

Influence of High-Pressure Compaction of Binary Mixtures on Solubility, Dissolution and Wettability of Borderline Poorly Soluble Drugs Employing Standard Excipients

Dissertation

zur

Erlangung des Doktorgrades (Dr. rer. nat.)

der

Mathematisch-Naturwissenschaftlichen Fakultät

der

Rheinischen Friedrich-Wilhelms-Universität Bonn

vorgelegt von

Bashar Ibraheem

aus

Homs, Syria

Bonn, Juli 2021

Angefertigt mit Genehmigung der Mathematisch-Naturwissenschaftlichen
Fakultät der Rheinischen Friedrich-Wilhelms-Universität Bonn

Promotionskommission:

Erstgutachter: Prof. Dr. Karl-Gerhard Wagner

Zweitgutachter: Prof. Dr. Alf Lamprecht

Fachnaher Gutachter: Prof. Dr. Gerd Bendas

Fachfremder Gutachter: Prof. Dr. Valentin Stein

Tag der Promotion: 30.11.2021

Erscheinungsjahr: 2021

Significant portions of Chapter 4 were previously published in an article entitled “Influence of high-pressure compaction on solubility and dissolution of ibuprofen binary mixtures employing nonfunctional excipients”, Ibraheem, et.al., IJPX, 2021. DOI: 10.1016/j.ijpx.2021.100075

Acknowledgements

First, I would like to thank Prof. Dr. Karl G. Wagner for giving me this great opportunity to carry out this Ph.D study in his group, for his great ideas, his personal precious and continuous support as well as for his scientific guidance and input throughout the supervision of my PhD thesis.

From University of Bonn, I would like to thank Franz-Josef Willems and Jürgen Hohmann (technical Workshop, Pharmaceutical Institute), Alexander Christen (Workshop for precision engineering, Institute of Physics), as well as the staff members of the glass workshop (Institute of Chemistry) for their technical proficiency, creative ideas and support to manufacture the die assembly for the preparation of IDR-disks under high pressure and to modify the dissolution tester for the performance of IDR testing, including also the new IDR instrument for neat excipients. The modified equipment as well as the new developed technique enabled performing valuable measurements, which were consequently used to establish certain correlations that enriched the study. I would like to recognize and thank PD Dr. Hubert Rein, who introduced me to wetting experiments for solid surfaces and shared his related experience.

I would also like to thank the members of the examination board, Prof Dr. Alf Lamprecht, Prof. Dr. Gerd Bendas and Prof. Dr. Valentin Stein, for participating and accompanying the PhD defense procedure. I also would like to express my gratitude to KAAD (Catholic Academic Foreign Services) for granting me the scholarship programme.

I would like to acknowledge and thank many colleagues for the cooperation I received during my research at the Institute of pharmaceuticals, for the unforgettable moments outside the working frame and for their productive discussions. Jan Kozak, Kai Berkenfeld, Mohamed Ehab Ali, Stefan Lorscheidt, Tawfek Yazeji, Markus Ries, Henusha Jhundoo, Merari Duarte, Ozan Hirlak, Alexander Ramich, Thomas Schmal, Florian Schorr, Maryam Shetab Boushehri, Bernadette Kettel, Esther Sophia Bochmann, Simone Putzke, Pia Steinlein, Kristina Steffens, Anna Katharina Krome, Chiwah, Katrin Grüneberg, Dnyaneshwar Kapote, John Youshia, their company made me feel at home. I miss already being together. Special thanks go to my office mates (Viktoria Riedel, Markus Jäger, Fabian Simons, Veronika Hagelstein, Daniel Jagudka and Tim lillotte), who have so generously donated much of their time sharing me the German culture, I will always remember the cheerful moments and the friendly working atmosphere.

I greatly appreciate Martina Gerlitz for supporting me by many bureaucratic hurdles, especially during my employee time at the institute.

I would extremely like to thank the fantastic Harry Potter fans, my trustful friends "Grizic Daris, Tugrul Mert Serim and Alvaro Lopez Marmol" for their invaluable unfailing friendship that began in Germany, for their support in all life's aspects., together we could overcome some hard times, for always being available to help sharing their knowledge and care.

I am extremely grateful to Mrs. Jennifer De Goursat for her critical correction of a considered part of the manuscript.

I wish to express tremendous gratitude to all Syrian long-time mates, thanks for having them in my life.

I would like to express my great gratitude in particular to my parents, brothers and sister for their love and prayers, without their faith and belief I could have not accomplished this work. Thanks to Hassan for always being there whenever I need.

And last but definitely not least, I would like to thank my Iliana for sharing her love, for taking care of me and keeping encouraging me even during the difficult times. Looking forward to living more joyful moments lifelong.

for my family

“Antwan, Najah, Sawsan, Ammar, Hassan, Ilina”

TABLE OF CONTENTS

Nomenclature	VI
Symbols.....	VI
Abbreviations.....	VIII
1 Introduction	1
2 Aims and scope of work	4
3 Model and literature background	6
3.1 Related aspects and perspectives on solubility and dissolution's improvement of poorly soluble drugs 10	
3.1.1 The impact of compaction pressure on dissolution rate	10
3.1.2 The impact of excipient on drug solubility and dissolution rate.....	11
3.1.3 The impact of the co-milling process on drug solubility and dissolution rate.....	12
3.1.4 Intrinsic dissolution test as evaluation method of solubility enhancement techniques	13
3.2 Possible mechanisms of compaction under high-pressure in combination with hydrophilic carriers for improving drug solubility and dissolution.....	14
3.2.1 The influence on crystal form (crystal modification).....	16
3.2.1.1 Effects of crystal habits and crystal defects.....	17
3.2.1.2 Effects of metastable polymorphs	18
3.2.1.3 Effects of amorphization.....	18
3.2.2 The influence on solid surface wettability, increased drug/excipient interactions and overall polarity.....	20
4 Influence of high-pressure compaction on solubility and dissolution of ibuprofen binary mixtures employing nonfunctional excipients	22
4.1 Introduction	22
4.2 Results.....	24
4.2.1 Dissolution studies of IBU-compacts	24
4.2.1.1 Intrinsic dissolution rate of IBU-compacts.....	24
4.2.1.2 Dissolution studies (non-Sink conditions) of IBU-formulations.....	26
4.2.2 Solubility determination of IBU-formulations	29
4.2.3 Kinetic and intrinsic solubility of IBU	31
4.2.4 Solid-state analysis of IBU-formulations.....	32
4.2.4.1 X-ray powder diffraction XRPD of IBU-formulations	32
4.2.4.2 Differential scanning calorimetry DSC of IBU-formulations	36

4.2.5	Compacts morphology of IBU-formulations SEM	39
4.2.6	The influence of amorphous form: Melt quenched IBU (IBU-MQ).....	43
4.2.6.1	Saturation solubility of IBU-MQ.....	44
4.2.7	Stability studies of IBU-HPC COM-Tab	45
4.2.8	Theoretical estimation of aqueous solubility improvement for IBU-MQ and IBU-compacts 46	
4.3	Discussion.....	48
4.4	Conclusion.....	60
5	Influence of high-pressure compaction on wettability of ibuprofen compacts prepared employing nonfunctional excipients: the impact of pure excipient properties	62
5.1	Introduction	62
5.2	Results.....	64
5.2.1	Wetting studies of IBU-compacts	64
5.2.1.1	Surface free energy SFE & wetting kinetics of IBU-compacts.....	64
5.2.1.2	Sorption behaviour of IBU-compacts.....	65
5.2.1.3	SFE and wettability of melt quenched IBU (IBU-MQ)	66
5.2.2	FTIR analysis of IBU-compacts (IBU/excipients interactions)	67
5.2.3	IBU-compacts porosity.....	72
5.2.4	Mercury porosimetry of IBU-tablets.....	73
5.2.5	Mercury porosimetry of IBU-granules	75
5.2.6	Milling effect on particle size distribution of IBU-mixtures	77
5.2.7	Specific area of IBU-granules	78
5.2.8	The influence of pure excipients properties on the compacts' performance	79
5.2.8.1	The effect of pure excipient and drug/excipients ratio on the wettability	79
5.2.8.2	IDR for pure excipients.....	80
5.2.8.3	Kinetic and intrinsic solubility of IBU in binary mixtures	81
5.2.9	The influence of high-pressure: 200MPa formulations analysis.....	82
5.3	Discussion.....	84
5.3.1	IBU-compacts characteristics.....	84
5.3.2	Effect of pure excipients	94
5.3.3	Principle component analysis PCA of IBU-compacts	97
5.4	Conclusion.....	99

6	The evaluation of application of high-pressure compaction employing nonfunctional excipients as a process to improve solubility and dissolution. A case study with indomethacin	101
6.1	Introduction	101
6.2	Results.....	102
6.2.1	Dissolution studies of IDM-compacts	102
6.2.2	Saturation Solubility of IDM-formulations.....	104
6.2.3	X-ray powder diffraction of IDM-formulations.....	105
6.2.4	Differential scanning calorimetry of IDM-formulations.....	108
6.2.5	SEM of IDM-formulations	110
6.2.6	FTIR of IDM-compacts.....	112
6.2.7	Wetting studies of IDM-compacts	116
6.2.7.1	Sorption behaviour of IDM-compacts (Tensiometer).....	117
6.2.8	IDM-compacts Porosity and Density.....	118
6.2.9	Particle size distribution of IDM-mixtures	119
6.2.10	Specific area of IDM-granules	119
6.2.11	Stability of IDM PVPVA COM-Tab	120
6.3	Discussion.....	121
6.3.1	Principle component analysis of IDM-compacts.....	133
6.4	Conclusion.....	135
7	Mechanistic understanding of incompatibilities of ibuprofen and copovidone during direct compression under high-pressure.....	136
7.1	Introduction	136
7.2	Results.....	138
7.2.1	Dissolution studies of IBU-PVPVA formulations	138
7.2.2	Solubility determination of IBU-PVPVA formulations.....	139
7.2.2.1	Shake flask method.....	139
7.2.2.2	CheqSol method.....	140
7.2.3	Solid-state analysis of IBU-PVPVA compacts	141
7.2.3.1	XRPD of IBU-PVPVA compacts	141
7.2.3.2	DSC of IBU-PVPVA compacts.....	143
7.2.3.3	Optical observation and SEM of IBU-PVPVA compacts	143
7.2.4	Wetting studies of IBU-PVPVA compacts.....	146

7.2.4.1	Shape drop analysis of IBU-PVPVA compacts	146
7.2.4.2	Tensiometer of IBU-PVPVA compacts.....	147
7.2.5	Density and porosity of IBU-PVPVA compacts.....	148
7.2.6	Hg-porosimetry of IBU-PVPVA granules	148
7.2.7	PSD of IBU-PVPVA mixtures	149
7.2.8	Effect of IBU: PVPVA ratio	150
7.2.9	IBU-PVPVA compacts under 200MPa	150
7.2.10	IBU and PVPVA interactions: FTIR.....	151
7.2.11	Dissolution profiles of stored IBU-PVPVA compacts.....	154
7.3	Discussion.....	154
7.4	Conclusion.....	158
8	Materials and methods.....	160
8.1	Materials	160
8.1.1	Ingredients for solid formulations	160
8.1.2	Chemicals for analytical assays	160
8.2	Methods.....	161
8.2.1	Preparations of the tablets using high-pressure 500MPa	161
8.2.1.1	ST-formulations.....	161
8.2.1.2	COM-formulations (the oscillating mill function)	161
8.2.2	Preparations of IDR disks	162
8.2.3	Dissolution studies	162
8.2.3.1	Dissolution profiles (non-sink conditions)	163
8.2.3.2	Intrinsic Dissolution procedure & Analysis (Modified apparatus)	163
8.2.3.3	Intrinsic dissolution test of pure excipients Novel instruments	164
8.2.4	Equilibrium solubility at different pH values by Shake flask Method	165
8.2.5	CheqSol	167
8.2.6	Solid-state analysis.....	168
8.2.6.1	X-Ray powder diffraction XRPD.....	168
8.2.6.2	Differential Scanning Calorimetry DSC Analysis.....	169
8.2.7	Scanning electron microscopy (SEM).....	170
8.2.8	Wetting studies	171
8.2.8.1	Drop Shape Analysis (SFE & wetting kinetics).....	171

8.2.8.2	Tensiometer: Sorption behaviour	174
8.2.9	Fourier transform infrared spectroscopy FTIR-ATR	175
8.2.10	Tablets Porosity.....	175
8.2.11	Mercury porosimeter	176
8.2.12	Particle size distribution (PSD) of ST and COM mixtures	177
8.2.13	Specific area	178
8.2.14	Preparation of melt quenched IBU (IBU-MQ).....	178
8.2.15	Data analysis	179
9	Summary and outlook	180
10	PUBLICATIONS.....	184
11	Appendix.....	185
12	References	189

Nomenclature**Symbols**

ΔC_p	difference of heat capacity
ΔG	free energy difference
ΔH_f	enthalpy of fusion
ΔS_f	entropy of fusion
A	surface area
COM	co-milled
COM-Tab/Gr	co-milled tablets/ granules
C _s	saturation aqueous solubility
D	diffusion coefficient
d ₁₀	10 percent of the particles' distribution lies below this value
d ₅₀	average diameter size of particles, where half of distribution lies above and half below this diameter
d ₉₀	90 percent of the particles' distribution lies below this value
d _{average}	average of pore diameter
D _o	dose number
dx/dt	dissolution rate
Gr	granules
h	boundary layer thickness
H _f	heat of fusion
K _s	kinetic solubility
m ²	square of absorbed water mass (Tensiometer)
Mix	mixtures
P _o	polarity
POR%	total porosity
R	gas constant
r ₅₀	pore radius at 50% of the maximum cumulative intrusion volume of mercury
S amorphous/S crystalline	solubility ratio

SF	solubility factor
ST	standard
ST-Tab/Gr	standard tablets/ granules
S_o	intrinsic solubility
T	temperature
Tab	tablets
T_g	glass transition temperature
T_g_{mix}	glass transition temperature of mixture
T_m	melting point/ melting temperature
V	medium volume
W	mass fraction
W_a	work of adhesion
W_i	work of immersion process
W_s	work of spreading
ΔH_c	cold recrystallization
ΔH_m	heat of fusion
ΔH_m^o	heat of fusion of 100% crystalline drug
θ	contact angle
σ_l	liquid surface tension
σ_s	total surface free energy
σ_s^d	dispersive part of surface free energy
σ_{sl}	interfacial tension liquid/ solid
σ_s^P	polar component of surface free energy

Abbreviations

API	active pharmaceutical ingredient
ANOVA	analysis of variance
ASD	amorphous solid dispersion
BCS	biopharmaceutics classification system
BET	Brunauer, Emmet and Teller method
BSE	backscattered electron detector
CheqSol	chasing equilibrium solubility
CMC	critical micelle concentration
DSA	drop Shape Analysis
DSC	differential scanning calorimetry
FTIR-ATR	Fourier transform infrared spectroscopy - Attenuated Total Reflection
FTIR	Fourier transform infrared spectroscopy
GIT	gastrointestinal tract
HBA	Hydrogen-bond acceptor
HBD	Hydrogen-bond donor
HCL	hydrochloric acid
HPC	hydroxypropyl cellulose
HPC-SSL	super special-low viscosity hydroxypropylcellulose
IBU	ibuprofen
IBU-MQ	melt quenched ibuprofen
IDM	indomethacin
IDR	intrinsic dissolution rate
ISO	isomalt
LV_{interface}	liquid-vapour
MANN	mannitol
MUPS	multiple unit pellet system
NSAIDs	non-steroidal anti-inflammatory drugs
OWRK	Owens-Wendt-Rabel-Kaelble method
PCA	principle component analysis

PM	physical mixtures
PVP	polyvinylpyrrolidone
PVPVA	polyvinylpyrrolidone vinyl-acetate copolymer/ Copovidone
PSD	particle size distribution
RH	relative humidity
RT	room temperature
SD	solid dispersion
SL _{interface}	solid-liquid
SV _{interface}	solid-vapour
SE	secondary electron detector
SEDDS	self-emulsifying drug delivery system
SEM	scanning electron microscopy
SEM-COMP	scanning electron microscopy-composition
SFE	surface free energy
SORB	sorbitol
UVD	Ultra Variable-Pressure Detector
VP mode	variable pressure operation
XRPD	X-ray powder diffraction

1 Introduction

The increasing number of new drug candidates, yielding from the combinatorial chemistry research, exhibiting poor solubility and inadequate dissolution properties within the past decade [1], resulted in various enabling principles to overcome the poor aqueous solubility and thereby potentially increase their bioavailability. Thus, the selection of appropriate delivery systems for these drugs is one of the challenges for the pharmaceutical development. The so-called “enabling formulations” aim to transfer drugs, which have low solubility, but reasonable membrane permeability (Biopharmaceutics Classification System **BCS** class II) into a dissolved state along the gastrointestinal tract **GIT**. This might potentially shift the absorption profile of these sparingly soluble entities close to that of BCS class I that has high solubility and permeability [2,3]. Several approaches of enabling formulations were already employed, such as the use of nanosuspension, complexation, incorporation of non-ionic surfactants, liposomal formulations, self-emulsifying drug delivery systems and amorphous solid dispersions **ASD** [3–9]. The most frequently used reference technology for enhancing solubility and bioavailability is the ASD [10].

Within an ASD and in an ideal condition, the drug is molecularly dispersed into a hydrophilic solid carrier or matrix to form a glass solution [7,10,11], which is a single amorphous system [12]. ASDs can be prepared by melting, solvent method, or melt-solvent method [13]. The ASD approach was implemented to enhance the solubility and release of several active pharmaceutical ingredients **APIs** using different vehicles [14–19]. Despite the effectiveness of ASDs as most favorable enabling formulations, this technique is still associated with some limitations that are manifested in the following points:

- i. **manufacturing processes:** such as degradation of some compounds due the mechanical forces upon processing like comminution, health and environmental concerns due to the use of organic solvents with possible residuals, as well as expensive costs by solvent methods. Moreover, temperature sensitivity issues and thermal degradation of the drugs should be investigated upon using melting methods [3]. In addition, the preparation of ASD is often time-consuming, involving multiple steps.
- ii. **decreased physical stability:** As ASDs represent thermodynamically instable systems [5,11], their physical stability is the main hurdle encountered by their development. Besides, ASDs are impaired by a potential precipitation after dissolution, taking into account that the maintenance of steady supersaturation over GIT is critical factor to govern the bioavailability [20].

- iii. **scale up aspects** [8]: The reproducibility of ASD that was obtained during the development stage, might be a scale up issue, especially when the rotary evaporation process is applied within the preparation [21].

The mentioned limitations of the ASD approach are a matter of concern as they may counteract its benefits. In this respect, it is useful to investigate whether desired benefits of ASDs overcoming their stability issues with acceptable preservation of supersaturation and a suitable way of preparation, could be achieved with conventional approaches. These approaches include the API in its crystalline form, emphasizing on oral dosage forms due to their prevalence and convenience as administration way [22].

Several conventional techniques are used for the improvement of solubility and dissolution that include: micronization, chemical modifications, crystal modification, solvates and salt formation etc. [1,4,6,8,9,23,24]. This also involves processes like wet granulation that includes applying high shear mixing with water or organic solvents, resulting in increased hydrophilicity of the system due to the presence of water-soluble binders and consequently improved wettability and dissolution kinetics. Yet, this method is impaired by the use of solvents, an obligate drying step, time and energy consumption [25].

Other conventional methods have been employed successfully, which rely on adding some functional excipients such as pH-modifiers, co-solvents or surfactants. For pH-dependent drugs, adding pH-modifiers as solubilizing excipients can adjust the environmental pH within the dosage form, such as a tablet or capsule, to a range where, the drug may potentially dissolve [26,27]. For example, an acid may precipitate in the stomach, but then dissolve subsequently in the intestine due to the ionization at higher pH values. Hence, in the case of a weakly acidic compound, some alkalizing agents are used as solubilizing excipients by increasing the surrounding pH to a higher value than the drug's pKa [26]. Under these circumstances, it is essential to ensure high concentrations of the dissolved drug and preserve this supersaturation at pH of up to value 4. The risk of precipitation with pH-adjustment technique is high as soon as the compound comes into contact with an aqueous medium with a pH where it is less soluble. As well, there is a high possible toxicity due to the application of a non-physiological extreme pH.

The term 'co-solvents' refers to adding some water miscible solvents in which the drug is also soluble, like PEG 400, propylene glycol or ethanol [28]. Although this technique is regarded as a potent method for solubility enhancement [29], the development of cosolvent-formulations is usually slow and costly. Its toxicity and tolerability are moreover a cause of concern when applying high levels of solvent, in addition to uncontrolled precipitation, which may take place upon dilution. However, the drug does not redissolve easily from the co-solvent mixture. As most cosolvents are liquid or semi-liquid, an adequate

concentration in a solid dosage form is usually critical. Thus, this approach is usually combined with liquid filled capsules, mostly as Self-Emulsifying Drug Delivery System (**SEDDS**).

The efficacy of employing surfactants to enhance the solubility of BCS class II molecules was also confirmed. In general, the surface-active agents are able to decrease the medium surface tension, thus improving the wettability of APIs. Furthermore, as the concentration of surfactants exceeds their critical micelle concentration **CMC** values, the micelles formation will be triggered with the hydrophobic drug molecules being included within the micelles. This is referred as 'solubilization by micellization' [30–32]. However, the effects on solubility and partition coefficient of the drug into micelles were found to depend on the type of surfactants and drug characteristics [31].

Hence, the selection of an enabling strategy needs to balance bioavailability over stability and manufacturing aspects, especially in case of borderline solubility-limited drug candidates in between BCS I and II or III and IV, respectively. As mentioned, interactions between APIs and functional excipients are often employed to improve solubility and dissolution kinetics in enabling formulations [33]. However, the question remains whether excipients regarded as non-functional or standard might establish similar interactions; subsequently, improvement of solubility when employed at unusual manufacturing process conditions. For us, the potential on wettability and solubility by compacting **API** and hydrophilic excipients at high-pressure, as could be performed via briquetting in a tablet machine for small scale [34,35] or in a roller compaction process for larger scale, is of special interest. The simplicity of the new potential strategy to be translated into final dosage forms and its convenience for manufacturing scale-up are essential issues to consider.

2 Aims and scope of work

In respect of all the aspects introduced above, a new strategy is proposed for borderline poorly soluble drugs, based on a conventional approach. The primary aim of this work is to implement formulations exhibiting improved solubility and/or dissolution rate, by compacting API in the presence of hydrophilic excipients at high-pressure. The process is intended to facilitate and enable the production of suitable dosage forms by a simple way of preparation, having comparable or superior performance of that obtained with often-applied conventional techniques (mentioned in the introduction). Consequently, an enhancement of solubility and dissolution will be achieved with reduced costs, no possible toxicity, high tolerability, less time and energy consumption. Besides, an improved reproducibility will be obtained for the prepared dosage forms in term of their physicochemical properties.

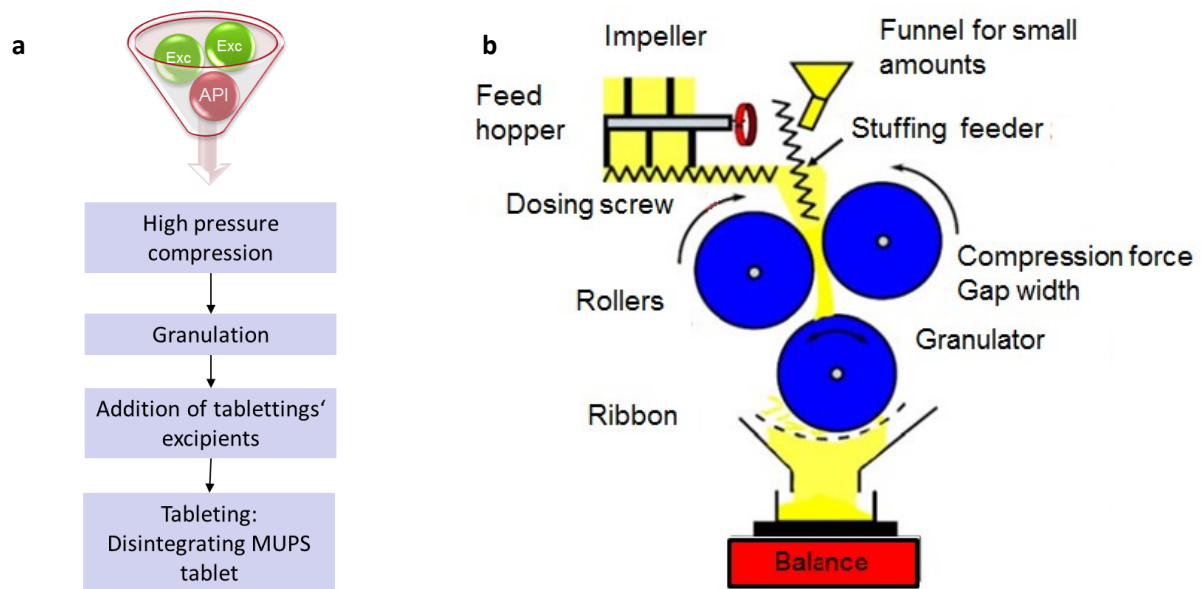


Figure 1 Schematic diagram of (a) the proposed approach, (b) Roller compactor according to R. F. Lammens

The proposed strategy is based on compaction of binary mixtures; consisting of a crystalline drug and a water-soluble non-functional excipient that has polar groups such as polyols, or polymers, through application of high compression pressure.

The direct compression process can be applied as a functional tool to produce the desired formulations (compacts). The problem caused by tablet compression at very high-pressure, however, is usually a prolongation of the disintegration process. Hence, these compacts should be regarded as a primary source for granules produced via briquetting. These granules would form multiparticulate tablets, where the dense granules could be dispersed in a disintegrating tablet matrix similar to Multiple Unit Pellet System

(MUPS) tablets (Figure 1a). This strategy can be regarded as surrogate development of a roller compactor process that would be able to produce these highly compacted granules (Figure 1b).

The secondary aims of this work were as follows:

- To investigate and evaluate the outcomes of the application of high pressure compaction in terms of crystal modification, drug/excipient interactions and the surface wettability.
- Evaluation of an additional milling step for the binary mixtures prior of compacting under high-pressure.
- Impact of the excipient type and its solubilizing efficacy in respect to supersaturation.
- Contribution of the disk-intrinsic dissolution rate IDR of neat excipient to the overall disk-IDR value of the formulations.
- Influence of drug to excipient ratio on the drug wettability obtained for the compacts.
- To apply IDR test as a key parameter to characterize all experimental drug formulations and to evaluate the potential dissolution benefit of the proposed approach.

3 Model and literature background

Ibuprofen (**IBU**) and indomethacin (**IDM**), as borderline BCS II candidates, were selected as model drugs from the aspects of their crystalline nature and weak acidity.

Both weakly acidic drugs have carboxylic acid group and have a low affinity to interact with water leading to the insolubility in aqueous media [36]. The existence of this specific group of the API molecule that can be deprotonated is important to obtain high potential interactions with the excipient.

Ibuprofen

Ibuprofen is a propionic acid and a representative for non-steroidal anti-inflammatory drugs (**NSAIDs**) [37] which is widely used in analgesic immediate release tablets. Ibuprofen with its low solubility and good permeability belongs to the BCS class II, therefore the absorption of IBU out of immediate-release oral dosage forms is primarily affected by solubility and dissolution. IBU's solubility is pH-dependent, it has a low solubility at low pH (stomach) and higher solubility at pH 6.8 [38].

IBU crystals are susceptible to be modified. Romero *et al.* monitored a change in the crystal habit of IBU upon only processing as mixing with excipients and tableting. This was explained by destabilization and fragilization of IBU intermolecular interactions based on investigating the IBU crystal packing and referring to the responsible molecules that are sensitive to the mechanical stress because they are not involved in the intermolecular interactions between the raw IBU crystals [39]. The existence of a crystalline metastable form of IBU was reported by Dudognon and colleagues 2008, however, the solubility and stability still needs to be addressed [40].

IBU has 2 counts of Hydrogen-bond acceptor (**HBA**) and 1 Hydrogen-bond donor (**HBD**); hence it can be involved in H-bonding interactions.

Indomethacin

IDM, just as IBU, inhibits the synthesis of prostaglandins generating its analgesic and anti-inflammatory effects as NSAID drug [41]. It is commonly prescribed for moderate to severe state of some diseases such as rheumatoid arthritis and osteoarthritis.

IDM belongs to BCS class II drugs that mostly suffer from dissolution-limited bioavailability [36].

Based on IDM chemical structure (Table 35), it is a monoprotic acid, which can be characterized with one proton donor site that linked to the OH group in addition to 4 HBA.

Different values of solubility were reported for IDM due to different polymorphic forms [42,43]. A transformation of IDM from the initial γ -form to the polymorph β -form or an amorphous component is possible upon processing [44].

Regarding the polymers, many previous studies confirmed the capacity of various hydrophilic polymers such as polyvinylpyrrolidone (**PVP**) and hydroxypropyl cellulose (**HPC**) to improve solubility as well as dissolution rate of poorly soluble drugs [45–48] and to inhibit the precipitation, maintaining the supersaturation state for reasonable time [49–53]. In this work polyvinylpyrrolidone vinyl-acetate copolymer (**PVPVA**) and HPC with super special-low viscosity (**HPC-SSL**) were selected as polymeric model excipient. Additionally, sugar alcohol based model excipient like isomalt (**ISO**), mannitol (**MANN**) and sorbitol (**SORB**) were chosen.

Hydroxypropyl cellulose

HPC is a pH-independent water-soluble polymer. HPC-SSL has a low Tg (28.3 °C) and relatively lower molecular weight, hence it can act as a solid-state plasticizer [20].

In a previous study, adding HPC-SSL in solid dispersions (**SDs**) contributed in gaining a tailored release profile of API with superior supersaturation over a certain pH range [20]. Moreover, HPC-based SDs, prepared using various pharmaceutical processes, proved to successfully improve the dissolution process, preserve the supersaturated state and maintain the chemical stability of poorly soluble drugs [51–53]. The ability of HPC to maintain supersaturation was explained by either inhibition of drug aggregation because of drug/ carrier interaction or by the influence of viscosity induced from dissolved polymer that can obstruct the crystallization process [49].

HPC has 8 counts HBD and 19 HBA [54]. The high level of API/HPC interaction is key factor to achieve the stabilization of drugs in amorphous state. The nonionic nature of HPC allows the contact between the polymer and low energy surfaces of a hydrophobic drug, resulting in enhanced wettability, showing the ability to decrease the surface tension of aqueous media upon dissolution of its molecules. [50].

Copovidone (PVPVA):

PVPVA (Copovidone) represents a copolymer of 1-vinyl-2-pyrrolidone and vinyl-acetate in a ratio of 6:4. PVPVA has a lower glass transition temperature and hygroscopicity than PVP, making it more compliant for ASDs production and from stability point of view [55]

PVPVA as hydrophilic polymer possesses 3 HBA (1 for PVP and 2 for VA) per repeating monomer, without any HBD site [56]. The ability of PVP to strongly interact with APIs was identified, mainly by the formation of hydrogen bonding resulting in higher anti-crystallization capacity [46,57]. The feature of PVP to inhibit the crystallization kinetics was likewise investigated and confirmed for amorphous IDM by preventing its self-association [58].

Isomalt, mannitol and sorbitol

Sugar-alcohols, on the other hand, were associated with a solubilizing effect showing marked increase in both the solubility and dissolution when applied as carriers for SDs [14,15,59–61]. Sugar-alcohols could be successful carriers in solid dispersion technique, due to the high glass transition temperature, the absence of physiological risks and browning reactions, the high thermal stability and the pronounced property as substrate for H-bonding [59]. Moreover, sugars-alcohols might inhibit the re-crystallization of amorphous API because of their abundant polyhydroxy and hence their strong formed H-bonding [60].

In a previous work, the remarkable improvement of dissolution rate for nifedipine SDs with mannitol was attributed to better wettability of nifedipine crystals due to mannitol particles that attached on the surface [15]. Mannitol can form considerable hydrophilic diffusion layers around drug particles, attracting the water molecules and mediating the necessary contact for solubilization [59].

Isomalt, mannitol and sorbitol are characterized with strong hydrogen bonding in water, due to the plenty of H-bonding groups presenting in their molecules. ISO has 11 HBA and 9 HBD, whereas MANN and SORB have 6 HBD and HBD each. As the molecules of sugar-alcohols dissolve in the aqueous solution, a more hydrophilic environment can be created around the drug molecules increasing their wettability. The mentioned properties make the selected sugar-alcohols valuable candidates in the approaches of solubility improvement.

Compacts' composition

Development batches of binary mixtures (drug/excipient) were prepared with a drug load of 20%. The mixtures were blended and the blends resulted were directly compressed to obtain tablets at a pressure of ≈ 500 MPa. Corresponding tablets were also prepared from mixtures with the same compositions but using co-milled mixtures. The milling was performed using a ball mill as a medial step prior to the compression process.

The produced tablets were subsequently broken (granulated) by a dry granulator to get dense granules.

The physical mixtures (**Mix**), tablets (**Tab**) and related granules (**Gr**) that have been prepared without a previous co-milling process are referred to as standard formulations (**ST**). Respectively, the corresponding mixtures, tablets and related granules that have been obtained from the milled blends are co-milled formulations (**COM**).

Figure 2 presents the preparation steps of the compacts under high-pressure, the compositions of the compacts are listed in Table 1, Table 2 and Table 3. More details of the preparation are described later (see section 8.2.1).

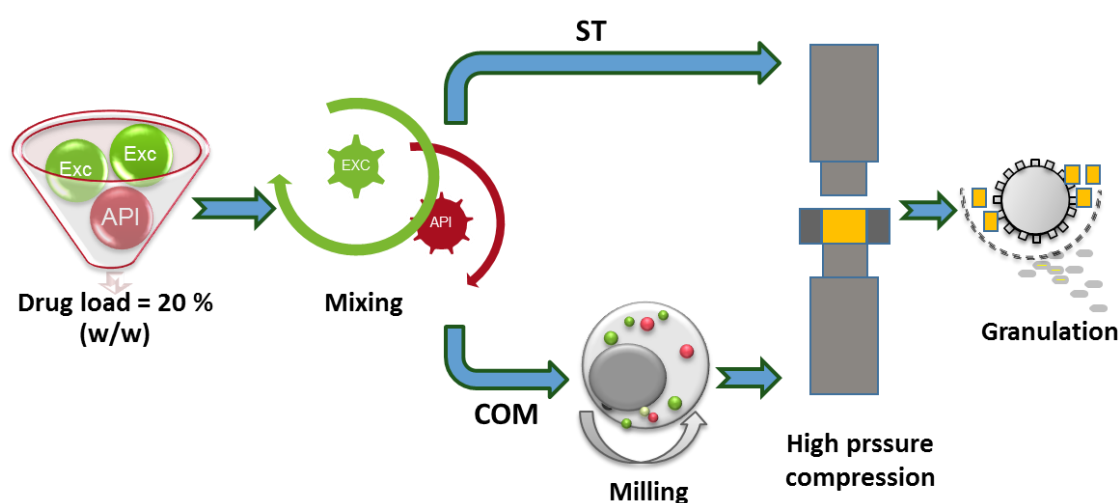


Figure 2 Illustration of the compacts preparation applying high-pressure

Table 1 Composition of IBU compacts (Chapter 4 and 5)

Formulation	Composition (Wt%)	Milling before compression
IBU-HPC ST-Tab/ Gr	ibuprofen/ HPC-SSL 20/80	No
IBU-HPC COM-Tab/ Gr	ibuprofen/ HPC-SSL 20/80	Yes
IBU-ISO ST-Tab/ Gr	ibuprofen/ isomalt 20/80	No
IBU-ISO COM-Tab/ Gr	ibuprofen/ isomalt 20/80	Yes
IBU-MANN ST-Tab/ Gr	ibuprofen/ mannitol 20/80	No
IBU-MANN COM-Tab/ Gr	ibuprofen/ mannitol 20/80	Yes
IBU-SORB ST-Tab/ Gr	ibuprofen/ sorbitol 20/80	No
IBU-SORB COM-Tab/ Gr	ibuprofen/ sorbitol 20/80	Yes

Table 2 Composition of IDM compacts (Chapter 6)

Formulation	Composition (Wt%)	Milling before compression
IDM-PVPVA ST-Tab/ Gr	indomethacin/ PVPVA 20/80	No
IDM-PVPVA COM-Tab/ Gr	indomethacin / PVPVA 20/80	Yes
IDM-ISO ST-Tab/ Gr	indomethacin / isomalt 20/80	No
IDM-ISO COM-Tab/ Gr	indomethacin / isomalt 20/80	Yes

Table 3 Composition of IBU-PVPVA compacts (Chapter 7)

Formulation	Composition (Wt%)	Milling before compression
IBU-PVPVA ST-Tab/ Gr	ibuprofen/ PVPVA 20/80	No
IBU-PVPVA COM-Tab/ Gr	ibuprofen/ PVPVA 20/80	Yes

3.1 Related aspects and perspectives on solubility and dissolution's improvement of poorly soluble drugs

Different aspects that relate to the proposed strategy can affect the solubility and dissolution process, such as the impact of compaction, milling process and excipient properties.

3.1.1 The impact of compaction pressure on dissolution rate

In relation to the compression pressure, conventional tableting has mostly shown unacceptable release for poorly soluble drugs displaying a water-solubility below 1 µg/ml [3]. However, various attempts were carried out to monitor drug dissolution profiles upon applications of different compaction pressures. Several authors stated that compression force has no effect on drug release in spite of the confirmed influence on tablet hardness. Similar release profiles were obtained from amorphous cefuroxime axetil out of milled, size-uniformed powders prepared from pellets compressed at different compression forces. It was indicated that the uniformity of the drug particle sizes prevailed over different pressures applied and is responsible to obtain comparable release rates [62]. However, prepared tablets from the same API revealed a decrease in the dissolution rate by increasing the pressure. The prolongation of disintegration time can however explain this finding.

Some researchers investigated the influence of tableting pressure on the dissolution process, represented by the intrinsic dissolution rate (**IDR**). IDR is defined as the dissolution rate of a drug under constant temperature, pH, agitation and surface area [63]. In these studies, no clear correlation between the compression pressure and IDR could be established.

Yu *et al.* investigated the outcomes of changing the experimental variables on the observed IDR and reported that compression forces did not have a significant effect on IDR values of the pure APIs studied [64]. Another study indicated that the IDR of non-disintegrating disks of salicylic acid, aspirin and a mixture of both was independent from compression pressures [65] and the materials particle size. Previous work addressed also no significant differences between IDR profiles of pure amorphous tadalafil (prepared using ball milling) compressed at different forces [66]. The same was reported by Tseng and colleagues, where the disk compression force revealed no significant effect on IDR of chloramphenicol using miniaturized rotating and stationary disk systems [63].

In this context and by evaluating the compaction effect on dissolution rate, the nature of drug solid-state must be considered. It was suggested that IDR values are overestimated for amorphous materials when the pressure is not high enough [67]. Moreover, the pH of medium can interfere with the obtained IDR data as an influencing factor for pH-dependent drugs. A less relevant effect on IDR of pure amlodipine besylate was obtained by employing different compaction pressures [68]. This observation was more obvious in acidic medium where amlodipine besylate is much more soluble.

Although it has been speculated that different compression pressures may affect IDR of a solid form, no distinct effect was observed among the mentioned studies. However, these trials mostly focused on compaction of pure APIs or they did not include applying and testing high-pressures. There is a lack in the scientific literature of experimental investigation employing high-pressure compaction of API/ excipient mixtures. Consequently, it is interesting to understand the response of binary mixtures when they are subjected to high mechanical stresses during the compression.

3.1.2 The impact of excipient on drug solubility and dissolution rate

Most strategies to improve drug solubility and dissolution rate are based on excipients and the assumption that the carrier properties can affect the solubility properties of the final form. Therefore, the characteristics of a drug delivery system and its performance after administration can be modified by means of combined carriers [5,69]. The extent of the excipient's contribution within the overall process of drug solubility or dissolution improvement is thus a matter of interest and has to be investigated.

Drug dissolution rates can be essentially influenced by the properties of pure excipients. Some co-dissolving excipients revealed either inhibition or promotion effect on the solubility and IDR of ibuprofen and paracetamol as applied in different concentrations [70]. Costa and his colleagues referred that the dissolution behaviors and physical characteristics of prepared pellets of ibuprofen depended also on the physical properties of used excipients, such as solubility, specific surface area, and density [69]. Different dissolution performances were addressed for ketoprofen SDs obtained with various hydrophilic carriers as e.g. polyvinylpyrrolidone K30 and Polyvinyl alcohol [71].

The drug/excipient ratio must be considered in the evaluation of the excipient's impact on drug solubility. An increased solubility of IDM in PVP 90 solutions was measured with increasing PVP concentrations. This was explained by possible interaction between IDM and PVP in solution, likely due to hydrogen bonding [72].

3.1.3 The impact of the co-milling process on drug solubility and dissolution rate

Associating the compaction with a previously applied co-milling step can induce higher level of crystal modifications/mechanochemical activation and drug/excipient interactions, leading to improved solubility and release kinetics. Generally, particle size reduction can be accomplished by mechanical crushing of the compaction process or by the milling process, due to the impact of high-pressure compression and friction [6]. The disruption of large crystals is normally accompanied with higher specific surface area and developing of cohesive powders with higher surface energy [50]. Moreover, a milling process can provoke a change in particle shape, in addition to milling-induced amorphization or structural disordering of the crystal. Drug dissolution and solubility could be improved by the mentioned implications of the milling [23].

The ability of ball milling was stated to prepare glass solutions of poorly soluble drugs together with polymeric compounds, exhibiting a single homogenous amorphous phase [6]. The dry milling of drug-excipient co-mixtures can induce high interactions by means of van der Waals forces or hydrogen bonding. Co-milling of a hydrophobic drug with a water-soluble excipient was also reported as potential method to improve the solubility [23].

Nevertheless, a co-milling process might lead to reveal both hydrophobic and hydrophilic groups of drug molecules on the surface. Upon applying mechanical fracture on particles, the crystals would break up differentially depending on their shape [73,74], therefore various facets will be exposed on the surface and hence, various functional groups would mainly contribute to the surface chemistry, resulting in different wettability. Modi *et al.* found that a milling process induced a decrease in the preferred orientation for compacts prepared from the milled materials associated by crystal surfaces with lower abundance of hydrophilic facets. Thus, it was suggested that not only the crystal molecular arrangement but, also surface molecular environment of the compacts should be considered to properly interpret IDR results [73]. A better wettability is expected to be related to higher exposure of hydrophilic groups on the compact surface.

In addition to a lower degree of texture (less-texturizing materials as the crystallites are allowed to be more randomly oriented [75]), triturated ingredients are also accompanied by higher free energies on the surface due to the internal induced strains and defects that develop around the dislocation core in crystals, beside the generated mechanochemically-activated particle surfaces [23,75]. These aspects must be considered by evaluating the impact of the milling on solubility and dissolution processes.

3.1.4 Intrinsic dissolution test as evaluation method of solubility enhancement techniques

For sparingly water soluble drugs, where the dissolution step is the rate limiting step in the absorption process, *in vitro* dissolution analysis can be used to predict the oral bioavailability of different formulations [26]. Bio-relevant sink conditions (medium volume is about 5 to 10 times greater than the volume correspond to the API saturated solution) during the test should be achieved, realizing that such conditions may appear *in vivo*, when the absorption of a drug from the gastrointestinal fluids occurred faster than the dissolution process [26].

As particle size and shape would have a major impact on dissolution kinetics and potentially extent, IDR testing was chosen as an area normalized characterization tool [63]. IDR measurement is of great importance to determine the dissolution rate. It describes the rate of solid mass transfer from specific surface to the liquid medium [76]. Extrinsic factors, such as pH, temperature, stirring speed and surface area will be maintained constant during IDR testing; hence, drug dissolution properties and the impact of different solid forms on the product performance can be assessed. This reduces the numerous factors affecting the normal dissolution test. Normalization of the IDR findings could be used for the prediction of the dissolution behavior of other shapes and sizes.

In the recent years, more focus was noticed regarding the use of IDR as a normalized measure, independent of shape, size of the tablets or the particles remaining after tablet disintegration. The automatization of the intrinsic dissolution apparatus makes this testing a relatively simple procedure. In comparison with conventional solubility testing, IDR test requires smaller quantities, at reduced test duration [68].

During IDR test, only a certain equal area is exposed to the dissolution medium for all investigated formulations, which allows proposing all possible forms of the substance (polymorphs, amorphous, crystalline, etc.) to the same conditions, thus eliminating surface area alteration that usually occurs during normal dissolution test and excluding particle size and pore influence. IDR could be presumably affected by several parameters such as preferred orientation, crystal habit, solubility, surface free energy (**SFE**) and crystal strains. In addition, this test facilitates comparison of the effect of different excipients and solid-states on the drug release. Any change of the drug solid-state, manifested in discontinuing of the release rate's linearity, can be monitored during the test.

Although the IDR procedure is not appropriately standardized yet, this method might correlate better to *in vivo* dynamic conditions to predict the drug behavior. Furthermore, it can be employed to observe the influence of surfactants and pH on the solubilization process of poorly soluble drugs, to investigate the mass transfer phenomena during dissolution and to provide the pH-dependent release profiles [64,77,78].

Several studies were performed to investigate the feasibility of applying IDR measurements for drug solubility classification. The IDR test was applied for the characterization of solid-state of IBU, and the evaluation of the dissolution process in different pH values with different excipients [79]. Investigations of 15 model BCS drugs, confirmed a good qualitative correlation between disk-IDR values and BCS classes of solubility [64]. Zakeri *et al.* concluded the suitability of drug categorization depending on their IDR and intestinal permeability values [76]. In addition, according to the results obtained by Dezani and colleagues, IDR testing was demonstrated to be superior technique for solubility studies as compared to conventional equilibrium method for determination of biopharmaceutical class [80].

Besides, the real solubility may not be correctly determined by equilibrium solubility method because of experimental variables, such as shaking time, temperature volatility, filtration, and quantity of substances [79], or due to the occurrence of potential changes in solvates, polymorphs and salt forms during the solubility test. IDR can help monitoring these different transformations and offer solubility determination before the incident of any transformation [64].

Considering all mentioned advantages, IDR was considered as a key parameter to characterize and evaluate all experimental drug formulations, and to test the potential dissolution benefit of the presented approach. The application of IDR test can be utilized to monitor possible physical changes of the tested drugs such as the particle morphology and degree of order, which would provide better understanding of relationships between the dissolution rate and the solid properties, determining the impact of employed strategy as well as the excipient contribution.

3.2 Possible mechanisms of compaction under high-pressure in combination with hydrophilic carriers for improving drug solubility and dissolution

The application of very high energy by the compaction process using high-pressure involves different mechanisms that can be responsible to enhance drug solubility and dissolution rate.

In general, the compaction includes brittle fracture and plastic deformation presenting new surface properties [81]. Thus, an intense deformation of the surface is expected to be triggered by applying high-pressure. An additional comminution before compaction can disorder the outside layers of a crystallite and might consequently transform it into amorphous form. Furthermore, the high-pressure compaction can boost a change in the structure of molecules which affect the solubility and wettability in different mechanisms [82]. Buckton and Newton reported a plastic flow compaction of Amylobarbitone, confirming notable changes in surface energy along with the compression pressure.

Dissolution is affected by both wettability and solubility; whereby bad solubility does not always relate to bad wettability. As can be concluded from Noyes-Whitney equation (Eq. 1), proposed by Rasenack and Müller that describes the dissolution process, accelerating the dissolution rate dx/dt can be achieved by various attempts. That includes enlarging the wettable surface area A of the drug, decreasing the contact angle θ of the solid with dissolution medium, or reaching higher saturation solubility concentration C_s to maintain the sink condition compared to the present dissolved concentration C_t [1]. The other two factors including diffusion coefficient D and boundary layer thickness h are drug-dependent and physiological-dependent respectively and could not be directly affected by drug delivery strategies.

$$\frac{dx}{dt} = \frac{A \cdot \cos \theta \cdot D \cdot (C_s - C_t)}{h} \quad \text{Eq. 1}$$

The improvement of the aqueous solubility C_s can be performed through crystal modifications converting the drug into high free-energetic state. In addition, increasing the interactions between the components (drug and hydrophilic excipient) would induce an increase in the drug hydrophilicity and the work of adhesion between the solid surface and aqueous medium, represented in lower θ value, thus better wettability. Accordingly, two potential effects of the proposed process can be induced on either C_s or θ values and hence on the physicochemical properties of the formulated drug, that could have an influence on its solubility and dissolution kinetics. These effects are discussed thoroughly afterwards. The factors, derived from Eq. 1 and could be affected by the proposed approach, are summarized in Table 4.

Table 4 Factors which can influence in-vitro dissolution rates and might be affected by high-pressure compaction

Term in Noyes-Whitney equation	Affected by	Possible effect of high-pressure compaction
A: wettable surface area of undissolved drug	Particles size of solid	Decrease in particle size due to accumulation of particles defects
	Dispersibility of particles in dissolution medium	The presence of hydrophilic excipient would hinder the trend of particle agglomerates formed by cohesion in the medium (3.2.2)
θ: contact angle of solid with dissolution medium	Drug crystal habits	Different crystal habits beside variances in relative abundance of diverse hydrophilic facets on the surface (3.2.1.1)
	Solid surface wettability	Increasing the overall solid polarity and surface free energy (3.2.2) Increasing drug/ excipient interactions 3.2.1.2(3.2.1.3)
Cs: solubility of drug in dissolution medium	Drug solid state	Effects on polymorphism and amorphization/ surface mechanochemical activation (3.2.1.2, 3.2.1.3)
	Presence of hydrophilic compounds	Excipients may work as solubilizing agents (3.2.2)

(based on a table proposed by [26])

3.2.1 The influence on crystal form (crystal modification)

The approach involves the application of high mechanical energy resulting in fracture of particles, which may reduce the particle size and can defect the crystal lattice of each single ingredient, similar to the impact obtained by grinding processes [23]. This might generate crystal modification, which could manifest in mainly three types of crystal modifications (Figure 3): either in (a) change in the drug morphology by producing crystal fractures reflected in crystal habit modification or (b) crystal defects/ new metastable polymorphic forms or (c) transformation into the amorphous state. These modifications would be associated with creating activated surfaces of elevated energy (mechanochemical activation), i.e. improved solubility [1,23,77,83–85].

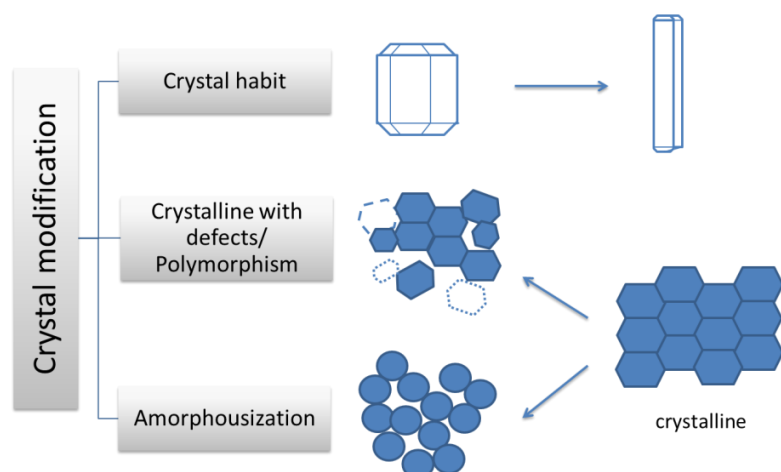


Figure 3 Schematic of possible aspects of crystal modifications induced by high-pressure compaction

3.2.1.1 Effects of crystal habits and crystal defects

The change in morphology might also induce anisotropic shapes affecting the flowability, particle behavior during compaction and the drug release kinetics [73,86,87]. Upon compression, the crystallites would be less randomly orientated (highly texturized), tending to adopt a new preferred arrangement along the surface of the sample. Consequently, it is expected that only specific crystal planes are represented on the tablet surface. This process is referred to as texturization [75].

Different crystal planes are assigned with different surface energies or with the exposure of different hydrophilic groups at various quantities on the surface. Thus, differential wettabilities and different dissolution kinetics could be revealed [73,88]. A higher IDR was linked to crystal shape exhibiting more polar crystal faces and consequently higher hydrophilic interactions with the aqueous medium [89,90].

The habit modification approach might suffice to improve the dissolution rate, without the necessity to induce polymorphic transitions [89]. Tenho *et al.* suggested that for poorly soluble and limited dissolved drugs, IDR would be influenced to a significant extent by the crystallites preferred orientation (texture degree). However, the presence of polymorphic, pseudo-polymorphic or amorphous forms might obscure this effect [75].

Beside habit modifications, the crystal energetics can affect the disk-IDR [77]. Herewith, the crystal energetics can be altered by changing the nature, concentration (density) and profile of the crystal imperfections (defects and impurities). A higher density of crystal defects and dislocations corresponds to higher internal and free energy and thus, higher thermodynamic activity, resulting in faster dissolution

behavior. Accordingly, it is valuable to attempt optimizing the crystal properties via only habit modification applying a simple method without inducing any polymorphic transformations.

3.2.1.2 Effects of metastable polymorphs

The compaction with a very high mechanical energy can enable the formation of a network matrix, converting API into a new crystal structure, which is weakly bonded and poorly organized (metastable physical forms). Inducing different relative positions and orientations of the adjacent molecules in the crystal lattice would generate different interactions so that the molecules would align differently to each other, producing different crystalline forms (polymorphs). Different analytical techniques can be utilized to screen and identify the polymorphism, such as X-ray diffraction, the thermal analysis; particularly differential scanning calorimetry, hot stage microscopy and infrared spectroscopy [91–93].

As compared to the most stable crystalline form, the metastable forms are generally less-stable, characterized with higher free released energy, increased solubility and hence, improved dissolution rates [26]. The importance of polymorphism with respect to enhanced solubility and dissolution properties was evidenced in various studies [92,94,95]. However, the enhancement degree depends on the differences in metastable/crystalline free energy. Only small differences in the solubility are expected between polymorphs having relatively small differences in their free energy [96].

The physicochemical stability of metastable forms is not only a challenge for the entire shelf life of the dosage form but also during the absorption process within GIT. The metastable form can convert easily to the more stable but less-soluble form in the GI media [97]. Indomethacin IDM is an interesting case of study. Three polymorphic forms of IDM were reported exhibiting different melting points, where the higher melting point was connected with lower solubility and more stability [72]. Thus, the challenge is to produce a stable polymorph exhibiting higher solubility without a potential conversion to another form within GIT.

3.2.1.3 Effects of amorphization

The amorphous form is normally associated with the absence of a crystalline structure [26]. The effect of the conversion of a crystalline to the amorphous state on improving the solubility and dissolution is well investigated by a plenty of studies where the amorphization led to an increase by many folds as compared

to the related crystalline form [17,20,47,48,83]. An improvement of solubility up to 1000-fold was reported between the amorphous and their corresponding crystalline forms [24].

Usually, from dissolution point of view, different solid forms of API would have the following release order: Amorphous form > metastable form > stable crystalline form [9]. Upon dissolution, amorphous forms can generate supersaturated solutions [98] and might initially precipitate (if ever occurs) as a metastable form that has a higher solubility than the most stable crystalline form (Figure 4) [13].

The reported enhancement of the solubility by amorphization varied depending on physicochemical properties of the treated substances and following their lowest energy crystalline forms. The amorphous IDM was reported to have 4.9 folds higher aqueous solubility to that of the crystalline form (γ -polymorph) [99]. Another work suggested 4 folds of solubility improvement for amorphous IDM (in SD prepared with crospovidone) as compared the crystalline IDM [100].

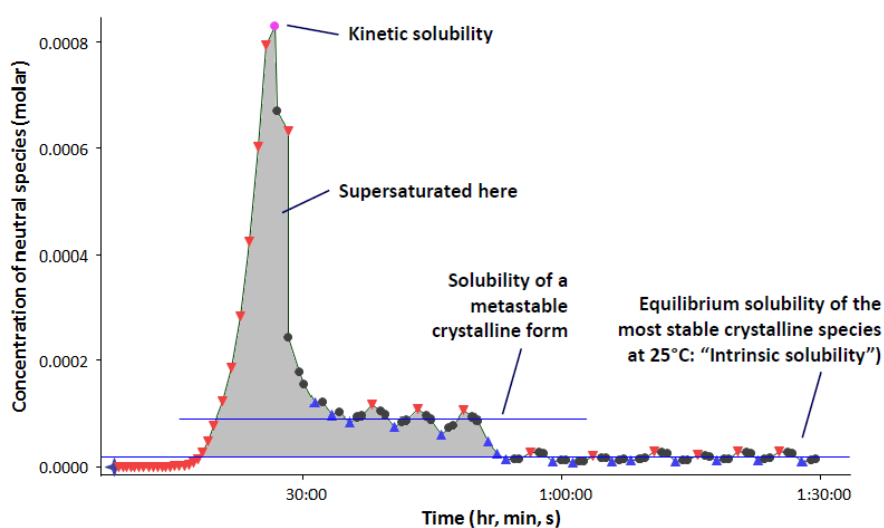


Figure 4 CheqSol experiment of piroxicam that precipitates initially in metastable form and then transforms to more stable crystalline form with lower solubility [101,102]

In fact, the physicochemical properties of neat amorphous forms for the same API can be influenced by the production methods, leading to different values of the solubility and dissolution rates, even when these forms own the same glass transition temperature [66]. On the other hand, the amorphous API within different ASD systems can behave identically with no significant difference between ASDs manufactured by the rotary evaporation, spray-drying method or hot melt extrusion [48,103].

Generally, the increase of solubility of amorphous forms to their crystalline forms can be theoretically estimated, but it was sometimes significantly higher than the experimental value when the recrystallization process during the experimental determination is rapid and not negligible [104].

In some cases, the dissolution rate of the crystalline form out of tablets could be unexpectedly higher than that of pure amorphous forms [66]. It was explained by the higher compressibility degree of the amorphous form due to the chaotic order of molecules, which results in a decreased porosity of the tablets and may cause slower dissolution rates. This confirms that, the pressure applied should be considered when comparing the crystalline with amorphous form of the same API.

3.2.2 The influence on solid surface wettability, increased drug/excipient interactions and overall polarity

Now the effects of high pressure on the neat API are extended to the solubility and dissolution effects of API/excipient mixtures compressed at high pressure. The second mechanism relates to the manipulation of the overall tablet solid surface.

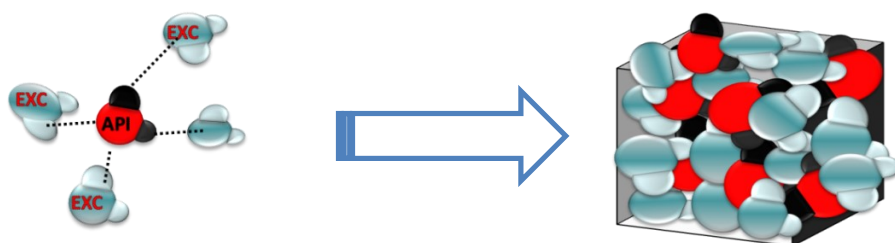


Figure 5 Illustration of excipient molecules as solubilizing agents and formation of coherent mass of both components

The employed hydrophilic excipients might work as solubilizing agents that, under the high-pressure applied, are able to reduce the interfacial tension between the aqueous medium and the hydrophobic drug surface. This system would ensure a new higher strength of intermolecular interactions between particle compounds. These intermolecular forces of attraction at condensed phases of drug and hydrophilic excipient result in the formation of condensed coherent masses (Figure 5), enhancing the dissolution step by increasing the overall polarity at a higher surface free energy **SFE**. Stronger attractive forces will be produced between the solid matrix surface and water, leading consequently to overall surface hydrophilization, optimizing the overall wettability characteristics of the drug surface from poor to good wettability (Figure 6) and promoting the dissolution process as a result. In other words, the proposed approach may produce higher strength interactions between the adjacent components in the

formed compact, possessing consequently increased SFE. This is reflected particularly, from a pharmaceutical point of view, by providing a rise of material wettability and changes in its properties.

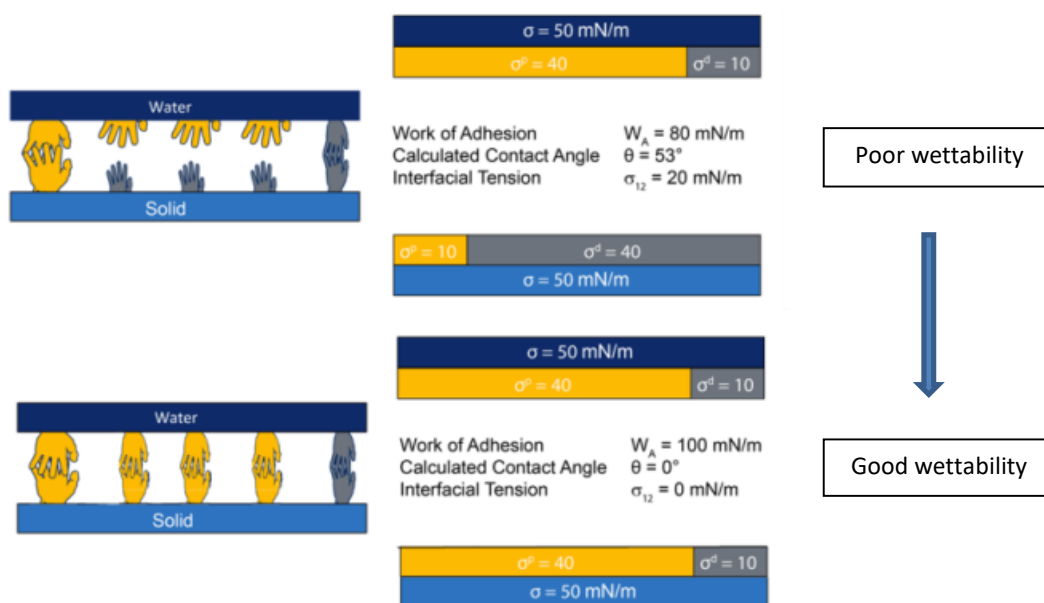


Figure 6 Schematic diagram of phase contact between aqueous medium and solid drug (KRÜSS technical note TN315e, modified). σ^p and σ^d refer to polar fraction and dispersive fraction of surface tension σ respectively.

Finally, a phenomenon similar to that of hydrotrophy or cosolvency systems could be induced [105]. Each water molecule could form four bonds resulting in a loose open structure with a large free volume. Upon incorporation of hydrophobic fragments into water, the densification of water structure occurs, causing shorten intermolecular distances between water molecules and driving out of hydrophobic drug molecules [106]. As molecules of the hydrophilic excipient dissolve in water, the resulted solution will be characterized by strong water/excipient intermolecular interactions due to the polar groups of the excipients, represented in H-bonding. Consequently, the densification as well as the overall intermolecular attraction of water molecules will decrease, increasing the ability of incubation of matrix-embedded hydrophobic particles within the aqueous medium. This restriction of water's self-association is referred to as solvent blinding effect [9,29].

All the mentioned mechanisms and consequences thereof for improving drug solubility/ dissolution rates are subject to testing and investigations in the following chapters.

4 Influence of high-pressure compaction on solubility and dissolution of ibuprofen binary mixtures employing nonfunctional excipients

4.1 Introduction

The application of high-pressure compaction in presence of a hydrophilic excipient is introduced as a potential technique to improve solubility and/ or dissolution kinetics of borderline BCS II candidates, which establishes a new substrate for formulation strategies.

Considering the dissolution of a crystal as the inverse process of crystal growth, its overall dissolution rate can then be estimated by the total of dissolution rates of individual crystal planes [75]. The manifestations of the possible crystal modification, which could be induced by the proposed technique, can be summarized in three attributes. The three solid-state attributes of drugs (namely crystallinity, crystal defects/polymorphism and crystal habits) can affect their physicochemical properties such as solubility, physical chemical stability and dissolution behavior.

Possible changes can occur to these attributes, particularly for crystalline substances, through modifying of the molecules' arrangement, crystal shape and mechanical properties. Changes in either the internal crystal structure (manifested as polymorphs or amorphous state) or in the external shape (crystal habits) can be generated, leading to different solid forms. The crystal modification can be considered as an effective strategy to improve the dissolution of BCS class II drugs [84]. The influence of crystal habit and exposure of different crystal facets on the API's wettability is well reported. The polarity and relative hydrophobicity of the crystals faces is governed by the molecular functional groups that emerge at the surface.

To sum up, depending on the inherent chemistry within the crystal lattice and the surface's groups, different chemical properties of the crystal face could be obtained [89] (more details in section 3.2.1). Therefore, the presence of any crystal modification due to the applied process was investigated in this chapter. Ibuprofen, as a model compound, as well as four excipients were used, which included: low-viscosity hydroxypropylcellulose as polymeric model excipient and three sugar-alcohols based model excipients, namely isomalt, mannitol and sorbitol. The formulations tested are listed in Table 1.

Certain effects can be induced via milling processes of pure ingredients on their own or the co-milling with a suitable adjuvant. Some examples of these effects, through which the drug dissolution and solubility could be improved [9,23], are summarized for the current used ingredients (Table 5).

4. Influence of high-pressure compaction on ibuprofen binary mixtures

Table 5 Examples on the milling or co-milling effects of the studied ingredients obtained from the literature

Ingredient	Adjuvant	observations	Ref.
Ibuprofen	-	reduction of the particle size to about 1/20 of the initial size, no chemical changes in the particles	[107]
Ibuprofen	-	Micronization to 2-3 μm , increased surface area, no induced Amorphization or change in crystal form, no chemical decomposition	[108]
Ibuprofen	kaolin	complete Amorphization of IBU	[109]
Ibuprofen	HPC	a partial loss in crystallinity of IBU, enlarged surface area and increased wettability	[50]
Ibuprofen	physical mixture containing PVP	changes in the IBU thermal properties that were related to some crystal modifications and higher intermolecular interactions	[39]
Sorbitol	-	a progressive polymorphic transformation upon increasing the milling time to the metastable crystalline form A	[110]
Mannitol	-	polymorphic conversion to the metastable form α , which reverses toward the stable physical state of crystalline form β after RT storage	[110]

Therefore, it is important to address whether the magnitude of mentioned changes can be achieved by applying the high-pressure compaction of the binary mixture independent of a prior co-milling step. This was evaluated by comparison of the resulted properties of co-milled formulations with that of the same formulations produced without a prior milling. The ball mill was used for the co-milling process, which might create various crystal structures on the particles surface, due to the high mechanical impact in the milling chamber between grinding balls and the wall of the chamber.

IDR test was applied as a method and primary parameter for the evaluation and comparison of the behavior of different IBU compacts prepared in different pH media. A modified intrinsic dissolution apparatus was developed based on the rotating disk system (8.2.1). This ensured the facilitation of the preparation and examination of IDR-disks compacted under higher pressure.

Furthermore, a melt-quenched IBU was prepared and tested, in order to estimate the specific contribution of the amorphous form to increase the solubility and IDR of an amorphous-based formulation.

The potential influences of the process were investigated and the characteristics of the obtained tablets and their granules were examined. Several factors and experimental parameters, including the increase degree of the aqueous solubility, the change in IBU solid state and IBU/ excipient interactions, were tested and correlated with the drug release. These correlations were performed to understand the relationship between resulted material properties and the compact performance.

4.2 Results

4.2.1 Dissolution studies of IBU-compacts

4.2.1.1 Intrinsic dissolution rate of IBU-compacts

As the accumulated dissolved amount of IBU per unit area was plotted against time (Figure 7), a linear gradient with acceptable correlation coefficients R^2 (0.97-0.998) was produced, confirming the feasibility and reliability of using the modified dissolution apparatus for IDR measurements. For the calculations of IDR at pH 5.5, only the data prior to a significant erosion or distortion of the tablet's surface were used [111]. Similar trends were observed in both media. All IBU-formulations showed statistically a significant increased IDR over the crystalline IBU-disk. Among the formulations tested, superior dissolution rates were obtained with HPC-compacts compared to the other excipients, followed by isomalt-compacts. ST-compacts with mannitol and sorbitol revealed the slowest IDR.

Table 6 Intrinsic dissolution rates of ibuprofen formulations and pure IBU

Formulation	IDR	
	pH 1.0 mg/min/cm ²	pH 5.5 mg/min/cm ²
IBU-HPC ST-Tab	0.468 ± 0.021	2.610 ± 0.230
IBU-HPC COM-Tab	0.892 ± 0.062	3.947 ± 0.079
IBU-ISO ST-Tab	0.350 ± 0.059	2.201 ± 0.117
IBU-ISO COM-Tab	0.162 ± 0.008	1.988 ± 0.157
IBU-MANN ST-Tab	0.118 ± 0.007	0.260 ± 0.037
IBU-MANN COM-Tab	0.133 ± 0.003	0.538 ± 0.070
IBU-SORB ST-Tab	0.117 ± 0.010	0.218 ± 0.016
IBU-SORB COM-Tab	0.123 ± 0.005	0.496 ± 0.088
IBU-CRY	0.025 ± 0.003	0.045 ± 0.001

In general, co-milled compacts resulted in higher IDR values compared to ST-Tabs, except for ISO-compacts (Table 6).

The differences between HPC-formulations and the other compacts, except for IBU-ISO ST-Tab, were significant and noticeable in the acidic medium. On the other hand, the difference between HPC- and ISO-formulations decreased at pH 5.5 as IBU partially ionized.

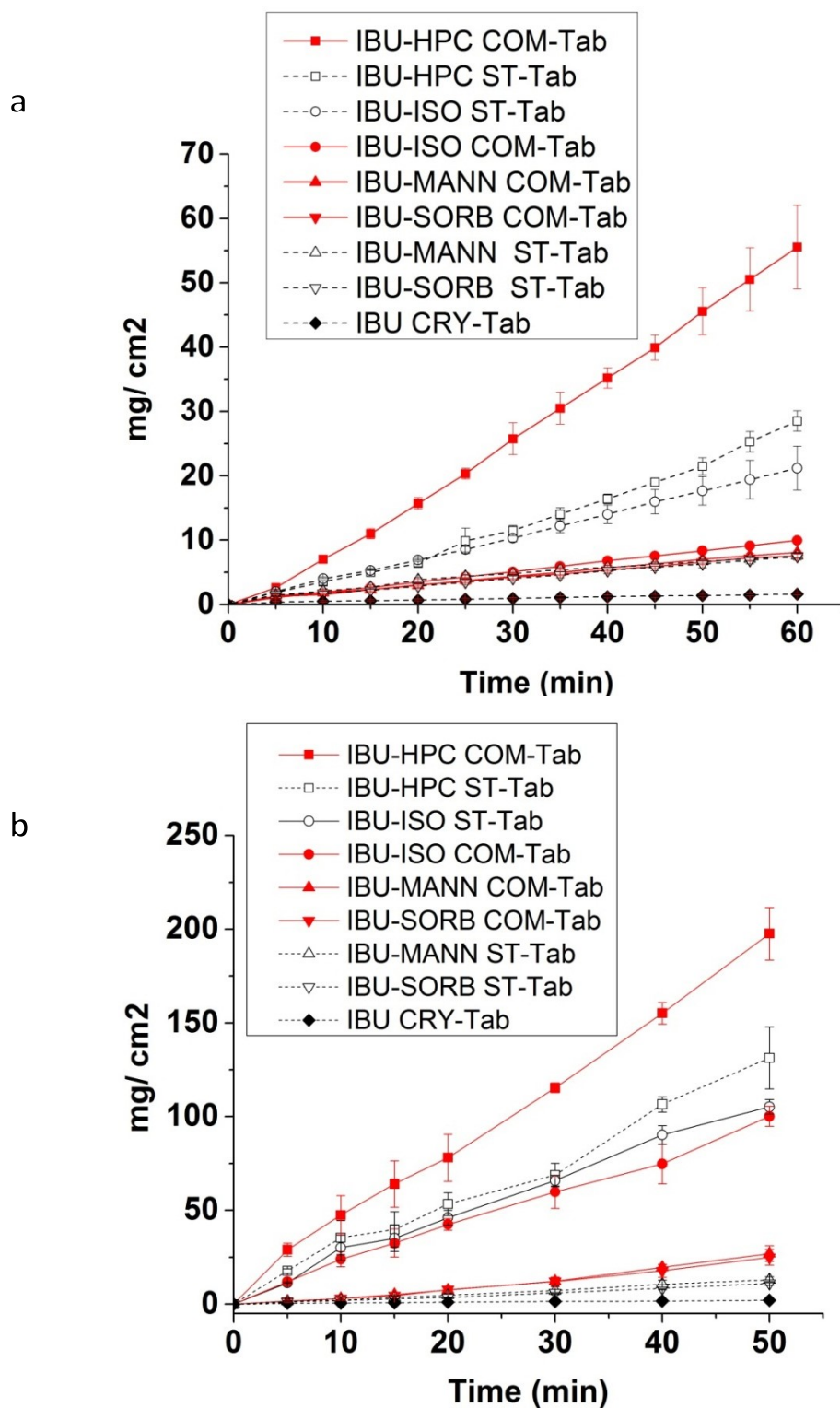


Figure 7 Intrinsic Dissolution profiles of ibuprofen formulations using a modified USP apparatus 1 at 37 °C, 100 rpm; medium volume 900 ml of (a) pH 1.0; (b) pH 5.5; mean \pm SD; n = 3

The IBU-HPC COM-Tab showed the highest rate of all tablets. Moreover, ANOVA analysis showed that IBU-ISO ST-Tab differed significantly from other sugar-alcohol compacts in both media. No significant differences could be observed of release rates within ST- or within COM-compacts of IBU-MANN and IBU-SORB by a comparative assessment at pH 1.0 and pH 5.5.

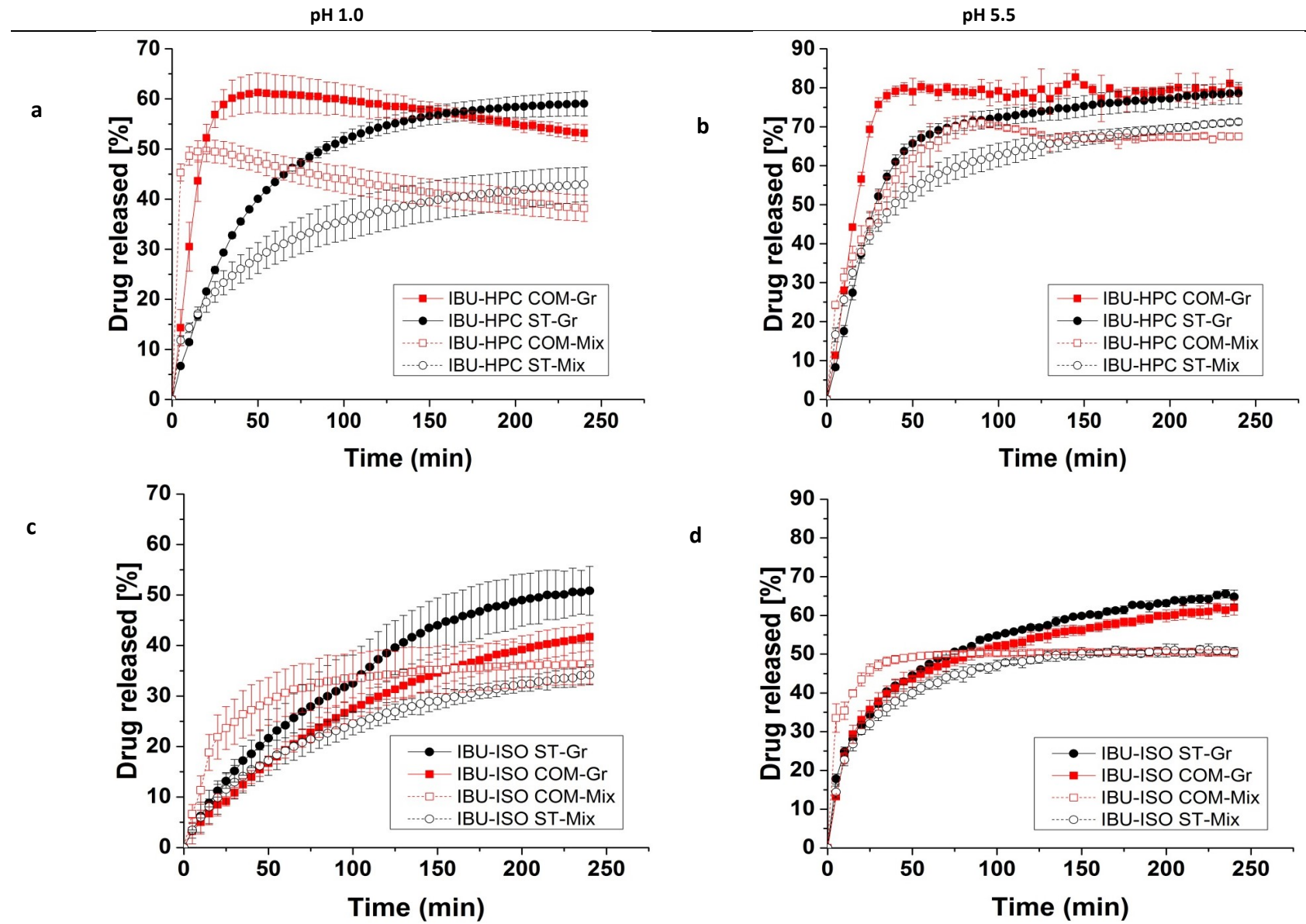
4.2.1.2 Dissolution studies (non-Sink conditions) of IBU-formulations

The release behaviors of IBU out of granules at non-sink conditions are summarized in Figure 8. Accelerated release kinetics were observed for IBU out of ST-compacts as compared to the neat IBU and corresponding ST-mixtures as well, in case of all excipients in both media. This influence was less significantly noticed for ST-compacts with SORB and MANN at pH 1.0 and pH 5.5, respectively.

Regarding the co-milled formulations, COM-Tab of HPC showed a faster release than the corresponding mixture in both media. However, the co-milled mixture revealed a faster initial release of for the first 15 minutes at pH 1.0, where the COM-mixture and -granules showed a reduction in the drug release after 20 min (from 50 to 38%) for the mixture and 50 min (from 61 to 53%) for the granules. On the other hand, the co-milled mixture of isomalt showed a higher release than the produced granules for, at least, the first 50 min at pH 1.0 and pH 5.5; the dissolution endpoint was however higher for the granules. Co-milled mixtures with MANN and SORB were obviously superior to the related granules at pH 1.0 and faster for the first initial minutes at pH 5.5 with a significantly higher endpoint for the granules.

Generally, both types of granules were superior to the neat IBU and the co-milled granules revealed faster releases than the corresponding ST-granules at both media (less noticed in case of mannitol and sorbitol granules, Figure 9). IBU-ISO granules were the only exception, where the ST-granules showed improved kinetics over the co-milled ones. The same order of the IBU release for the granules was obtained as that recorded from the IDR test for matching tablets. HPC-granules were again much faster than all other granules, followed by isomalt granules.

4. Influence of high-pressure compaction on ibuprofen binary mixtures



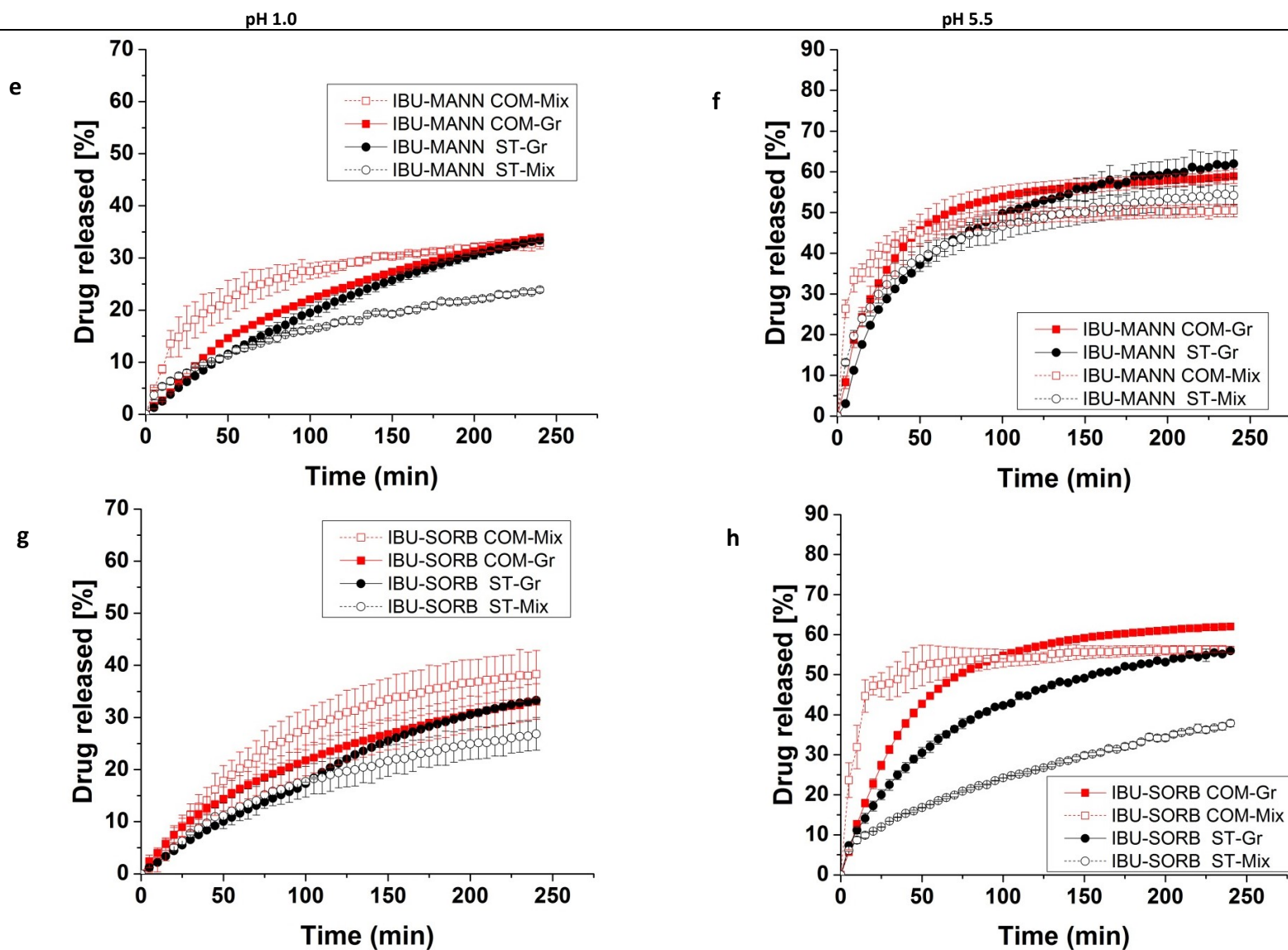


Figure 8 IBU release out of compacts granules as compared to related physical mixtures at pH 1 and pH5.5 (non-Sink conditions). Trials were performed in 900 ml at 37 ± 0.5 °C (100 rpm, USP. Apparatus 1), mean value \pm SD (n=3). a & b: IBU-HPC, c & d: IBU-ISO, e & f: IBU-MANN, g & h: IBU-SORB

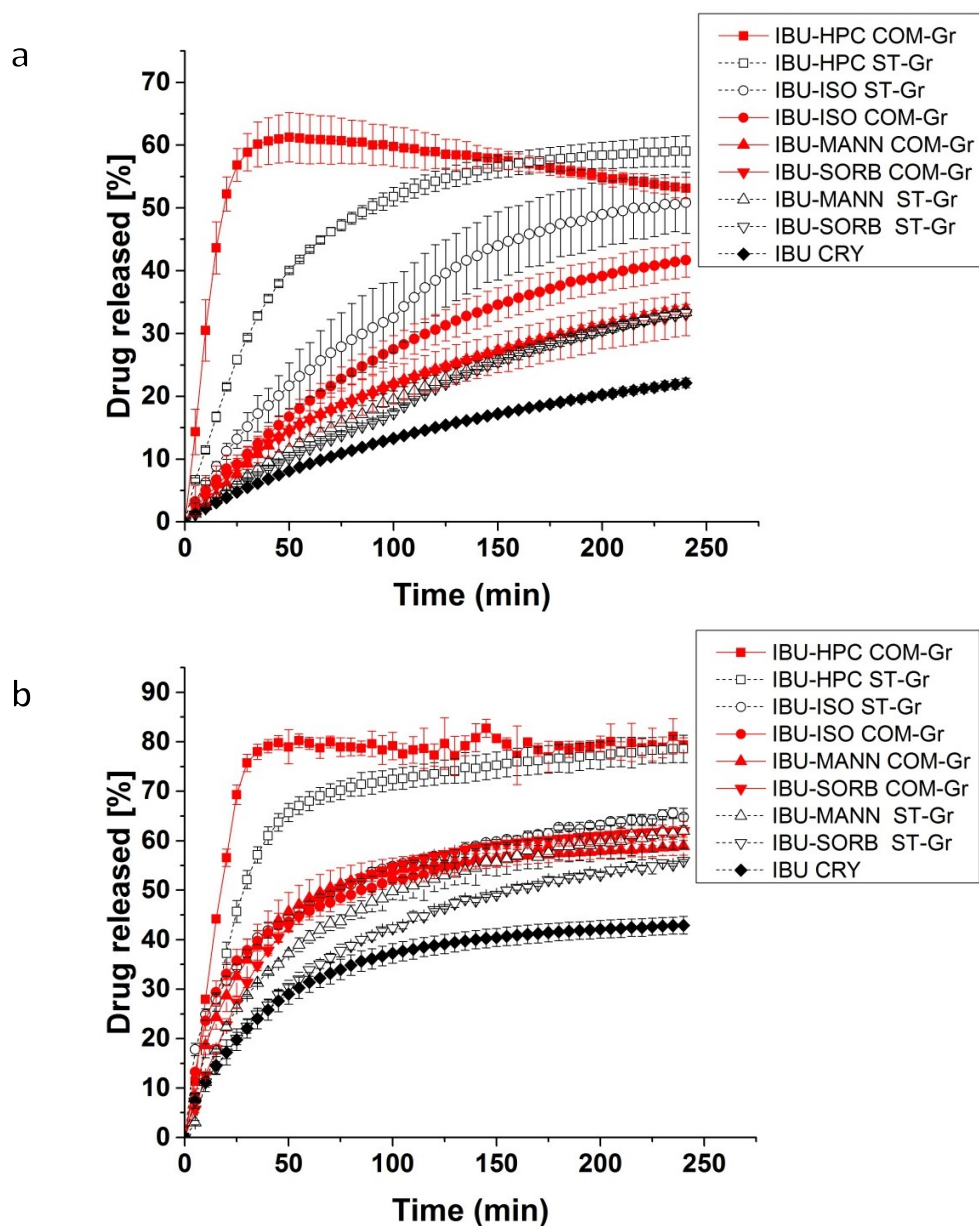


Figure 9 Drug release profiles of ibuprofen formulations using USP. Apparatus 1 at 100 rpm, 37 ± 0.5 °C; medium volume 900 ml of (a) pH 1.0; (b) pH 5.5; mean value \pm SD; n = 3

4.2.2 Solubility determination of IBU-formulations

The saturation solubility measured for the pure IBU was 0.0302 ± 0.0025 and 0.4212 ± 0.0712 mg/ml at pH 1.0 and pH 5.5, respectively. The saturation solubility of IBU out of the prepared formulations was improved in the range of 12- to 45% at pH 1.0 and from 3 to 54% at pH 5.5, compared to the saturation solubility of the neat, crystalline IBU. All results are summarized in Appendix; Table 54.

At pH 1.0, all excipients had a similar impact on increasing the solubility for standard physical mixtures of about 10% (Figure 10 A). However, the IBU aqueous solubility increased out of the compacted granules in the following order: HPC-Gr > ISO-Gr > MANN-Gr > SORB-Gr, where SORB-granules showed practically no improvement compared to the related mixture ($p=1$). Excluding ISO, all excipients showed even a higher increase in solubility when the materials were co-milled prior to compaction, maintaining the above-mentioned rank order.

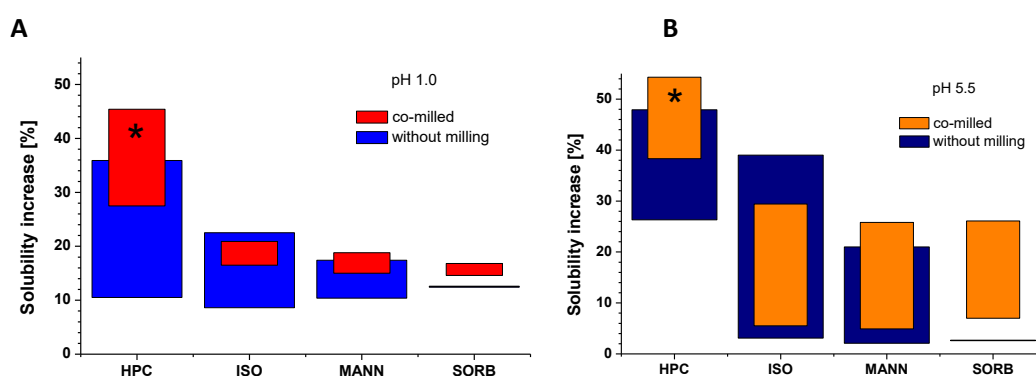


Figure 10 Solubility increase [%] of IBU dependent on pH (A: pH 1.0; B: pH 5.5), two ingredients mixing conditions: without milling or co-milled. The bottom of the bars represents values for the physical mixtures; the top of the bars represents the granules obtained from high pressure compaction
* partially amorphous (~ 38%)

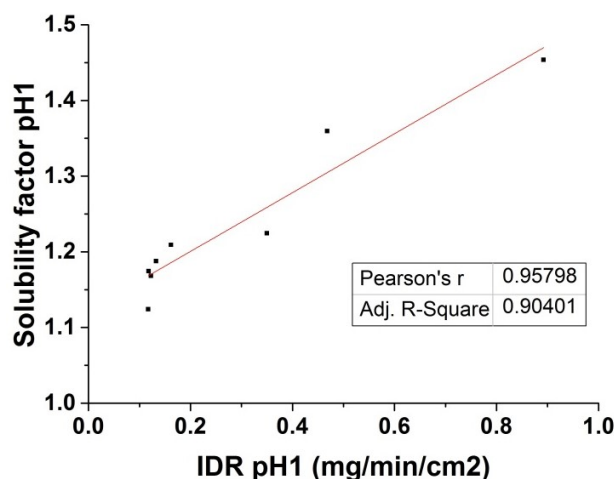
At pH 5.5, the increase degree in IBU solubility decreased for the physical mixtures compared to the values at pH 1.0, while it was more pronounced for the ST-granules. However, SORB-Gr showed similar increase of IBU solubility as the related mixture ($p=0.151$). The additional co-milling increased further the solubility to higher extent than ST-mixtures and granules with the exception of ISO-granules.

Similarly to the presented IDR data, the compacts with HPC and isomalt were superior to other excipients, with a particular advantage for IBU-HPC COM-Gr followed by IBU-HPC ST-Gr. Among the sugar-alcohols, only the isomalt ST-formulation showed a remarkable increase in the equilibrium solubility and the closest to HPC-compacts. An increase was observed in Cs of IBU out of co-milled compacts as compared to ST-formulations in the both media, presenting the same trend that was obtained by IDR testing, the IBU-ISO ST-granules were again the only exception. This was estimated by expressing the solubility increase as solubility factor **SF** ($C_{s,form}/C_{s,IBU}$; Table 7), which refers to the extent of solubility increase of IBU out of the compacts as compared to neat IBU.

Table 7 Solubility factors of IBU formulations (physical mixtures, granules) and pure IBU

Formulation	SF	SF	SF	SF
	Mix (pH 1.0)	Gr (pH 1.0)	Mix (pH 5.5)	Gr (pH 5.5)
IBU-HPC ST	1.105	1.359	1.263	1.479
IBU-HPC COM	1.275	1.454	1.383	1.543
IBU-ISO ST	1.086	1.225	1.031	1.390
IBU-ISO COM	1.165	1.209	1.055	1.294
IBU-MANN ST	1.104	1.174	1.021	1.210
IBU-MANN COM	1.150	1.188	1.049	1.258
IBU-SORB ST	1.126	1.124	1.026	1.027
IBU-SORB COM	1.146	1.168	1.070	1.261

Interestingly, plotting SF against the IDR values revealed a linear relationship (Figure 11).

**Figure 11 IDR correlation with solubility factor for IBU compacts at pH 1.0**

4.2.3 Kinetic and intrinsic solubility of IBU

IBU is a monoprotic acid with a $pK_a = 4.38$, which was obtained from the extrapolation of three p_sK_a values measured by the UV-metric method using Inform apparatus at methanol percentages of 24.97, 34.59 and 46.82% v/v. This value was in good agreement with the literature-reported value [112]. Based on the measured pK_a and CheqSol experiments (Table 8), the pure IBU showed 0.036 and 0.143 mg/ml for intrinsic solubility S_o and kinetic solubility K_s respectively. These values were significantly lower than the reported values (0.050 and 0.180 mg/ml for S_o and K_s respectively) using the same method [112] and slightly higher than the values measured by Etherson *et al.* (0.0299 and 0.141 mg/ml for S_o and K_s respectively) [113].

Table 8 Experimental solubility data measured by CheqSol at 25°C, experiments were replicates in n = 4 (mean ± SD)

Sample	Intrinsic Sol mg/ml	Kinetic Sol mg/ml	estimated Sol pH 1.0 mg/ml	estimated Sol pH 5.5 mg/ml	supersaturation ratio K_s/S_0
IBU	0.0363 ± 0.0003	0.1436 ± 0.0092	0.0363 ± 0.0003	0.5141 ± 0.0043	3.96

The supersaturation ratio is defined as the kinetic solubility divided by intrinsic solubility. IBU precipitated initially with a kinetic solubility of 0.144 mg/mL before converting to a stable form with an intrinsic solubility of 0.036 mg/ml.

4.2.4 Solid-state analysis of IBU-formulations

4.2.4.1 X-ray powder diffraction XRPD of IBU-formulations

XRPD was used to examine any modification of the crystalline form for all compacts [93]. Besides, it was applied for the quantification of the crystallinity of HPC-formulations.

The X-ray pattern of pure IBU and sugar-alcohols displayed the presence of numerous distinct peaks, which refers to their crystalline nature. Pure HPC demonstrated experimentally a hollow pattern, referring to a completely amorphous form [114,115]. For this reason, a quantification method of crystallinity could be established in case of HPC-formulations (8.2.6.1). This amorphous structure of HPC with no peaks in the XRPD pattern was stated before [20]. However, it was not consistent with another study where HPC with some degree of crystallinity exhibiting a very small melting peak at 188 °C was reported [50].

In respect to the calibration curve of crystallinity%, there was no influence of compression process on the overall crystallinity of IBU-HPC-ST tablets as well as the physical mixture (Table 9). The tablets revealed, however, to undergo a kind of crystal modification as clarified later.

In general, XRPD diffractograms (Figure 12, Figure 13 and Figure 14) of all samples showed the prominent peaks of IBU at specific 2θ values (at 16, 20 and 22°), conforming its crystalline nature [87]. All peaks of the crystalline IBU were present in the physical mixtures with a lower intensity because of dilution effect. Upon compaction and as compared to IBU-HPC ST-MIX, the intensity of the peak at 22° 2θ increased and became sharper, whereas the intensity of other peaks at 16.5, 20, 28.5 2θ decreased (Figure 12). Additionally, some peaks almost disappeared at 14, 15, 34, 43 two Theta; the one at 37° totally disappeared and a different shape at 16.5, 28.5 2θ was observed. The intensity of these changes was also clear in case of ISO-compacts, where different intensities of some peaks as well as different peak shapes were monitored at 16.5, 20, 22°, besides the disappearance of the peaks at 19, 25, 34 2θ . The MANN-

compact showed either reduced or increased intensities at different peaks such as at 20, 34 and 36 2θ , and a change in the peak shape at 16.5°. The compacts with SORB exhibited the less changes, like the change in the peaks shape at 16.5 and 20 2θ .

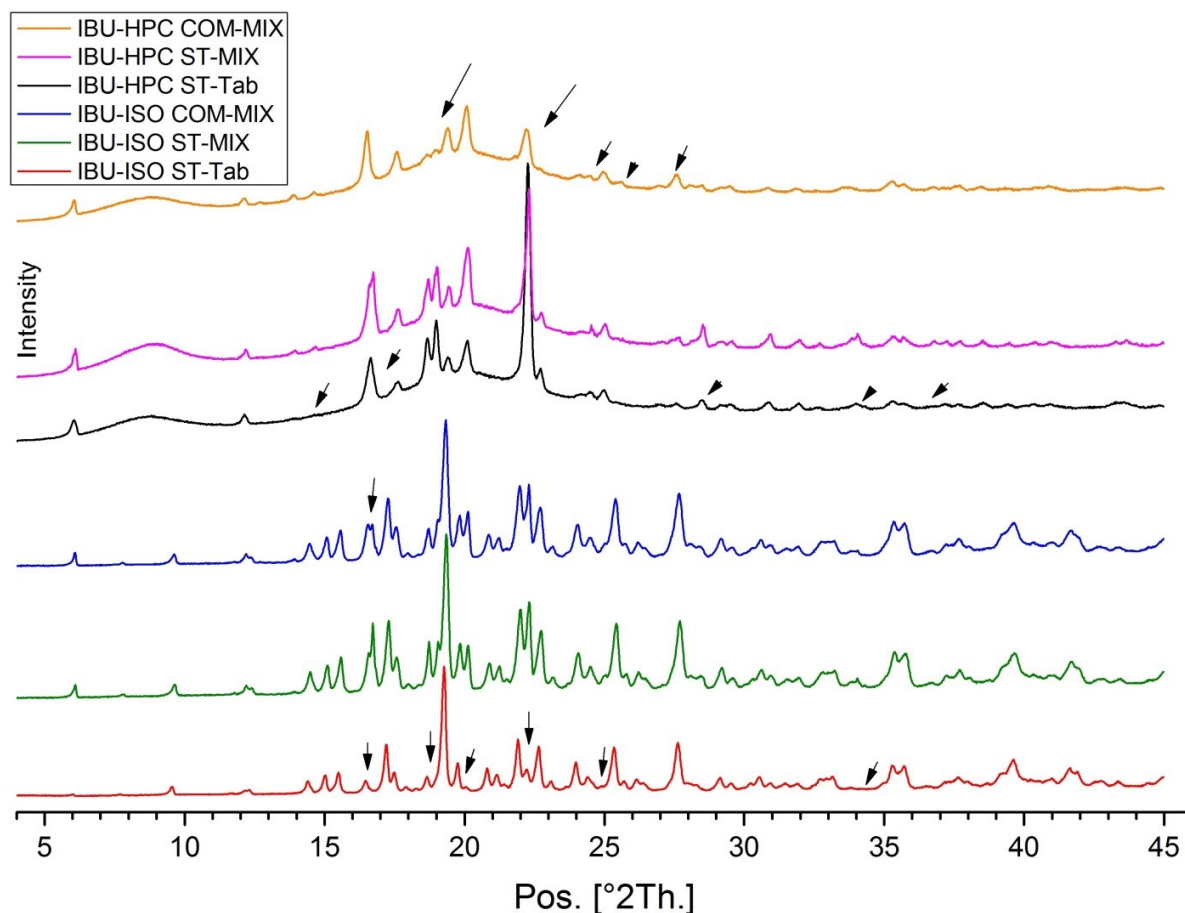


Figure 12 X-ray Diffractogram of standard tablets and milled mixtures as compared to ST-Mix: IBU-HPC, IBU-ISO

Moreover, higher degrees of peak changes were even observed due to co-milling process and the diffraction peaks broadened due to the crystallite size reduction.

The highest impact of the co-milling process was with HPC, resulting in a pronounced decrease in intensity of the most peaks such as at 18, 19 and 22 2θ , a different shape at 24, 27, 28 2θ ; a disappearance of the peaks at 32.5 and 34 2θ , and the new peak appeared at 25.5°. Moreover, a partial loss in crystallinity was calculated for IBU with a lower overall intensity of IBU peaks. An amorphous form of IBU (around 38%) was induced. The absence of some diffraction peaks as well as the appearance of more halo regions indicates the presence of the amorphous form. The co-milling impact was also evident with SORB and MANN (Figure 13), resulting in a different shape of some peaks and different intensities. The influence

was less expressed with ISO, which was reflected in the defect of the peak shape at $16.5\ 2\theta$ and in some differences in the intensities.

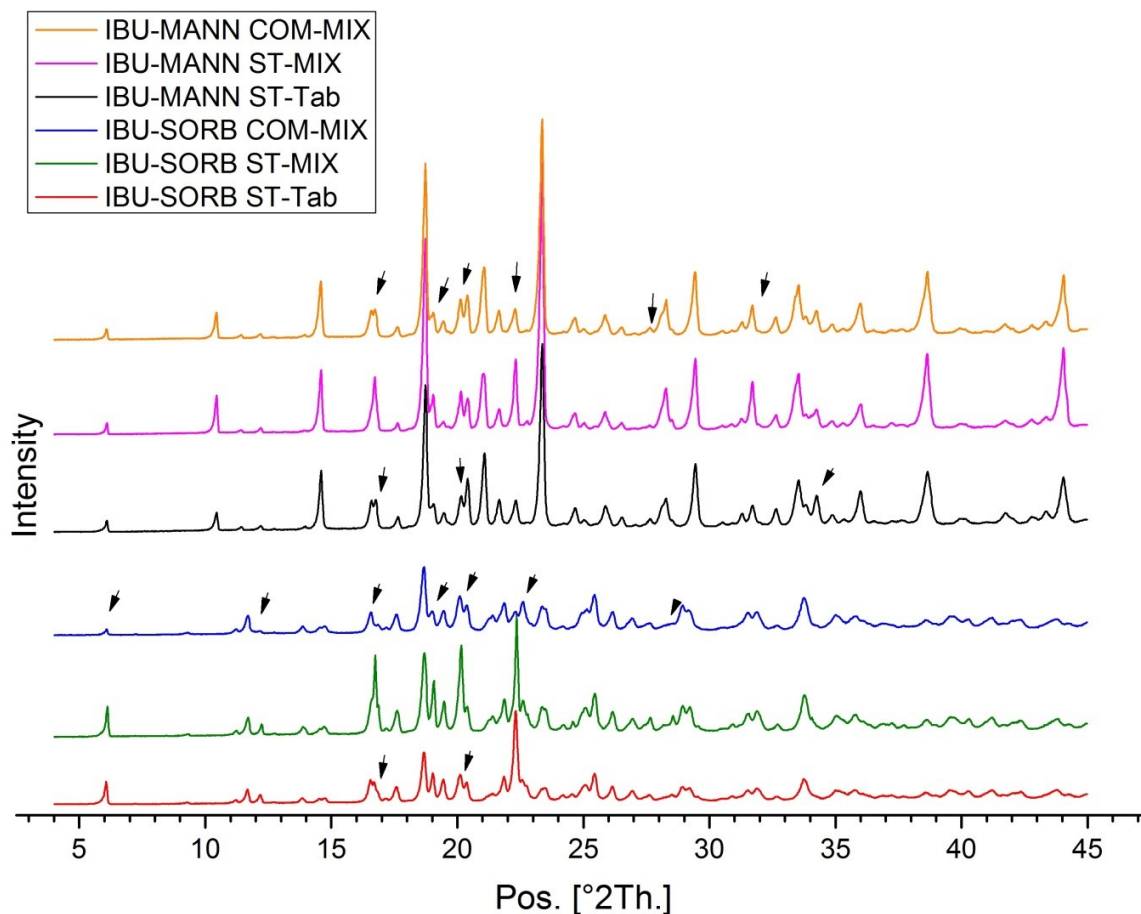


Figure 13 XRPD patterns of standard tablets and milled mixtures as compared to ST-Mix: IBU-MANN, IBU-SORB

The compaction process, in turn, after the co-milling triggered a crystal change to some extent (Figure 14). Additional changes were observed in the peak intensity of some peaks of ISO COM-compact when compared to the corresponding co-milled mixture, in addition to some minor changes in the peak shapes at 16.5 , 20 , $22\ 2\theta$. The COM-compacts of MANN and SORB also exhibited the same trend, with a changed shape of the peaks at 17 , $20\ 2\theta$ and at $20\ 2\theta$ respectively.

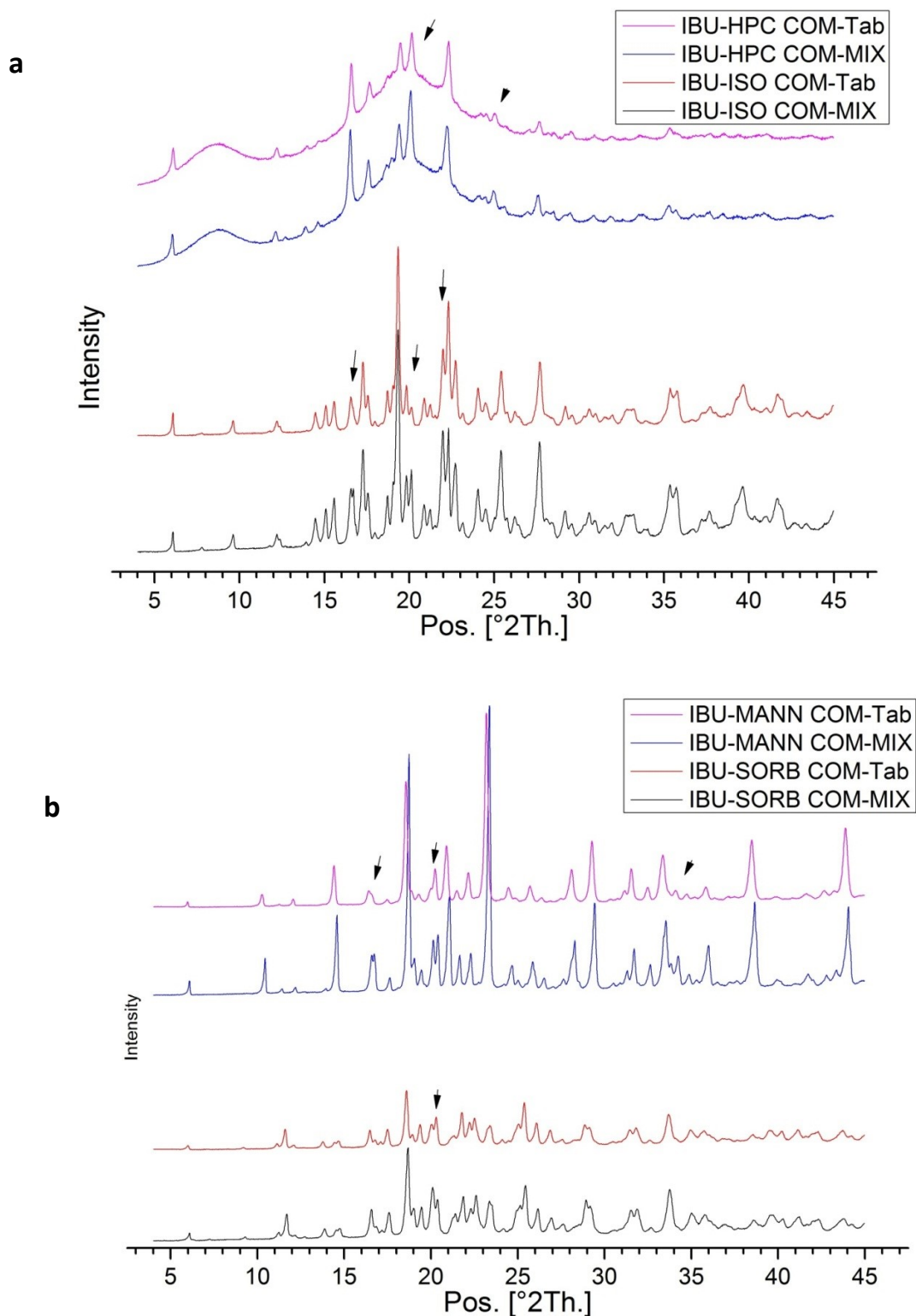


Figure 14 X-ray Diffractogram of co-milled tablets as compared to milled mixture: a) IBU-HPC, IBU-ISO, b) IBU-MANN, IBU-SORB

Table 9 Crystallinity determination of HPC-SSL formulations

Formulation	Sum of net intensity (cts)	Crystalline IBU%
IBU-HPC ST-MIX	1332606	100
IBU-HPC ST-Tab	1347465	100
IBU-HPC COM-MIX	811802	62
IBU-HPC COM-Tab	726002	55

4.2.4.2 Differential scanning calorimetry DSC of IBU-formulations

Table 10 Content of crystalline IBU, onset of melting peaks for all compacts and corresponding mixtures by DSC measurement

Sample	Melting onset temperature °C (MIX)	IBU load% (Crystalline) (MIX)	Melting onset temperature °C (Tab)	IBU load% (Crystalline) (Tab)
IBU-HPC ST	70.49 ± 0.89	20.20 ± 1.98	65.24 ± 0.61	19.02 ± 0.81
IBU-HPC COM	44.89 ± 0.18	06.24 ± 0.63	43.99 ± 1.30	05.43 ± 0.82
IBU-ISO ST	75.40 ± 0.09	21.55 ± 1.90	74.01 ± 0.28	21.96 ± 1.22
IBU-ISO COM	75.15 ± 0.09	20.43 ± 2.01	73.90 ± 0.17	20.97 ± 0.03
IBU-MANN ST	75.33 ± 0.51	20.25 ± 1.26	74.50 ± 0.05	21.64 ± 0.80
IBU-MANN COM	75.02 ± 0.03	22.17 ± 1.94	72.91 ± 0.18	20.26 ± 1.65
IBU-SORB ST	75.00 ± 0.28	21.83 ± 1.16	74.37 ± 0.12	18.05 ± 1.81
IBU-SORB COM	74.94 ± 0.01	21.40 ± 1.95	73.28 ± 0.13	20.87 ± 0.76
Pure IBU	75.64 ± 0.06			

IBU exhibited a sharp distinct melting point with the onset at 75.64 °C. It also revealed a glass transition temperature **T_g** at circa -46.34 °C.

No melting point **T_m** was found in the DSC thermogram of the pure HPC. The absence of a melting peak confirmed the amorphous characteristics of the polymer. The first heating run showed a broad endotherm ranging from 50 to 110 °C, which was ascribed to the loss of residual water from the hygroscopic polymer upon heating.

Neat isomalt, mannitol and sorbitol showed an endothermic peak at 161.6, 169 and 103.3 °C, respectively that related to their melting points. Isomalt contains two water molecules in the inner crystal structure. The thermal analysis of isomalt revealed a broad endotherm peak around 90 °C due to the dehydration process of glucopyranosyl mannitol-bihydrate. Nevertheless, the measurements of IBU thermal parameters within the ISO-formulations could be performed. The high energy $\Delta H = 72.76 \text{ Jg}^{-1}$ accompanying the dehydration process of ISO suggests strong interactions between the inner water molecules and the plenty of hydroxyl groups existing in isomalt.

As compared to the neat IBU, all physical mixtures other than HPC-mixtures showed essentially a similar melting onset around 75 °C; however, there were smaller due to the sample's dilution, indicating no significant physical interactions upon blending process. The IBU-HPC ST-Mix showed a relatively sharp peak, corresponding to the melting endotherm of IBU, shifted to a lower temperature at 70 °C (onset), in addition to the measured T_g around -4.8 °C that is at a lower temperature than that of HPC.

The co-milled mixtures showed a depression in the melting onset. Additionally, a lower ΔH_m was measured for IBU-HPC COM-MIX.

DSC thermograms of all ST- and co-milled compacts displayed the existence of the IBU melting peak indicating the presence of the crystalline IBU. However, some differences were noticed in T_m of IBU for the compacts as compared to the corresponding mixtures (Table 11, Appendix; Figure 63 to Figure 66). The melting endotherm was not as sharp as observed for related mixtures (particularly with HPC) and the T_m onset decreased to 65.24 - 74.5 °C. The ST- and COM-Tablets of IBU-HPC showed a glass transition in the first heating at -9.1 and -15.8 °C respectively.

The crystallinity for the compacts and related mixtures was calculated based on the measured ΔH_m° 104.4 ± 3.9 J/g for 100% load of the crystalline IBU (see 8.2.6.2). Except for IBU-HPC COM, similar values of enthalpy of fusion were obtained for all formulations (Table 10), suggesting no pronounced change in crystallinity during the compaction or co-milling processes. The calculated IBU load for the mixtures and compacts ≈ 20%, was assigned to the initial drug load. Approximately, the IBU residual crystallinity was 5.4 and 6.2% for IBU-HPC COM-compacts and mixture respectively.

Table 11 The reduction in the onset of T_m for the compacts as compared to the related mixtures and pure IBU

Sample	Reduction in T _m onset (°C) Tab / Mix	Reduction in T _m onset (°C) Tab / pure IBU
IBU-HPC ST	5.25	10.40
IBU-HPC COM	0.90	31.65
IBU-ISO ST	1.39	1.63
IBU-ISO COM	1.25	1.74
IBU-MANN ST	0.83	1.14
IBU-MANN COM	2.11	2.73
IBU-SORB ST	0.63	1.27
IBU-SORB COM	1.66	2.36

Statistically, all compacts showed a significant reduction of the T_m onset as compared to pure IBU (Table 11), except for MANN and SORB ST-Tabs. The T_m onset depression of IBU was significantly higher for HPC

ST- and COM-compacts than for the other compacts. IBU-HPC and IBU-ISO ST-compacts differed significantly from their related mixtures, whereas no significant differences were obtained between IBU-SORB, IBU-MANN ST-compacts and their corresponding mixtures; this observation was however inverted for the co-milled compacts.

After the cooling run and upon the reheating run, all tested samples exhibited no melting endothermic peak, erasing the initial crystallinity. Upon rapid cooling, no time was available for IBU to develop a significant crystalline component and recover its original crystallinity. Mannitol formulations only, revealed an exothermic peak due to the cold recrystallization process in the second heating run. Anyways, the comparison of the enthalpies associated with cold crystallization and the following melting indicated no initially presence of IBU crystalline structure after the cooling step. All samples showed, however, a single T_g in the reheating run, which refers to the formation of single-phase amorphous systems.

The cellulose with a high molecular weight is usually characterized with a low T_g [116], HPC showed a phase transition at 28.27 °C. For IBU-HPC formulations, the DSC experiments revealed a single glass transition upon second heating with no melting peak suggesting the formation of one phase system [17], with a depression of T_g of HPC.

As compared to ST-mixtures, the ST-compacts with HPC showed lower values of T_g in the first heating run accompanied with a higher ΔC_p that could refer to a higher IBU/HPC interaction of upon compaction and thus a higher depression of HPC T_g.

The T_g of HPC-compacts has increased over the low T_g of pure IBU (-46.34°C). Increasing of T_g might refer to a lower molecular mobility for IBU within the compacts.

Gordon-Taylor equation (Eq. 2) was applied to calculate the theoretical T_{g,mix} of IBU-HPC glass solution, based on T_g, the mass fraction W, and the quotient K of changes in the heat capacity (ΔC_p) at T_g of both components ΔC_{p2}/ ΔC_{p1}.

$$T_{g_{mix}} = W_1 T_{g1} + K W_2 T_{g2} / W_1 + K W_2 \quad \text{Eq. 2}$$

A theoretical T_g value of -13.51 °C was obtained for the IBU-HPC glass solution. The experimental T_g of the IBU-HPC formulations was -10.285 °C determined from the second heating run, which was close to the theoretical estimation.

In the first heating run, IBU-HPC COM-Tab showed a Tg around -15.8 °C. Residual moisture of 2.513% was measured for these compacts.

Taking this amount into consideration and assuming the homogenous distribution of moisture, the theoretical calculation for a Tg glass solution of ternary components (IBU, HPC and water) was performed applying Flory-Fox equation (Eq. 3).

$$1/Tg_{I,II} = W_I/Tg_I + W_{II}/Tg_{II} \quad \text{Eq. 3}$$

where Tg_{i, ii} is the Tg of the ternary mixture, Tg_I is the Tg of the IBU-HPC glass solution (second heating) and Tg_{II} is the Tg of water (135 K) [117], w_I and w_{II} are the weight fractions of the IBU-HPC mixture and water, respectively. A value of -16.4 °C was theoretically calculated for the Tg of the IBU/HPC/water homogeneous amorphous ternary mixture.

As compared to the related co-milled mixtures, the IBU-HPC COM-compacts showed slightly higher values of ΔCp at the first heating Tg (0.3255 to 0.2997 Jg⁻¹K⁻¹).

4.2.5 Compacts morphology of IBU-formulations SEM

The surface of the tablets was optically smooth, massed and homogeneous.

The shape of the particles was also explored prior to compaction, all ingredients' shape can be seen in the images of ST-mixtures (Figure 16). The neat IBU showed needle-like rods, with an acicular morphology form. HPC-SSL has a roundish-particle shape, whereas isomalt appeared as spherical agglomerates with rough surfaces. Mannitol appeared as dense rounded crystalline agglomerates with smooth surfaces and sorbitol showed a crystalline granules form.

The morphological transformations of pure ingredients were visible within the formulated compacts at the ×100 magnification (Figure 15, SE images). In general, all compacts' surfaces appeared comparable as a smooth condensed flat bulk, but only at a very high magnification, slight abrasions of some tested compacts could be seen, like IBU-ISO and IBU-MANN ST-compacts. Ibuprofen particles became fairly fine with stiff surfaces. The COM-compacts demonstrated generally smoother surfaces in comparison to the compacts prepared without co-milling. The compacts exhibited almost one homogenous phase (especially HPC-compacts), showing a melted-like appearance, which could refer to some changes of the IBU crystalline form.

No particle boundaries could be detected on SEM-COMP images obtained by BSE detector and discrete phases of the two ingredients could be hardly recognized (Figure 15). This was more evident regarding

the COM-formulations, emphasizing the additional impact of the co-milling process to generate a new morphology. However, the images of IBU-SORB ST-Tab revealed that the two ingredients could be still distinguished (Figure 15, d) and identified. Some particles of magnesium stearate could generally be seen adhering to the compacts surface.

IBU-HPC compacts were different as compared to the compacts prepared with other excipients. The deformation degree was more intensive (Figure 15. a, e). The particles appeared to sinter forming a smooth glossy surface, which might indicate to some extent of crystals fusion or plastical deformation of the particles at the surface, which was in direct contact with the punches during the compaction, as a result of the provided mechanical energy.

As compared to the related ST-Tab, IBU-HPC COM-compacts showed more homogenous areas, where the surface appearance changed from white opaque to partially translucent.

Furthermore, the compacts were gently broken apart to monitor the cross-sections, trying to avoid extra shear forces that can cause additional crystal defects.

Generally, the physical mixtures showed needle-like rods distributed between roundish particles, agglomerates, or granules in respect of the excipient used. After compaction, this turned into less spherical particles and more random shapes; no original agglomerates or granules could be monitored anymore. The cross-sections illustrated different irregular morphologies of both ingredients, comprising of particles with rough surfaces sticking together to form bigger masses (Figure 16). The images revealed an inhomogeneous particle size and shape, an unorganized reticulated mass. The IBU network looked to be resulted from sintering of the ingredients crystals during processing.

The analysis indicated a decrease in the particle size upon compaction. The images revealed non-porous nature of the inner structure with accumulations of crystals defects in the bulk.

The IBU-HPC compacts possessed a particulate structure, characterized by a concrete-like multi stacked layers. The consistence of IBU-HPC COM-Tab showed sharp edges of sticking particles. The co-milled samples showed distinctly fewer areas of discernible particles.

While ST-mixtures had a quite regular shape as shown at higher magnification, the COM-mixtures revealed a significant reduction of particles size. Their particles were very fine and irregular and some broken particles reassembled to form bigger ones.

4. Influence of high-pressure compaction on ibuprofen binary mixtures

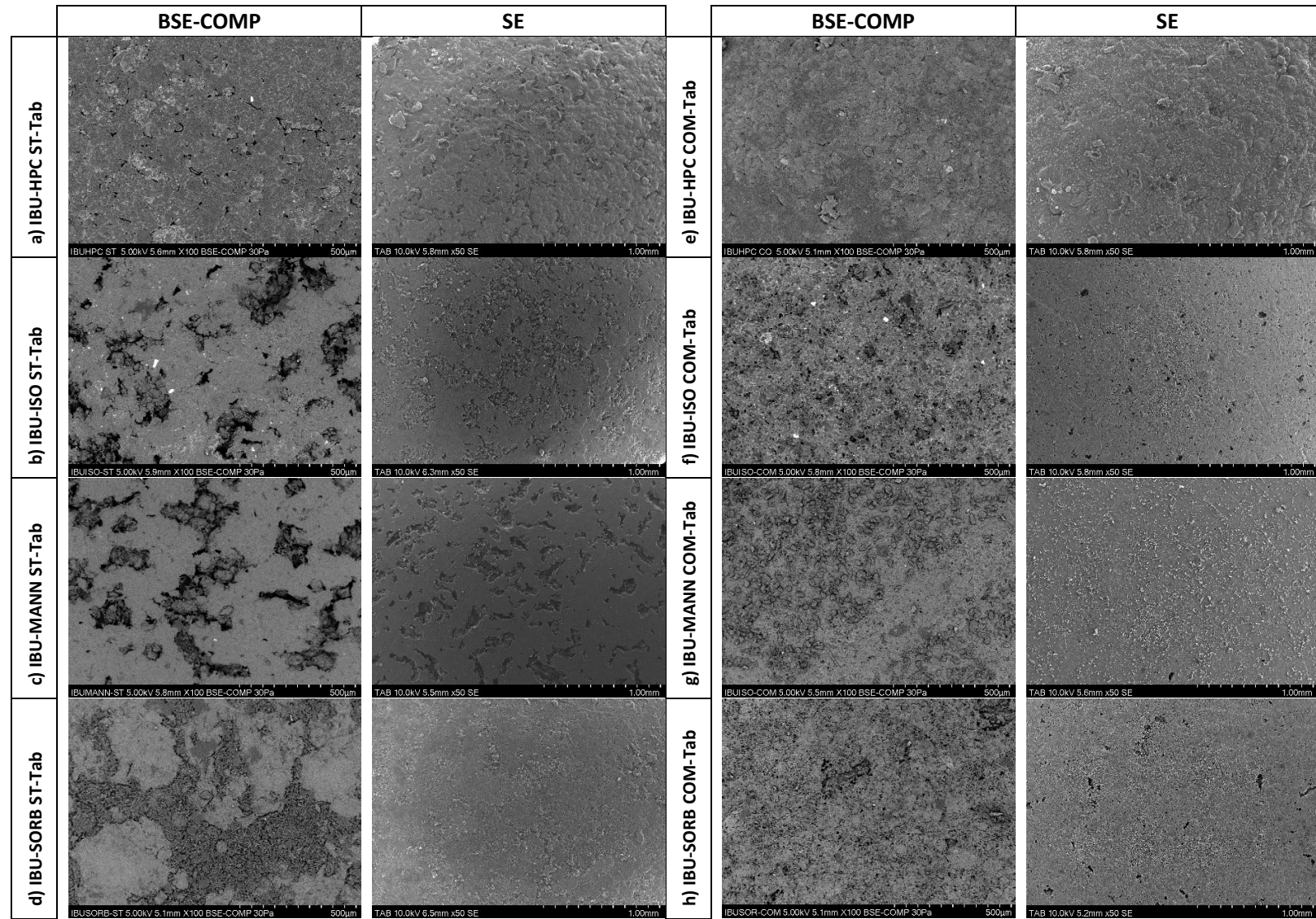


Figure 15 SEM micrographs of compacts surface BSE-COMP obtained by BSE detector (x100 resolution) as well as surface images by SE detector (x50 resolution)

4. Influence of high-pressure compaction on ibuprofen binary mixtures

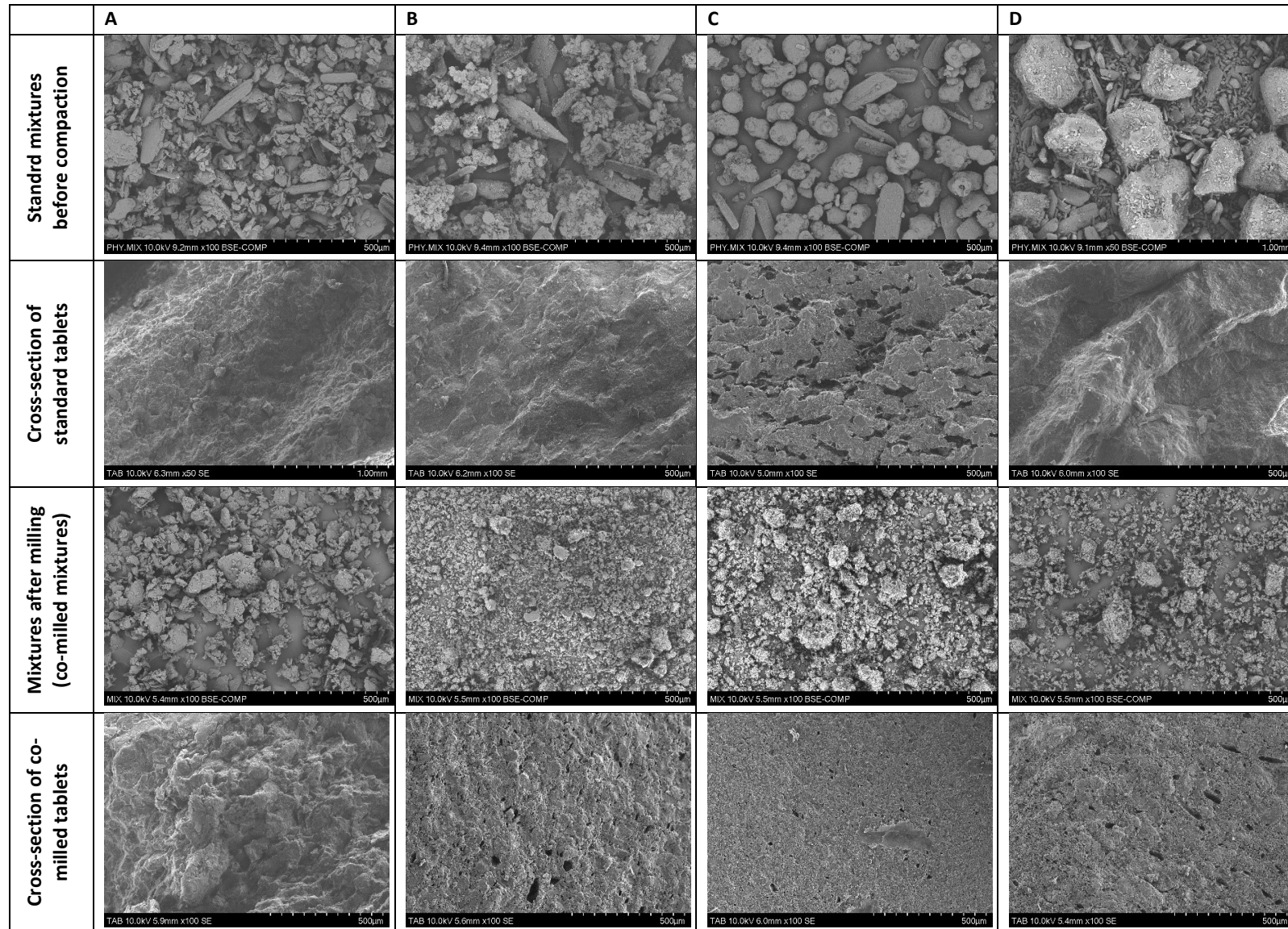


Figure 16 SEM photographs of mixtures and cross-sections of A: IBU-HPC, B: IBU-SO, C: IBU-MANN, D: IBU-SORB. From top to bottom: ST-mixtures, cross-sections of ST- compacts, COM-mixtures, cross-section of COM-compacts

4.2.6 The influence of amorphous form: Melt quenched IBU (IBU-MQ)

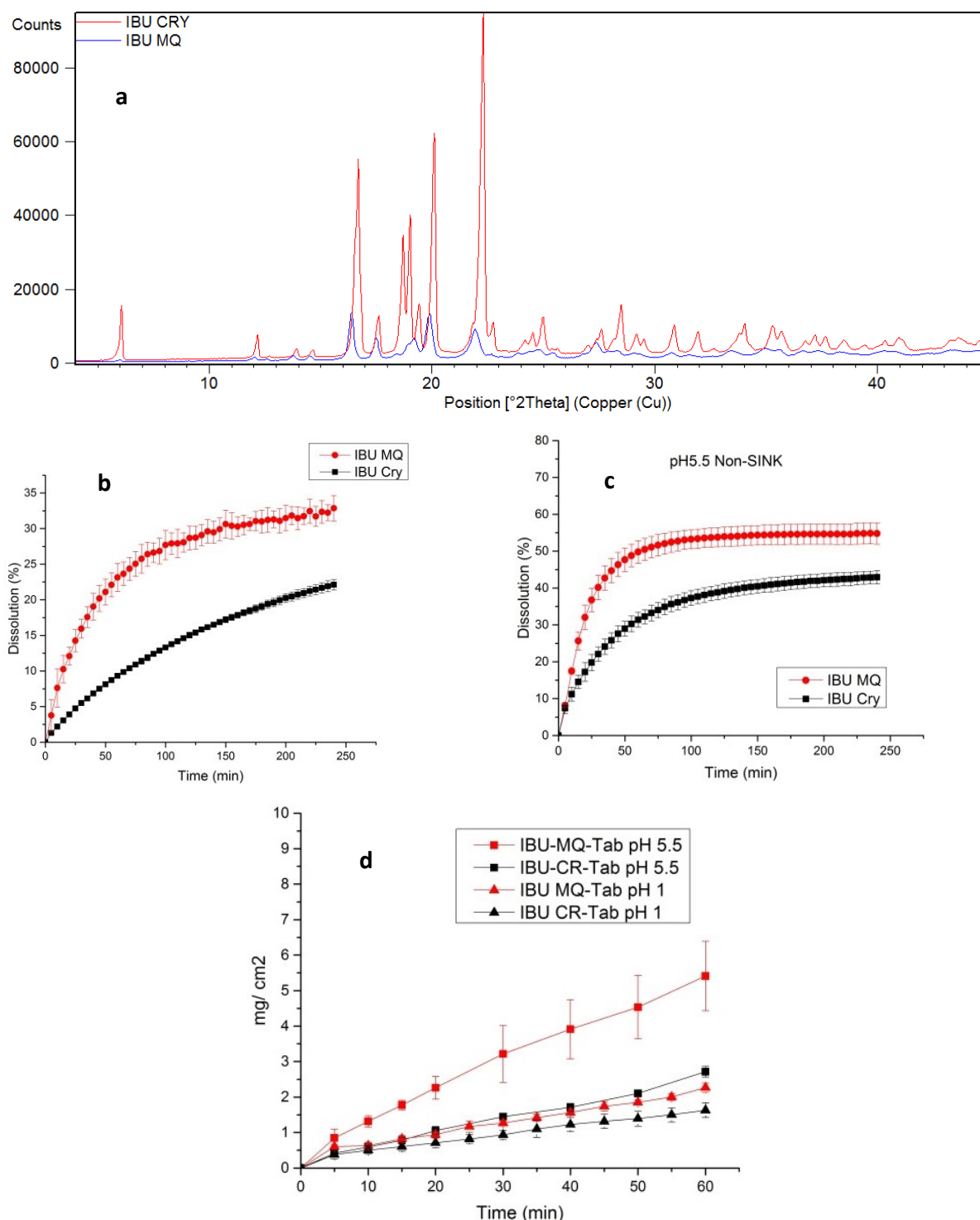


Figure 17 (a) X-ray Diffractogram of melt quenched IBU, release profiles of both forms at pH 1.0 (b) and at pH 5.5 (c) in non-sink condition, (d) IDR of IBU-MQ compared to crystalline form. Trials were performed in 900 ml at 37 ± 0.5 °C (100 rpm, USP. Apparatus 1), mean value \pm SD (n=3)

A reduction in the IBU total crystallinity could be observed by XRPD measurement due to the melt quenching process, beside the polymorphic transformation of the ibuprofen solid-state (Figure 17, a). As compared to the neat crystalline IBU, the IBU-MQ spectrum revealed, in general, less defined and broader peaks with lower intensities, like the three peaks between 18 and 19 Theta, confirming the presence of an amorphous component. Some diffracted peaks almost vanished in the range of 28 to 45 Theta, like the peaks at 28, 31, 32 and 34°.

Approximately, 68% of amorphousness was calculated for the melt-quenched IBU by applying the same determination procedure as described in 8.2.6.1.

The increase degree in the solubility and drug release by conversion of 68% of IBU to an amorphous material was determined. The IDR testing of the melt quenched IBU was performed at pH 1.0 and pH 5.5 (Figure 17, d). The IDR of IBU-MQ was 1.3 and 2.2 folds higher than that of the crystalline IBU at pH 1.0 and pH 5.5 respectively, which can be attributed to the 68% amorphization. The increase in IDR was more significant at pH 5.5. Moreover, the increase of the release rate was more obvious for IBU-MQ as compared to the crystalline IBU during the drug release test of free powders at non-sink condition in both media (Figure 17, b and c).

4.2.6.1 Saturation solubility of IBU-MQ

The equilibrium solubility of IBU-MQ was determined using the traditional shake flask method at pH 1.0, pH 5.5 media and compared to that of the crystalline IBU. The results indicated that IBU-MQ had an improved aqueous solubility at pH 1.0 and pH 5.5 by 1.55 and 1.3 times respectively (Table 12). These improvement degrees differed relatively from that predicted for 68% amorphous IBU (1.97 folds), with respect to the theoretical enhancement estimation for 100% amorphous IBU of 2.9 and 2.2 folds at 25 and 37 °C, respectively, as described further in 4.2.8.

Interestingly, IBU-MQ compacts showed an improved IDR by 1.3 times as to IBU crystalline at pH 1.0, this was close to the theoretical estimation of 68% amorphous IBU at 37 °C (1.5).

Based on XRPD data, the IBU-HPC COM-Tab contained 45% amorphous material. The predicted improvements of solubility, achieved upon a 55% reduction in the crystallinity, were 1.3 and 1.1 times at 25 and 37 °C respectively. These values matched the experimental benefit on the solubility achieved by IBU-HPC COM-Tab as compared to the corresponding ST-Tab (1.1 times).

No influence of the melt quenching process was obtained on the kinetic and intrinsic solubilities measured by CheqSol method. Since the assay starts where API is totally ionized and dissolved, the properties related to the processing history will be blinded and eliminated.

Table 12 Experimental and predicted solubility ratios for IBU-MQ as to crystalline IBU and for IBU-HPC COM-Tab as to ST-Tab

Sample	Theoretical estimation ^a		Experimental			
	Shake flask 25°C	Shake flask 37°C	Shake flask pH 1.0	Shake flask pH 5.5	IDR pH 1.0	IDR pH 5.5
IBU-MQ (68% A)	1.97	1.5	1.55	1.3	1.3	2.2
IBU-HPC COM-Tab (45% A)/ ST-Tab	1.3	1.1	1.1	1.1	1.9	1.5

^a based on (Parks and Hoffman), A: amorphous

In addition to amorphous form, the processing of melt quenching induced a marked decrease in the particle size of IBU (Figure 18). d_{50} was reduced by melt quenching to a half value as that of the crystalline IBU. The following values of IBU-MQ were recorded for d_{10} , d_{50} , d_{90} and span respectively: 3.56 ± 0.31 , 22.98 ± 1.19 , 61.83 ± 1.09 and 2.54 ± 0.10 as compared to that of IBU: 10.06 ± 1.83 , 50.98 ± 1.01 , 119.29 ± 3.86 and 2.14 ± 0.00 .

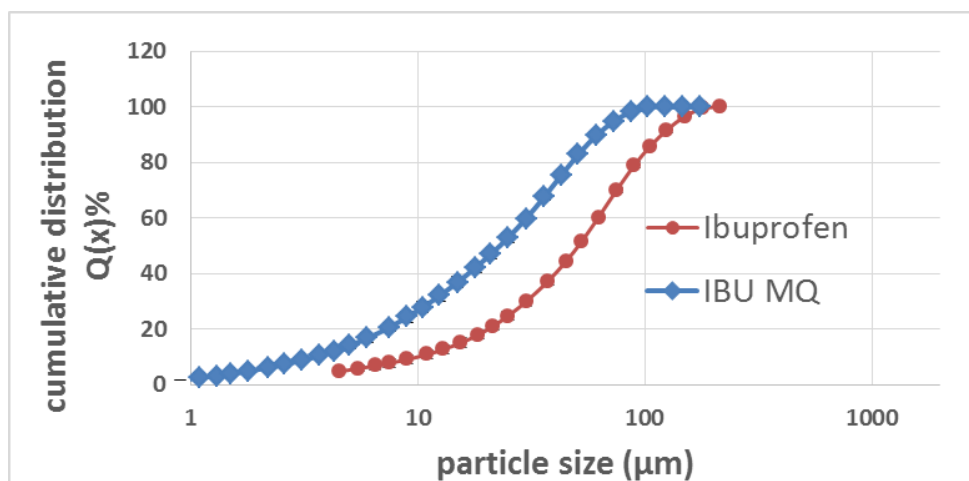


Figure 18 Particle size distributions of the crystalline IBU and IBU-MQ

4.2.7 Stability studies of IBU-HPC COM-Tab

The presence of polymorphism may promote phase transformations, which could be critical for the dosage form performance upon storage. Due to the amorphous content, the focus was on IBU-HPC COM-compacts, which were subsequently subjected to accelerated stability conditions at 40 ± 2 °C/ 75%

RH \pm 5% for 4 months, where the samples were kept in opened containers and analyzed by XRPD. In addition, samples were stored for six months at room temperature RT and analyzed.

Table 13 XRPD solid-state of IBU-HPC COM-Tab as Initial, after accelerated stability studies for 16 weeks and after 6 months storage at RT

Composition (%)	XRPD Initial	40°C, 75% r.h., 4 weeks	40°C, 75% r.h., 8 weeks	40°C, 75% r.h., 16 weeks	RT, ambient r.h., 6 months
IBU-HPC COM-Tab	55% crystallinity	41%	39%	38%	49%

The tablets showed no significant change in the crystallinity after 6 months of storage at RT and ambient conditions (Table 13) and the difference measured is rather within the method's analytical error. For the accelerated stability studies, the compacts did not reveal any significant differences in their XRPD diffractograms after 4, 8 and 16 weeks (Figure 19). However, a decrease in the crystallinity was observed. The first measurement after 4 weeks indicated a minor decrease in the crystallinity to 41% that corresponds to the higher amount of amorphous form of IBU. No extra reduction was further observed.

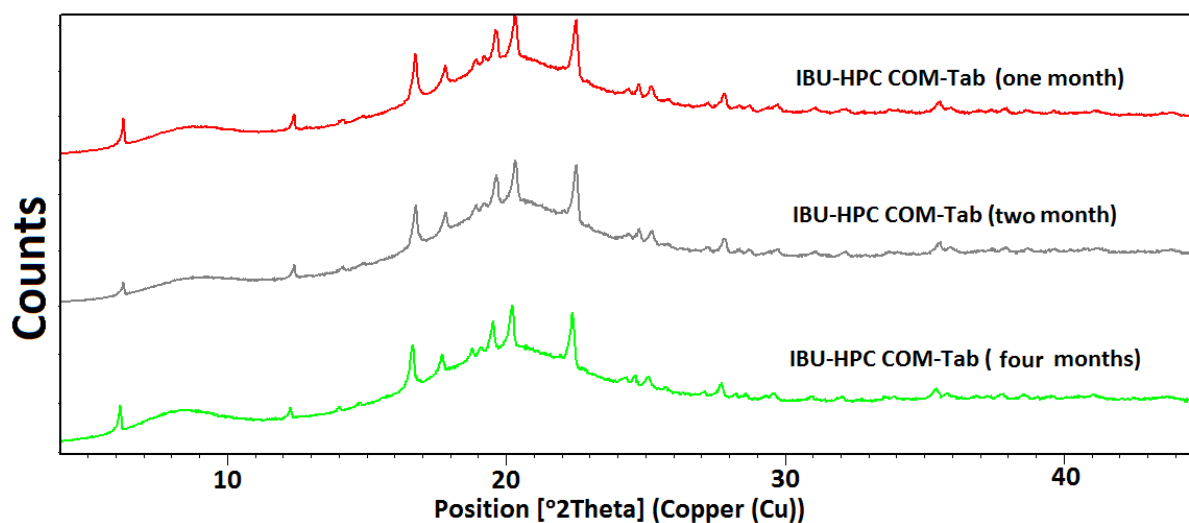


Figure 19 X-ray Diffractogram of IBU-HPC COM-Tab upon storage during the accelerated stability study

4.2.8 Theoretical estimation of aqueous solubility improvement for IBU-MQ and IBU-compacts

The application of data from DSC measurements and equations (Eq. 8 and Eq. 9) estimated approximately 2.9 folds solubility of the amorphous IBU to that of the crystalline IBU at 25 °C in purified water. This value, however, decreased to 2.2 folds at 37 °C. Based on the equilibrium solubility of 0.0303 mg/ml in pH 1.0 at 25 °C for the crystalline IBU as seen by the shake flask method, an aqueous solubility of amorphous IBU is

predicted to be 0.08787 mg/ml. Hence, an improvement degree of 1.97 folds for the IBU-MQ could be predicted.

On the other hand, the theoretical maximum increase of the solubility for the metastable forms S_0^m as to crystalline IBU S_0^c was estimated to be from 1.04 to 7 folds at 25 °C and from 1.04 to 4.5 folds at 37 °C, based on the approach proposed by Hancock and Parks (see section 8.2.4, Eq. 10 and Eq. 11) .

The prediction of solubility ratios for the compacts to the crystalline IBU are summarized in Table 14.

The experimentally determined thermal properties that were used for the calculations are: $T_g = -46.34$ °C with $\Delta C_p T_g = 0.305$ J/gK for IBU, and T_m^c for the different IBU induced forms as listed in Table 10. Since DSC measurements showed no change in the degree of crystallinity except for IBU-HPC COM-Tab, thus, ΔH_f^c was considered to be constant (104.4 J/g) for all compacts and the value of 28.37 J/g was applied for IBU-HPC COM-compacts that has a partial amorphization. In addition, the difference of capacity ($\Delta C_p T_g$) between the glassy and equilibrium super-cooled liquid form for IBU was obtained at T_g and also used for the solubility predictions.

The predicted increase of solubility for the different compacts varied from 1.03 to 7 folds of the crystalline IBU solubility, depending on the applied ΔC_p values ($\Delta C_p=0$, $\Delta C_p=\Delta S_f$, $\Delta C_p=\Delta C_p$ at T_g). In general, the experimental solubility ratios revealed relatively higher values than the predicted ones in both media. The predicted solubility ratios of IBU-HPC compacts showed, as experimentally, the same trend, having the higher ratios compared to other excipients-compacts. For IBU-HPC ST-Tab, the measured solubility ratio was in an acceptable agreement with the predicted values.

Only IBU-HPC COM-compacts showed a lower measured ratio than the predicted value.

Table 14 Experimental and predicted solubility ratios for induced polymorphs as to crystalline IBU

Formulations	forms	^a Predicted solubility ratio 25 °C	Experimental solubility ratio pH 1.0	Experimental solubility ratio pH 5.5	^a Predicted solubility ratio 37 °C
IBU-HPC ST-Tab	IBU-compact / crystal	1.4-1.49	1.36	1.48	1.42-1.49
IBU-HPC COM-Tab	IBU-compact / crystal	5.9-7	1.45	1.54	4.2-4.6
IBU-ISO ST-Tab	IBU-compact / crystal	1.05-1.06	1.22	1.39	1.05-1.06
IBU-ISO COM-Tab	IBU-compact / crystal	1.06-1.07	1.21	1.29	1.06-1.07
IBU-MANN ST-Tab	IBU-compact / crystal	1.03-1.04	1.17	1.21	1.03-1.04
IBU-MANN COM-Tab	IBU-compact / crystal	1.09-1.11	1.19	1.26	1.09-1.11
IBU-SORB ST-Tab	IBU-compact / crystal	1.04-1.05	1.12	1.03	1.04-1.05
IBU-SORB COM-Tab	IBU-compact / crystal	1.08-1.09	1.17	1.26	1.08-1.09

^a The reported range of values is related to different ΔC_p values applied for the calculations

The predicted solubility ratios decreased as the temperature increased. The impact of applying different ΔC_p approximations was small on the prediction at the applied temperatures, as both temperatures are close and above T_g . The approximation $\Delta C_p = \Delta S_f$ produced an intermediate prediction independent of the temperature applied.

4.3 Discussion

As expected, varied IDR values were observed depending on pH values of the media (Table 6), whereby higher values were in connection with higher pH. The IDR of IBU increased out of the formulations from 5 to 36 folds and from 5 to 88 folds at pH 1.0 and pH 5.5 respectively. These observations confirmed that, the examination of compaction process effects can be facilitated by IDR testing over the pH range of gastrointestinal tract [118]. No deviation from linearity could be observed within the IDR profiles, indicating that no superficial transformation of IBU occurred into another polymorph of different solubility [79] and referring to an acceptable stability of the compaction-induced forms over a reasonable period. The IDR of compacts prepared from the co-milled mixtures was, in general, higher than that of the related ST-Tabs. IBU-ISO ST-Tabs were the only exception, showing higher IDR than the co-milled tablets with 14 and 49 fold at pH 1.0 and pH 5.5 respectively. This was in line with previous studies that reported the same observation and it was attributed to the decrease in preferred orientation degree of hydrophilic facets upon milling [73,75]. The varied relative intensities of some XRPD peaks for ST-compacts as compared to the related mixtures may be attributed to the preferred orientation (texturization) of crystallographic planes after compaction. This observation was more noticeable for IBU-ISO ST-Tab (Figure 12). Upon compression, the crystallites would strongly tend to be orientated more one way than all others with specific facets aligning preferably along the surface of the sample. Moreover, this texturization decreased when the tablets are prepared from milled materials. Hence, the ST-compacts are expected to be associated with a higher texturization as compared to the COM-compacts. For a highly texturized sample, only specific crystal planes are expected to be represented on the tablet surface. Accordingly, IBU-ISO ST-Tab might be characterized with a higher texturization and more abundance of crystal planes that are rich with polar OH groups on the surface of compacts. The IBU-ISO ST-compacts showed more pronounced changes to the co-milled compacts in XRPD analysis, such as the higher intensity of XRPD peak at 20° . Thus, the preferred orientation of polar faces as well as the partial production of metastable form seemed to have a dominant impact than the milling-induced lattice defects on the IDR and solubility for IBU-ISO compacts. In addition, the co-milling process can reveal both hydrophobic and hydrophilic groups on the surface depending on the original crystal shapes. This can also clarify the uneven

performance for co-milled compacts as to ST-ones. However, the IDR values of co-milled compacts still varied, indicating to the dominant impact of different crystal energetics for these compacts.

As XRPD and DSC data indicated, different dissolution behaviours might correlate to the induced polymorphism (most likely to a partial extent) or to the different physicochemical properties of different exposed crystal faces on the compacts surfaces and their ability to build hydrophilic interactions with the dissolution medium. The new generated physicochemical properties were obvious for the HPC-compacts and to a less extent for MANN and SORB-compacts. The variation found among the ST-compacts can be also related to different crystal habits and hydrophilic facets involved in the dissolution process after compression [73]. Generally, a less increase was obtained regarding the IDR, non-sink dissolution rates and solubility values for IBU-MANN and IBU-SORB ST-compacts, without significant differences between both formulations. The less increase in IDR can be explained by a less strength of contribution of these additive molecules to introduce a high level of impurity defects and associated dislocations within the crystal lattice of IBU as that exhibited with ISO and indicated by XRPD and DSC data. Since the tablets were prepared out of different isotropic crystals, therefore the surface energies of the induced planes can differ, thus possessing different dissolution kinetics [90].

The considerable increase in the drug release values for HPC compacts correlated with the higher level of crystal modifications and IBU/HPC interactions. By forming one condensed unit with HPC as referred by SEM images, the contact area of IBU with the dissolution medium increases. In addition, the proposed technique can enable the dispersibility of IBU as very fine particles within the hydrophilic matrix that leads to a better wettability.

The dissolution profile at non-sink condition confirmed the influence of high-pressure compaction to produce a faster drug release as compared to the related ST-mixtures. This was observed to different extents according to the compressed excipient and the pH of dissolution medium, which underlines the role of used excipient in the proposed approach applied. In general, a higher increase of the dissolution rate was obtained in the acidic medium and with HPC and ISO as excipients. The compaction after co-milling produced additional benefits for IBU-HPC COM-granules by increasing the level of supersaturation state and maintaining it for a longer period (50min) compared to 20min for the co-milled mixture. For the co-milled mixtures, the particle size effect seemed to be more dominant than the compaction impact, especially during the initial minutes leading to a faster release than the granules. However, the endpoint

of dissolution was higher for the granules referring to a higher solubility reached, except for MANN and SORB granules at pH 1.0.

The HPC behavior upon dissolution should also be considered by evaluating the superior release for HPC-compacts. HPC can induce hydrophilic hydration due to HPC/water H-bonding [106]. Hence, the HPC solutions are characterized with strong H-bonds. This penetration of HPC-molecules can aid the inclusion of the interacted IBU-molecules into the cavities of the water structure, facilitating the dissolution step of IBU.

The comparison of dissolution profiles for granules with the IDR profiles of the compacts revealed the same order. However, the dissolution profiles were generally similar for MANN and SORB granules (ST and COM) in both media. The IBU release out of ISO-granules was not close to that out of HPC-compacts at pH 5.5, as seen and expected based on the IDR test. Nonetheless, the release for the first 10-15 minutes was much comparable for both formulations, before any great change of granules size has been occurred. As soon as the first 20 minutes had passed, the release of IBU from HPC-granules accelerated. Due to the low T_g of HPC, the water can easily plasticize the polymer, increasing its flexibility and molecular mobility to make more space. IBU molecules are then facilitated to be dissolved within HPC chains, forming H-bonds with the polymer and assisting the diffusion of the dispersed drug molecules into the medium. The dissolution studies indicated that, IDR testing can be applied as an indication and forecasting tool for the drug release that simply discriminate between formulations, at least for the first phase of release.

Since IBU is a pH-dependent drug, the extent of solubility is likely be affected as the drug passes through the gastrointestinal tract upon oral administration [119]. The compacts had mostly a higher magnitude of the solubility increase as compared to the related mixtures at pH 5.5 than at pH 1.0, which might indicate a higher influence of the process in the medium, where IBU exists partially in an ionized form. The same effect was observed from the IDR test.

Interestingly, the formulations impact on the equilibrium solubility measured after 7 days and the dynamic value of the IDR measured during 60 min, led to the same rank order. Plotting SF against the IDR, even revealed a linear relationship (Figure 11). The extent of increment was obviously higher for IDR values than the solubility as compared to pure IBU, referring to a higher impact of the proposed approach on dissolution than on solubility.

No obvious impact of the compaction process was found on solubility in case of IBU-SORB ST-compacts. The solubility values obtained might be underestimated, in particular, the saturated solubility of IBU from

MANN- and SORB-formulations. The possibility of transformation to the IBU stable crystalline form during the long equilibrium period of 7 days cannot be excluded. The measured increase of solubility for IBU-HPC COM-compacts was lower than predicted, which might be caused also by a change in the phase over 7 days, which could be mediated by the dissolution and supersaturation state of IBU in the aqueous medium. Hancock and Parks also stated that the magnitude of solubility increase for indomethacin amorphous forms was experimentally much lower than predicted, as compared to the crystalline counterparts[42].

Due to the relatively small differences in the free energy between IBU within the compacts and crystalline IBU, the magnitudes of predicted advantages on solubility were generally low. However, the measured solubility factors were in an acceptable agreement with the predicted values, showing the same tendency regarding the HPC-formulations and the co-milled compacts as to ST-compacts, other than ISO-compacts. Although the experimentally determined results might shift from the predicted possible improvements, the application of Hancock and Parks approach is still a good indication of the in-vitro solubility for amorphous- or metastable forms.

Moreover, since the solubility for compacts after one week did not reveal returning to the IBU thermodynamic solubility. Hence, the induced IBU forms achieved a long-term of supersaturation, which might provide a sufficient time for the dissolved drug molecules to be absorbed under in vivo conditions

Additionally, the solubility values obtained of all compacts increased approx. 12-15 times from pH 1.0 to pH 5.5 (consistent with the solubility increase of pure IBU= 14 times), whereas the IDR results did not reflect the same magnitude, showing a less multiplication ratio (2 to 12 times). This was not compatible with other studies, that presented a similar trend of the solubility and IDR values' increase at different defined pH values [64,76]. Despite the good correlation obtained between the IDR and solubility values, yet some discrepancies may still exist between the IDR test and the solubility method [76]. Yu *et al.* pointed to some inconsistencies existing when drugs have either extremely low or higher doses [64]. A low pressure has been mostly used in those studies to prepare IDR disks (a range of 2 to 34 MPa), which might lead to an overestimation of IDR values. In that context, the current research indicated that a certain pressure is necessary to obtain high-dense disks, minimizing the interference of porosity on the outcomes. Besides, two IDR values were reported (0.1 and 1 mg/min/cm²) [64,76], under which the drug is considered as insoluble and belongs to BCS I or II. This disagreement in the literature regarding the IDR watershed value, may also lead to some muddle. IDR is a rate phenomenon, while the shake flask method relates to the equilibrium state. Hence, the IDR application is presumed to offer higher correlations to in

vivo dynamic of the dissolution [79]. It can help monitoring any transformation, offering solubility determination before the occurrence of any changes. For all points mentioned, the difference in the magnification ratio (pH 5.5/pH 1.0) observed between IDR and solubility values cannot be considered as unusual.

A correct determination of solubility by the shake flask method can be affected by many experimental variations (see section 3.1.4). Various employed protocols were reported, which was reflected in a notable diversity of the published data [79,112,120]. It was reported that, the sparingly soluble drugs need to be stirred or shaken for longer time to reach equilibrium [120]. Shaking for 24 h to 7 days was reported [112]. The IBU solubility obtained after shaking for 7 days at pH 1.0 was much close to the measured intrinsic solubility from CheqSol findings, which was expected since the intrinsic solubility refers to the values where IBU is fully neutral. This agreement promoted to shake for this long period in order to ensure reaching equilibrium solubility. The estimated solubility from CheqSol at pH 5.5 was also comparable to the value obtained from shake flask method after 7 days.

The kinetic solubility, which refers to the maximum reached solubility and indicates to the extent of supersaturation achieved by the system [113], was higher than the intrinsic solubility value. This confirms that IBU can undergo a certain degree of supersaturation, before it starts to precipitate and chase the equilibrium. Hence, IBU can be considered as a Chaser [112].

The carried-out DSC analysis indicated that, the thermal properties of IBU did not drastically change upon physically blending with the sugar-alcohols; suggesting no significant interactions. On the contrary, some changes were observed in the compacts' thermograms. Further investigation suggested some differences in the IBU melting profile. Similar values of the enthalpy of fusion were obtained for all formulations except for IBU-HPC COM, suggesting no alternation of the overall crystallinity during compaction or co-milling processes. However, the transformations of the solid form, even partially, could not however be excluded. The shift in the melting point towards a lower temperature might indicate the presence of new forms of IBU, as compared to the more stable crystalline IBU. This depression of the onset melting can also suggest higher IBU/excipients interactions induced [47]. These higher interactions would act similarly to an impurity, showing fronting of the melt endotherm; subsequently, an earlier onset temperature. Romero *et al.* also reported some changes in IBU thermal properties, observed by tableting or grinding of the physical mixture and were attributed to higher intermolecular interactions after compression [39].

The greatest melting point depression was particularly detected with HPC, whereby less strength of depression was connected to MANN and SORB ST-compacts. However, the tense of reduction in the melting onset for standard compacts was in the following order: IBU-HPC > IBU-ISO > IBU-MANN > IBU-SORB, which is in agreement with IDR data exhibiting the similar trend (Table 6 and Table 11).

Besides, the co-milled formulations showed, in general lower melting onsets than ST-formulations referring to a higher level of crystal defects or IBU/excipient interactions. This was more remarkable for COM-compacts of MANN and SORB as compared to the related ST-compacts but less noticed for ISO COM-compacts. The differences in the thermal properties were generally small for sugar-alcohols compacts, suggesting a partial polymorphic transition.

Various changes were observed either in the intensity or the shape of some IBU prominent peaks in the diffraction pattern for the compacts when compared to the corresponding ST-Mixtures; other IBU peaks disappeared. Hence, IBU appeared to undergo some sort of crystal modification in the tablets, especially for HPC-compacts, whose changes in peaks deflection by XRPD were more obvious [39]. However, the diffraction patterns and DSC thermograms of IBU induced within the compacts did not correspond to the metastable form of racemic ibuprofen identified by Dudognon and colleagues 2008.

The variation in the relative intensity of some characteristic peaks, including small angles, may be attributed to either crystals size reduction or to crystal habit modification; as the relative abundance of planes exposed to X-ray beam are different, or could be related to the preferred orientation of crystallographic planes upon compaction [73,75,87,121]. These changes are connected with different hydrophilicities or molecular groups exposed on the surface and thus different ionization degree or connected with higher crystal energetics (i.e. defects and/or solvation [77]) as new forms of IBU were induced, which can explain the higher IDR values obtained as compared to neat IBU. The involvement of these aspects would differ according to the crystal behavior under compaction and co-milling. However, the presence of unchanged original IBU peaks suggested only partial modifications of the crystals, most likely on the surface.

The different IDR values, possessed by tested tablets, indicated different crystal planes, or surfaces associated with different energy. The induced partial amorphization is most likely the main factor responsible for the obtained IDR improvement in case of IBU-HPC COM-Tab, whereas the high-induced energy and the mechanical activation, due to high level of crystal defects and disorder, could describe the higher IDR and solubility of COM-Tabs of IBU-MANN and IBU-SORB as compared to their ST-compacts.

The IDR of poorly soluble and limited dissolved drugs will be affected by the preferred orientation to a bigger extent. However, the presence of polymorphic or pseudo-polymorphic forms or amorphous form might obscure this effect of texture [75], which can explain higher values of IDR for co-milled compacts of HPC, MANN and SORB.

Considering that XRPD peak width correlates with the material particle size [122], the diffractograms of COM-mixtures presented accordingly less sharp peaks as compared to their ST-mixtures, this was less observed in case of ISO-compacts. Beside the less crystallinity revealed by IBU-HPC COM-Tab, alterations in some peaks shape might confirm the change in the crystal form. In the literature, higher amorphization was seen in samples with higher drug-polymer interactions [71], thus, it might be concluded that higher IBU-HPC interactions were triggered upon co-milling.

The induced amorphization for IBU-HPC COM-formulations most likely resulted from the dispersion of IBU molecules into the amorphous HPC. The physical stabilization of the resulting amorphous mixture and IBU/HPC-interactions may have a thermodynamic origin, where the IBU dispersed into HPC is below the solubility limit at room temperature at a 1:4 ratio IBU:HPC so that IBU and HPC form a stable amorphous molecular alloy at room temperature. This was indicated by the observation of no change in the amorphous content after 6 months of storage at ambient conditions.

Furthermore, the compacts of co-milled IBU-HPC did not reveal a significant variation in peak intensities and shapes when compared to co-milled mixture, which might indicate to less effect of high-pressure compaction on milled mixtures regarding crystal modification, in particular that contain an amorphous form. The partial loss in crystallinity of IBU-HPC was mainly caused by co-milling, which is compatible with previous study of HPC [50] and, to a rather negligible extent, by high-pressure compaction.

The higher reduction of T_m onset for IBU-HPC mixtures and tablets was probably related to the partial molecular dispersion/ dissolution of IBU into the HPC matrix upon heating in DSC that could lead to an "eutectic impurity" of IBU. As an amorphous substance and having low T_g, HPC possesses a high molecular mobility and plasticity and can cause API melting point depression. However, the T_m onset for the tablets was still lower than the corresponding mixtures referring to higher IBU/HPC interactions within the tablets and to the effect of the process applied. Additionally, the co-milled IBU-HPC COM mixture revealed obviously a lower melting point than ST-mixture, indicating also to higher IBU/HPC interactions and/or to a new metastable form of IBU induced by co-milling. This supports the polymorphic transition in IBU as suggested by XRPD.

The integration of the melting points for IBU-HPC COM-formulations confirmed the partial decrease in crystallinity degree. DSC findings evidenced that a metastable state with higher energy could be formed due to IBU and HPC interactions. The higher intermolecular hydrogen bonding between IBU and HPC in addition to the less mobility of IBU, as it was entrapped in polymer matrix upon compaction and co-milling, may be responsible for this conversion. However, the lower calculated crystallinity by DSC as compared to XRPD estimation might be related to the intense contact, interactions and the dissolution of induced metastable IBU into the HPC matrix upon heating in DSC that could lead to a fractional conversion of IBU, which interfered with heat of fusion obtained, taking the low T_g of HPC into account. The same tendency was reported for co-milled sample of ketoprofen with PVA [71].

The decrease of the HPC T_g for IBU-HPC formulations upon second heating might be resulting from destroying the H-bonding of HPC molecules, causing weaker HPC intermolecular interactions [116].

Applying the Gordon-Taylor equation can help inspecting the possible plasticizing effect of one component on another and the homogeneity of the compacts. The application of this equation assumes no interactions existing between the drug and the polymer. The theoretical T_g value of a homogeneous amorphous blend is proposed to be between the two T_g s of the single pure amorphous components. The single T_g , revealed by IBU-HPC formulations during the reheating run, referred to a one homogenous amorphous phase. However, the deviation of this value from the theoretical calculated $T_{g_{mix}}$ can relate to interactions presenting between IBU and HPC [83].

The T_g of IBU-HPC COM-Tab from the first heating was between the T_g s of neat IBU and HPC and might be attributed to the formation of an amorphous phase resulting from the co-milling step [123]. The T_g was, however, lower as compared to the water-free homogeneous glass solution of IBU-HPC obtained from the second heating run (-10.285 °C), which could be explained by the residual water content within the formulation. As mentioned before, the hygroscopic feature of neat HPC was obvious from DSC thermogram of the first heating run. Due to the moisture uptake of HPC during the preparation of the compacts, a depression in T_g may be observed via the plasticization effect of water.

The theoretical estimated T_g of the IBU/HPC/water ternary mixture $T_{g_{I,II}}$ and the experimental T_g of IBU-HPC COM-Tab were matching, which confirmed that the measured T_g is ascribed to the formation of a ternary amorphous phase of IBU, HPC with the residual moisture [123].

The higher ΔC_p of IBU-HPC COM-compacts to the related co-milled mixture indicated some increasing of the IBU-HPC glass solution component (a higher fraction of amorphous IBU) upon compaction [124]. The disappearance of the T_g of pure HPC might indicate that all amount of HPC was involved to form the IBU-HPC glass solution system. ΔC_p values were proportionally correlated to the amorphous amount of IBU in the sample. A comparison of $\Delta C_p = 0.3255 \text{ Jg}^{-1}\text{K}^{-1}$ for T_g of the COM-compacts with ΔC_p for the IBU-HPC fully amorphous glass solution ($\Delta C_p = 0.4515 \text{ Jg}^{-1}\text{K}^{-1}$) suggested the conversion of approx. 72% (w/w) of IBU into an amorphous phase with HPC, which correlates to 5.6% of the residual crystalline IBU. These findings were along with the findings from the melting-based DSC analysis (Table 10).

The magnitude of changes observed in XRPD for the ST-compacts was in the following rank order: IBU-HPC > IBU-ISO > IBU-MANN > IBU-SORB. Depending on the changes observed by both XRPD and DSC, a change in IBU crystal habit for MANN- and SORB-compacts may be concluded rather than a change in the internal structure that was speculated for HPC- and ISO-compacts. However, ibuprofen remained crystalline upon compacting with HPC and upon compacting or co-milling with ISO, MANN and SORB. All mentioned observations out of XRPD and DSC go along with IDR data of the compacts and confirm the employment of IDR testing to have better understanding of relationships between dissolution rate and the solid crystalline form.

Depending on the used excipient and type of processing (with or without co-milling), high-pressure compaction seems to be able to generate destabilization, rearrangement and fragilization of IBU intermolecular interactions, and trigger new IBU/excipient interactions, leading to varied arrangements between the molecules i.e. packing polymorphism, where the molecules possess quasi the same conformation [91]. The change is then, how the molecules in the crystals are packed based on the new interactions formed between the components. The new formed hydrophilic network could be the assistant factor for the drug dissolution.

Some APIs like ibuprofen does not display plastic deformation, which makes the formation of a compact difficult [125]. Based on XRPD and SEM analysis as well as the melt-like appearance on the surface, the application of high-pressure and in combination with a hydrophilic excipient seemed to promote the occurrence of a partial fusion of particles at the surface. Besides, it would promote a plastic flow of deformation of the crystals throughout the compact, generating a migration of lattice defects through all layers, followed by emerging of the defects and disappearing at the crystal faces. Consequently, the

nature and the concentration of crystal defects can affect IDR values, which explain the different IDR values obtained.

The properties of the crystal entity are affected by crystal morphology [89]. SEM analysis showed differences in the morphology within the compacts surfaces that revealed a kind of deformation. The original external appearance of ingredients was changed and varied within the compacts used for IDR experiments. These observations correlated with the crystal modification suggested by XRPD and DSC analysis. This was more obvious with IBU-HPC compacts; where the melted-like appearance confirmed the change of the IBU crystalline form and referred that most original crystalline IBU and polymer particles had disappeared in favor of the dispersed integrating matrix.

Upon compaction, enough mechanical energy was available to generate sintering of crystals of the two adjacent ingredients shell. The co-milling process induced even an additional deformation. The COM-compacts exhibited visible homogeneous areas. The partially translucent appearance of IBU-HPC COM-compacts is most likely representing the created amorphous form in case of IBU-HPC COM-Tab.

The increased strength of interparticulate bonding, besides, the possible increase of local temperature at the contact level above T_m of IBU (78 °C), may induce a fusion of particles at surface and decrease in void spaces, which could be the reason of the new morphological characteristics. A possible crystal disruption and lattice rearrangement for IBU due to the compaction was also suggested previously [39].

In addition, the SEM images of cross-sections showed packs of IBU-excipient networks with a homogeneous concrete-like structure, confirming the morphological changes triggered. The compaction induced apparently single component regions that assembled together with deformed edges. The images referred to a homogenous application of pressure throughout the compact, thus, the texturization of inner regions is expected to be as much as that on the surface. The images indicated a crystal lattice fragilization of each ingredient; the particle boundaries were not obvious anymore. Upon milling, a further intense crystal disruption appeared. SEM analysis referred that compaction can also operate in reducing the particle size, producing compacts with a low porosity.

The differences observed by XRPD, DSC and SEM suggested certain changes in the crystalline form during compaction, which might have been strongly occurred at the compacts surface. The exhibited changes were in respect with the untreated materials properties and the induced IBU/excipient interactions. The IBU

release data were generally consistent with the measured decreases in T_m (onset) induced and corresponded well with increases in the concentrations of crystal defects as seen by SEM.

The results confirmed the impact of high-pressure compaction to modify certain characteristics of raw ingredients in a way that can determine the overall performance of the final dosage form.

Based on the data of IBU-MQ, a higher significant impact of the IBU amorphous part (68%) could be seen at pH 5.5; which was in line with IDR data obtained with IBU-HPC COM-Tab that confirms this hypothesis. The increase in IDR value for IBU-MQ as to the crystalline IBU was consistent with dissolution profiles obtained from free powders at non-sink condition. However, the magnitude of the increase in IDR was not as high as observed from free powders dissolution for the first 40 minutes, especially at pH 1.0. This can be explained by two factors: the smaller size of IBU-MQ particles (Figure 18) and the variable compressibility under high-pressure. The compressibility of amorphous material is higher, resulting in lower porosity of tablets, which may cause a lower dissolution rate [66].

The IDR of IBU-HPC COM-Tab was 36 and 88 folds that of IBU-Tab at pH 1.0 and pH 5.5 respectively. The amorphous portion of IBU could not merely explain this increase, based on the values of IBU-MQ. However, a significantly higher impact on solubility and dissolution is expected to be obtained for amorphous systems with HPC than for neat amorphous substances. In this context, API in ASD systems proved to show additional improvement on dissolution rates as compared to the free amorphous form of drug [83]. The solubilizing effect of HPC, the crystal modification's degree as well as proven IBU/HPC higher interactions should be considered.

On the other hand, the estimated increase in solubility and IDR for IBU-HPC COM-Tab (corresponding to 45% amorphous) to IBU-HPC ST-Tab, based on the measurement of IBU-MQ (corresponding to 68% amorphous), matched to big magnitude the experimental values, other than IDR values at pH 1.0. This might indicate that the contribution of IBU amorphous portion would not be able to cover and explain the whole increase of 1.9 folds of IDR at pH 1.0.

The estimated solubility for IBU-MQ using the described model (Parks and Hoffman) seemed to fit more at pH where the drug is unionized and to describe the IDR values. Besides, the conversion possibility of amorphous IBU of IBU-MQ to the more stable crystalline IBU during shaking for a long period might be responsible for measuring lower values of the aqueous solubility as predicted.

In relation to co-milled IBU-HPC, the amorphous forms are associated thermodynamically with a higher disorder of molecules and hence, a higher Gibb's free energy. Thus, these forms are unstable and may experience recrystallization into the poorly-soluble crystalline forms.

The ability of polymer carriers with high molecular weights, such as PVP and HPMC, was reported to kinetically stabilize the amorphous state by interacting with API, thus inhibiting the recrystallization process, in addition to the solubilization effect on API into the polymeric matrix. The presence of HPC enhanced the dissolution profiles of IBU and moreover, prevented the recrystallization, as no changes in the diffraction peaks were observed by XRPD for IBU-HPC COM-Tab upon storing at room temperature. This confirmed the stabilizing ability of HPC on IBU amorphous form.

Usually, the milling-produced forces, including Van der Waals, electrostatic forces or inter-particulate cohesive, stimulate the particles agglomeration [23], especially for very fine particles $\leq 30 \mu\text{m}$. However, the co-milling with HPC would physically hinder this trend of agglomeration by adsorbing onto IBU particles surfaces, providing certain coverage. This produces a higher steric stabilization. Simultaneously, the strong IBU-HPC interactions, via Van der Waals forces or H-bonding, would protect the activated status of IBU and obstruct the recrystallization.

At higher relative humidity, the absorbed water might act as plasticizer, causing a reduction of Tg of HPC. The reduction in Tg would enable the polymer chains to solubilize and surround IBU, inhibiting the recrystallization process [47] and increasing the dissolved amorphous part. This might explain the reduction of crystallinity upon accelerating stability study. The decrease of the polymer viscosity can also contribute facilitating the dissolution of drug within the polymer chains [83]. .

Moreover, IBU-HPC COM-granules exhibited a maintenance of the supersaturation state for IBU over 50min at pH 1. Previous studies showed the ability of HPC to inhibit the precipitation for a reasonable period increasing the chemical stability [49,51–53]. The ability to maintain supersaturation state was explained by either inhibition of drug aggregation as a result of drug/carrier interaction, or the influence of viscosity because of the polymer that obstruct the crystallization.

Sugar-alcohols were also reported to maintain the chemical stability because of the abundance of their polyhydroxy and hence, their strong formed hydrogen bonding [60]. In general, the resultant high IBU/excipient interactions would assure kinetically the stabilization of IBU dispersed within the induced crystalline excipient-matrix, which reduce the tendency of any polymorphic transition.

4.4 Conclusion

High-pressure compaction of IBU with polyols, namely isomalt, improved the aqueous solubility and intrinsic dissolution rate significantly, without changing the crystalline state of IBU. In combination with the polymer HPC, the effect on solubility and dissolution was even more pronounced; however, with a high degree of IBU transformed into an amorphous state for the co-milled formulation. Based on the testing results of the melt quenched IBU, the amorphous portion could explain the noticeable increase in solubility and IDR of HPC co-milled tablets compared to the corresponding tablets without co-milling. In general, the magnitude of increase in solubility and IDR was carrier-dependent and did not necessarily require a co-milling step of the binary mixture prior to compaction.

The linearity obtained during IDR testing confirmed the phase stability of the solid state of the compacts, i.e. no change in polymorphs occurred. The enhanced solubility of IBU, based on the solubility determination data after shaking for 7 days, is expected to provide sufficient time for dissolved drug molecules to be absorbed under in vivo conditions. In addition, acceptable shelf-life stabilization was monitored of IBU in an amorphous state regarding HPC co-milled compacts.

The modified intrinsic dissolution apparatus was confirmed as a feasible and reliable procedure to measure IDR of the compacts prepared under high-pressure. The IDR test was verified as a primary parameter to assess the drug dissolution properties and evaluate the impact of different solid properties on the product performance. The testing could be applied as an indication and forecasts tool for the drug release at non-sink condition. This tool can simply discriminate between formulations, at least for the first phase of release.

XRPD and DSC analysis suggests changes in the internal crystal structure of IBU (probably to a partial extent) or in the external shape and/or increasing IBU/excipient interactions within the prepared compacts. XRPD and DSC findings were in line with IDR results. Higher magnitude of change was connected with higher IDR and solubility values.

The compacts from co-milled mixtures showed mostly higher degree of changes in XRPD as well as lower melting onsets in the DSC than that of related ST-compacts referring to a higher level of crystal defects. Hence, the high crystal energetics, associated with the co-milling process, could be the dominant effect on IDR in the case of co-milled compacts.

As has been concluded from IDR and solubility values, a higher impact of the process applied was observed at $\text{pH} > \text{pK}_a$ of IBU. Moreover, the overall effect of the tested approach was higher to increase the dissolution rates rather than the aqueous solubility, as compared to pure IBU.

The results of this chapter suggest screening high-pressure compaction as a means to potentially improve solubility and IDR in a roller compaction process. The combination with co-milling of the substrates prior to compaction should be evaluated carefully, as milling did not always improve solubility and IDR performance of IBU and posed a higher likelihood to facilitate the formation of an amorphous drug.

5 Influence of high-pressure compaction on wettability of ibuprofen compacts prepared employing nonfunctional excipients: the impact of pure excipient properties

5.1 Introduction

The high-pressure compaction of a binary mixture, consisting of a drug and a nonfunctional hydrophilic excipient, was proposed and introduced as a new technique to improve the solubility and dissolution rate of borderline insoluble drugs. The approach demonstrated an increase in the solubility and dissolution rate of ibuprofen especially with HPC-SSL and isomalt (chapter 4). Two potential impacts can be induced by this process on the physicochemical properties of API within the formulated product (3.2). In the previous chapter, the first impact of the proposed process was evaluated considering the ability to induce any crystal modification on the neat API.

The second potential impact relates to the manipulation of the overall tablet solid surface and its wettability. The drug's release rate can be increased by enhancing the drug wettability by aqueous systems (see section 3.2.2). Accordingly, the wetting properties of the prepared compacts (see Table 1) are assessed in this chapter. This is important because it might explain their improved dissolution rates and the supersaturation levels achieved.

For this purpose, the surface free energy SFE studies were primarily performed to investigate the contact between surfaces having different degree of polarity and to examine the effect of a change in the polarity induced by high-pressure compaction. In this context, the drug/excipient interactions were evaluated in terms of released free energy of the compacts surface, which can correlate to the strength of interaction with water.

A quantitative assessment of the water-compact interactions was done by wetting kinetics. This was done to investigate the specific relevant phase in the drug absorption, i.e., the wetting step, but not the mechanism of drug release. The produced compacts are then characterized with regard to wettability, density, porosity, and correlated with the manufacturing type (with or without a prior co-milling).

In the previous chapter, the level of induced crystal modification of IBU was found to be excipient-dependent. In addition to the influence of API properties on the created compact system, the dissolution rates of API out of a system can be affected by the properties of pure excipients [5,69,71]. The delivery of the drug from a formulation might be assisted or even controlled by the excipient's solubility as well as

the carrier's release [6]. Therefore, the influence of pure carrier properties should be assessed and estimated (3.1.2). In this chapter, the selected excipients (isomalt, mannitol, sorbitol and HPC) were also examined to inspect whether the produced compact-systems can be also considered as carrier-dependent in respect of wettability.

In this relation, the proposed approach may promote the dispersion of IBU into the excipient's network, which can increase the surface area of IBU, displaying similar phenomena to what observed in solid dispersions [126]. Upon a high level of dispersion and as the hydrophilic carrier starts to dissolve; the drug can simultaneously be released as very fine particles out of the compacts, having facilitated transportation to the medium. The employed hydrophilic carriers would assure an increased dispersibility besides hindering the aggregation of drug particles. This highlights the importance of excipient pure properties affecting the produced system.

IDR was successfully applied as an evaluation method of the prepared enabling formulations. However, there is a lack in specific information about the contribution of pure excipient's proportion dissolving in the medium on the overall dissolution rate of the dosage form. Therefore, the estimation of the carrier contribution in the overall dissolution performance is of great importance. To achieve this, the determination of IDR for pure excipients is needed, which can be complicated from analytical point of view. Thus, a new procedure was developed, which can be simply used to quantify the mass dissolved of pure excipients.

Several experimental parameters were investigated regarding the surface properties and wetting kinetics of the compacts, as well as the influence of pure individual excipient on the compacted composites. All the related variables, including the findings obtained in the previous chapter, were analyzed by principle component analysis (**PCA**) and correlated with IDR order of involved formulations.

In addition, two formulations of IBU-HPC and IBU-ISO were compacted under less pressure (200MPa) to identify the influence of the high-pressure on the solubility, IBU release rate and tablets wettability.

5.2 Results

5.2.1 Wetting studies of IBU-compacts

5.2.1.1 Surface free energy SFE & wetting kinetics of IBU-compacts

As compared to neat IBU, all compacts expressed generally a spreading wetting type; showing rather hydrophilic surfaces with respect to the lower contact angles measured with water, revealing significantly higher SFE with significant increases in the polar component. The very big contact angle of pure IBU-compacts indicated the poor wetting attribute as well as a hydrophobic character of the IBU molecules. Among compacts tested, IBU-ISO and IBU-HPC compacts showed significantly smaller contact angles and higher SFE compared to the IBU-MANN and IBU-SORB compacts (Table 15).

Generally, IBU-ISO ST-Tab possessed the highest total SFE among all formulations with significantly the highest value of the polar energy and the lowest dispersive component. However, the difference was only not significant with IBU-HPC COM-compacts ($p=0.054$).

Moreover, the calculated $\sigma_{sv}^p / \sigma_{sv}^d$ ratio referred to a remarkable trend toward the polar part in case of HPC and ISO-compacts.

The co-milled compacts showed higher values of the total SFE as compared with the related ST-compacts. Only ISO ST-compacts accompanied reversely with a higher energy than ISO COM-compacts. The co-milled compacts of sugar-alcohols showed an increase in the dispersive energy as compared to the corresponding standard compacts.

Table 15 SFE Components and values of Wa, Wi and Ws calculated for IBU compacts

Sample	¹ surface free energy mJ/m ²			P ₀ %	² Wetting kinetics J/m ²		
	total	dispersive	polar		Wa	Wi	Ws
IBU-HPC ST-Tab	66.33 ± 0.31	31.71 ± 0.46	34.62 ± 0.77	52.19	137.05	256.77	-8.67
IBU-HPC COM-Tab	68.00 ± 0.62	28.60 ± 0.48	39.40 ± 0.14	57.94	139.37	266.04	-6.35
IBU-ISO ST-Tab	70.41 ± 0.46	26.07 ± 0.67	44.34 ± 1.13	62.97	143.25	281.55	-2.47
IBU-ISO COM-Tab	65.60 ± 1.51	27.75 ± 0.33	37.85 ± 1.84	57.68	136.11	252.99	-9.61
IBU-MANN ST-Tab	52.47 ± 0.93	36.54 ± 0.34	15.93 ± 0.59	30.35	114.30	165.77	-31.42
IBU-MANN COM-Tab	58.95 ± 0.32	38.92 ± 1.19	20.03 ± 0.87	33.99	121.99	196.52	-23.73
IBU-SORB ST-Tab	47.54 ± 0.67	33.37 ± 0.14	14.17 ± 0.53	29.80	108.44	142.33	-37.28
IBU-SORB COM-Tab	50.20 ± 0.16	35.17 ± 0.34	15.03 ± 0.50	29.94	110.46	150.39	-35.26
IBU-CRY	40.45 ± 0.99	38.71 ± 0.29	1.74 ± 0.73	4.28	76.76	15.59	-68.96

¹ Water and Diiodomethane was used as probe liquids

² Water was used as probe liquid

All measured contact angles used for SFE calculation are summarized in Appendix; Table 55.

With respect to the SFE determination, the surface polarity P_0 of all compacts was estimated as the quotient of the polar component to the total SFE (Eq. 4). Polarity values ranging from 30 to 63% were calculated for the formulations, compared to 4% for pure IBU-compacts.

$$P_0 = \frac{\sigma_S^P}{\sigma_S} \times 100 \quad \text{Eq. 4}$$

Both IBU-ISO and IBU-HPC compacts showed a very high work of adhesion and the highest improvement of the immersion and spreading processes (Table 15). The highest values were considerably assigned to IBU-ISO ST-Tab. On the other hand, no significant differences were found in the work values between IBU-MANN and IBU-SORB-compacts, where both compacts connected with the lowest values. No statistical difference between the IBU-ISO ST and IBU-HPC compacts was indicated by ANOVA analysis.

5.2.1.2 Sorption behaviour of IBU-compacts

As demonstrated in Figure 20, IBU-ISO and IBU-HPC-compacts exhibited the smallest contact angles. The both compacts displayed the highest amount of absorbed water and proved to have significantly a faster initial rate of sorption (slope g/s) as compared to MANN and sorbitol-compacts separately.

IBU-ISO ST-Tab was superior to the others, whereas IBU-SORB tablets pointed the lowest sorption amount and biggest contact angles following the IBU-MANN formulations. On the contrary, IBU-SORB formulations showed the highest sorption of n-Hexan followed by IBU-MANN formulations. The contact angle of water was significantly higher on IBU-HPC ST-Tab (29.9°) than IBU-ISO ST-Tab (22.4°). However, the differences diminished upon co-milling process, in which the co-milled tablets of IBU-HPC and IBU-ISO showed a contact angle of 27.3° and 30.2° respectively. The measurement of pure IBU compacts was not applicable.

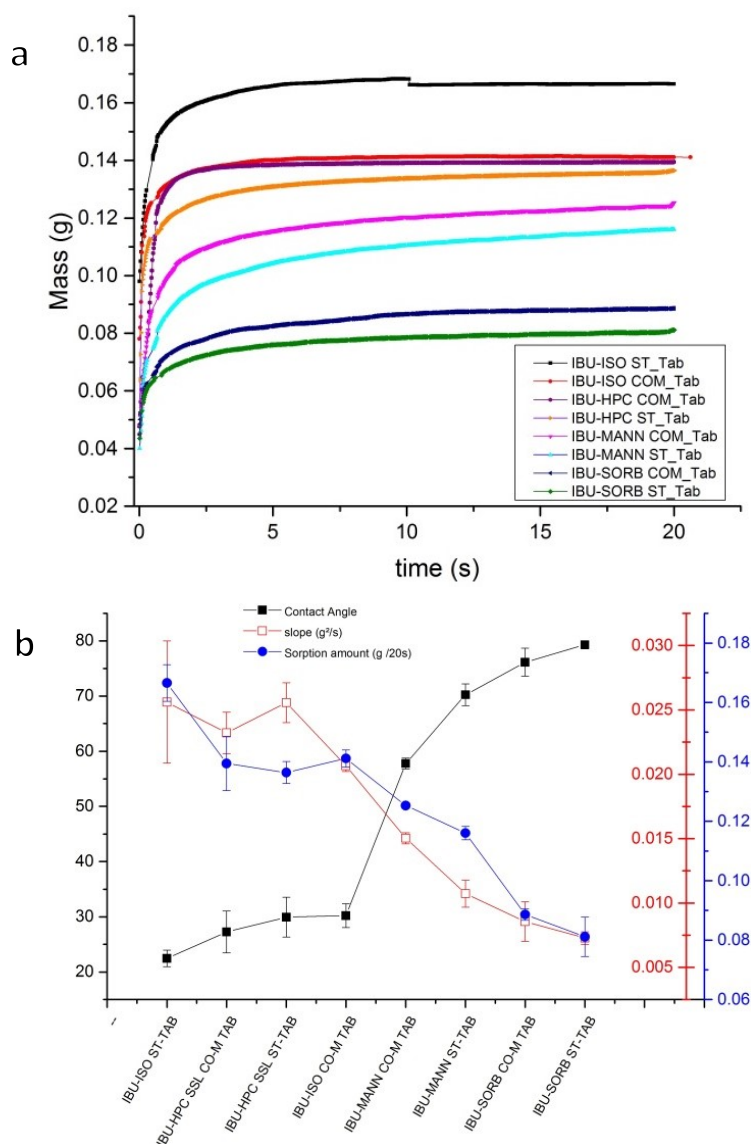


Figure 20 (a) the mass uptake of water into all IBU-compacts bed, (b) values of contact angle, slope and sorption amount of all tested compacts

5.2.1.3 SFE and wettability of melt quenched IBU (IBU-MQ)

Since IBU-HPC COM-Tab was evidenced to have an amorphous part, the SFE studies of IBU-MQ compacts were performed to determine the contribution of the amorphous amount of IBU in the wettability improvement of this formulation as compared to IBU-HPC ST-Tab, where no change in crystallinity was recorded. The data showed an improved polarity by around 6 folds for IBU-MQ (68% amorphous) as that of IBU in the crystalline form (Table 16). The amorphous form was also reflected in the wettability by a boost in σ^p by 7.5 folds, beside a betterment of the wetting kinetics.

While no measurement of the contact angle for crystalline IBU could be done by Tensiometer, the measurement could be performed for IBU-MQ compacts (Table 17).

Table 16 SFE Components, calculated values of W_a , W_i and W_s for the compacts of pure IBU compacts

formulation	σ^p	σ^d	σ_s	Po%	W_a	W_i	W_s
IBU-CR	1.74 ± 0.73	38.71 ± 0.29	40.45 ± 0.99	4.28	76.76	15.59	-68.96
IBU-MQ	13.08 ± 1.20	35.75 ± 0.22	48.83 ± 1.32	26.75	107.55	138.77	-38.17

Table 17 Wetting values of pure IBU-MQ compacts from Washburn method

formulation	contact angle	slope g^2/s	amount $g/20s$
IBU-MQ Tab	74.17 ± 2.33	0.0111 ± 0.0009	0.1029 ± 0.0012

5.2.2 FTIR analysis of IBU-compacts (IBU/excipients interactions)

The chemical structures of all ingredients utilized in the IBU-compacts are summarized in Table 18.

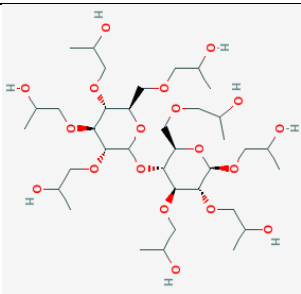
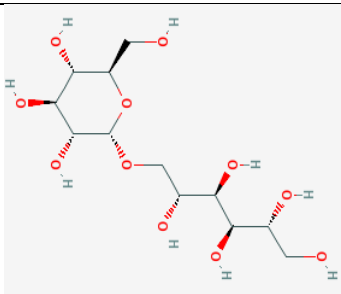
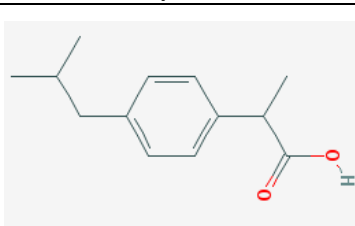
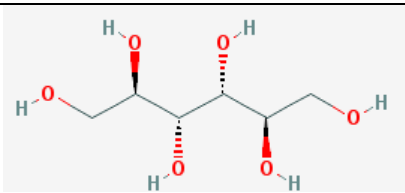
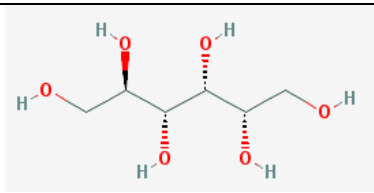
When IBU acts as HBD, the most significant changes will be observed on hydroxyl OH-band absorption. The spectrum of crystalline IBU demonstrated a sharp well-defined band at 1708.7 cm^{-1} , which corresponds to the stretching vibration of isopropionic acid's carbonyl C=O. The main multiplied peaks around 2953 cm^{-1} are attributed to the stretching OH vibration. Any change, observed at the level of these peaks for the compacts, is indicative to changes in the IBU molecular level [87]. The specific bands of IBU aromatic ring are at the wavelengths, where there is no interference or overlapping with excipient bands, such as the in-plane ring deformation of stretching aromatic C-C bonds at 1507 cm^{-1} . Besides, a sharp peak at 778 cm^{-1} is assigned to the out-of-plane deformation of bending C-C group of the aryl substituents [127]. The band at 1460 cm^{-1} is allocated to the C-H asymmetric bending of CH₃ and to the C-H scissoring of CH₂. The spectrum of pure HPC contained strong and very broad peaks of OH stretching vibration in the pyranose ring around 3438 cm^{-1} [116,128], that is indicative of H-bonded hydroxyl groups. The several absorption bands at 2932 and 2967 cm^{-1} are connected to the CH and CH₂ stretching vibration [128], and the one at 1373 cm^{-1} is related CH bending.

By the analyses of IR spectrum of IBU-HPC ST-Tab, some changes could be observed in the most informative regions where possible IBU/HPC interactions can take place (Figure 21, a). As compared to neat IBU, the vibration peaks at ~ 2630 and 2730 cm^{-1} , related to the stretching vibration of cyclic dimerized OH groups, were almost missing. The characteristic peak of stretching C-O vibrations was also much diminished in the fingerprint region at 1183 cm^{-1} , which indicated a certain degree of interaction via hydrogen bonding of OH groups. In addition, the OH stretching peaks were further broadened; as a very less defined peak between 2850 to 3000 cm^{-1} (especially for the co-milled compacts) and the IBU

peak at 2953 cm^{-1} was almost embedded. Besides, a broadening and shifting of C=O from 1708.7 to a higher wavenumber 1715 cm^{-1} was recorded. Marked changes were also monitored in the “fingerprint” region, presented as less intensity of the strong peak at 778 cm^{-1} . The peak at 1007 cm^{-1} disappeared in both ST and COM-compacts. Apart from that, the specific peak of stretching ether moiety C-O-C at 1047 cm^{-1} was much broadened as compared to neat HPC and the IR-absorption of OH at 3438 cm^{-1} was much broadened within the range of $3150\text{-}3600\text{ cm}^{-1}$.

The mentioned manifestations were more evident in IBU-HPC co-milled compacts; where less defined and broader peaks were detected for several functional bands of IBU such at 1715 , 1506 , 1047 cm^{-1} and the ranges of $3150\text{-}3600$, $400\text{-}800\text{ cm}^{-1}$. Besides, the peak of C=O at 1715 cm^{-1} was characterized with a relatively less sharpness and the band at 2953 cm^{-1} was embedded to a high extent, displaying a higher broadness.

Table 18 Chemical structure of the materials used in IBU-compacts*

HPC	isomalt	ibuprofen
		
mannitol		sorbitol
		

*National Center for Biotechnology Information. PubChem Database, <https://pubchem.ncbi.nlm.nih.gov/>

The next characteristic peaks could be defined for the neat isomalt: Strong broad peaks at 3283 cm^{-1} , which relates to OH stretching of alcohol [129]; the strong characteristic band at 1154 cm^{-1} because of strong dipole moment, related to the stretching asymmetrical aliphatic ether C-O-C [129]; several peaks of aliphatic CH stretching vibrations at 2960 and 2900 cm^{-1} , and the stretching vibrations associated to CO at 1037 and 1062 cm^{-1} as primary and secondary alcohol respectively. Finally, the vibrations recorded around 1346 cm^{-1} were assigned to the OH bending (in-plane).

Some changes could be seen for IBU ISO-compacts as compared to ISO (Figure 21, b) that included: An apparent broadness of OH region with a minor bathochromic shift at 3281 cm^{-1} ; the OH bending vibrations at 622 cm^{-1} (out-of-plane) almost disappeared with a blueshift to a higher wavenumber in the fingerprint region. Additionally, the two peaks related to CO stretching showed reverse intensities, the peaks of CH bending vibrations at 1425 cm^{-1} were integrated in the IBU peak at 1419 cm^{-1} that showed a longer and sharper shape. In comparison to neat IBU, the OH stretching was also broadened showing higher intensity with lower frequency around 2920 cm^{-1} (more evident in ST-Tab), besides, a downshifting was obtained of the peak from 2953 to 2946 cm^{-1} .

The neat mannitol presented a very broad band at 3280 cm^{-1} , representative of stretching vibrations of the OH axial deformation with intermolecular H-bonds [130,131]. The characteristic peaks set, observed at 2950 and 2918 cm^{-1} , represent the linking stretching vibration of CH and CH₂ [59,130,131]. The bands at 1077 and 1018 cm^{-1} are ascribed to the stretching of CO of the alcohol group (secondary alcohol) [131] and of the primary alcohol respectively. Several peaks of CH bending vibrations are observed between 1260 and 1390 cm^{-1} .

The following changes could be noticed for the IBU-MANN compacts as compared to neat MANN (Figure 22, a). The OH bending at 702 cm^{-1} (out-of-plane) was less defined and shifted to 687 cm^{-1} with less intensity; the OH bending at 1308 cm^{-1} (in-plane) was blueshifted to 1318 cm^{-1} in COM-Tab. Besides, the peaks of CH bending were shifted and integrated within the peak at 1417 cm^{-1} ; the peak of OH stretching became broader showing an extra shoulder around 3330 cm^{-1} (more obvious in COM-Tab). The bands of CH and CH₂ at 2950 cm^{-1} disappeared, integrating within the OH stretching peaks of IBU, which demonstrated a possible interaction MANN/ IBU. On the other hand, certain observations were collected compared to IBU: A broadening of OH stretching peaks (higher observed in COM-Tab) with a minor downshift to 2951 cm^{-1} . The co-milled compacts showed additionally broader peaks of OH bending of IBU at 1230 cm^{-1} .

5. Influence of high-pressure compaction on wettability of ibuprofen compacts

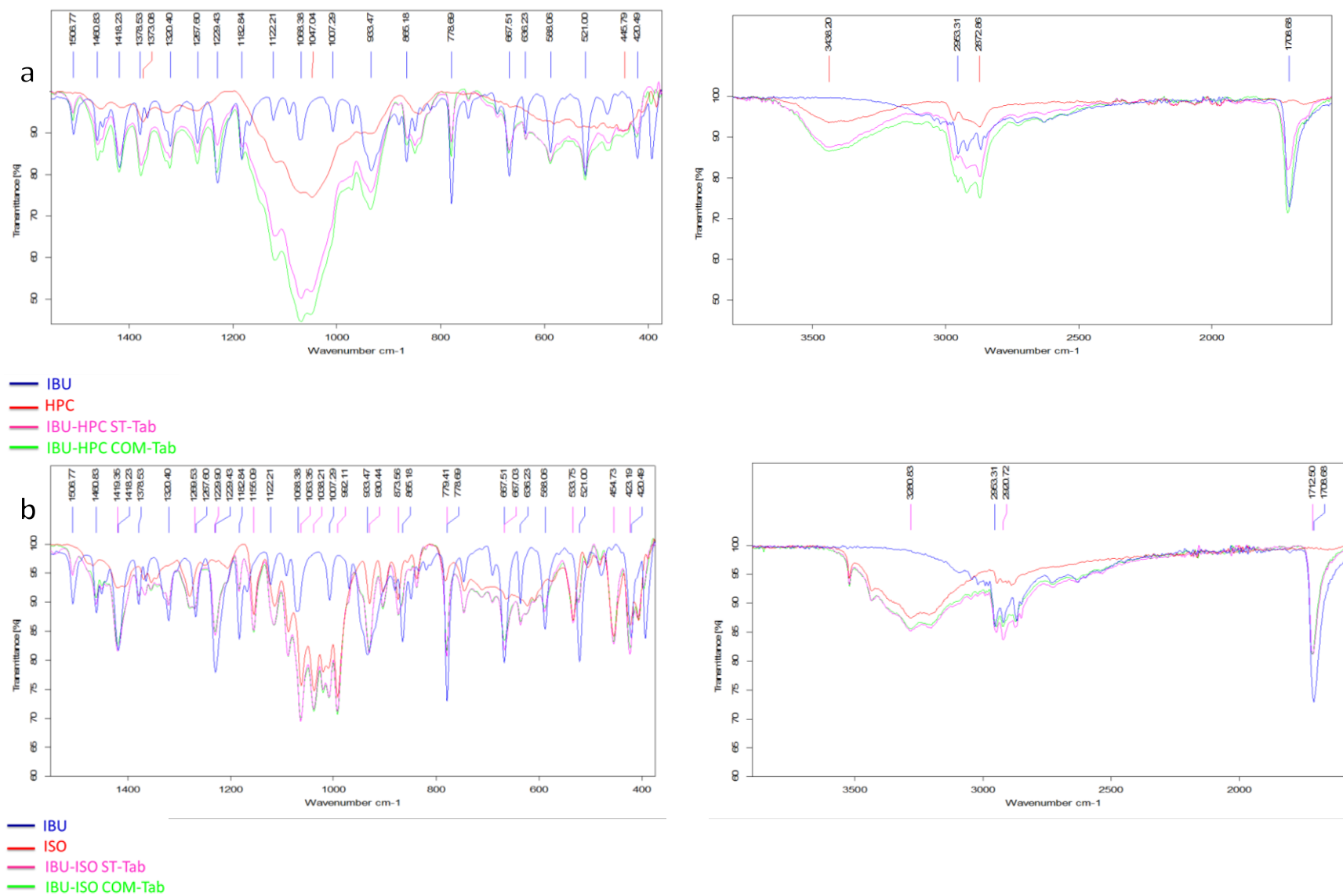


Figure 21 FTIR spectra of (a) pure crystalline IBU, pure HPC, IBU-HPC ST and IBU-HPC COM compacts. (b) pure crystalline IBU, pure ISO, IBU-ISO ST and IBU-ISO COM compacts, the presented ranges refer to bands where prominent changes occurred

5. Influence of high-pressure compaction on wettability of ibuprofen compacts

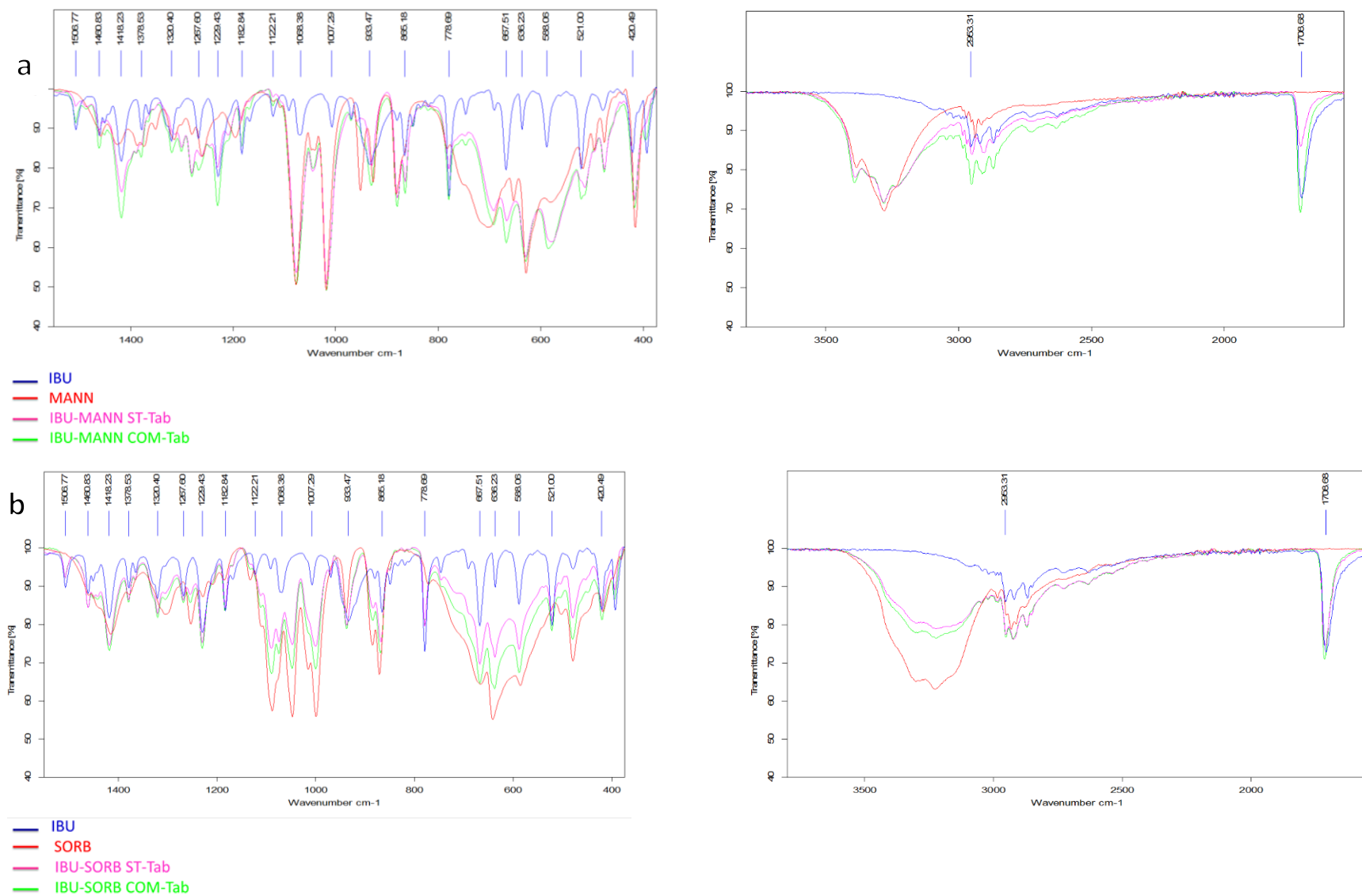


Figure 22 FTIR spectra of (a) pure crystalline IBU, pure MANN, IBU-MANN ST and IBU-MANN COM compacts. (b) pure crystalline IBU, pure SORB, IBU-SORB ST and IBU-SORB COM compacts, the presented ranges refer to bands where prominent changes occurred

The pure sorbitol possessed very strong broad peaks of OH stretching at 3226 cm^{-1} ; the CO stretching (primary alcohol) at 1047 cm^{-1} , and a peak at 2930 cm^{-1} corresponding to the CH stretching. The several peaks between 1252 and 1415 cm^{-1} were related to CH bending vibrations [132].

The following observations were obtained for the compacts as compared to neat SORB (Figure 22): The minor redshift of the OH stretching to 3222 cm^{-1} , that showed a less intensity as that of pure SORB. The COM-compacts exhibited, however, a broader peak of OH stretching than that of ST-ones. The OH bending at 641 cm^{-1} (out-of-plane) shifted to 636 cm^{-1} and the peak at 1087 cm^{-1} , related to CO stretching vibrations (secondary alcohol) [132], showed a minor shift to 1089 cm^{-1} . The OH bending at 1309 cm^{-1} (in-plane) was less defined and integrated within the IBU peak at 1320 cm^{-1} ; the peaks of CH bending became sharper. Finally, the OH stretching of IBU was broadened compared to pure IBU.

All sugar-alcohols compacts displayed a blueshift of C=O stretching of IBU to a higher frequency (1712 cm^{-1}). This shift was more pronounced in the co-milled tablets (1714 - 1716 cm^{-1}).

5.2.3 IBU-compacts porosity

All compacts expressed, generally, a low porosity (around 4-5%; Table 19), which was expected considering that the mixtures were condensed by application of high-pressure, leading to less voids volume. The porosity of IBU-ISO ST-compacts was the only exceptional value, showing relatively higher value that was significantly more porous than other compacts. The porosities of co-milled compacts were much comparable ($p > 0.05$) and only IBU-HPC and IBU-MANN -compacts were significantly different. The co-milled compacts showed significantly lower porosity than their matching ST-compacts.

Table 19 The mesured porosity of IBU-compacts

Formulation	Average
IBU-HPC ST-Tab	4.996 ± 0.136
IBU-HPC COM-Tab	3.489 ± 0.216
IBU-ISO ST-Tab	7.002 ± 0.437
IBU-ISO COM-Tab	3.838 ± 0.159
IBU-MANN ST-Tab	5.410 ± 0.167
IBU-MANN COM-Tab	4.323 ± 0.221
IBU-SORB ST-Tab	5.575 ± 0.140
IBU-SORB COM-Tab	4.041 ± 0.152
IBU-CR Tab	4.280 ± 0.319
IBU-MQ Tab	1.710 ± 0.321

Besides, IBU-MQ compacts significantly presented a lower porosity than the crystalline IBU-compacts, confirming the hypothesis that was introduced preciously in 4.3 regarding the higher compressibility of amorphous materials.

Table 20 Density values of the tablets and related mixtures, all values in g/ cc

	Tablet Density	True density (MIX)	*Apparent density (MIX)
IBU-HPC ST-Tab	1.1422 ± 0.0016	1.2023	0.299
IBU-HPC COM-Tab	1.1534 ± 0.0026	1.1951	0.394
IBU-ISO ST-Tab	1.3047 ± 0.0039	1.4010	0.411
IBU-ISO COM-Tab	1.3565 ± 0.0008	1.4117	0.280
IBU-MANN ST-Tab	1.2978 ± 0.0005	1.3736	0.427
IBU-MANN COM-Tab	1.3287 ± 0.0010	1.3873	0.346
IBU-SORB ST-Tab	1.3094 ± 0.0020	1.3879	0.594
IBU-SORB COM-Tab	1.3478 ± 0.0018	1.4060	0.366

*Apparent density was determined by measuring the volume of a known mass of an untapped powder sample into a graduated cylinder

The measured tablets density was much closer to the true density of related mixtures, which explained the induced low porosities obtained (Table 20). The density of a mixture bed is mainly affected by the outer shape of crystals components. Other than IBU-HPC mixtures, the apparent densities of the mixture beds were lower for the co-milled mixtures than that of matching ST-mixtures, but they showed, in contrary, higher true densities than of ST-mixtures. The higher apparent densities for ST-mixtures of IBU-ISO, IBU-MANN and IBU-SORB are related to the crystal habit and the surface form of spray dried granules, which facilitate the particles arrangement during the filling, packing and pressing. Thus, they possess a high tableability and compressibility [133].

5.2.4 Mercury porosimetry of IBU-tablets

The values of $d_{average}$, and the median pore radius (r_{50}) are listed in Table 21,

The mercury porosimetry displayed relatively higher porosity values than that measured based on solid fraction calculations (5.2.3), but it demonstrated, anyways, the same trend (Table 21).

In general, ST-tablets were characterized by a higher porosity than COM-tablets. A higher porosity was observed for each ST-compact as compared to the co-milled counterpart, presenting significantly higher values for total pore surface area as well (except for SORB-compacts). The COM-tablets were accompanied with a smaller median pore diameter than that of ST-tablets. A separate comparison within

ST- or only within COM-tablets revealed that HPC-tablets had the lowest porosity to the other excipient-Tabs in each case.

Table 21 The measured values of all compacts by mercury porosimetry

PASCAL 140+440	Total pore surface area (m ² /g)	Porosity%	r50 (nm)	d _{average} (nm)
IBU-HPC ST-Tab	26.69	9.40	11.59	12.33
IBU-HPC COM-Tab	19.36	5.19	5.15	9.29
IBU-ISO ST-Tab	21.40	12.16	16.29	17.46
IBU-ISO COM-Tab	12.09	5.87	8.57	14.28
IBU-MANN ST-Tab	32.19	11.70	7.16	11.20
IBU-MANN COM-Tab	23.97	7.85	6.15	9.85
IBU-SORB ST-Tab	17.83	11.35	57.44	19.47
IBU-SORB COM-Tab	18.61	7.02	7.15	11.18

Figure 23 (a) shows the cumulative intrusion volume of mercury plotted versus the mean pore diameter of all formulations. Figure 23 (b) shows, as an example, the relative intrusion volume% versus the pore radius ranges for IBU-SORB ST-Tab. All studied tablets presented one class of trend, in which the most pore volume corresponded to the mercury intruded volume up the high-pressure step (nanoporosity). Generally, the change of intruded mercury against the applied pressure did not tend to a maximum step or at least a minimum plateau.

As can be seen, no significant differences in the respective frequency of the pores diameters for COM-tablets were observed. The pores distribution for ST-Tabs of IBU-ISO and IBU-SORB presented a notable higher frequency at a higher range of pore diameters, which can clarify the relative high values of their median pore diameters.

The pore size distribution of all tablets showed a very high trend towards very fine pores in the nanometer scale. Only IBU-SORB ST- and relatively IBU ISO ST-tablets displayed some distribution in a bigger range of sizes. The two approaches (r50 and d_{average}) showed some variability in estimations of the pore size; the values obtained were, however, in consistent with the porosity order.

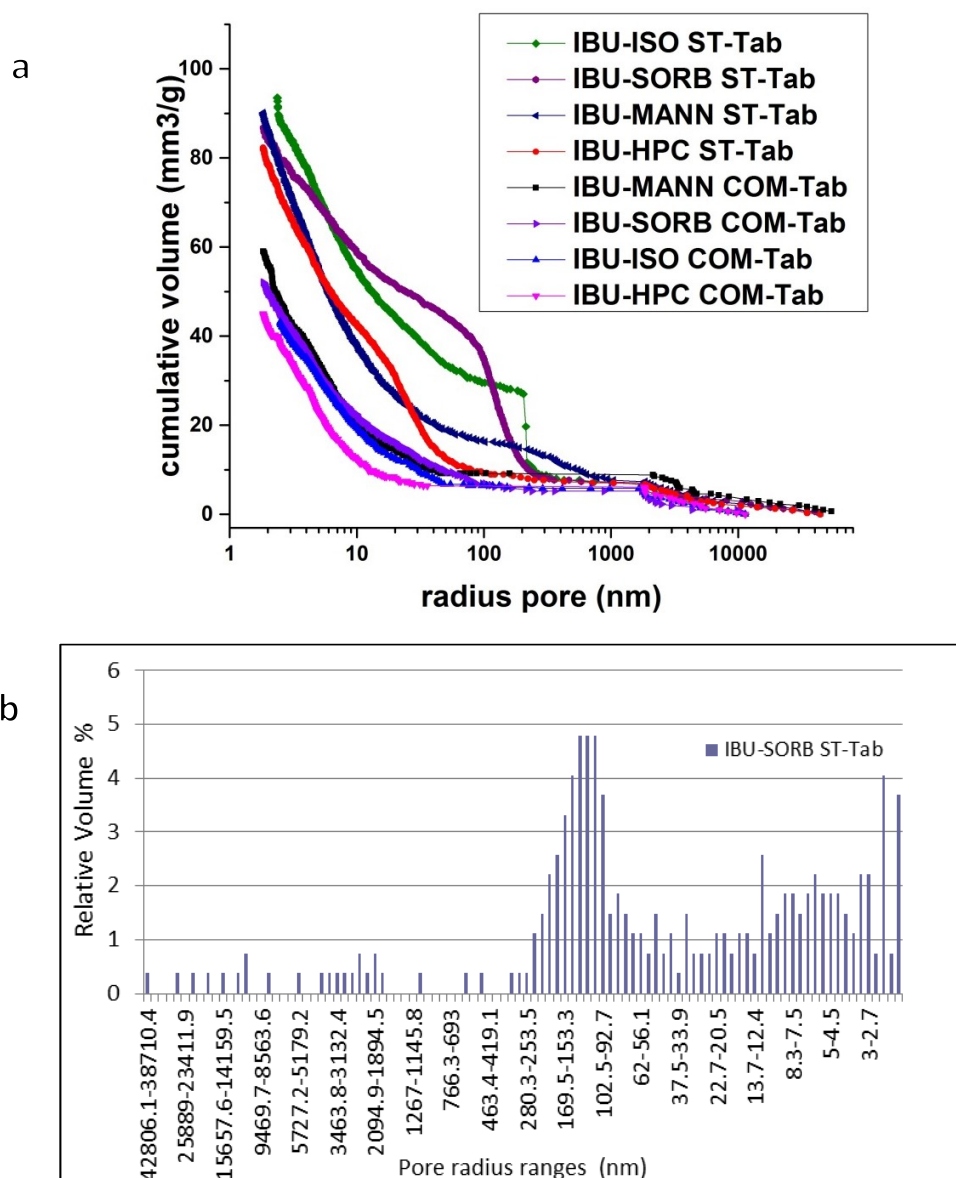


Figure 23 (a) Mercury intrusion curves for all tablets, (b) pore size distribution of IBU-SORB ST-Tab

5.2.5 Mercury porosimetry of IBU-granules

The porosity values were, in general, lower than the measured ones for the corresponding tablets (see Table 21 and Table 22).

The ST-granules were also characterized by a higher porosity as compared to COM-granules. The IBU-HPC granules (both ST/COM) and the co-milled granules showed very low porosities. All ST-granules exhibited higher porosities than the co-milled counterparts, but in contrary to what observed by the tablets analysis, they did not present higher values for the total pore surface area (except for HPC-compacts), which is

perplexing. The total pore surface areas of COM-granules were higher than those of ST tablets, and associated with a smaller median pore diameter.

Table 22 Density, total surface area, porosity and pore diameter of granules from mercury porosimeter analysis

Offset	Bulk density (g/cm ³)	Apparent density (g/cm ³) calculated	Total pore surface area (m ² /g) calculated	Porosity (%)	r50 (nm)	d _{average} (nm)
IBU-HPC ST-Gr	0.12	0.12	27.73	1.01	8.39	12.20
IBU-HPC COM-Gr	0.21	0.21	17.22	0.91	6.26	9.98
IBU-ISO ST-Gr	1.22	1.30	17.01	6.02	53.55	11.63
IBU-ISO COM -Gr	0.19	0.19	20.83	1.07	6.22	10.74
IBU-MANN ST-Gr	1.23	1.30	10.90	6.07	1972.25	18.18
IBU-MANN COM-Gr	0.19	0.19	22.08	1.37	10.92	12.97
IBU-SORB ST-Gr	1.34	1.45	12.44	7.46	788.32	17.94
IBU-SORB COM-Gr	0.19	0.19	17.34	0.99	9.68	11.92

Figure 24 shows the cumulative intrusion volume of mercury plotted versus the mean pore diameter of all granules. The co-milled granules showed that the most pore volume was related to the mercury intruded volume in the nanometer range. Generally, ST-granules displayed a certain distribution in the micrometer range. The pore size estimation showed considered deviations between the both approaches (r50 and d_{average}).

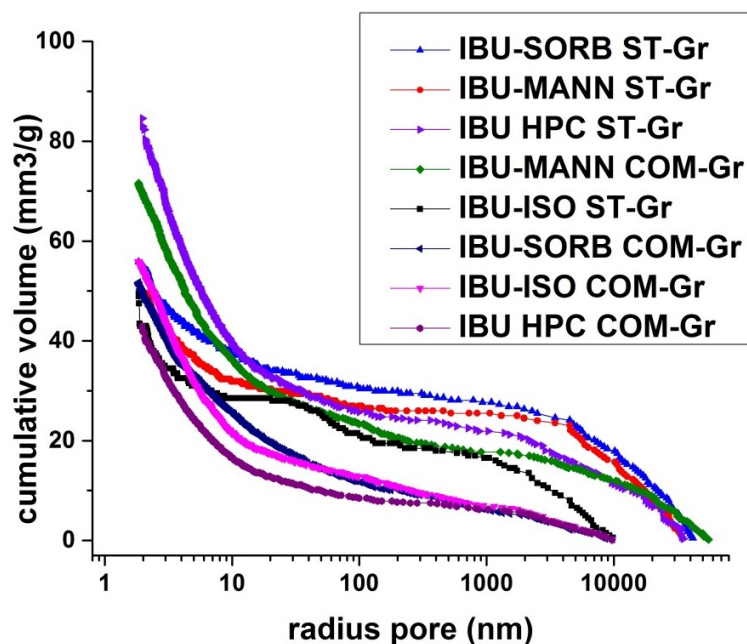


Figure 24 Mercury intrusion curves for all IBU formulation granules

5.2.6 Milling effect on particle size distribution of IBU-mixtures

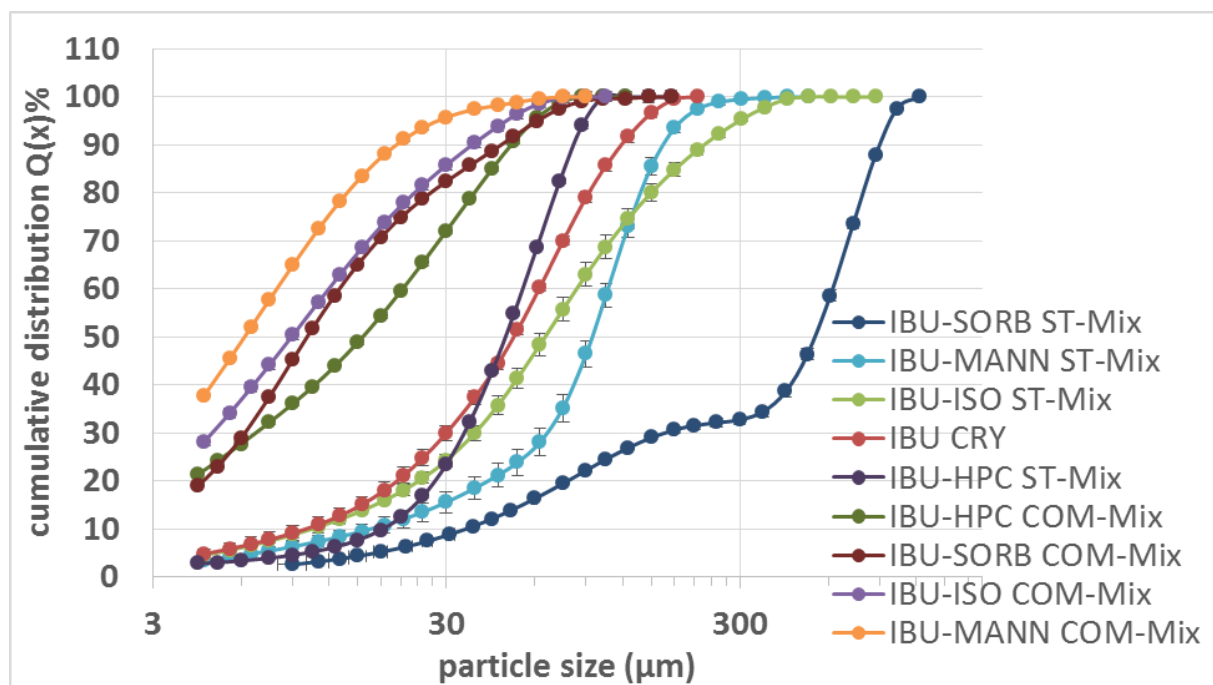


Figure 25 Particle size distribution of pure IBU (crystalline) and all IBU mixtures before and after milling

IBU-SORB ST-Mix displayed big sizes of particles ($d_{50} = 539 \mu\text{m}$), the volume median diameters of the particles for the rest of ST-mixtures ranged from $47 \mu\text{m}$ up to $94 \mu\text{m}$.

The analysis of particle size distribution confirmed major differences and a considerable reduction in the particles size upon co-milling. The most effectiveness on particle sizes was obtained in case of sorbitol mixtures, followed by mannitol mixtures, which was rational considering the big size of sorbitol granules. A less degree in the particle size decrease was marked in case of HPC mixtures after co-milling. The d_{10} , d_{50} , and d_{90} values for pure IBU (crystalline) and all IBU mixtures before and after co-milling are summarized in Table 23.

In general, all mixtures have rather a wide asymmetrical particle size distribution. Span values between 1.3 and 4.3 were calculated. The ST-mixtures showed, however, a more narrow symmetrical distribution as compared to co-milled ones. After the co-milling process, the co-milled mixtures were found to have a very low average diameter d_{50} that did not exceed $15 \mu\text{m}$ (Figure 25). The efficacy of the co-milling process was in the following order for the binary mixtures: IBU-SORB > IBU-MANN > IBU-ISO > IBU-HPC.

Table 23 Particle size distribution of IBU and IBU binary mixtures (before and after milling)

	ST-MIX				COM-MIX			
	d ₁₀	d ₅₀	d ₉₀	Span	d ₁₀	d ₅₀	d ₉₀	Span
IBU-HPC	18.27 ± 0.96	47.82 ± 0.82	82.18 ± 0.45	1.34 ± 0.03	1.96 ± 0.08	15.61 ± 0.09	50.07 ± 0.20	3.08 ± 0.03
IBU-ISO	10.54 ± 0.76	65.48 ± 3.76	227.22 ± 11.87	3.31 ± 0.17	1.92 ± 0.03	8.94 ± 0.27	36.82 ± 0.69	3.90 ± 0.06
IBU-MANN	17.04 ± 3.36	94.31 ± 3.35	166.47 ± 4.69	1.59 ± 0.05	1.56 ± 0.00	6.19 ± 0.00	20.42 ± 0.39	3.05 ± 0.06
IBU-SORB	35.21 ± 0.90	539.90 ± 9.17	905.13 ± 7.15	1.61 ± 0.02	2.49 ± 0.08	10.10 ± 0.03	46.29 ± 1.94	4.34 ± 0.18
IBU-Cr	10.06 ± 1.83	50.98 ± 1.01	119.29 ± 3.86	2.14 ± 0.00				

5.2.7 Specific area of IBU-granules

No formulation of granules showed a great value of specific surface area measured by Brunauer, Emmet and Teller method (BET). The COM-granules possessed higher values as compared to ST-granules (Table 24). The analysis of specific area revealed that the ST-granules of each formulation have only an area per unit mass about two third of that of the related COM-granules.

However, IBU-SORB ST-granules showed the lowest specific surface area, possessing not even half of that of related COM-granules. IBU-HPC COM-granules showed the highest specific surface area, whereas IBU-MANN granules showed the highest value within the ST-granules.

Some additional experiments were carried out on some ST- and co-milled mixtures, which revealed, as expected, significantly higher values than the correlated granules, especially for the co-milled mixtures, such as the co-milled mixture of IBU-ISO and IBU-MANN.

Table 24 Surface area of formulated granules

	Spec. surface area [m ² /g] Gr	Spec. surface area [m ² /g] Mix
IBU-HPC ST-Gr	0.4085	n.t.
IBU-HPC COM Gr	0.6488	1.8782
IBU-ISO ST-Gr	0.3565	1.6206
IBU-ISO COM-Gr	0.4958	2.0608
IBU-MANN ST-Gr	0.4241	n.t.
IBU-MANN COM-Gr	0.6181	2.8108
IBU-SORB ST-Gr	0.2215	n.t.
IBU-SORB COM-Gr	0.5891	n.t.

n.t. not tested

5.2.8 The influence of pure excipients properties on the compacts' performance

5.2.8.1 The effect of pure excipient and drug/excipients ratio on the wettability

Compacts of pure ingredients (with and without milling) as well as compacts prepared with another API/excipient ratio (40: 60) were also prepared (applying the same conditions under high-pressure) and examined, to investigate the contribution of excipient's wettability as well as excipient's concentration on the overall wettability of the related formulations. It can be subsequently extrapolated, whether the wettability of prepared formulations is an excipient-dependent phenomenon and a linear regression of the increased excipient's ratio.

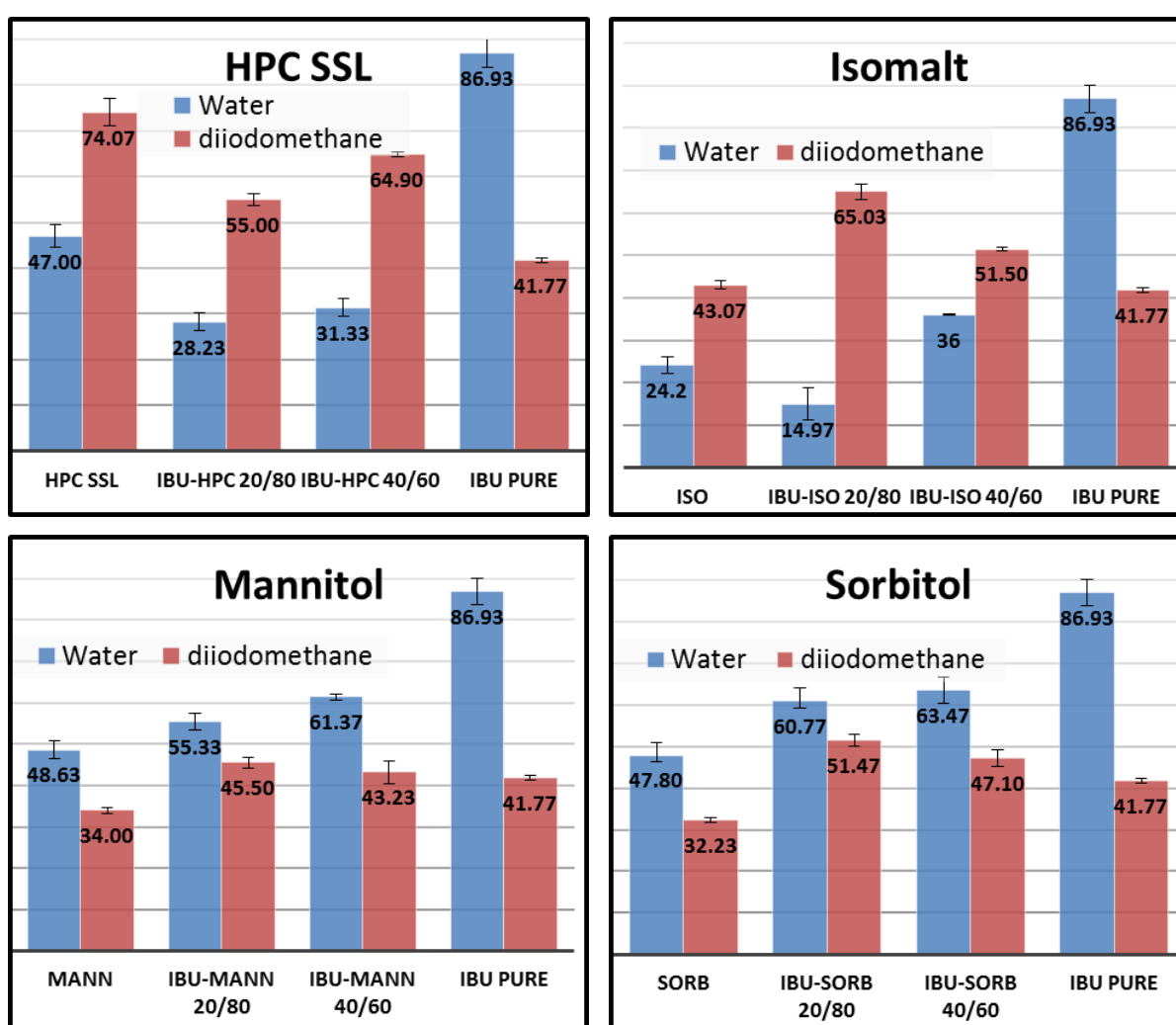


Figure 26 Contact angle values of the compacts of pure ingredients and of different IBU/excipient ratios

In general, the contact angles obtained from compacts of pure excipients were $< 50^\circ$. The pure ISO-compacts revealed higher wettability as compared to other neat excipients (Figure 26). Additionally, the

20/80 compacts of IBU-ISO and IBU-HPC displayed an improved spontaneity in the wetting process over the individual components, showing a lower contact angle with water as compared to those of the related compacts from pure components. This was not the case for the compacts of IBU-MANN and IBU-SORB, where a decrease in the contact angles with water and thus, an improvement of W_a values was observed over the pure IBU-compacts, but not over the pure mannitol- and sorbitol-compacts respectively. All 20/80 compacts displayed a better wettability than the compacts with 40/60 ratio.

5.2.8.2 IDR for pure excipients

Depending on the developed method described in 8.2.3.3, the end-point of IDR for pure excipients was firstly determined for the disks prepared without a previous milling in pH 1.0 and pH 5.5 media. No significant differences in IDR values resulted between the both media, which refers to the pH-independent solubility nature of the tested excipients (Table 25 and Table 57 in Appendix). Accordingly, the disks of pure excipients prepared with a previous milling were only tested at pH 5.5.

The optic observation during the pre-studies proved the disappearance and vanishing of the disks at the endpoint of the experiments, except for HPC-compacts. As soon as the HPC-disk came in contact with the aqueous medium, the compact surface wetted and the polymer began to hydrate, forming a gel-like layer on the surface, leading to a prolongation of the dissolution process. Similar observations were also collected for the disks of neat PVPVA.

Table 25 IDR measurements of disks prepared from pure excipients at pH 5.5

Excipient	IDR mg/min/cm ²
ISO	28.779 ± 3.952
ISO milled	26.458 ± 3.332
MANN	17.706 ± 2.650
MANN milled	23.498 ± 3.656
SORB	11.460 ± 1.645
SORB milled	20.546 ± 2.780

The pure isomalt-compacts demonstrated the faster IDR compared to the other two sugar-alcohols (Table 25). Sorbitol ST-compacts on the other hand, showed the slowest IDR values. A minor improvement was observed in IDR of the milled excipients as compared to disks prepared of the same excipient without milling (only significant in case of sorbitol compacts $p=0.0337$).

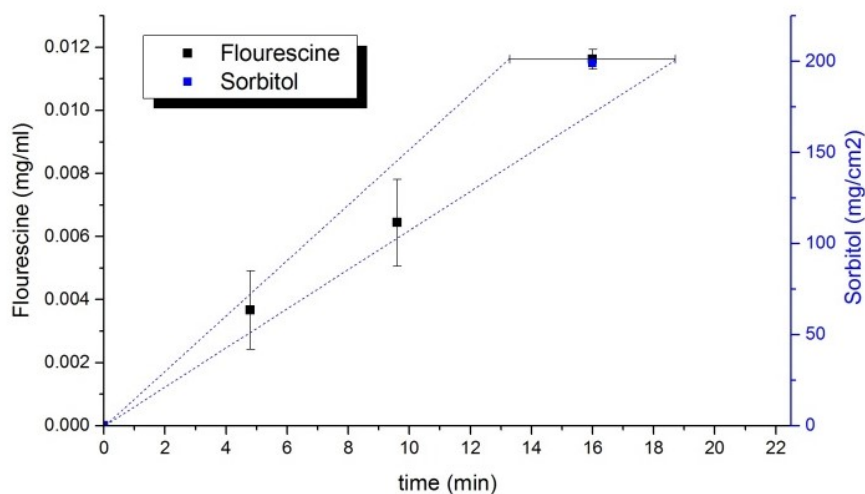


Figure 27 IDR measurement of pure sorbitol by the developed equipment with the verification of the method by determination of the dissolved fluorescein

In order to assess the feasibility and reliability of using the developed method and to ensure that the measured end-point corresponds to the complete dissolution of the tested disk, the procedure was validated by addition of ($\approx 9\%$ w/w) fluorescein, which was homogeneously mixed with the sugar-alcohol powder before pressing to form an integrated compact. The verification of the method was performed for each sugar-alcohol in triplicate. During the dissolution, samples were drawn out of the dissolution vessel at predetermined time intervals and the concentration of fluorescein released in the media was analyzed by UV spectrophotometer; the data of fluorescein calibration are listed in

Table 52. The results for the pure sorbitol, as an example, can be seen in Figure 27 ; all the measured concentration points for fluorescein were within the range of the triplicate obtained end-points for the pure sorbitol, with an acceptable linearity, confirming the reliability of this procedure to determine the IDR of soluble non-polymer excipients. The results of validation for the other two sugar-alcohols are presented in Appendix; Figure 62.

5.2.8.3 Kinetic and intrinsic solubility of IBU in binary mixtures

The analysis covered all binary formulations. Differences were observed in the intrinsic S_0 and kinetic K_s solubilities depending on the involved combined excipient and as compared to pure IBU. The final values are summarized in Table 26.

All binary formulations showed higher S_0 and higher K_s than neat IBU. S_0 was maximally increased by 1.4 folds with HPC, followed by 1.2 folds with ISO as compared to neat IBU, whereas the lowest increase was measured in presence of sorbitol.

For all samples in this study, the supersaturation ratio showed positive values (Table 27). IBU precipitated at a concentration that is at least 4 times of the IBU intrinsic solubility in the presence of tested excipients. No correlation was found between the intrinsic and kinetic solubilities. The kinetic solubility K_s refers to the maximum reached solubility, and indicates to the extent of supersaturation achieved by the system [113]. The IBU-HPC mixture exhibited the least difference between S_o and K_s values.

Table 26 Experimental solubility data measured by CheqSol at 25 °C, experiments were replicates in n = 8

formulation	S_o mg/ml	K_s mg/ml	Estimated Sol pH 1.0 mg/ml	Estimated Sol pH 5.5 mg/ml
IBU-HPC	0.0508 ± 0.0010	0.1560 ± 0.0143	0.0509 ± 0.0010	0.7202 ± 0.0143
IBU-ISO	0.0442 ± 0.0010	0.1602 ± 0.0290	0.0442 ± 0.0010	0.6215 ± 0.0131
IBU-MANN	0.0420 ± 0.0008	0.1627 ± 0.0172	0.0420 ± 0.0008	0.5958 ± 0.0108
IBU-SORB	0.0397 ± 0.0011	0.1474 ± 0.0125	0.0397 ± 0.0011	0.5625 ± 0.0157
IBU	0.0363 ± 0.0003	0.1436 ± 0.0092	0.0363 ± 0.0003	0.5141 ± 0.0043

Table 27 The increase of intrinsic and kinetic solubility and supersaturation ratio for binary mixtures

formulation	S_o increase	K_s increase	KS/ S_o	Supersaturation ratio KS/ S_o (IBU)
IBU-HPC	1.40	1.09	3.07	4.30
IBU-ISO	1.22	1.12	3.63	4.42
IBU-MANN	1.16	1.13	3.87	4.49
IBU-SORB	1.09	1.03	3.72	4.07
IBU	1.00	1.00	3.96	3.96

5.2.9 The influence of high-pressure: 200MPa formulations analysis

Formulations were compacted under less pressure to differentiate, whether the observed increase in solubility and IDR is certainly related to the impact of high-pressure. Considering that IBU-HPC and IBU-ISO compacts were superior to other formulations, showing a higher enhancement in both solubility and IDR, therefor, two corresponding standard formulations were prepared under 200MPa without a previous co-milling and tested in comparison with that of 500MPa.

Generally, no significant changes in XRPD of both 200MPa-compacts were monitored, the recorded patterns were comparable to that of physical mixtures (Figure 29). Besides, the crystallinity was unaffected for 200MPa-tablets of IBU-HPC, as confirmed by the calculation of the crystallinity degree. These observations were reflected in a less improvement of the IBU saturation solubility for 200MPa formulations at pH 1.0, as revealed by shake flask method, showing a solubility factor of 1.2 and 1.1 for

5. Influence of high-pressure compaction on wettability of ibuprofen compacts

IBU-HPC and IBU-ISO granules respectively, compared to 1.35 and 1.22 for the correlated 500MPa granules (Figure 30).

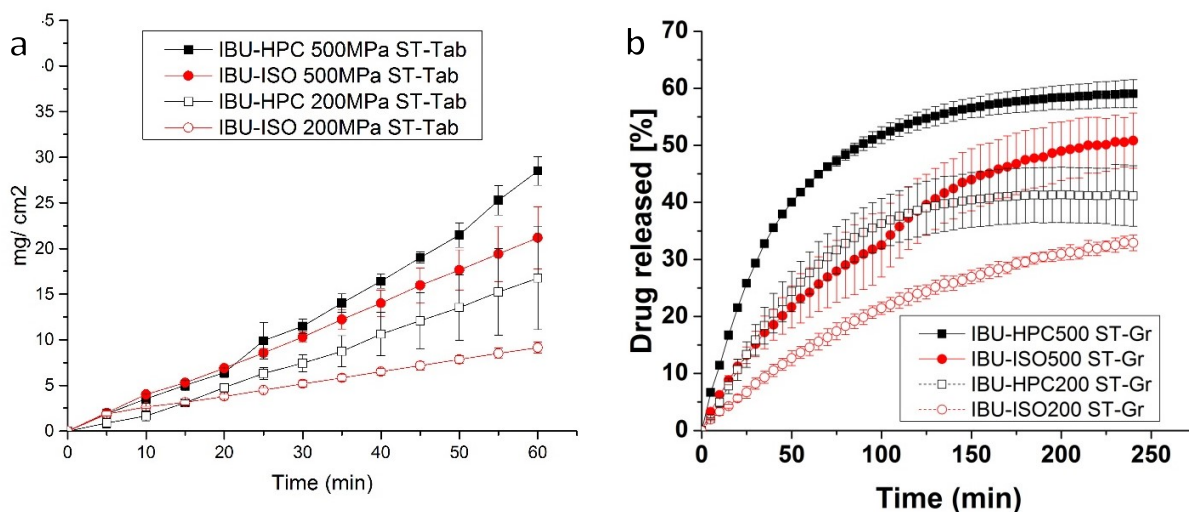


Figure 28 IBU-HPC and IBU-ISO compacts prepared at 200MPa as compared to 500MPa compacts at pH 1.0 (a) IDR (b) dissolution test of granules at non-sink condition

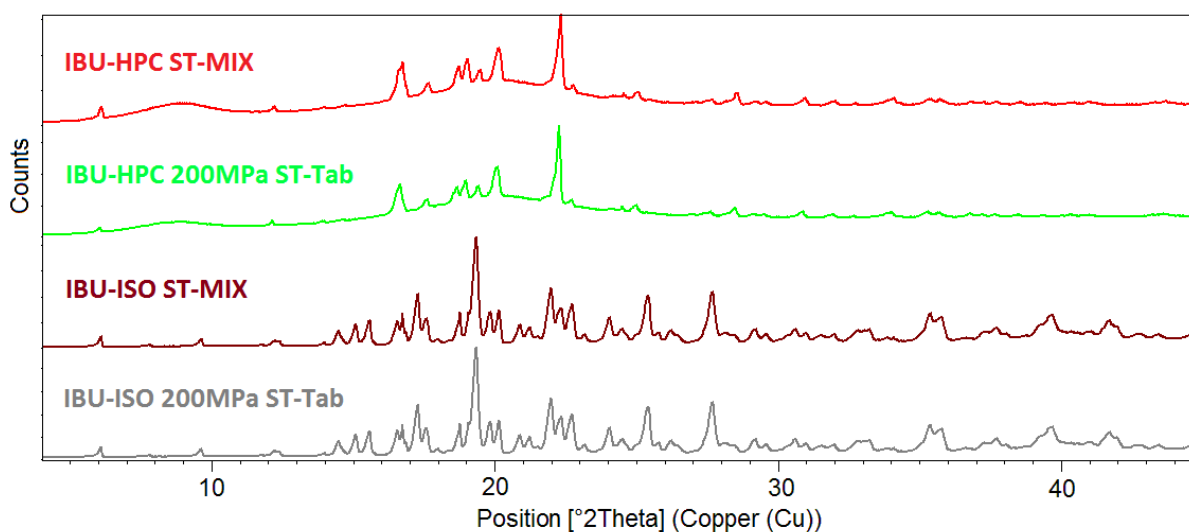


Figure 29 XRPD of 200MPa-compacts and related mixtures

The compacts under less pressure had significantly slower IDRs and consequently slower dissolution rates of the granules at non-sink condition as compared with the release data of high-pressure compacts with the same drug/excipient ratio (Figure 28). A comparison of SFE of same formulations prepared under different pressures, demonstrated a lower total SFE for the 200MPa compacts. The σ_p value of IBU-HPC ST-200MPa compacts was, however, similar to that possessed by 500MPa-compacts (Figure 30).

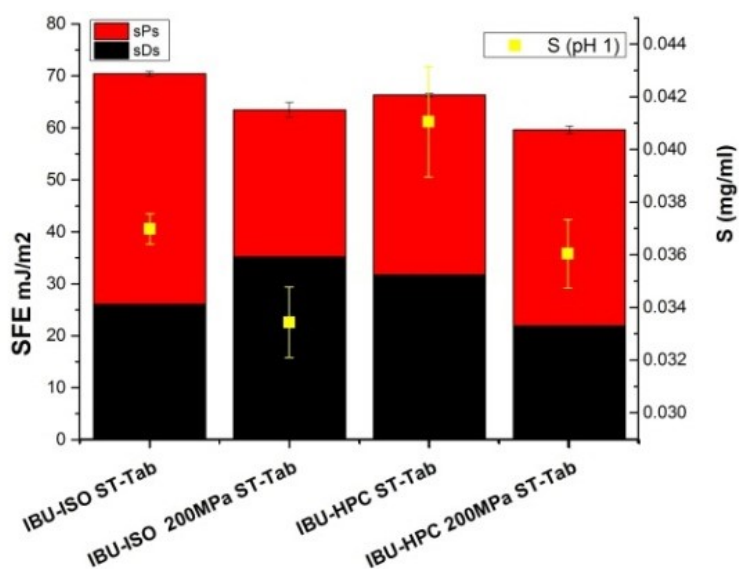


Figure 30 IBU-HPC and IBU-ISO compacts prepared at 200MPa as compared to 500MPa compacts: SFE and saturation solubility

As expected, both compacts of 200MPa displayed higher inner porosities and lower densities than that of 500MPa-compacts (Table 28).

Table 28 The measured porosity and density of IBU-HPC and IBU-ISO ST-compacts prepared by 200MPa

Formulation	Porosity%	Density g/cc
IBU-HPC200 ST-Tab	8.8860 ± 0.311	1.0955 ± 0.0037
IBU-ISO200 ST-Tab	10.333 ± 0.325	1.2562 ± 0.0046

5.3 Discussion

5.3.1 IBU-compacts characteristics

According to OWRK method, London dispersion forces are primarily responsible for the dispersive component, whereas all other forces, including predominantly hydrogen bonding are for the polar interactions. The two-component model of OWRK suggests that the interfacial tension between two phases is ruled by the fact, whether the polar and disperse parts of one phase can interact with analogous parts of the opposite phase. Hence, the calculated SFE and polarity values are exclusively a good indication of the compact surface interaction with aqueous phase [82].

SFE findings were, generally, in consistent with IDR results for the compacts (Chapter4). The different measured values of polar and nonpolar components indicated the variation of the major facets available on the compacts surface. The higher polar component and lower dispersive component for ISO and HPC-

compacts might be ascribed to a higher exposure of polar groups on the surface [73]. These high polarities played the main role causing high works of adhesion, leading to higher wettability.

The dispersive part seems to be, on the other hand, of great important for mannitol and sorbitol compacts. Their lower polarity, as compared to other excipients-compacts, would demonstrate a low value of $\sqrt{\sigma_{sv}^p \sigma_{lv}^p}$ and hence, a small contribution of polar interactions forces to reduce the interfacial tension with water.

The partially IBU amorphous material within the co-milled HPC compacts (4.2.4.1) contributed to increasing the polarity as a higher strength of IBU/HPC interaction is available, which explains the improved wettability as compared to ST-Tab. However, apart from higher interactions of amorphous IBU/HPC, the amorphous material has a higher polarity itself that can be seen from the results obtained for IBU-MQ tablets. Moreover, the dissolved HPC can act decreasing the surface tension of water [50], that would facilitates the contact with low energy surfaces of the hydrophobic drug and ease the wetting process.

Beside the possible changes on surface and shapes, milling can also generate mechanochemically high activated surfaces of the particles, thus a higher SFE obtained. The higher dispersive part exhibited by COM-compacts as compared to their ST-compacts might be related to the greater provided surface area available for contact upon milling, leading to greater dispersion forces. IBU-ISO COM-Tab showed different trend to the other excipients, manifested by a lower polarity than ST-Tab, which could refer to lower abundance of hydrophilic facets on the crystal surfaces as a result of reduction in preferred orientation [73]. The 63% polarity of IBU-ISO ST-Tab indicated a preferable trend to strongly interact with polar entities of water.

Alcohol-sugars can attach on the drug's surface, leading to the formation of more hydrophilic diffusion layers around API particles. Similar effects were reported previously regarding mannitol [15,59]. The polarity values of MANN- and SORB-compacts were significantly higher than of IBU but relatively lower to other compacts; which is critical, as values under 40% can express rather non-wetted solids. Although both mannitol and sorbitol are very water soluble, the process failed however, to produce a high level of interactions as much as with HPC and isomalt. Contact angles of their formulations indicated a mixture of hydrophilic as well as hydrophobic character. IBU might consequently struggle to dissolve out of their

compacts in water, which was presented in slower IDR (Table 6). The smaller contact angles with Diiodomethane confirmed the high dispersive nature of their surfaces energy.

The compacts surface will be characterized by intermolecular bonds between the components and dislocation. As referred by the polarity data, more functional hydrophilic groups that emerge at the surface are presenting in case of HPC- and ISO-compacts [90]. Since the surface tension of water has proportionally a dominant polar component (70%) than dispersive one. Therefore, it is anticipated that HPC and ISO-compacts are easily accessed by water molecules. However, the water molecules might adsorb slower onto MANN and SORB-compacts.

The preformed study of wetting kinetics facilitated understanding the mechanisms of interactions and any variances in the wetting process. The thermodynamic driving force for each wetting process is represented by the corresponded work value [73,134]. Positive values of W_a and W_i , observed for all compacts, are indicative of the spontaneous nature of both adhesion and immersion process with a significant improvement as for pure IBU. However, the negative values of spreading coefficient (spreading pressure) W_s refer that spreading and wetting of aqueous phase on the compacts surface is not complete. The highest W_a values, exhibited by IBU-ISO Tabs with a superiority for ST-compacts as compared to other compacts, specified stronger interactions with water so that a high work must be executed on the interface solid/water area to reversibly separate them [81,135]. Their highest W_i indicated a better spreadability of water than other formulations, and that water covered the compact's surface without changing the initially area of liquid-gas interface to a big extent [81,134,135]. This improved immersion process was reflected for IBU-isomalt and IBU-HPC formulations in the faster initial dissolution rates as well as the fast initial uptakes of water by Tensiometer and may have contributed to the higher values of slope from IDR test. A complicated difficult change of the solid-vapour interface to solid-liquid interface could be stated for pure IBU-compacts, due to the too low W_i value.

The calculated kinetics revealed that, strong adhesion and immersion of water were obtained over the surface for the formulations with highest SFEs and polarities.

The relationship between the enhanced IDR and wetting kinetics are thought to depend on the compacts composition; the strength of changes in physicochemical properties such as crystalline form and/or preparation steps (with or without milling). Lippold *et al.* reported a linear increase of the effective surface area A_{ef} by decreasing the measured contact angle down to 40 degrees for hydrophobic drugs[136]. The

smaller contact angles of ISO and HPC-compacts can then be associated with bigger effective areas and thus, faster releases of IBU. This linear correlation is however, conditional on the assumption that the boundary layer thickness is constant.

The correlation between the wettability findings and IDR might establish a tool to predict whether the proposed approach will be effective or not, directly from the analysis of drug and excipient structures and their ability to interact by calculating the polar component of SFE. Buckton determined that powders are capable to disperse and immerse into water, when obtaining spreading pressure values > -23.2 mN/m, which corresponds to the dispersion component of water σ_{lv}^d [137,138]. Accordingly, all tested compacts showed rather the ability for water spreading, due to the W_s values exhibited. However, the water might not have a sufficient force to spread appropriately on IBU-SORB and IBU-MANN compacts (especially IBU-SORB ST-Tab) as they revealed relatively lower W_s . The neat IBU is almost impossible to wet because of the large difference between the provided water's driving force (23.2 mN/m) and the required force for water spreading on IBU compacts (68 mN/m). The high W_s values of ISO- and HPC-compacts, close to zero, suggested that the dispersion process can take place without a resistance [81,138].

The induced crystal modifications or new molecular orientation [139] and/or the higher strength of drug/excipient interactions can explain the changes in the physical surface properties for the compacts and be responsible for showing different contact angles. The wetting assessment helped as an indication of the interactions level between formulation components.

The time of drop shape measurement was fixed to 60 seconds after placing of the drop on the compacts surface to avoid any problem regarding the surface's structural integrity (swelling or deformation). However, the dynamic nature of contact angle should not be negligible, as the reduction of the initial contact angle θ for water as a function of time was not identical for all formulations. This effect was more obvious for HPC compacts. After water came in contact with HPC-compacts, θ gradually decreased to some extent. The surface of a polymeric system would move rapidly after contacting water to minimize the interfacial free energy, leading to a decrease in θ [82]. Furthermore, the penetration of the drop below the surface into the compact bulk and the reorientation of interface's molecules could be generally also responsible for the dynamic decrease of θ . The mentioned factors might have been involved in producing underestimated apparent θ for the IBU-HPC 200MPa-compacts, which were additionally categorized with a higher porosity. Nevertheless, the outcomes of drop shape analysis are capable to describe the nature

of solid's interaction with a specific liquid [137], and to reveal differences among samples or different arrangements of crystals packing. It represents a good empirical assessment of the solid wettability.

Although SFE describes the energetics of total compacts surfaces, but it might fail to represent the energy of each crystal lattice, which is usually reflected in the aqueous solubility values. This is important, considering that the dissolution rate of the compact can be estimated to be the sum of dissolution rates of all individual crystal planes. Hence, some inconsistencies could be found between SFE and solubility or dissolution results.

No method could be considered as an ideal method for the measurement of contact angles. Thus, the results are relative and highly dependent on the applied method. A reasonable degree of agreement was obtained within both applied methods. The same trend of θ values was noticed for all formulations, but with higher values obtained invariably from Washburn approach, that indicated the higher wetting tendency for IBU-ISO ST-compacts (Figure 20). The same observation was reported earlier [81,135,138], confirming the relative nature of wetting studies.

As water will often not penetrate into a hydrophobic powder [82,135], the water failed to wet pure IBU compact and a very low mass was adsorbed over time. The Washburn liquid penetration is not suitable to be applied when contact angles are larger than 90° ; or there is a variation of the effective pore size within the powder bed or the sample has internal pores [139]. On the other hand, the fast rate of adsorption for IBU-ISO and IBU-HPC compacts indicated the rapid water uptake from the solid surface. The amount of water sorption was identical for COM-Tabs with HPC and ISO. Both formulations seemed to have a similar number of binding sites on the solid, which controls the interaction and the arrangement of water molecules. However, different solids with various hydrophobic natures might show similar amount of water adsorption but bind differentially [82,135].

The contact angle was reduced for co-milled compacts of MANN and SORB as compared to ST-compacts -, by over 18% and about 3% respectively, indicating the improved drug surface wetting when co-milling is introduced into the process.

As FTIR analysis referred, the relatively low wavenumber of C=O for pure IBU relates to the stable IBU dimeric form [127]. IBU-molecules can undergo self-association, where the carboxylic acid groups form H-bonding through cyclic symmetric acid-acid dimers. Accordingly, the absorption band of OH was also seen

at a lower frequency, whereas the non-hydrogen bonded OH groups possess normally a strong sharp absorption in a higher range 3700-3584 cm^{-1} .

Upon compaction, the internal H-bonds between IBU molecules seemed to become weaker or be broken. Thus, the blueshift of absorption band C=O for the compacts might imply that, the dimeric structure of IBU was damaged and the most carbonyl groups are no longer hydrogen-bonded with IBU OH groups [125,127].

Taking into account that the free non H-bonded C=O is normally associated with a band around 1735 cm^{-1} [109]. The C=O band for the compacts was yet at a relatively low frequency. This can relate to the simultaneously new formed H-bonds of IBU with the excipient that can be estimated from the observed broadening of OH stretching band. However, the presence of defined peak and the minor shifting of C=O indicated limited interactions involving the carbonyl moiety in IBU molecule.

IBU can act either as HBA or HBD [140]. HPC was reported as HBA [141]. For HPC ST-compacts, both the position and the apparent broadening nature of stretching OH for IBU and HPC are characteristic of H-bonded hydroxyl groups.

The apparent change of both C=O and OH bands implied the participation of these moieties (to less extent regarding C=O) in IBU/HPC interactions for the compacts system, which might explain the higher polarity for the compacts surfaces and consequently the faster IDR. Regarding IBU-HPC COM-Tab, the broader less defined nature of several functional bands of IBU, including the fingerprint region, indicated amorphous-rich regions of IBU. In addition, the mentioned broadening at 2953 and 1715 cm^{-1} is indicative of higher intermolecular H-bonds between IBU and HPC, resulting from IBU availability in an amorphous state. The presence of amorphous fraction may lead to a loss in specific vibrational modes or to more widely spread vibrational modes as compared to more condensed restricted vibrations of IBU crystals [130], which in turn resulted in the loss of peaks and broadening in the fingerprint region.

The merging or masking of some IBU bands in IR spectra collected for IBU-HPC compacts, in particular of the co-milled, might imply high molecularly interactions and that the IBU molecules dissolved to some extent into HPC matrix, mainly through H-bonding interactions. For example, the CH and CH₂ stretching bands of HPC (and also of ISO) superimposed over the OH-stretching band of IBU.

For pure alcohol-sugars, the broader nature of OH-stretching vibrations is an evidence of the distribution of these groups over different sites, showing varied internal interactions between OH-groups [132]. After the compaction with isomalt, mannitol or sorbitol, the OH-stretching region of ibuprofen was much

broadened, indicating the presence of intermolecular hydrogen-bonding involving OH groups. The H-bonding of OH is normally accompanied with a shift of corresponding stretching bands to a lower frequency (3550-3200 cm^{-1}), exhibiting a broad nature.

The less degree of changes in IBU characteristic peaks, in the spectra of MANN and SORB compacts, indicated to less IBU/excipients interactions as compared with HPC and ISO, which is in agreement to the findings obtained from both XRPD and DSC measurements.

In general, a higher intensity of blueshift for the carbonyl band was recorded with COM-compacts of ISO, SORB and MANN as compared to the ST counterparts, referring to a more intensive damage of the IBU dimer structure. Nevertheless, the vibration peaks around 2630 and 2730 cm^{-1} , related to cyclic dimerized OH groups, were still presenting (but to less extent) in ISO, MANN and SORB-compacts. Hence, the dimeric-IBU still partially exists. The drug/ excipient interaction degree would be affected by the particle size and available contact area of both components upon compaction. This will clarify that IBU dimers may still be remaining and why, for example, the compacts of co-milled mixtures showed a higher damage of IBU dimers.

Moreover, the intensity of some peaks for ST-compacts was not as high as for COM-compacts, which indicated the availability of different solid-state in each system. Due to different changes induced of the crystalline IBU within the compacts, different conformation arrangements are generated. Hence, various intermolecular forces were obtained and reflected in different FTIR spectra.

Since the level of interaction controls the strength of change induced, a higher extent of interaction can be considered for IBU-HPC compacts and especially for COM-Tab, which is in line with higher amorphization [71]. The intensity of interactions within the compacts was in the following order: HPC COM > IBU HPC ST > IBU ISO > IBU MANN, which coincided with the SFE results, and directly matched with the IDR enhancement. Interestingly, the same order was also obtained from SEM, XRPD in term of the degree of crystal modification (see chapter 4). In this context, the presence of specific parts within API molecules that can be either protonated or deprotonated (like ibuprofen) is crucial to obtain a high potential of interactions.

The low porosity for the compressed samples can be considered as preferable for wetting studies and IDR experiments, because the interference of water penetration through the pores and capillaries is limited.

The application of high-pressure boosts an increase in the molecules density per unit volume, as the ingredients are forced together, with removing of voids which would otherwise contain air.

Generally, an optimization of the procedure for IDR testing must be considered to minimize the interference of porosity%. According to USP 38, the compression at 15 MPa for 1 minute is suggested to be sufficient to prepare IDR-disk for many crystalline compounds. Nevertheless, it was referred to the necessity to evaluate the formation of capillaries and individually adjust the procedure depending on the tested substance. The IDR values might be overestimated for the compacts prepared with a relatively low pressure, due to some erosions of the surface during the test. Herewith and for a certain substance, more investigations are required to specify the most appropriate pressure, by which the intrinsic properties of ingredients are expressed, excluding any change in the physical properties. More informative IDR values will then be obtained, which would optimize the interpretation of IDR values and the correlation to the formulations properties.

By comparison of measured porosity values for all compacts, no remarkable differences could be found and all values were relatively low. Thus, the porosity as a total might not have played a crucial role in the observed dissolution process. However, the more porous structure for IBU-ISO ST-Tab could, to a small extent, interfere with the contact angle studies, and might affect the water sorption rate.

In spite of similar porosities revealed by all formulations, the pores geometry and shape could vary and hence affecting the dissolution. SEM images displayed, in most of the cases, very fine irregular-structures pores that were hardly to be distinguished.

The different densities (true and apparent), exhibited by COM-mixtures, indicated changes in the crystal form or crystal habits as compared to ST-mixtures. The co-milled particles were characterized with extremely fine particles with polyhedral aspects, they might have a higher ability to impend each other and be consolidated, that led to fill the small intra-spaces; decrease the voids volume, and consequently to low porosities. The higher ability of densification for COM-mixtures resulted in higher values of the true density than exhibited by ST-mixtures and accordingly in higher COM-tablet densities.

Additionally, the higher density displayed by IBU-HPC COM-Tab as to ST-Tab can be particularly related to the partial presence of the amorphous material that has higher compressibility. The same can stand regarding the low porosity of IBU-MQ Tab. IBU crystallized out from the molten phase as a very fine powder which had significantly, as seen by PSD analysis, smaller particle size as compared to the crystalline form.

Based on laser diffraction analysis, the micronization influence of triturating was obvious using the oscillating mill. The measured big size of sorbitol particles without co-milling might hinder a high level of interactions with IBU within the ST-compacts; the same was noted but to a less degree with mannitol. A certain range of particle size of both ingredients might be required to facilitate the interactions; taking the increased interactions accompanied the co-milled formulations of MANN and SORB into account; whose mixtures showed the highest intensity of particle size reduction.

The porosity, total pore surface area and median pore diameter can affect the drug dissolution rate, but they undergo some changes during the dissolution test. Thus, a future in-situ investigation during the dissolution test might be important to correlate the changes with dissolution behaviours. By comparison between the pores size distribution graphics of Mercury porosimeter for the tablets and the values of r_{50} or $d_{average}$, the $d_{average}$ calculation appeared to be more reliable. The Mercury data indicated that the co-milling process led to a decrease in the porosity, pores size and pores surface area except for sorbitol-compacts, where the total pore surface areas did not match the same order of porosity values. However, a higher porosity does not always mean a higher specific surface area [142], and a higher porosity does not always correlate with a bigger median pore diameter [69].

As can be seen in Figure 23, the intrusion of mercury was still continuing at high values of pressure and did not demonstrate a plateau level. Hence, the volume readings could be early done before equilibrium, which can lead to smaller pores sizes and volumes measured [143]. Thus, the real total porosities may be higher than measured in Table 21 that showed underestimated values.

The higher pore surface area, exhibited by ST-tablets, might be related to a higher amount of the entrapped mercury inside pores, where the inner pore diameter and dimensions are sometimes larger than pore entrance diameter, i.e., Ink-well shape of pores. The presence of this pores shape can explain the high values of total pore surface areas, deviating significantly from the specific surface areas determined by the gas adsorption method (BET technique) that showed lower values. A high-pressure is required to enable the mercury intrusion through a narrow entrance into the big inner pore dimensions, which will be estimated as a large volume intruded inside the narrow pores, resulting in calculation of extremely high surface areas. This observation was reported by Costa *et al* [69].

The obstruction of mercury flow, through the small pore channels, can be primary the factor that led to small porosity values for COM-Tabs. The SEM images showed a smother surface for COM-tablets referring

to their tiny pores entrance diameters. Regarding IBU-ISO ST-Tab, the measured frequency of pore range 2-10 nm might rather relate to more pores having a big inner shape with 2-10 nm entrances.

The same porosity rank order was reflected in the results of mercury porosimetry for the tablets and related granules, but the values were obviously lower for the granules. In general, lower porosities and pore sizes were also observed for COM-granules. Nevertheless, the data obtained from the granules revealed some differences as compared to that of the results obtained from tablets regarding the measured densities. The obtained values of bulk and apparent densities, for the co-milled granules as well as IBU-HPC ST-granules, were not rational or comparable to the measured values of the compacts as seen in 5.2.3.

However, the higher total areas of pore surfaces for COM-granules indicate larger wettable contact surfaces with the release medium and contributed mostly to the faster drug releases for COM-granules than ST-granules. The results were compatible with BET data for the granules, where the specific surface areas of COM-granules were also higher. This was correlated with the first 15 min of the dissolution test in case of HPC, MANN and SORB COM-granules. On the other hand, the higher porosities and bigger pore diameters of ST-granules can compensate the effect of lower total surface areas [69].

Generally, there are some important limitations by the mercury porosimetry [143] that should be considered and can lead to some errors within the data, such as the considered pores geometry and shape, the presence of very small pores and the rough precision of density measurement. Despite these limitations, the analysis is useful for comparison studies.

The low value of specific area obtained for IBU-SORB ST-granules by BET could contribute to the slower power of their dissolution rate. Considering that the granules examined were rather uniform in term of granules size, the analysis of the specific surface area can indicate their dissimilar surface porosity and morphology, even when the differences in IBU release were sometimes not significant.

As mentioned, the high mechanical forces applied upon compacting might induce a reduction in the particle size. Additionally, the milling process showed a significant decrease in the particle size and an increase in specific surface area that might influence the dissolution process. However, the impact of particle size could be offset after compaction regarding IDR testing [89]. The porosity and specific surface area data indicated an increase in specific surface area and a decrease in the total porosity for the co-

milled formulations. Although SEM images did not reveal a plenty of surface pores possessed by the COM-compacts, the BET data might be linked to a high percentage of broken defected facets that led to higher specific surface areas values.

The higher values of specific area, obtained for some tested co-milled mixtures as compared to their granules, could explain their higher release rates at the initial time of dissolution testing (Figure 8).

The low compression pressure (200MPa) correlated with a higher porosity, which might lead to an easier penetration of the medium through the particles of the compact. However, the calculated SFEs referred to less intermolecular interactions triggered upon compaction with 200MPa that was reflected in lower IDR values. The compaction, accomplished by a lower pressure, might be insufficient to extensively induce any crystal modifications expressed in -an insignificant number of crystal defects or to ensure a high degree of IBU/excipient interactions. The lower values of solubility for 200MPa-compacts were compatible with the IDR studies.

Although the IBU-HPC ST 200MPa compacts exhibited bigger contact angles with water but they showed also bigger angles with Diiodomethane. Their σ_{sv}^p was consequently similar to that of 500MPa as a percentage of the total measured energy. This indicates that the total values of SFE should be considered when evaluating the polar component values. It might refer to some deficiencies or shortcomings accompanied by the estimation using this method. However, the overall porosity for the 200MPa-compacts was higher compared to the 500MPa-compacts. The higher porosity might interfere with contact angle measurements through the higher sorption force of water, leading consequently to smaller contact angles. In addition, other factors can interfere considering the polymer systems, which were mentioned already and can involve in the dynamic decrease of contact angles.

The difference of IDR could be undervalued between the IBU-HPC compacts prepared at different pressures. The presence of HPC could be responsible to form a small gel-like layer on the surface during the test. The formatted layer might represent a diffusion layer, through which the drug has to diffuse before being released and dissolved. This may affect the dissolution process resulting in underestimated IDR values for the 500MPa-Tablets.

5.3.2 Effect of pure excipients

The superiority of HPC-formulations to increase the solubility and IDR was observed to less extent at pH 5.5, which might indicate to a more pronounced influence of the excipient's properties at pH < pKa of IBU, i.e. before any significant ionization.

The adhesion process was spontaneous for all pure excipients; this was confirmed by the Wa values calculated for individual excipients.

In general, the contact angles with water for IBU/excipient compacts increased as the level of excipient content was reduced (Figure 26), with mainly a linear regression only for the MANN and SORB-compacts. Hence, the amount of these mentioned excipients seemed to be the dominant factor controlling the wettability properties of the tablets.

The varied extent of dissolution increase using various sugar-alcohols can be attributed to differences in their own hydrophilicity, which may have affected the overall wetting of the IBU-compacts. Among sugar-compacts, the pure ISO showed the lowest contact angles with water. The improvement of wettability for the compacts was correlated to some extent with the individual wettability of the pure excipient used. Mannitol and sorbitol are isomers and their pure compacts revealed similar wettabilities; nevertheless, the smaller contact angles exhibited by IBU-MANN compacts could be as a result of more available planes of OH groups for MANN related to the crystal habit and particle size, which could be responsible for showing stronger polar interactions with IBU as compared to neat sorbitol. The OH stretching band for pure sorbitol was even broader than that for IBU-SORB compacts, reflecting a higher degree of inter/intramolecular H-bonds between the sorbitol's molecules. This may explain the lower polarity obtained for IBU-SORB Tabs as to pure sorbitol tablets. Sorbitol failed to intensively interact with IBU, thus a lower effectiveness on solubility and dissolution was obtained.

The compacts with 60% excipient's load exhibited lower Wa values as compared with 80%, tablets, confirming that the introduction of a higher level of the polymer or soluble polyol to IBU improved the wettability of the composite.

The high density of the compact and the suitable amount of the excipient can assure a better contact between the drug and excipient particles that leads to intense interactions and a higher released energy. Therefore, a certain IBU/excipient ratio (in our case 1:4) is necessary to provide an optimal environment for higher drug/excipient interactions. The data certified the importance of an appropriate level of the hydrophilic carriers to achieve better wetting characteristics, and/or to modulate crystal modifications with a higher released energy.

The developed IDR method for pure excipients cannot be considered as applicable method for polymers, due to the prolongation of dissolution process after the formation of a gel-layer. HPC has both hydrophilic

and hydrophobic groups and was reported to form Gel-like layers (specified with hydrated HPC upon contacting water. Thus, it can also be used for extended release formulations [53]. The signals recorded during testing of neat HPC-Tabs might relate to the water leakage through the disks.

However, the IDR results of sugar-alcohols confirmed the dependence of the systems performance on properties of the pure carrier (concentration; SFE; polarity and IDR). The IDR of the three sugar-alcohols correlated to some degree with IDR values of their corresponding formulations (Figure 31). However, more tests with plenty of excipients have to be done to establish certain correlations.

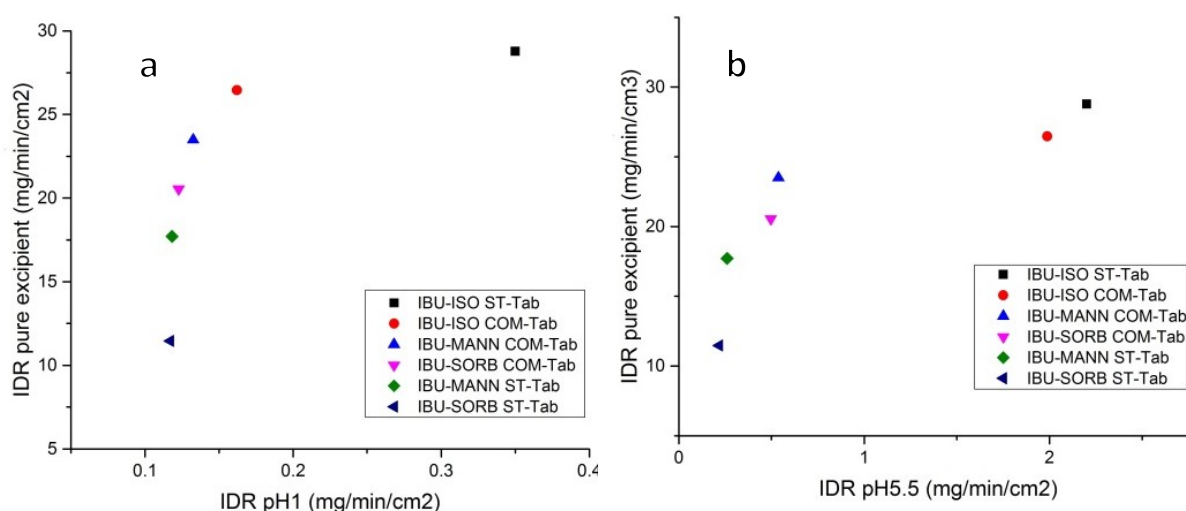


Figure 31 IDR (compacts)-IDR (pure excipient) correlation at (a) pH 1.0 and (b) pH 5.5

Moreover, the CheqSol data showed significant differences of solubility in respect of the used excipient. The presence of all tested excipients increased the intrinsic as well as kinetic solubilities of IBU, confirming the solubilizing efficacy of these excipients. The measured kinetic solubilities were varied but greater than their equilibrium solubilities, confirming that IBU undergoes a certain degree of supersaturation. The exhibited strength of excipient to increase the intrinsic solubility of IBU was in the following rank: HPC > ISO > MANN > SORB and the values were significantly different. The same order was seen for the IDR analysis. As compared to the intrinsic solubility of IBU, a higher supersaturation ratio was assigned to the formulations of HPC, ISO, and mannitol as that of sorbitol.

Since the assay of CheqSol starts where API is dissolved and ionized, the properties related to the processing history will be blinded and eliminated. By application of CheqSol, the influence of excipients that are presenting and dissolving in media could be investigated on the drug supersaturation ratio and

intrinsic solubility. The solubility of IBU increased by around 39% and 22% for HPC and ISO formulations respectively as compared to pure IBU. A less significant increase was found regarding the kinetic solubility (9%).

In general, ISO, MANN and HPC formulations showed to some extent the ability to maintain the supersaturation state without an acute precipitation (spring and parachute aspect) as it presented the lowest differences between the measured kinetic and intrinsic solubilities. These obtained information provided a crucial insight about the impact of each excipient on the solubility. The results confirmed that CheqSol is valuable to determine the enhancement of solubility of certain API, induced by solubilizing excipients, which was also demonstrated by other studies [113].

A big deviation in the obtained K_s was noted; this was also reported by Etherson *et al* [113]. In the current research, a poor index and correlation to the intrinsic solubility could be provided from the K_s data. The kinetic solubility is however, less reproducible and strongly affected by the experimental conditions. Hence, the K_s values failed to be a reliable guide to the intrinsic solubility values and are considered as variable, when high-quality solubilities are required [112].

The estimated values of solubility by CheqSol method differentiated from the saturation solubilities obtained by the shake flask method. However, both delivered the same trend in term of excipient's impact on the solubility increase. A good agreement was obtained between the solubility values measured for pure drugs by CheqSol and that published in the literature [112,113]. Nevertheless, no comparisons were reported for the API/excipient mixtures. Moreover, some major deviations of the S_0 measured by CheqSol were also reported as compared to the computed calculated or published values [144] [43].

5.3.3 Principle component analysis PCA of IBU-compacts

The selected dataset that was obtained for the 8 compacts formulation regarding 30 variables (that were measured and reported in this and the former chapters) was investigated by PCA. PCA was used to reveal relationships between the variables themselves and between the variables and observations (the compacts) focusing on the performance in terms of IDR values. The PCA analysis, including initially the IDR values as a variable, revealed high correlations between IDR at pH 1.0 and solubility factors; intrinsic solubility; T_m onset reduction to pure IBU and to some extent with IDR of pure excipients. The IDR at pH 5.5 was additionally highly correlated with SFE, W_a and σ^p values.

Based on the initial PCA correlation matrix, the multiple measured variables could be reduced to 14 that can affect the IDR values, and still explain all variances in the matrix of the original variables. Therefore, the following 14 factors were included in a further PCA analysis: SFE; solubility factor; W_a ; water sorption; σ^d ; porosity; pore radius; amorphousity%; K_s ; T_m onset reduction to pure IBU; T_m onset reduction to the related mixture; IDR excipient; σ^p excipient and W_a excipient. Some data were presented in the previous chapter (Table 6, Table 7, Table 9 and Table 11).

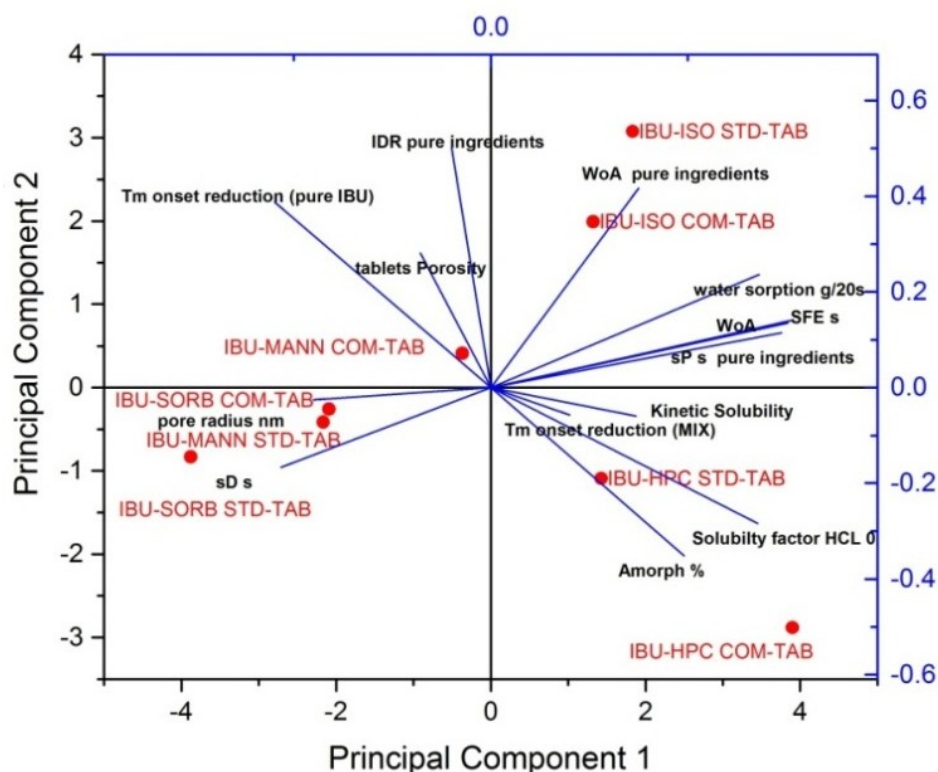


Figure 32 Biplot of all IBU-tablets for PC1 and PC2

The PCA of the 14 variables is demonstrated in Figure 32. The biplot shows both the loadings each variable (coefficients of PCs, as blue lines) and the projection of all observations scores (as red spots) for the first two selected principle components PC1 & PC2 in parallel. Each red point represents a compact formulation in the original data. The scores of each observation, obtained for PC1 and PC2, described around 70% of the diversity in the descriptor space. The vectors, corresponding to σ^p pure ingredients; W_a ; SFE; kinetic solubility and inverse pore radius, aligned with the x-axis (i.e. they have similar heavy loadings for PC1). The vectors corresponding to IDR excipient and tablet porosity aligned more with the y-axis. The other variables were more evenly distributed.

The formulations covered all four quadrants of the PCA plot (biplot), confirming the physicochemical heterogeneity of the dataset. Dominant patterns and major trends in the data were obtained. The IBU-HPC compacts, which showed the highest IDR values, were clustered around amorphousness; solubility factor; kinetic solubility and T_m onset reduction; indicating the dominant influence of these factors to induce higher IDR values. While the IBU-ISO formulations depended more on W_a pure ingredient; SFE; W_a ; water sorption and σ^p excipient. The ST-compacts for MANN and SORB were more affected by σ^d and the pores radius.

5.4 Conclusion

The compaction of IBU with polyols or with HPC applying high-pressure generated certain modifications in the surface nature. This modified nature was manifested by the exposure of more polar functional groups on the solid surface and was represented in the high ultimate surface energetics and wettability of the tablets as obtained from SFE studies. The highest magnitude of increase in tablets polarity was for ISO-compacts and was even more pronounced for the formulation compacted without a prior co-milling process. HPC-compacts demonstrated also high polarity; however, with higher values for the co-milled formulation due to the partial presence of IBU in the amorphous form.

Wetting studies suggest a higher strength of interactions produced between the adjacent components IBU/excipient in the formed matrix, especially for HPC- and ISO-tablets, that possessed accordingly a higher degree of solid/water interactions. This was reflected particularly from a pharmaceutical point of view by an improvement in the wetting kinetics.

As FTIR data referred, the main IBU/excipient interactions occur preferentially via H-bonding at the OH groups' level, which was identified by the apparent broadening of OH stretching vibration of both components in the compacts system as compared to the pure ingredients. The coexistence of the hydrophilic excipients, particularly HPC, could hinder the self-association of IBU molecules, obstructing its dimers-form for the favor of new IBU-excipient interactions.

FTIR data also confirmed the crystal modification of IBU within the compacts that was suggested previously based on XRPD, DSC and SEM analyses. The conversion to IBU amorphous form for the co-milled compacts of HPC contributed with inducing higher drug/ excipient interactions and wettability.

For the prepared compacts, the dissolution process can be considered as carrier dependent as well as drug dependent process. The properties of the used excipient are crucial for forming a high level of interactions with IBU, and are determinant of the overall generated effects regarding the compacts

wettability and dissolution performances. The intensity degree of the proposed process to increase the wettability and IDR appeared to be as a function of: a higher excipient load, higher solubilizing efficacy of the excipient to produce supersaturation state of IBU and last but not least, higher IDR of pure excipient for the sugar-alcohols. In this context, the new IDR developed procedure was successfully implemented to quantify the mass dissolved of pure polyols-disks.

The low values of tablets porosity as well as small pore sizes obtained underlined the importance of the applying IDR test with certain pressure to demonstrate and stress only the intrinsic properties of IBU within the solid compacts.

Based on PCA, the high amorphousity, solubility factor, kinetic solubility and the reduction of T_m onset were more potent factors relevant to higher IDR values.

The results of this chapter suggest an ability to modify and manipulate the surface properties of binary mixtures per high-pressure compaction, which would provide an efficacious advantage to the pharmaceutical industry regarding poorly soluble drugs.

6 The evaluation of application of high-pressure compaction employing nonfunctional excipients as a process to improve solubility and dissolution. A case study with indomethacin

6.1 Introduction

The design of solid formulations, based on high-pressure compression of binary mixtures consisting of an API and a nonfunctional hydrophilic excipient that has polar groups, was proposed as a new technique to improve solubility and/or dissolution rate of borderline poorly soluble drugs. Ibuprofen was chosen and tested as the first drug model and four excipients were also selected (isomalt, mannitol, sorbitol and HPC) and examined (see Chapters 45). The impact of the proposed technique was investigated and the approach revealed an ability to generate IBU/ excipient interactions and to manipulate either the IBU solid-state and/ or the compacts surface properties.

The previous results revealed promising improvement of solubility and dissolution rate of IBU with pH-independent water-soluble polymer HPC-SSL and isomalt as polyols. In this chapter, the effectiveness of the technique was further investigated with another weak acid (indomethacin IDM) using isomalt as sugar-alcohol based model excipient and applying another polymer, namely vinylpyrrolidone vinyl-acetate copolymers PVPVA as polymeric model excipient.

IDM has one proton donor site that linked to the OH group, in addition to 4 hydrogen bonding acceptors, which together make IDM a good candidate for this approach in respect to the potential API/excipient interactions. Additionally, IDM can present in different polymorphic forms that have different values of solubility (see Chapter 3). Depending on these last two aspects, it is important to address, whether observations, influences and correlations will be obtained for IDM, which are similar to what collected applying the technique on IBU-binary mixtures. This confirms the previous interpretations and expected mechanisms for improving the solubility and release profiles.

Different formulations of IDM were produced by direct compression under high-pressure (500MPa) with and without a previous co-milling process and evaluated. The potential benefits of the process as well as the effect of processing and formulation on IDM solubility and dissolutions rate was investigated. The formulations tested in this chapter are listed in Table 2. The release of IDM, out of the compacts prepared, was correlated to the influencing factors and the differential solid properties.

6.2 Results

6.2.1 Dissolution studies of IDM-compacts

A similar tendency of IDR was resulted in both media (Figure 33). The IDR as well as the non-Sink dissolution studies (Figure 34) showed faster dissolution rates for the compacts than the pure IDM, where the IDR increase was statistically significant. Only IDM-ISO COM-Tab, which had the slowest IDR, revealed no significant difference with IDR of pure IDM at pH 1.0.

IDR factors were calculated as the increase of IDR of the compacts compared to pure IDM. Among the formulations tested, faster superior dissolution rates were obtained for PVPVA-compacts compared to isomalt-compacts, with significant differences that were noticeable in the acidic medium (Table 29). On the other hand, IDR values of PVPVA- and ISO-formulations were much closer at pH 5.5, where IDM is partially ionized, showing no significant differences between IDM-PVPVA COM-Tab, IDM-PVPVA ST-Tab, and IDM-ISO ST-Tab. However, IDM-PVPVA COM-Tab displayed the highest dissolution rate. ANOVA analysis showed that, IDM-ISO ST-Tab differed significantly from the related COM-compacts by a comparative assessment at pH 1.0 and pH 5.5.

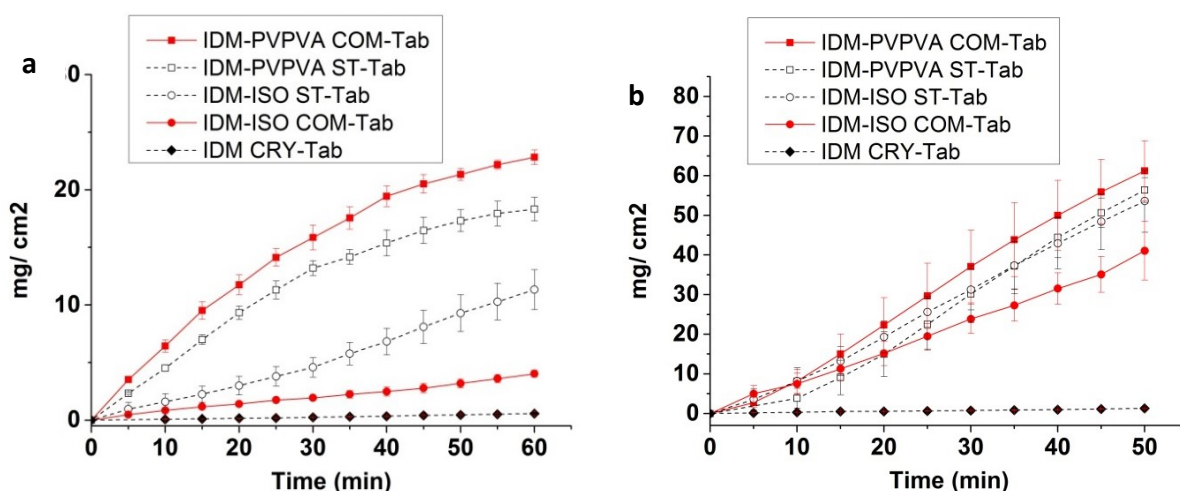


Figure 33 Intrinsic Dissolution profiles of IDM formulations using modified USP apparatus 1 at 100 rpm; medium volume 900 ml of (a) pH 1.0; (b) pH 5.5; mean \pm SD; n = 3

The influence of high-pressure compaction of binary mixtures on the release behavior of IDM was investigated as shown in (Figure 34). Accelerated release kinetics as well as higher release amounts were observed for IDM out of the granules as compared to neat IDM at both pH values. The same was obtained as compared to the related mixtures in case of ST-formulations for both excipients in both media; but with a less significant increase for ISO ST-Tab at pH 5.5.

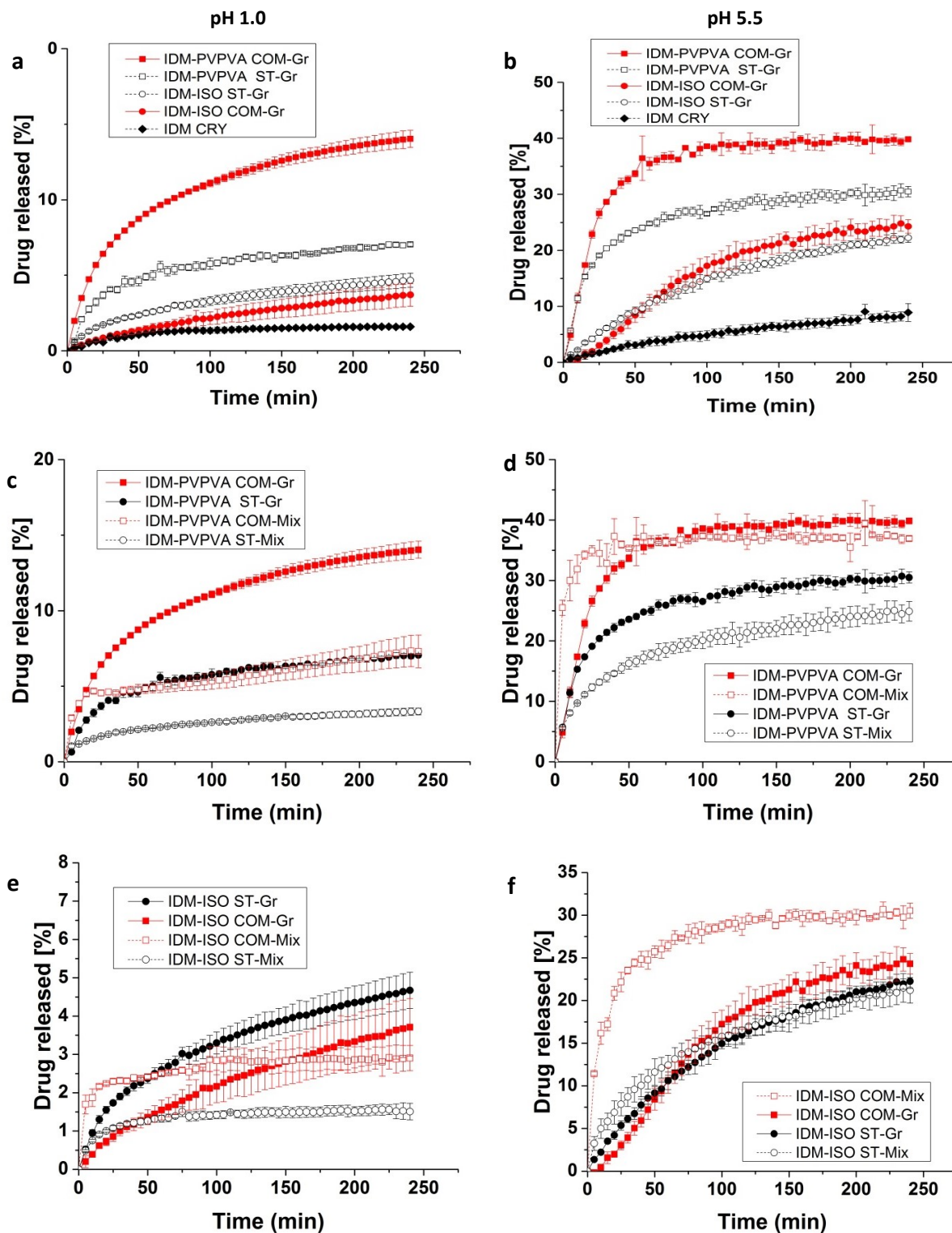


Figure 34 Dissolution profiles of IDM compacts granules as compared to related mixtures using USP apparatus 1 (basket) at 100 rpm; medium volume of 900 ml at pH 1.0 and pH 5.5, a & b: all granules compared to neat IDM, c & d IDM-PVPVA, e & f: IDM-ISO; mean \pm SD; n = 3

The co-milled granules of PVPVA showed a faster release than the corresponding mixture at pH 1.0, whereas a similar dissolution was observed at pH 5.5, with a faster initial release of co-milled mixture during the first 20 minutes. On the other hand, the co-milled mixture of isomalt showed a higher release than produced granules for the first 2 hours at pH 1.0 and obviously superior to the granules at pH 5.5. The end-point was, however, higher for the granules at pH 1.0.,

Some visual changes were observed during the dissolution test of IDM-PVPVA co-milled mixture at pH 1.0, the dissolution medium was whitey-yellow during the first minutes, then the yellow color became less intense (after 10 min) and the solutions became turbid.

Table 29 Intrinsic dissolution rates of indomethacin formulations and pure IDM

Formulation	IDR	IDR	IDR factor	IDR factor
	pH 1.0 mg/min/cm ²	pH 5.5 mg/min/cm ²	pH 1.0	pH 5.5
IDM-PVPVA ST-Tab	0.3528 ± 0.0224	1.2342 ± 0.0625	38.1	50.6
IDM-PVPVA COM-Tab	0.4253 ± 0.0136	1.3031 ± 0.1708	45.9	53.4
IDM-ISO ST-Tab	0.1804 ± 0.0314	1.1124 ± 0.1640	19.5	45.6
IDM-ISO COM-Tab	0.0595 ± 0.0120	0.7973 ± 0.1259	6.4	32.7
IDM-Tab	0.0093 ± 0.0012	0.0244 ± 0.0010		

6.2.2 Saturation Solubility of IDM-formulations

Table 30 Solubility factors of IDM formulations (physical mixtures, granules) and pure IDM

Formulation	Solubility factor	Solubility factor	Solubility factor	Solubility factor
	Mix (pH 1.0)	Gr (pH 1.0)	Mix (pH 5.5)	Gr (pH 5.5)
IDM-PVPVA ST-TAB	1.904	3.019	1.900	2.539
IDM-PVPVA COM-TAB	2.125	3.101	2.745	2.978
IDM-ISO ST-TAB	1.092	2.229	1.725	1.966
IDM-ISO COM-TAB	1.154	1.857	2.297	2.047

Mix physical mixture, Gr granules

The saturation solubility of IDM was measured to be 1.5 and 12 µg/ml at pH 1.0 and pH 5.5 respectively. The experimentally measured solubilities of IDM out of the granules were significantly greater than that of pure IDM in both media at room temperature and over a period of 7 days. All results are summarized in Appendix; Table 58.

At pH 1.0, the measurements revealed a significant improvement of the IDM equilibrium solubility for the investigated granules as compared to the corresponding mixtures (Table 30). A similar trend was obtained at pH 5.5, except for the case for IDM-ISO COM-granules; where the related co-milled mixture showed a

higher increase of solubility. However, the differences were not significant in this medium between the granules of IDM-ISO ST, IDM-ISO COM, IDM-PVPVA COM and the related mixture respectively.

Similar to IDR data, the compacts with PVPVA were superior to isomalt-compacts, with a particular advantage for IDM-PVPVA COM-compacts, which showed a higher impact on solubility improvement of IDM compared to the ST-compacts at both pH values. The COM-compacts of ISO demonstrated higher values than monitored for the related ST-granules at pH 5.5, but this was conversed at pH 1.0. The differences were not significant at the acidic medium within both PVPVA-compacts or within both ISO-compacts.

The calculation of solubility factor for the granules revealed a tendency of higher solubility factors at pH 1.0 in comparison with pH 5.5, excluding the IDM-ISO COM-Gr.

Additionally, the increase of IDR values from pH 1.0 to pH 5.5 did not reflect the same multiplication ratio obtained from the solubility values of all granules (Table 31). This was discussed before for the case of IBU.

Table 31 The increase in IDR and solubility of all compacts and pure IDM by increasing pH value

Formulation	IDR pH 5.5/ IDR pH 1.0	SOL pH 5.5/ SOL pH 1.0
IDM-PVPVA ST-Tab	3.5	6.9
IDM-PVPVA COM-Tab	3.1	7.9
IDM-ISO ST-Tab	6.1	7.2
IDM-ISO COM-Tab	13.4	9.0
IDM	2.6	8.2

6.2.3 X-ray powder diffraction of IDM-formulations

The presence of several peaks in the diffraction of IDM indicates its high degree of crystallinity. By comparing the diffractogram of IDM with its XRPD patterns in the literature, it can be indicated that the initial used IDM corresponds to γ -polymorph [44,67]. The diffraction peaks, collected at 11.6, 16.9, 19.6, 26.6 and 29.3 2θ are characteristic for the γ -form [145–148], especially the very distinct reflection at 21.8 2θ . Contrarily, PVPVA exhibited no crystallinity as evidenced by the amorphous “halo” pattern.

All standard mixtures contained the diagnostic representative peaks at 11.6, 19.6, 21.8 and 29.3 2θ , confirming the presence of the crystalline IDM γ -form. Depending on the binary mixture, XRPD of the ST-mixtures showed a combined diffraction pattern of the pure γ -polymorph IDM with either pure PVPVA or pure isomalt.

As seen in (Figure 35, a), some obvious changes were recorded within the ST-compacts relatively to pure IDM. This was represented for IDM-PVPVA ST-Tab in a new peak generated at 5.4 2θ ; a disappearance of the peak at 42.8 2θ ; the almost disappearance of the peak around 25.4 2θ and the changed shape of some peaks at 30.3 2θ ; the ranges of 34 - 35.5 2θ and at 10.1 2θ with a shift. Moreover, some changes regarding the intensity were observed, such as the higher intensity at 19.6 and 21.8 2θ and the lower intensity at 11.6 and 16.9 2θ . However, no change in the overall crystallinity was observed as clarified later. On the other hand, IDM-ISO ST-compacts showed less sharpness of peaks at the ranges 14-16 and 25-28 2θ ; a different shape with minor shifts of peaks around 17.3, 19.3, 26.6, 39.7 2θ and the disappearance of peaks at 19.6, 26.9 and 33.6 2θ .

The influence of co-milling process on the solid-state and crystallinity was obvious in case of IDM-PVPVA (Figure 35, b). A reduction in the sharpness as well as intensities was monitored at some peaks of IDM-PVPVA COM-mixtures such at 11.6, 16.9, 19.6 and 29.6 2θ , in addition to the almost hollow pattern in the range from 39 to 45 2θ . Moreover, the peak at 30.7 2θ disappeared and the one at 20.9 2θ much diminished; the change in the triplicate peaks at 16 -17.5 2θ might also reflect a change in the crystal habit. The increased hollow regions and lower intensity of IDM distinct peaks indicated a partial loss in crystallinity upon co-milling. The compression after co-milling triggered a very slight crystal change as well, represented in a minor decrease in some intensities and some changes in the shape, for example at 19.6 and 27.4 2θ .

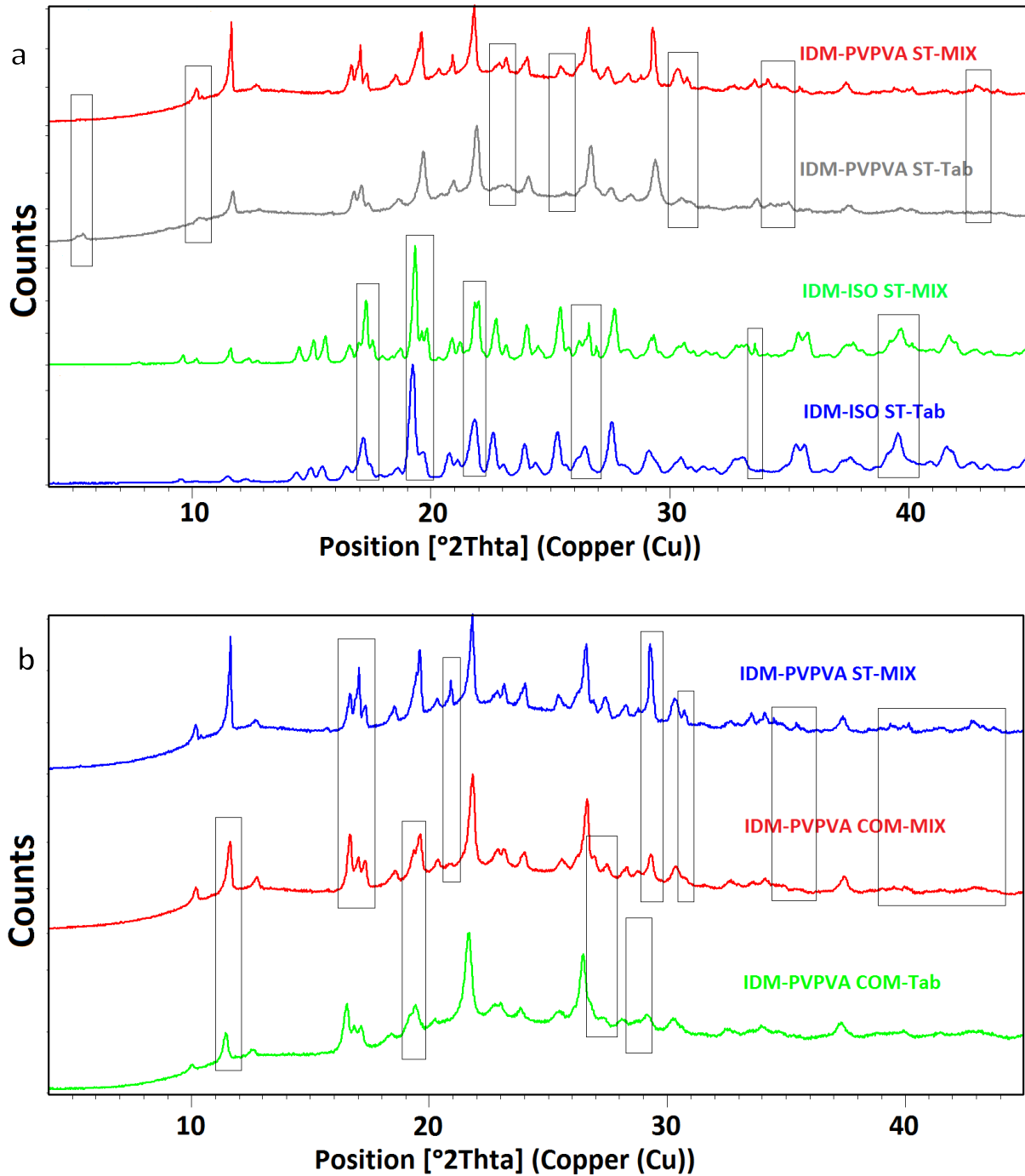
The isomalt co-milled mixtures showed some changes in some peaks shape like at 16.5, 22, 26.6 and 29.3 2θ ; the peak at 33.5 2θ disappeared, in addition to an alteration in some intensities (higher at 19.3 2θ and lower at 19.6 2θ). The compression after co-milling did not induce significant changes in the peaks shape (only at small values of theta) but generally a slight shift of all peaks.

The calculation of residual crystallinity regarding IDM-PVPVA formulations revealed no influence on crystallinity degree in case of the standard compacts, whereas a conversion of 20 to 27% into an amorphous form was estimated for the co-milled mixture and compacts respectively (Table 32).

Table 32 The crystallinity determination of IDM-PVPVA formulations

Formulation	Sum of net intensity (cts)	Crystalline IDM%
IDM-PVPVA ST-MIX	1292551	100
IDM-PVPVA ST-Tab	1257640	100
IDM-PVPVA COM-MIX	1050979	80
IDM-PVPVA COM-Tab	969939	73

The involvement of the crystalline isomalt interfered with the calculation of residual crystallinity by XRPD measurements for ISO-formulations, hindering a proper quantification of the IDM crystallinity.



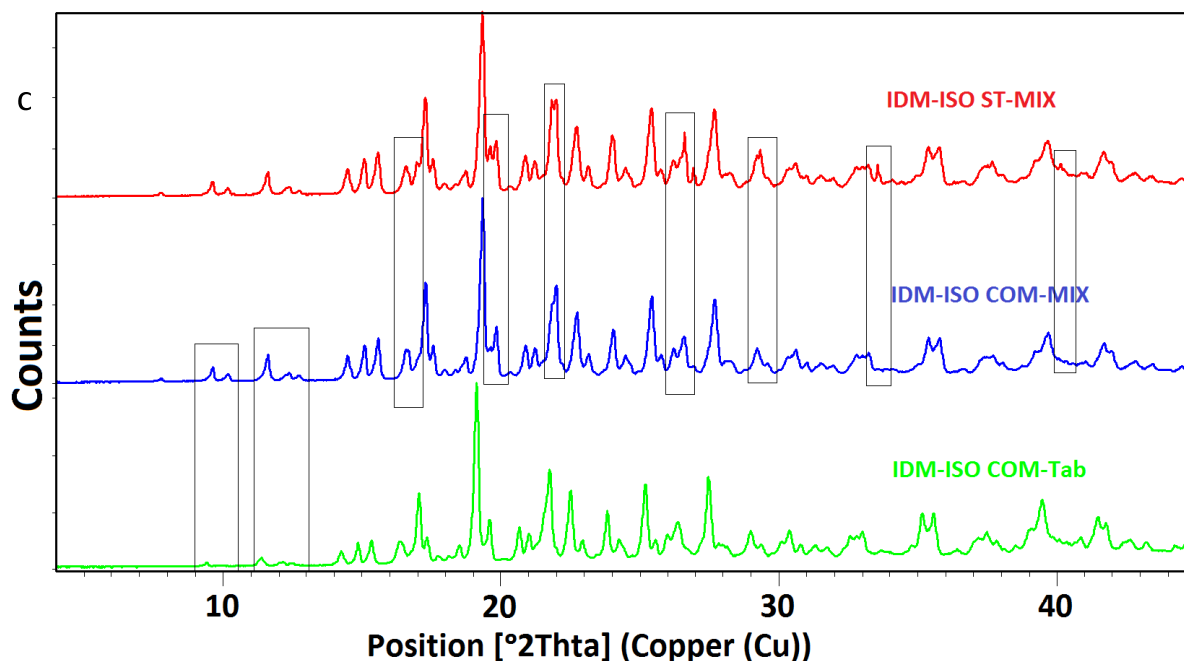


Figure 35 Graphical presentation of XRPD diffractograms of a) IDM ST-compacts, b) IDM-PVPVA COM-compacts, c) IDM-ISO COM-compacts as compared to the physical and co-milled mixtures

6.2.4 Differential scanning calorimetry of IDM-formulations

The neat IDM revealed a melting endotherm peak at 163.9 °C (onset 160.3 °C). The amorphous IDM, produced by quench cooling during the DSC measurement, showed a glass transition at 43.6 °C. The heat of fusion of IDM γ -polymorph was calculated as the mean of three independent measurements of the area under melting endotherm that were adjusted by the amount of IDM. A value of 100.9 J/g was obtained, which was close to reported values [42,149,150].

The neat PVPVA showed no melting point and a T_g at 107.7 °C (Peak), with a change in the heat capacity at T_g ($\Delta c_p = 0.238$ J/g/k). The enthalpy relaxation of amorphous PVPVA was around 64 °C above the T_g of neat IDM.

As mentioned before in 4.2.4.2, the first endothermic peak of isomalt was related to the residual water and the second peak was assigned to the melting endotherm (onset at 148.8 °C; peak at 161.6 °C) that overlapping with the IDM melting peak. Hence, the DSC curves of IDM-ISO mixtures and compacts revealed a merged endothermic peak around 160 °C. The T_g of pure ISO was recorded at 57.79 °C.

The DSC thermographs of IDM-PVPVA formulations revealed a first broad endotherm in the range of 60-110 °C, assigned to the dehydration of PVPVA [57]. A weight loss up to 6% (w/w) was measured for IDM-PVPVA COM-Gr upon drying.

The freshly prepared IDM-PVPVA ST-mixtures revealed at the first heating a broad endothermic peak near 157 °C (onset) that was not as sharp as the one of pure IDM, they showed also two Tgs at 49.38 and 103.97 °C, assigned to neat IDM and PVPVA respectively. The related ST-compacts demonstrated a small endothermic peak close to 156 °C (onset), and a new broad peak around 126 °C (onset). No melting peaks could be detected at all for the co-milled formulations. Upon second heating, two Tgs (Tg₁ at 46.32 and Tg₂ 99.78 °C) were further recorded for IDM PVPVA ST-Mix, whereas only one Tg at 81 °C was detected for the ST-compacts, indicating a higher degree of interactions generated within the compacts.

The IDM-ISO mixtures also exhibited the broad peak of ISO dehydration and one broad melting point, ascribed to the melting process of both ingredients. The related compacts demonstrated anyways the same endotherms with a clear depression of T_m as compared with the corresponding mixtures (Table 34); especially for the ST-compacts. No significant difference was measured between IDM-ISO compacts (ST and COM) regarding the impact to depress the melting point of IDM. The second heating for IDM-ISO ST- and COM-compacts showed a Tg at 46.39 and 40.54 °C respectively, whereas two Tgs were observed for the IDM-ISO ST-mixture at 45.25 and 58.78 °C, assigned to IDM and ISO respectively.

The calculated crystallinity was around 100% for the isomalt mixtures and compacts (Table 33). A slight decrease in IDM crystallinity was obtained for IDM-PVPVA ST-MIX, showing 16% load of the crystalline IDM. The IDM %enthalpy obtained from both melting points of IDM-PVPVA ST-Tab decreased to %very small values and became almost negligible for the co-milling formulations.

Table 33 The content of crystalline materials, onset of IDM melting peaks for IDM compacts and corresponding mixtures by DSC measurement

Sample	T _m onset °C (MIX)	load% of crystalline materials (MIX)	T _m onset °C (Tab)	load% of crystalline materials (Tab)
IDM-PVPVA ST*	157.18 ± 1.39	16.08 ± 3.73	T _{m1} 126.77 ± 1.75 T _{m2} 156.22 ± 0.77	n.a.
IDM-ISO ST**	157.56 ± 2.00	99.40 ± 2.41	148.05 ± 1.11	96.59 ± 4.40
IDM-ISO COM**	152.74 ± 0.84	98.06 ± 2.02	148.51 ± 0.87	97.88 ± 0.08
Pure IDM	160.32 ± 0.60	-	-	-

* crystallinity target: 20% (IDM)

**crystallinity target: 100% (20% IDM and 80% ISO); n.a. not applied

Table 34 The depression in the onset of T_m for the compacts as compared to the related mixtures and pure IDM

Sample	Depression in T_m onset ($^{\circ}\text{C}$)	
	Tab / Mix	Tab / pure IDM
IDM-PVPVA ST/ T_{m1}	30.41	33.55
IDM-PVPVA ST/ T_{m2}	0.96	4.10
IDM-ISO ST	9.51	12.27
IDM-ISO COM	4.23	11.82

6.2.5 SEM of IDM-formulations

The SEM images of pure IDM revealed irregularly rhombic plates with smooth borders, which is indicative for γ -form, whereas needle-like forms are the typical habit for α -form or β -form crystals [44]. The pure PVPVA appeared as irregularly rounded spheroids with empty core and a plant of cracks and fissures.

No pores were clear on the white surface of IDM-PVPVA ST-Tab (Figure 36), the surface appeared to be melted and flat with some cracks that were most likely formed by the pressure applied from the upper punch. Two phases could still be recognized.

Upon milling, the IDM-PVPVA COM-Mixture appeared as a very fine yellow-powder with irregular dimensions of IDM, referring to the amorphous material.

The surface of IDM-ISO ST-Tab was very flat with no porosity or cracks (Figure 36). The two components could clearly be identified. Unlike the co-milled mixture with PVPVA, fine particles were obtained upon milling with ISO, but the crystals of IDM were still easily to recognize.

In general, no inner pores were obtained for the COM-compacts, where both components integrated in a large homogenous bulk with a very smooth flat surface. The two components were less distinguishable as compared with the ST-compacts; and the cross-sections showed obviously rather one phase.

SEM of cross-sections showed packs of IDM/excipient networks (Figure 37). The compaction triggered different morphology inducing crystals with rough surfaces, comprising both IDM/excipient particles, sticking together to form one block and the particle boundaries of each component were not obvious. When taken together, the SEM images suggest a lower porosity of both ST- and COM-compacts. Only single-phase regions appeared that assembled together with deformed edges. The original structure of particles disappeared after compaction and changed into a homogeneous phase with small air pockets.

6. Influence of high-pressure compaction: The case of indomethacin

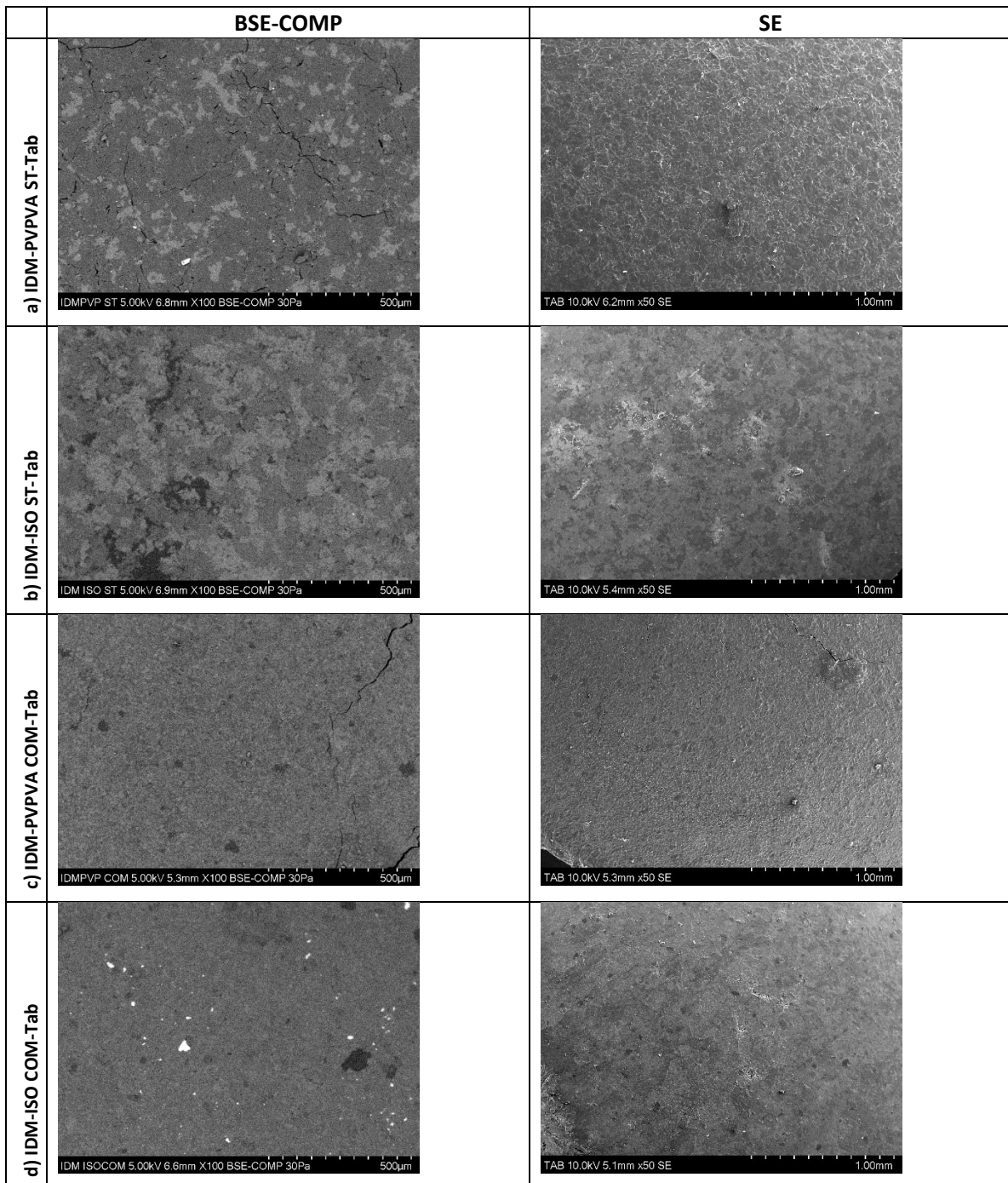


Figure 36 SEM images of IDM compacts surface BSE-COMP obtained by BSE detector (x100 resolution) as well as surface images by SE detector (50x resolution)

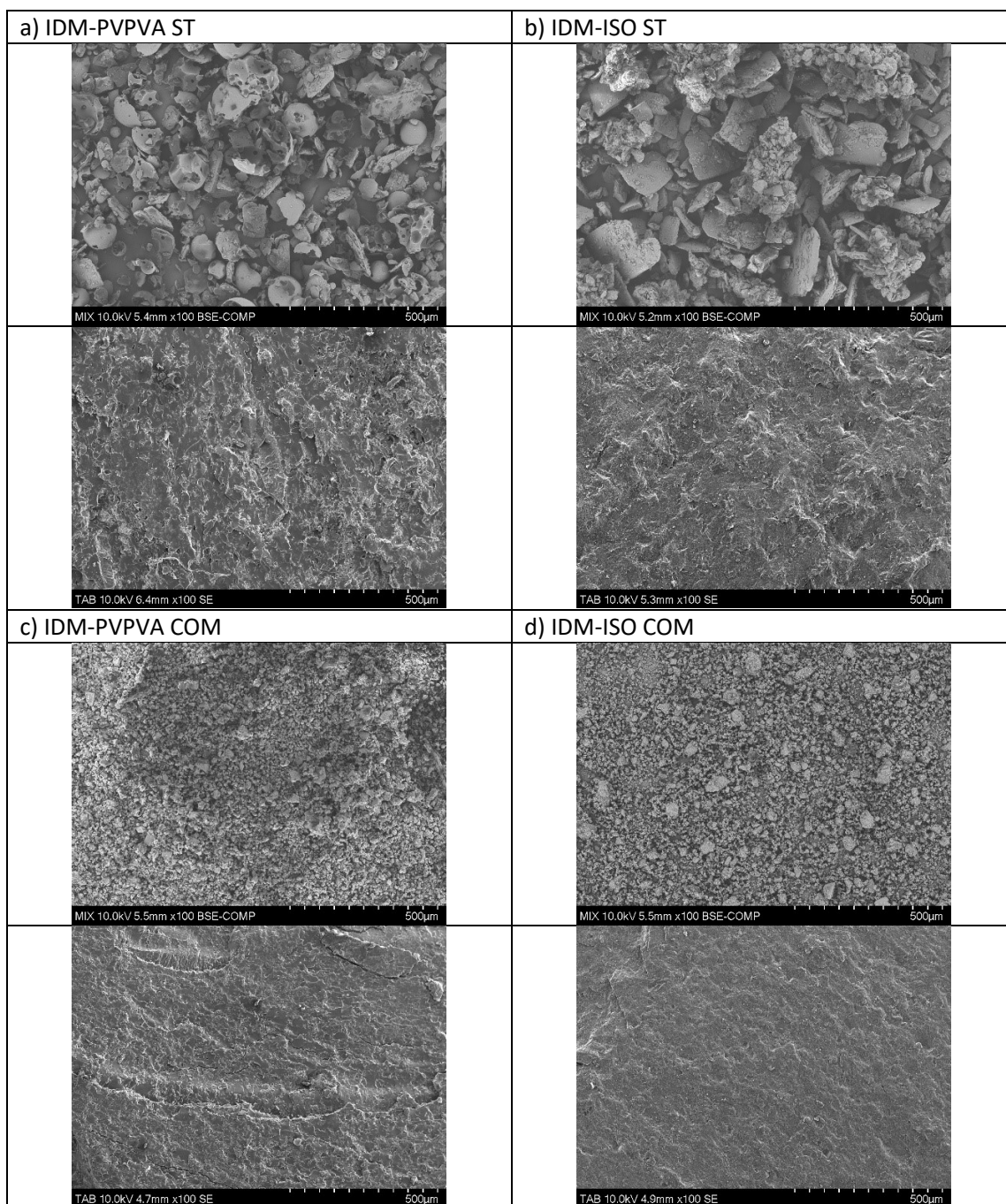


Figure 37 SEM photographs of mixtures and cross-sections of IDM-PVPVA and IDM-SO. From top to bottom: ST-mixtures, cross sections of ST- compacts, COM-mixtures, cross-section of COM-compacts

6.2.6 FTIR of IDM-compacts

The neat IDM showed two stretching absorptions of the carbonyl groups C=O (Table 35). The first one assigned to the carboxyl moiety at 1712 cm^{-1} , related to H-bonds of the asymmetric acid C=O---HO of cyclic dimer, and the second one C=O at 1689 cm^{-1} that associated to the benzoyl group. Additionally, CH

stretching was recorded as bands around 2900 cm^{-1} , overlapping with the weak stretching of OH at 2925 cm^{-1} . This OH stretching manifested as a broad vibration between 2600 and 3300 cm^{-1} referring to H-bonded OH [58], including the stretching of cyclic dimerized OH groups at 2728 and 2630 cm^{-1} . The peak at 1587 cm^{-1} corresponds to the C=C aromatic stretching vibration.

PVPVA showed two stretching carbonyl bands, dedicated to the strong C=O characteristic band of amide carbonyl in PVP at 1659 cm^{-1} and to the vinyl-acetate ester at 1730 cm^{-1} [151,152]. PVP is also characterized by the CH₂ stretching modes that assigned to some overlapping bands around 2900 cm^{-1} [153,154] and the CH deformation modes at 1422 and 1368 cm^{-1} [154]. Besides, the absorption band of bending C-N of the pyrrolidone can be seen at 1286 cm^{-1} [154]. The vinyl-acetate VA exhibited specified bands at 1433 cm^{-1} [152] and an IR absorbance at 1019 cm^{-1} , assigned to the stretching C-O vibration [155]. In addition, the peak at 1232 cm^{-1} corresponds to the stretching vibration of ether group C-O-C of vinyl-acetate [155,156].

The data obtained for the crystalline IDM and pure PVPVA as well as for the representative compacts with and without co-milling are illustrated in (Figure 38, a). The PVPVA-compacts exhibited a change in the broad peak of stretching vibrations of the IDM cyclic dimerized OH groups, such the disappearance of some peaks at 3022 , 2728 and 2630 cm^{-1} (especially in case of COM-compacts), and a shift of the band at 2830 to 2850 cm^{-1} (more obvious in ST-compacts). The OH region became, in general, sharper and more distinct as compared to pure IDM.

Figure 38, (a) shows a zoom of the spectrum in the wavenumber range of carbonyl group. The peak assigned to C=O dimers at 1712 shifted to 1718 cm^{-1} for the IDM-PVPVA compacts. The C=O absorbance peak of VA was embedded into the shifted IDM acidic carbonyl as a shoulder around 1728 cm^{-1} . The C=O band of benzoyl integrated into the dominant C=O band of PVP, forming a broad peak and almost disappeared in case of the COM-compacts. A minor shift was observed of IDM peak at 1221 cm^{-1} , assigned to the OH deformation bending.

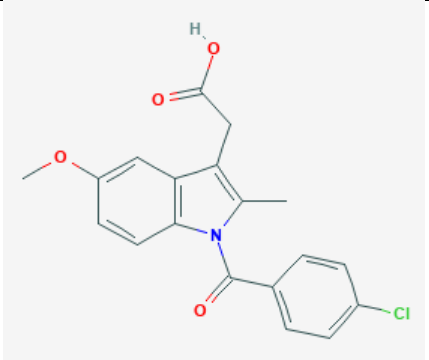
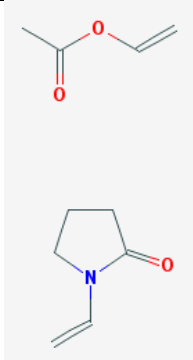
The peaks of COM-compacts were generally less sharp and mostly with lower intensity than that of ST-compacts, in addition to some change monitored around 600 cm^{-1} as compared to both IDM and PVPVA.

The bands assignments of pure isomalt are described previously in 5.2.2. The IDM-ISO compacts showed similar changes as recorded for the IDM-PVPVA compacts in the stretching vibration of IDM dimerized OH groups.

Moreover, the broad OH stretching of ISO, at 3283 cm^{-1} , became broader especially in case of ST-Tab (Figure 38, b). The peak assigned to C=O dimers at 1712 cm^{-1} shifted to 1720 and 1721 cm^{-1} for ST- and COM-compacts respectively. The IDM assigned peak disappeared at 1147 cm^{-1} in the range of OH bending; many peaks disappeared in the range of $600\text{-}900\text{ cm}^{-1}$, related to the out of plane CH deformation for substituted aromatic, such as at 590 , 770 and 832 cm^{-1} , in addition to 433 cm^{-1} in the fingerprint area. A slight shift was observed of the carboxylic OH (out of plane deformation) of IDM from 924 to 927 cm^{-1} and a shift of isomalt OH bending (in plane) at 1346 to 1356 cm^{-1} .

The intensity of COM-compacts differed from that of ST compacts, especially in fingerprint region, the intensity of C=O benzoyl decreased with a minor shift to 1691 cm^{-1} .

Table 35 Chemical structure of IDM and PVPVA used in this study*

IDM	PVPVA
	

*National Center for Biotechnology Information. PubChem Database, <https://pubchem.ncbi.nlm.nih.gov/>

6. Influence of high-pressure compaction: The case of indomethacin

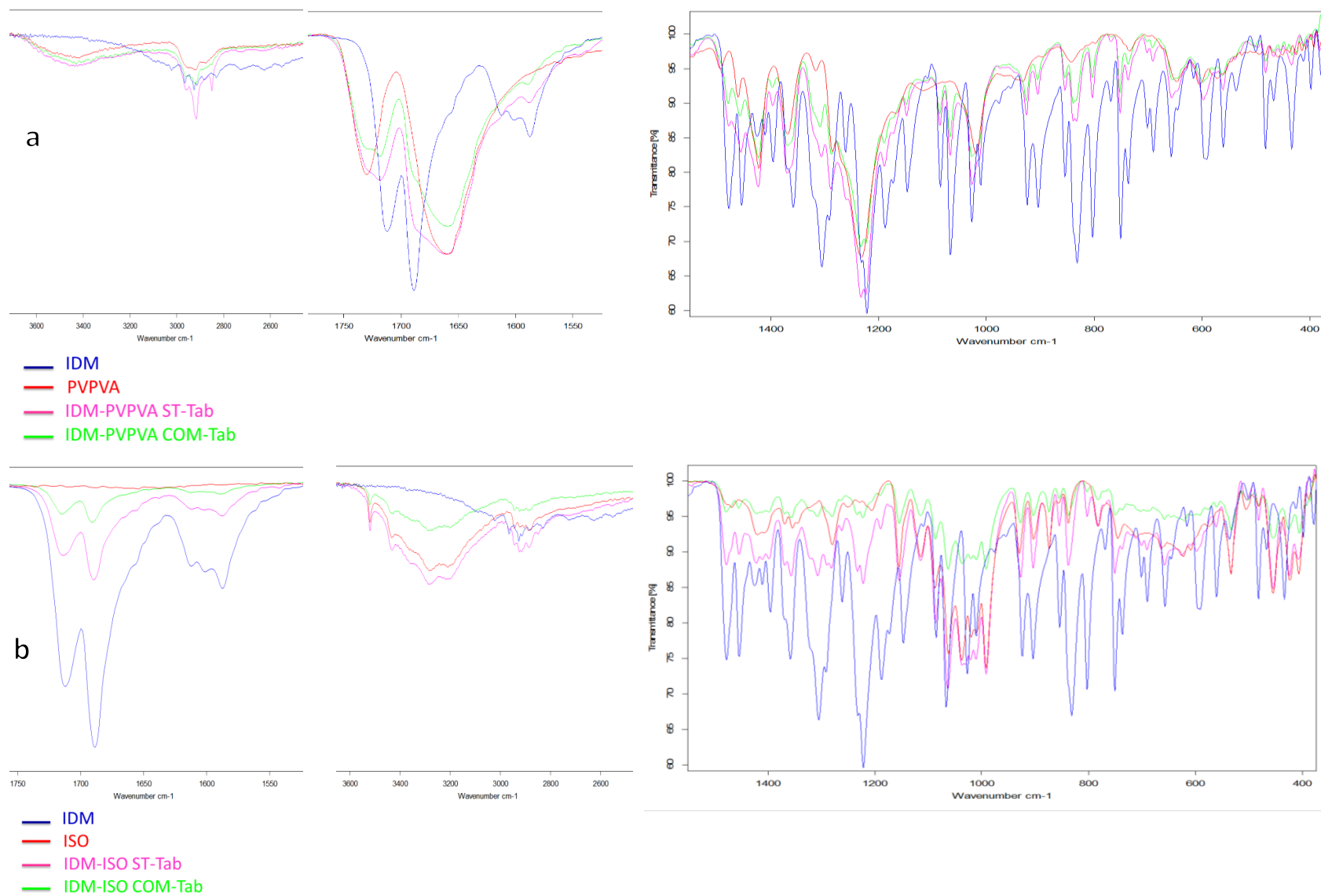


Figure 38 (a) FTIR spectra of pure crystalline IDM, pure PVPVA and IDM-PVPVA ST, IDM-PVPVA COM compacts. (b) FTIR spectra of pure crystalline IDM, pure ISO, and IDM-ISO ST, IDM-ISO COM compacts, the presented ranges refer to bands where prominent changes occurred

6.2.7 Wetting studies of IDM-compacts

All compacts were characterized for their surface free energy using OWRK method. For this purpose and to calculate the components of SFE, the data of measurements with water and DIM were applied (Appendix; Table 59).

As compared to pure IDM, all compacts expressed smaller contact angles with water. The PVPVA-tablets showed smaller contact angles with water and higher total SFEs than the compacts with ISO.

As SFE data revealed (Table 36), the IDM-PVPVA ST-Tab showed the highest total SFE with highest polar part that caused a high work of adhesion and led to higher wettability.

A negligible polarity was measured for pure IDM. All formulations exhibited significantly a higher total SFE as compared to pure IDM, where the dispersive part appeared to be the major component for all compacts (about two folds as that of the polar component). The calculated values of polar/ dispersive ratio (less than 1) indicated also to a remarkable higher tendency toward dispersive forces.

Table 36 SFE Components and values of W_a , W_i and W_s calculated for IDM compacts

Sample	¹ surface free energy mJ/m^2			$P_0\%$	² Wetting kinetics J/m^2		
	total	dispersive	polar		W_a	W_i	W_s
IDM-PVPVA ST-Tab	72.97 ± 0.79	46.97 ± 0.43	26.00 ± 0.96	35.63	136.95	256.36	-8.77
IDM-PVPVA COM-Tab	71.31 ± 1.52	48.44 ± 0.47	22.86 ± 1.23	32.05	133.43	242.28	-12.29
IDM-ISO ST-Tab	60.62 ± 0.74	40.11 ± 0.58	20.51 ± 0.17	33.84	123.93	204.27	-21.79
IDM-ISO COM-Tab	60.92 ± 1.26	46.55 ± 0.86	14.37 ± 0.82	23.59	117.95	180.36	-27.77
IDM	50.33 ± 0.18	50.26 ± 0.12	0.07 ± 0.12	0.14	68.20	-18.64	-77.52

¹ Water and Diiodomethane was used as probe liquids

² Water was used as probe liquid

No significant differences of the total SFE were observed within ST and COM-compacts for the same excipient, but a varied contribution of the components was noticed in case of ISO compacts.

Polarity values ranging from 23 to 35% polarity were calculated for the formulations compared to 0.14% for pure IDM-tablets.

The analysis of wetting process was performed covering three aspects, namely, adhesion, immersion, and spreading.

The adhesion process was spontaneous for all investigated compacts; this was indicated by the calculated W_a values with a significant improvement to that of pure IDM-tablet. Both types of PVPVA-tablets showed very high works of adhesion. IDM-PVPVA ST-Tab exhibited the highest W_a values as compared to other compacts, indicating stronger interactions with water.

The same could be determined for the works of immersion, where higher values for the PVPVA-formulations were further reflected by an improved immersion process and initial faster dissolution rates. The only negative value of W_i was demonstrated by pure compacts of IDM.

The negative values of W_s are indicative of a disfavoured complete spreading of water on all compacts surfaces. However, all formulations exhibited an improvement of the spreading process. The highest W_s value for the IDM-PVPVA ST-Tab indicated a better spreadability than the other formulations.

6.2.7.1 Sorption behaviour of IDM-compacts (Tensiometer)

The determination of the contact angles based on sorption behavior was also performed.

The contact angles with water were significantly smaller on IDM-PVPVA ST- and COM-compacts (35.0° and 44.5° respectively) than that of the corresponding IDM-ISO tablets (54.8° and 64.6° respectively). IDM-PVPVA ST-Tab was superior to the others, showing the highest value of slope as well as reduction in the contact angle, whereas IDM-ISO COM-Tab pointed the smallest slope and biggest contact angles (Table 37). In general, all compacts showed a similar behavior against n-Hexan, except for IDM-PVPVA COM-compact that showed a high value of absorbed mass (data not shown). This formulation, however, exhibited the highest absorbed amount with water as well.

Table 37 Values of contact angle, slope and sorption amount of all tested IDM-compacts

formulations	Contact angle	slope g^2/s	amount $g / 20s$
IDM-PVPVA ST-Tab	35.0 ± 1.6	0.0202 ± 0.0004	0.1249 ± 0.0091
IDM-PVPVA COM-Tab	44.5 ± 3.8	0.0169 ± 0.0011	0.1505 ± 0.0134
IDM-ISO ST-Tab	54.8 ± 2.8	0.0147 ± 0.0013	0.1027 ± 0.0021
IDM-ISO COM-Tab	64.6 ± 3.4	0.0105 ± 0.0013	0.1271 ± 0.0058

Figure 39 shows the mass uptake of water into the IDM-compacts bed. A fast rate of adsorption was appreciably obtained for the IDM-PVPVA compacts. The water failed to wet pure IDM compact and a very low mass was adsorbed as a function of time.

The absorbed amounts of water were statistically identical from the IDM-ISO ST-Tab and IDM-PVPVA COM-Tab. The contact angles increased in the presence of water by over 27% and about 17% for the co-milled compacts with PVPVA and ISO respectively, as that of related ST-compacts, indicating to a declined drug surface wetting when the co-milling was implemented into the process.

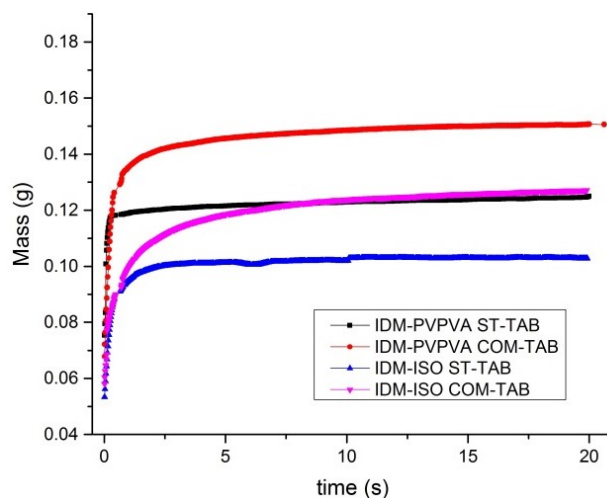


Figure 39 The mass uptake of water into all IDM-compacts bed

6.2.8 IDM-compacts Porosity and Density

The tablets showed high values of the mass per measured unit volume; the measured porosity was between 2.5 - 5% (Table 38). Except for IDM-PVPVA ST-Tab, no significant differences could be found between the measured porosities%. Lower porosities were observed for the COM-tablets as compared to their ST-compacts. The true densities of PVPVA mixtures were significantly lower than those of ISO mixtures.

Table 38 Porosity & Density values of IDM-tablets and related mixtures, all density values in g/ cc

formulation	Tablet porosity%	Tablet density	True density (MIX)	*Apparent density (MIX)
IDM-PVPVA ST-Tab	5.131 ± 0.097	1.187 ± 0.001	1.2507 ± 0.0021	0.236
IDM-PVPVA COM-Tab	3.619 ± 0.365	1.205 ± 0.005	1.2501 ± 0.0003	0.317
IDM-ISO ST-Tab	3.370 ± 0.195	1.424 ± 0.003	1.4732 ± 0.0004	0.424
IDM-ISO COM-Tab	2.537 ± 0.179	1.445 ± 0.003	1.4827 ± 0.0002	0.338

*Apparent density was determined by measuring the volume of a known mass of an untapped powder sample into a graduated cylinder

The apparent density of the ST-mixture bed was higher for the sugar-alcohol (isomalt) than related the co-milled mixture, whereas the COM-mixture for the polymer (PVPVA) showed in contrary a higher apparent density than its ST-mixture. The true density of mixtures with and without co-milling was, however, identical for the same excipient. The tablets densities were much close to the true densities of related mixtures.

6.2.9 Particle size distribution of IDM-mixtures

The micronization effect of triturating was obvious on particle size using the oscillating mill.

A high particle size reduction was obtained for both excipient mixtures after co-milling (Figure 40). The standard mixtures with either PVPVA or ISO demonstrated no significant differences in the particle size distribution. The volume median diameters of particles without co-milling ranged from 56 to 63 μm . No significant differences in the particle size were also monitored for the co-milled mixtures. After co-milling, the mixtures appeared to be very fine with a very low average diameter d_{50} that did not exceed 15 μm . The d_{10} , d_{50} , and d_{90} values of all IDM powder mixtures are summarized in Table 39. In general, all mixtures have rather a wide asymmetrical particle size distribution, which was more intense with co-milled mixtures. Span values from 1.4 to 3.6 were calculated.

Table 39 Particle size distribution of IDM mixtures, before and after milling

	ST-MIX				COM-MIX			
	d_{10}	d_{50}	d_{90}	Span	d_{10}	d_{50}	d_{90}	Span
IDM-PVPVA	16.69 \pm	63.52 \pm	110.65 \pm	1.48 \pm	3.17 \pm	10.93 \pm	33.52 \pm	2.78 \pm
	0.96	1.45	4.87	0.03	0.16	0.42	1.22	0.01
IDM-ISO	11.04 \pm	56.33 \pm	116.11 \pm	1.87 \pm	2.70 \pm	14.32 \pm	54.00 \pm	3.60 \pm
	0.47	1.31	2.30	0.09	0.19	1.29	1.53	0.24
IDM-Cr	6.45 \pm	29.13 \pm	74.72 \pm	2.34 \pm				
	0.20	0.70	2.31	0.04				

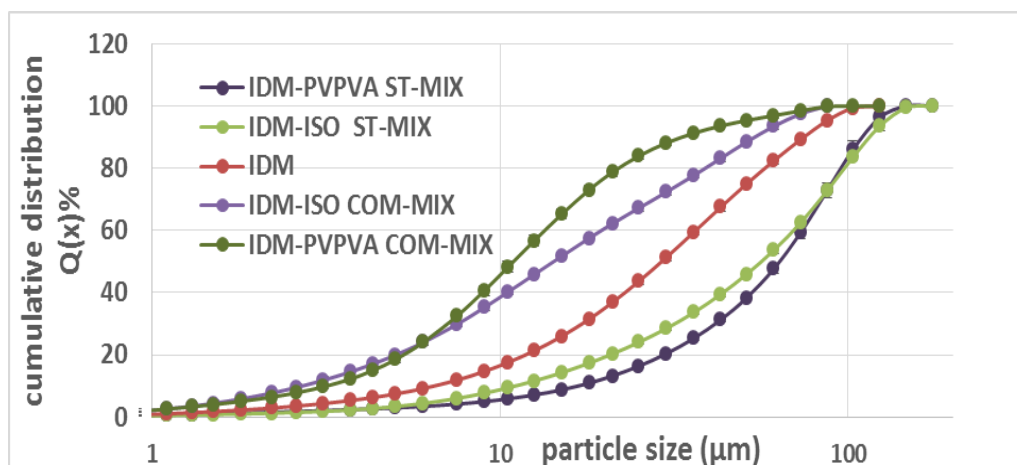


Figure 40 Particle size distribution of pure IDM and all IDM mixtures before and after milling

6.2.10 Specific area of IDM-granules

The formulation granules showed different specific surface areas, with exceptional relatively higher values obtained for IDM-PVPVA COM-granules (Table 40). The analysis revealed that the ST-granules for both

excipients have lower areas per unit mass than two third of those of the related COM-granules. An additional experiment was carried out on IDM-PVPVA COM-mixtures, which revealed significantly higher values of surface area as compared to their allocated granules.

Table 40 Surface area of IDM formulated granules

formulation	Spec. surface area	Spec. surface area
	[m ² /g] Gr	[m ² /g] Mix
IDM-PVPVA ST	0.7746	
IDM-PVPVA COM	1.2689	2.2742
IDM-ISO ST	0.5482	
IDM-ISO COM	0.8755	

6.2.11 Stability of IDM PVPVA COM-Tab

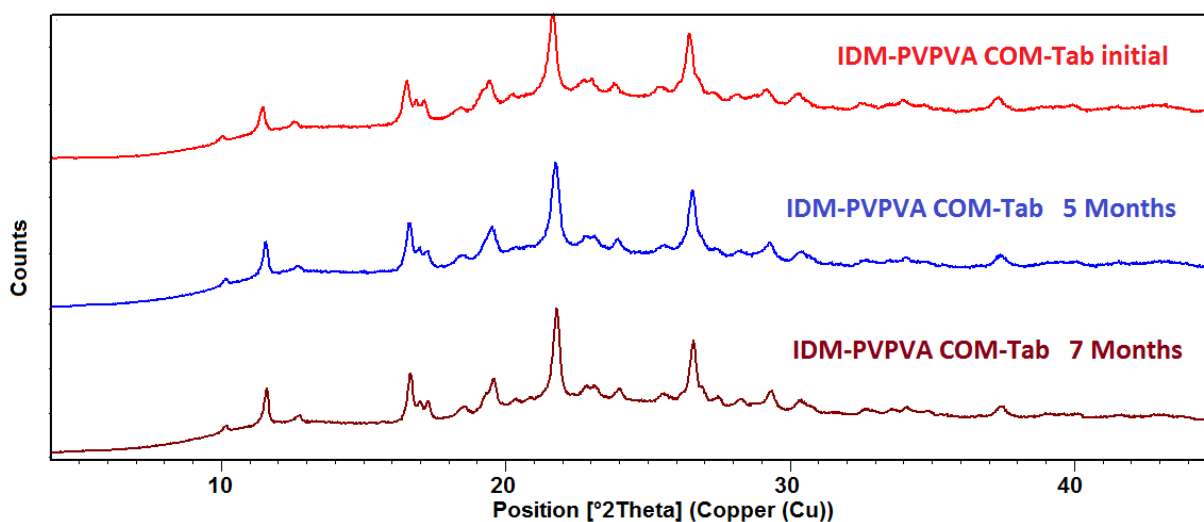


Figure 41 X-ray Diffractogram of IDM-PVPVA COM-Tab upon storage during the accelerated stability study

The samples of IDM-PVPVA COM-Tab were stored in a drying chamber at 40 °C within a desiccator that was maintained at 75% relative humidity (RH) using saturated solutions of NaCl. Figure 41 illustrates the representative diffraction patterns of the indicated compacts obtained after five and seven months of storage at 40°C, 75% r.h. No changes were observed in the crystallinity (Table 41) or in the XRPD pattern that might indicate any transformation in the crystal form and solid-state for IDM. However, during the stability test under the high humidity, the tablets surfaces deformed and became glassy in appearance.

Table 41 XRPD solid-state of IDM-PVPVA COM-Tab as Initial, after accelerated stability studies for 7 months

Composition (%)	XRPD Initial	40°C, 75% r.h., 5 months	40°C, 75% r.h., 7 months
IDM-PVPVA COM-Tab	73% crystallinity	75%	74%

6.3 Discussion

The network of pure IDM within the IDR-disk possessed a hydrophobic nature that limited the drug release, showing a very low IDR value.

The dissolution data confirmed the beneficial effect of high-pressure compaction of IDM binary mixtures on dissolution kinetics, also without a prior co-milling.

The linearity of IDR for all compacts excluded the occurrence of any change in the solid-state upon dissolution. The presence of PVPVA and ISO improved the dissolution properties of IDM with a stronger effect for PVPVA. This increase of the dissolution rate, obtained by the compacts as compared to pure crystalline IDM, was in line with previous studies of SDs of IDM/ PVP [72] [67].

Despite the partial amorphousity for the PVPVA co-milled compacts, their IDR results did not much deviate from the related ST-Tab. A high amorphousity does not always mean a faster release [71]. Interestingly, Fini and colleagues reported that the crystalline SDs of IDM/PVP showed a comparable release rate to related ASD systems [57]. Another study revealed that solid dispersions of IDM with a residual crystallinity showed a higher or similar dissolution rate than fully amorphous glass solutions [123]. The IDR testing might minimize the usual enhancement associated with an amorphous form due to the limited available release area. In addition, the surface of IDM-PVPVA compacts appeared glossy after the dissolution test, which might be related to the formation of a gel-like layer by PVPVA upon contact with the medium. This layer represents a diffusion layer for IDM and can lead to an underestimated impact of the amorphous part on IDR. Thus, the surface changes and compressability (especially regarding amorphous materials) should be considered by the evolution of IDR values. However, the impact of the amorphous portion was more recognizable in case of dissolution testing for granules at non-sink condition as more diffusion layers were present and the co-milled granules showed obviously a faster release than ST-granules.

The previous chapter confirmed the important role of IDR of pure ISO in the overall dissolution process of the formulation. In this chapter, the role of the excipient used was readily distinguishable in the acid medium. A higher degree of interactions could be expected for IDM with PVPVA as with ISO. The IDM release for ISO-compacts was not as fast as for PVPVA compacts, which did not agree with a previous work, where SD of IDM/ISO (30/70) showed higher dissolution rates as compared to IDM/PVP SDs [47].

The changes in color of the dissolution medium for IDM-PVPVA co-milled mixture indicated a certain degree of IDM recrystallization into other polymorphs during the release. A similar observation was

reported for another IDM system in 0.1N HCL [157]. A transformation of the amorphous IDM to the less soluble α and γ polymorphs can be expected in aqueous solution, which was observed previously over relatively short time [99]. However, no drop was recorded in the released IDM, particularly out of co-milled compacts. An investigation of the polymorphic transformation for the residual solid IDM recovered at the end of the dissolution test (by vacuum drying and then XRPD) must be considered in the upcoming studies.

Regarding the co-milled formulations, the particle size effect seemed to be more dominant than the compaction impact, especially at pH 5.5 that led to faster release of the mixtures. The dissolution endpoint at pH 1.0 was however, higher for the granules referring to a higher solubility reached for the granules-compacts.

Similar observations to IDR testing were obtained from the shake flask method. A strong correlation between IDR values and solubility factors was seen at pH 1.0. The solubility factors indicated relatively a higher influence of the applied strategy to increase the saturation solubility of IDM in the acidic medium, whereas the magnitude of IDR increase was higher at pH 5.5.

Different values for IDM solubility were reported in the literature, this discrepancy might be explained by various proportions of polymorphic forms that make the measurement of its solubility challenging [42,43]. The saturation solubility for pure IDM measured at pH 1.0 was much comparable to the value of intrinsic solubility measured by Comer *et al.* (8.8 $\mu\text{g}/\text{ml}$) [43], which is expected considering IDM presents in non-ionized neutral form in this acidic medium. However, the Curve Fitting experiment, which starts at low pH and with the original solid, revealed a less soluble form (3.3 $\mu\text{g}/\text{mL}$).

Higher values of solubility factor were obtained for the PVPVA compacts, producing an increase in solubility of about 3 folds. The dissolved PVP molecules can build hydrogen bonding with IDM leading to a greater solubility of indomethacin [72]. This ability of interaction is highlighted by the FTIR study.

The co-milled granules with PVPVA showed the highest increase of IDM solubility but much comparable to the related ST-granules, especially at pH 1.0 where 27% amorphousness produced only 2% improvement of solubility. The amorphous IDM was reported to have 4.9 folds higher solubility than γ -polymorph [99]. The solubility of co-milled samples might undergo a change in the IDM physicochemical properties during the long shaking period. Hence, the saturation solubility obtained may reflect an alteration in the phase of IDM, which could be mediated by the dissolution and supersaturation state in the aqueous medium, and led to experimentally a lower increase predicted [42]. However, IDM-PVPVA COM-Gr proved to be stable during the dissolution tests over 4 hours. Besides, the 3 folds of solubility increase obtained was

higher than reported values for co-grinded mixtures of IDM-PVP that increased the IDM apparent equilibrium solubility at 37.0 °C in the range of 1.4 to 2.6 fold [158,159]. Moreover, the measured increase was also higher than the expected increase based on the experimental solubility improvement of 4.5 fold (complete amorphous/ γ -crystal) obtained by Hancock and Parks [42], which refers to the dominant influences of the process and polymer on the observed increase for the compacts.

The impact of partial amorphization was not significant on the wettability and SFE, which showed no major differences between IDM-PVPVA ST- and COM-counterparts, probably due to the gel-like layer formed by the polymer upon depositing the water drop on their surfaces.

It is important to enhance the supersaturation rate and duration for drugs that have poor solubility under gastric conditions. For acidic pH-dependent compounds, it is essential to ensure high concentrations of the dissolved drug and prevent precipitation in the stomach. All compacts exhibited more or less a similar effect on the solubility improvement irrespective to the testing medium.

There is a considered possibility of a high degree of IDM/ISO interactions due to plenty of OH groups in ISO. The isomalt-compacts possessed higher solubilities than neat IDM, however lower solubility factors than PVPVA compacts, referring to a less degree of crystals defects (as indicated by XRPD) as well as drug/excipient interactions (as indicated by DSC and FTIR).

IDM is well known to exist in three polymorphic forms α , β and γ [72,147]. The two polymorphs, γ -form (form I) and α -form (form II), are often obtained and recognized [145,149]. The β -form (form V) is metastable. Two other polymorphs were also reported that are, like β -form, metastable and convert easily to forms α or γ [44].

The identification of polymorphic form for the used IDM and the investigation of the process-induced forms were carried out by XRPD, DSC, and infra-red spectroscopy. In general, the characteristic peaks patterns, coincided with the gamma form of IDM, were obtained by XRPD diffractograms for all samples. Thus, IDM maintained its crystalline nature within the compacts. However, the changes in diffraction patterns for the ST-compacts to the ST-mixture indicated that compacting IDM with PVPVA or ISO appeared to trigger some changes in its solid-state structure. Besides, the differences in some intensities for the tablets referred to a possible modification in the crystal habit or changes in the preferred orientation of the crystals [160]. The high-pressure compaction might generate different orientations

between the aromatic indole and phenyl rings, which can also cause the changes observed. A higher strength of these modifications was obtained in presence of PVPVA.

Unlike high-pressure compaction or the co-milling process, the XRPD analysis indicated no effect of physical mixing on the solid-state of IDM. No matching was found between IDM XRPD patterns for the compacts and the reported known polymorphic forms [44,145–148,160].

The compression process on its own did not generate a change in the IDM total crystallinity within the PVPVA ST-compacts. Additional changes were, however, evident either in peak intensity or the shape of some peaks as compared to the corresponding physical blends. The characteristic diffraction peak at $2\theta = 5.80$ was only reported for B-form [44], but its other specific peaks were not recorded, which excludes the possibility of IDM converting into that polymorph upon compaction.

The mechanical activation, accompanying the mechanical treatment via co-milling process, might explain the improved dissolution rate for the COM-compacts. IDM is partially molecularly dispersed in the polymeric matrix as amorphous material in case of PVPVA-COM formulations, thus a higher IDM/PVPVA interaction can be deduced [71]. The relative decrease of diffraction peak intensities approved the reduction in crystallinity% after the co-milling process. The co-grinding was previously confirmed to trigger the formation of IDM/PVP H-bonding with a conversion of IDM (either partially or completely) into an amorphous form [158].

Apart from the change in crystal habit, the process-induced reduction in the particle size can lead also to this variation in the relative intensity of some peaks, as different relative plenty of planes are exposed to the X-ray source. However, the co-milling process did not produce intense changes for IDM-ISO.

The reported five polymorphs of indomethacin exhibit melting points at different temperatures [161]. A lower T_m is associated with a higher solubility. The DSC of used pure IDM revealed the characteristic of crystalline γ -polymorph [44,146,160], which is the monotropic form [145].

DSC data indicated that neither the polymorphic form nor the crystallinity degree did alter during the physical mixing. However, the results clearly pointed out that the compacts were not identical regarding the melting profiles as compared to their mixtures. The data for isomalt-compacts suggested no effect of the compaction process on the crystallinity degree, but a modification in the solid-state cannot be excluded, as indicated by the depression of the IDM melting point.

The presence of 80% PVPVA affected the melting process of IDM for the prepared compacts and to less extent for the physical mixture. DSC findings for the IDM-PVPVA compacts (ST and COM) were not consistent with XRPD data regarding the crystallinity degree, and showed obviously lower values. This can relate to the partial molecular dispersion/ dissolution of IDM into the PVPVA matrix upon heating. Moreover, the observation of new broad peak, depressed around 148 °C, indicated new high interactions between IDM and PVPVA. Based on hot-stage microscopy **HSM** [57], PVP proved to interact with IDM upon heating over 100 °C, causing a depression of IDM melting temperature. The mentioned points can also explain the slight drop in crystallinity and the depressed endothermic peak for IDM-PVPVA ST-MIX. Similar observations were reported by Fujii *et al.* for systems consisting of IDM and crospovidone, where XRPD showed a different crystallinity compared to the DSC data [100]. The observed phenomenon might be PVPVA load-dependent. In a previous study, PVP did not appear to have an influence on IDM solid state for solid dispersions prepared at lower PVP ratios < 30% [72]. On the other hand, solid dispersions of IDM/PVP contained $\geq 30\%$ PVP revealed neither residual crystallinity by XRPD, nor melting points by DSC [44].

The DSC technique possesses a high sensitivity regarding the crystallinity quantification for IDM binary systems. However, a possible drug/excipient interaction or conversion of the crystalline to amorphous form during the heating run of DSC must be excluded. Therefore, the possibility of IDM transformation from one polymorph to another upon heating can limit quantifying the crystallinity degree by DSC [160].

Two separated melting peaks were observed upon heating the IDM-PVPVA ST-Tab above 120 °C; the first one at ca. 142 °C (peak) and a small one at 160 °C. The first peak might be explained by IDM transformation into the α -form or form III and the second peak would be assigned to the form β or the most stable γ -form. The transformation of IDM into other polymorphs was reported upon heating [44]. However, the current data generally referred to strong IDM/PVPVA interactions produced by high-pressure compaction and even to a higher strength of interactions upon co-milling as no T_m was detectable for the co-milled formulations.

Furthermore, the absorbed moisture within compacts interfered collaterally with the extent of the drug/polymer interactions during the DSC analysis. The absorbed water from PVPVA would act as plasticizer in PVPVA-formulations and caused a decrease in the polymer T_g . As a result, the polymer chains could be able to surround and solubilize the drug molecules as amorphous form [47]. The available humidity would also decrease the polymer viscosity and increase its disorder degree, facilitating the

dissolution of IDM within the disordered regions of polymer chains. The level of resulted amorphization would then depend on the PVPVA amount and IDM/PVPVA interaction's strength.

The depression in T_m was also observed for the ISO-compacts as compared with their mixtures, referring to induced IDM/ISO interactions, but to less extent than for IDM/PVPVA. Khodaverdi *et al.* also confirmed high IDM/ISO interactions within SD systems[47].

The presence of two T_g s in a tested system indicates multi phases, whereas the single T_g referred to a high molecular miscibility producing one phase [162]. Except for IDM-PVPVA ST-Mix, the DSC experiments revealed a single glass transition at 82.95 °C upon second heating for IDM-PVPVA glass solutions that were obtained after the cooling run of all IDM-PVPVA formulations with no melting peaks suggesting the formation of one phase system. The observed T_g was depressed to that of PVPVA and close to the theoretical T_g calculated by Gordone Taylor equation (85.76 °C).

The measured T_g for IDM-PVPVA ST-Tabs was around 64 °C at the first heating, which is lower than the T_g of full amorphous system. It can be related to the residual water, as a T_g of 53.53 °C was theoretically calculated by Flory-Fox equation that considered the measured water content of 5.498% \pm 0.19 (determined by the Karl Fischer method). A similar observation was obtained from reversing heat flow curves for IDM/PVPVA 20:80 solid dispersions [44]. In that context, Zecevic *et al.* also observed one phase for the IDM/Kollidon VA64 amorphous system with a T_g at 89 °C, whereas their extrudates showed a T_g at 61 °C [162].

Unlike COM-formulation, IDM-PVPVA ST-compacts showed a white appearance indicating that IDM remained crystalline. In general, the SEM images referred to non-pores compacts and a melted-nature for PVPVA compacts, with very smooth surfaces, especially for the COM-compacts. The two phases of components were obvious to a higher extent than what was obtained for IBU-HPC ST-Tab (chapter 4), but that was less pronounced after co-milling. The partial amorphization in PVPVA COM-Tab was reflected in homogenous light-yellow areas on the surface, which is indicative for an amorphous IDM [100]. The particles seemed to sinter together, producing very smooth and more melted nature surfaces with no pores.

The SEM of cross-sections confirmed the morphological changes upon compaction; it referred to the crystal disruption of both components that merged in one matrix. The changes were even more pronounced upon co-milling.

Generally, the solubility and IDR data indicated no changes in IDM phase during enough time to be absorbed through the gastrointestinal tract, without transforming into the more stable form.

All compacts expressed a spreading wetting type; exhibiting more hydrophilic surfaces as the measured contact angles with water were $\ll 90^\circ$. The very big contact angle for pure IDM tablets (≈ 93) indicates the very poor wetting attribute as well as hydrophobic character of IDM molecules.

The process achieved to produce a very high level of hydrophilic nature, particularly with PVPVA that showed a higher strength of improved wettability than ISO-compacts. The smaller contact angles for PVPVA compacts with water can be associated with a bigger effective area and thus, a faster release of IDM [136]. However, IDM might be covered by PVPVA particles, as fine precipitate multiple layers onto the surface [57], which may lead to underestimated differences between ST and COM PVPVA-compacts during the IDR testing.

The addition of a hydrophilic excipient such as isomalt resulted in enriching the surface of compacts with polar hydroxyl groups that caused an increase in the critical surface tension, thus, a better wetting. In spite of the ISO impact to reduce IDM contact angles with waters, the values are still, anyways, relatively big (45 and 51), which was presented in slower dissolution rates than PVPVA-compacts. In this context, the results of SFE were in consistent with the IDR profiles, which indicated lower wettability properties and less hydrophilic character for isomalt compacts.

The relatively small contact angles with Diiodomethane, confirmed the high dispersive nature of the compacts surface energy. As polarity values indicate, a higher tendency toward dispersive forces is obtained and a non-complete wetting process is probably dominant.

The comminution process has an influence on the ultimate surface properties as well as on the particle size. The COM-formulations could provide a greater surface area available for contacting, so greater dispersion forces, which led to the observed increase in the dispersive part and decrease in the polar part

of SFE as compared to ST-compacts. Despite the same total SFE calculated for ST- and COM-compacts of PVPVA, the ST-Tab exhibited, however, a higher contribution of polar forces. Thus, a high access of water molecules onto their surfaces with less entropic hindrance is expected [82].

The results indicated that high-pressure compaction could be able to adapt the surface, changing its nature and properties, which will be reflected in the measured contact angles [138], and increasing the scattered binding sites of water on the surface. The last is crucial for the first occurring solid/liquid interaction during the dissolution.

The wetting data referred to, in general, more homogenous natures for the surfaces with no spreading of values. As W_i results indicated, a fast initial dissolution was seen for the PVPVA-compacts as compared to ISO-compacts. This confirmed the importance of the analysis of wetting kinetics as an indication of the dissolution progress. A complicated difficult change of the solid-vapor to solid-liquid interface could be presumed for pure IDM tablets, due to the too low W_i value.

The negative W_s values imply rather a poor spreadability of an aqueous phase on the compacts surfaces and that the spreading of water is not complete. However, the PVPVA compacts and ST-compacts of ISO are dispersible and their particles have a less aggregation tendency in dissolution medium, since the measured resistances (spreading coefficients) were smaller than the water dispersive component, which describes the potential favourable solid/liquid interaction[138]. The higher W_s for PVPVA compacts was reflected in a faster release during the further dissolution stages.

A good correlation between the contact angles measured by tensiometer and the slopes of the ascending part of the curves (absorbed mass² Vs time; g^2/s) could be established. On the contrary, no specific correlation with water absorbed amounts after 20 s could be obtained. The smaller contact angle of IDM-PVPVA ST-Tab was not accompanied with a higher amount of sorption, which was acquired by IDM-PVPVA COM-Tab and might be caused by the partial presence of an amorphous material.

In terms of contact angles, the rank order obtained by the liquid penetration was identical to what acquired from the shape drop analysis but with rather higher absolute values. The same was collected previously during the analysis of IBU-compacts.

The PVPVA-compacts showed lower contact values and higher slopes indicating a higher wettability; and their fast rate adsorption indicated that water rapidly wetted the solid surface.

The increase in contact angles upon co-milling might be referred to the decrease in surface's polarity that led to less wettability. This was consistent with the previous chapter with IBU regarding ISO, whereas the presence of polymer PVPVA could interfere with the measured values as discussed before.

Since the application of this method is limited for the measurement of contact angles $>90^\circ$, hence, the measurement for pure IDM was not applicable and its tablet could not be penetrated by water. The existing of 80% part of either PVPVA or ISO can facilitate the penetration process of water molecules. Khodaverdi *et al.* referred to less wettability and consequently, a slower dissolution rate as the IDM to carrier ratio increased [47].

The solubility is controlled by the structure of the entire molecules, and not only related to surface's properties as SFE. Thus, the increase of solubility for PVPVA co-milled compacts to ST-compacts, in spite of the lower SFE, can be related to the higher degree of crystals defects and the partial amorphousity. Hence, the wetting can be considered as independent parameter of solubility.

Regarding FTIR analysis the observation of C=O moieties which act as HBA, or OH moieties which act as HBD, is of big importance for IDM and excipients molecules.

Indomethacin molecules might be potentially involved in a self-association as dimeric or catermeric structure by cohesive hydrogen bonding of carboxylic acids, with 4 other functional HBA. The characteristic FTIR spectra of the compacts were in line with the results obtained from XRPD and DSC data, confirming that the initial IDM used in the experiments was assigned to the polymorph γ [56]. The crystalline stable γ -indomethacin exists basically as cyclic dimers [58] and it has a lower solubility than the other metastable forms.

The damage of IDM dimer structure could be evident in the region of 1600 to 1750 cm^{-1} , based on the positions of vibrations bands related to the carbonyl dimer, benzoyl and free carboxylic acid. Depending on the solid-state of IDM (polymorph or amorphous), the C=O vibration's position of COOH and benzoyl will differ [56,58,163]. The non-H-bonded carboxylic C=O in a monomer or at the end molecule of a chain vibrates at a higher wavenumber at 1735 cm^{-1} (presented in neat amorphous IDM). The C=O related to H-bonded acid in chains (no dimers) vibrates at 1649 cm^{-1} . Accordingly, these frequencies were especially most valuable for comparison of the molecular state of IDM to identify any changes.

The resulting broad peaks around 1670 and 1720 cm^{-1} for the IDM-PVPVA compacts masked the single peaks, showing no clear-identified orderly peaks (recorded as a weak shoulder) for C=O of IDM (benzoyl)

and C=O of PVP (VA) respectively, which might indicate a higher degree of interactions. The observed broadening for C=O stretching mode of PVP might imply the involvement of this moiety in H-bonding interactions.

However, a remarkable shift of IDM C=O (COOH) frequency can still be respected. The shift to the higher wavenumber (1718 cm^{-1}) of IDM C=O as well as the change in the stretching vibration of IDM cyclic dimerized OH groups might refer to a decrease in the fraction of dimeric H-bonded acid [56]. It can be presumed that the C=O of PVP is H-bonded to the hydroxyl of IDM at the expense of IDM-IDM dimers. Within the indomethacin-PVP systems, PVP can form H-bonds with IDM that accompanied with a shift of its C=O vibration or with a change in the C=O (COOH) vibration of IDM [151]. The C=O of PVP can form stronger H-bonds with OH of IDM carboxylic acid rather than with H of NH, as the potential of electron sharing in COOH leads to a weak OH bond as that of NH [56].

When PVP is considered as a monomer, the 1/2 mole ratio of IDM/PVP corresponds to 1/1 (w/w). The 1/4 ratio (IDM/PVPVA w/w) within the compacts provides superabundant PVPVA and can ensure H-bonding for all IDM molecules with PVP chains. Hence, an excess of non H-bonded PVP is still offered. In case of the partial amorphization for the COM-compacts, the non-H-bonded C=O in a monomer or as an end molecule of a chain is hardly to be found, thus, no presence of IDM C=O (COOH) at a high wavenumber (1735 cm^{-1}) was observed.

The broad nature of OH stretching vibration, in addition to its position for the compacts, is indicative of a hydrogen bonded OH group.

The above-mentioned changes correspond to potential interactions between OH of IDM and the amide C=O of PVPVA and that the drug molecules interacted with excipients molecules at the expense of IDM-IDM internal interactions

Considering that the vibrational modes of molecules are much widely distributed in an amorphous system, the very broad nature of vibrations for the IDM-PVPVA COM-Tab is an indication of IDM being present in the amorphous form. For example, the OH stretching peak at 2925 cm^{-1} had pronouncedly less sharpness. This broadening can correlate with the increased intermolecular IDM/PVPVA hydrogen bonding for the co-milled system because of partial presence of IDM in the amorphous state. The amorphous IDM was further directly confirmed by the overall smoothing of several sharp peaks in the fingerprint region, which were originally present in the pure IDM spectra, resulted in broadening of the spectrum in the range of $400 - 750\text{ cm}^{-1}$.

The carbonyl peaks of IDM could be distinguished from isomalt, because they were observed in spectral regions with no overlapping or interferences. For ISO-compacts, the more shift of IDM C=O to a higher wavenumber (1720, 1721 cm^{-1}) as well as the disappearance of some peaks related to IDM cyclic dimerized OH groups would refer to a certain destroy of the IDM dimeric structure. Kaminska *et al.* observed several changes on IDM upon heating of IDM/saccharides SD through the high thermal energy introduced, which included the reconstruction or destroying of the dimer structures or the conversion of IDM to α -IIDM form [163]. Apparently, the high-pressure compaction could deliver enough energy to trigger certain changes.

The mentioned changes in the relative width and position of specific vibrational modes among the compacts, assigned to functional groups (carbonyl or OH), besides the disappearance of some peaks, would indicate to some changes at molecular level. The significant broadening of OH stretching in case of ISO ST-compacts is clearly indicative to the higher degree of interactions, involving OH as compared to the pure ingredients. This was supported by the disappearance of the indomethacin OH bending peak and the shift of isomalt's OH bending.

All tablets expressed generally a high density; the mixtures were condensed by means of high-pressure applied, leading to less voids volume.

The produced very fine COM-particles were more compliant to rearrange and slip at the initial stage of compression, decreasing the bulk bed porosity. This facilitated a higher strength of inter-particle interactions during the subsequent stage of compression that led to reach a higher bed densification for the compacts. This can explain the lower values of porosity for COM-compacts, which was confirmed by the cross-section of SEM analysis. The higher density of PVPVA co-milled compacts can also be explained by the higher compressibility, which is usually exhibited with amorphous materials.

The measured higher density of the compacts highlighted the better contact of particle-particle (API-Excipient). A higher compliance for the particles to be arranged during filling and compaction is normally connected with higher apparent and taped powder densities [133], resulted from malleable crystal shapes and surfaces as that of isomalt. However, in spite of differences between the apparent densities of mixtures, the compaction under high-pressure achieved to generate tablets with a much close to true density.

The co-milling step can increase the risk of agglomeration due to bigger cohesive forces that leads to a poor flowability [23], which was noticed during the compaction process of co-milled mixtures, especially

with ISO. The co-milling using a long chain polymer such as PVPVA would physically hinder this trend of agglomeration by adsorbing onto the particles surfaces.

The compacts low porosity was in line for the performance of IDR testing, where disks with low porosities are preferred to avoid more interferences with the results. Besides, the porosity values were convenient for the measurement of contact angles.

The relatively higher porosity for IDM-PVPVA ST-Tab was not evident by SEM, where the images did not reveal big pores, but demonstrated rather a plenty of fine branching pores.

The true density of co-milled mixtures differentiated slightly from their standard mixtures; nonetheless, it might indicate changes in the crystal form to some extent.

The analysis of PSD confirmed the considerable reduction in particle size upon co-milling. The relatively small D₅₀ value for ST-mixtures may ensure a suitable environment for IDM/excipient interactions.

Although the surface area is controlled during IDR testing, the influence of particle size factor on the results of IDR could not be excluded [164]. When the reduction in particle size is associated with new habits and facets exposed to the medium or with lattice defects, another dissolution profile is then anticipated. Thus, the most appropriate pressure used for production of IDR-disks must be carefully and individually determined for each specific system.

Considering the uniformity of granules size for all formulations (after sieving), the data of specific surface area can indicate their dissimilar morphology that interfered with the obtained differences in solubility and non-Sink dissolution rates at pH 5.5, where the effect of ionization process is superior.

The data indicated an increase in specific surface area for the co-milled compacts despite the possessed lower porosity. This might relate to different crystal habits of the particles within the COM-compacts, exhibiting different multifaceted planes that lead to higher specific surface areas.

The higher disorder state of an amorphous substance is to be accompanied with higher free energy, entropy and chemical reactivity. Upon storage, possible transformations of amorphous IDM were reported into either the stable γ -form (below T_g) or into the α -form (above T_g) [44,151]. However, this trend to recrystallize upon storage can occur even at temperatures much lower than the T_g.

In the current research, the IDM-PVPVA COM-Tab did not reveal any change regarding the crystallinity as well as crystalline form in the accelerating test for 7 months. The induced IDM/PVPVA interactions (including H-bonds) are essential for the stabilization of IDM [163].

The data agreed with previous studies, which suggested that PVP and PVPVA could interact with IDM in amorphous molecular dispersion, showing less molecular mobility of IDM, with no observation of recrystallization [56][58,165]. This was attributed mainly to H-bonds of IDM/polymer, hindering parallel IDM self-association through the formation of IDM dimers, which is necessary to form γ -crystals. The presence of PVPVA, that has a higher glass transition temperature than that of IDM, increased the T_g of whole prepared systems and hence, decreased the recrystallization potency [57].

A high stability is also expected for IDM-ISO compacts. The large number of hydroxyl groups available in isomalt molecule provides a suitable substrate and enables more interactions between IDM and ISO, which can assure a very high physical stability for IDM/ISO systems. [47].

6.3.1 Principle component analysis of IDM-compacts

A further analysis was done applying PCA to differentiate, which factors in case of IDM-compacts were considered as dominant and major contributors to the dissolution and solubility increase. These factors included the induced crystal modification, the total energy of the bulk compacts represented as SFE and its polar components and the excipient's impact.

The selected dataset that obtained for the 4 formulations regarding 27 variables (measured factors) was analyzed. PCA revealed certain relationships between the variables themselves and between the variables and observations (formulations). The analysis, including IDR values as a variable, revealed high correlations of IDR at pH 1.0 with wetting kinetics, the solubility factor, porosity, sorption slope, σ_p , SFE of excipient and the reduction of indomethacin T_m onset (as compared to the related mixture). The IDR at pH 5.5 was highly correlated with the polarity, PS and to less extent with the sorption slope, whereas it was not highly correlated with wetting kinetics, the solubility factor and the reduction of indomethacin T_m onset.

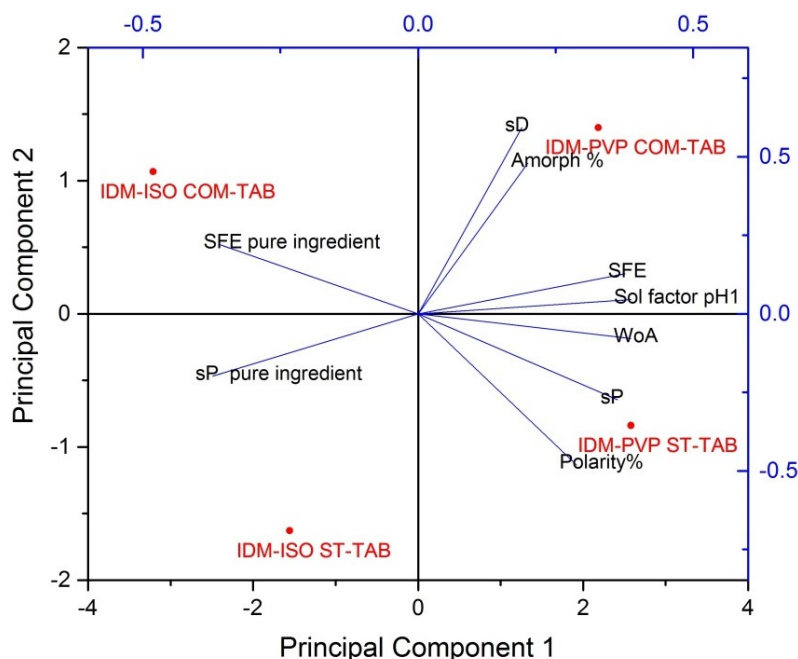


Figure 42 Biplot of IDM-tablets for PC1 and PC2

Based on the PCA correlation matrix and loading plot, the multiple measured variables could be reduced to 9 that can affect the IDR values, and still explain all variances in the matrix of original variables. For example, a high correlation was obtained between the reduction of T_m and SFE. Accordingly, the following 9 factors were included after merging in a further PCA analysis: Solubility factor; σ_p of pure excipient; SFE of pure excipient; SFE; polarity%; σ_p ; amorphousness%; σ_D and WoA .

The PCA of the 9 variables at pH 1.0 is demonstrated in the biplot (Figure 42). Each blue line represents the coefficients of each variable regarding the first two principle components, and the red spots represent the projection of all compacts (observations) scores in the original data. The scores obtained for the first two principal components (PC1 and PC2) could describe around 92% of the diversity in the descriptor space. The vectors, corresponding to WoA , SFE and solubility factor, aligned with the x-axis (i.e. they have similar heavy loadings for PC1). The vectors, corresponding to σ_D and amorphousness%, were highly matching with the y-axis. The other variables were more evenly distributed.

The 4 formulations covered all four quadrants of the PCA plot (biplot), confirming the physicochemical heterogeneity of the dataset. Dominant patterns and major trends in the data were obtained. IDM-PVPVA COM-compacts, which showed the highest IDR values, were clustered around amorphousness%, solubility factor and σ_D , which indicated the dominant influences of these factors to induce a higher IDR. While

IDM-PVPVA ST-formulation correlated highly with W_a , σ_p and polarity of the tablets. The isomalt compacts were more affected by the properties of pure excipient.

6.4 Conclusion

Similar to what obtained with ibuprofen, the applied approach revealed the ability to generate certain modifications in the IDM solid-state as well as in the properties of the compacts surface. This confirmed the effectiveness of the proposed technique with another weak acid using isomalt and PVPVA as hydrophilic excipients.

The association between IDM and the used hydrophilic excipients under high-pressure proved to significantly increase the IDM solubility and produce rapid dissolution profiles. The enhancement was carrier-dependent (higher for PVPVA-formulations) and did not necessarily require a co-milling step of the binary mixture prior to compaction.

The process promoted a high degree of IDM/excipient interactions without a necessary changing in the IDM crystalline state. The presence and the type of interaction were detected and indicated by DSC and FT-IR spectroscopy. The effect obtained was even more pronounced for the co-milled compacts of IDM-PVPVA that were associated with a partial amorphousization and characterized with higher interactions. A damage of IDM characteristic dimeric interactions to the favor of IDM/excipient binding appeared to occur, producing a decrease in the dimer population of IDM, which was more evident in IDM compacts with PVPVA.

The application of the proposed strategy appeared to trigger changes in the solid-state structure of IDM, indicated by the induced obvious changes in X-ray diffractogram. Furthermore, the compacts' surfaces demonstrated modified surface properties, expressed as a significant improvement in wettability and polarity. As observed with IBU, the higher magnitude of changes for IDM correlated to higher IDR and solubility values.

The linearity of IDR curves, solubility values after 7 days and the stability study referred to an acceptable phase stability of the IDM solid state of the compacts, even in the supersaturation state as well as the shelf-life stability for the partial amorphous IDM of the co-milled PVPVA compacts.

Based on PCA, a faster release of IDM out of the compacts, in terms of IDR, was highly affected by higher amorphousity%, higher solubility factor, higher polar component of SFE, higher W_a and to less degree by wetting properties of the pure excipient. Similar correlations and observation were recorded with IBU; however, to not an intense degree regarding the impact of SFE and W_a .

7 Mechanistic understanding of incompatibilities of ibuprofen and copovidone during direct compression under high-pressure

7.1 Introduction

The application of high-pressure compaction was tested as a potential strategy to improve the solubility and dissolution rate of IBU and IDM when applied on binary mixtures. It revealed promising results for IBU in the presence of HPC or ISO and for IDM in the presence of PVPVA (see Chapters 4, 56).

Testing the proposed approach on the IBU/PVPVA mixture is also of high interest due to the possible resulting API/excipient interactions. The potential of PVP and PVPVA to enhance the dissolution of poorly soluble APIs was well established, mostly in solid dispersions (see section 3.1.2), and particularly, with drugs that have a carboxyl group (like IBU, IDM, Ketoprofen etc.). IBU contains a carboxylic acid moiety, which has strong dipoles and can thus form a strong H-bonding interaction with other capable substrates. On the other hand, PVPVA molecules can interact with the drug molecules in different forms including electrostatic bonds, van der Waals forces and H-bonds resulting in an agglomeration or polymorphism of the drug.

Some published data confirmed these IBU/PVP interactions but showed that the binary mixture of crystalline ibuprofen/PVP undergoes spontaneous transformation into supersaturated one-phase amorphous form by grinding [166] or even by merely physical mixing during storage at ambient conditions [167]. This could provoke technological issues within the development of the solid dosage form. Another work clearly stated that PVP is incompatible with the micronized IBU in a mixture [168]. To the best of our knowledge, this issue was not investigated deeply for the case of copovidone.

The IBU/excipient incompatibility can influence the formulation's performance. It contributed partly to the reduction in the dissolution rate of IBU out of a ternary mixture including PVP and lactose [169].

Additionally, BASF indicated that IBU is physically incompatible with PVP and PVP-containing materials, and the use of those materials combined with IBU must be avoided under all circumstances. BASF referred to a dramatic decrease in the release rate of IBU tablets prepared with PVP as binder after 3 months of preparation [170]. The mentioned incompatibility is, however, reported to not be strong with crosslinked PVP; hence, the use of crosslinked PVP with IBU was left to customers' evaluation.

The spontaneous transformation of ibuprofen into amorphous form was also reported to occur with another polymer; namely polyethylene oxide 100,000 in compacts with a high polymer content of 90%, which were stored at a high relative humidity 94% [171]. Interestingly, this phenomenon was not the case for naproxen and PVP despite the presenting of the propionic acid within naproxen structure [166].

Various factors could impact and control these induced IBU/PVP interactions, such as the arrangement of IBU crystal structure [166] and the particle size of IBU [168]. Sekizaki *et al.* found that a higher decrease of IBU crystallinity was obtained by increasing the storage temperature, standing (contact) time, weight ratio of PVP (from 0.25 to 0.75) in the mixture, the moisture content of PVP and by decreasing the molecular weight of PVP [167].

This incompatibility issue is challenging from a stability point of view, especially in the case of prepared formulations with either a certain residual crystallinity of IBU or an initially full amorphous phase of IBU/PVPVA before storing. This leads us to address, whether the same phenomenon will be obtained applying high-pressure compaction using PVPVA, which has a lower hygroscopicity than PVP and thus, is expected to be less influenced by the humidity [55]. As well, it possesses 2 HBA more [56], which might generate a different degree of interaction with IBU on its own or as a consequence of the applied process itself.

Accordingly, the aim in this chapter was to evaluate the influence of high-pressure compaction, with and without prior co-grinding, on IBU/PVPVA-copolymer mixture, investigating the stabilization of IBU solid-state within the manufactured compacts as well as the formulation's performance in terms of drug release. The prepared compacts were generally characterized, focusing on their stability aspects and the dominant factors affecting it.

Further, this section has aimed to analyze and mechanistically understand the incompatibility between IBU/PVPVA as well as the nature of their interactions in the solid-state upon compaction. The various factors, which can affect and control IBU/PVPVA interactions, are investigated, monitoring any change in the crystal structures of both components. The formulations tested in this chapter are listed in Table 3.

7.2 Results

7.2.1 Dissolution studies of IBU-PVPVA formulations

Very much faster dissolution rates, either in terms of IDR or in the dissolution profiles (at non-Sink conditions) were obviously obtained from the formulations compacts as compared to pure IBU in both media (Figure 43).

Higher dissolution rates were obtained for the co-milled compacts as compared to the standard compacts. The IBU-PVPVA COM-Tab showed the highest dissolution rates.

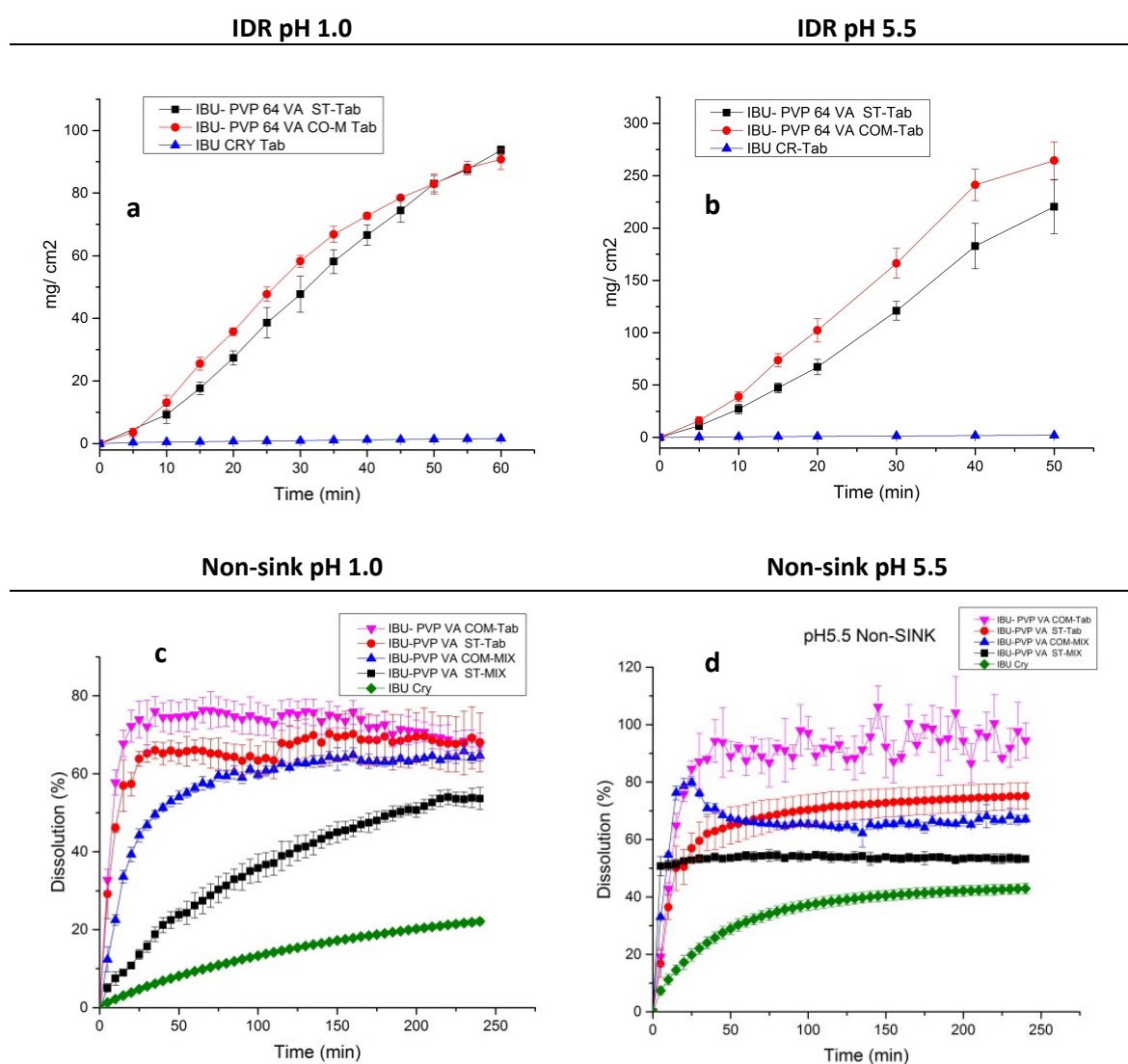


Figure 43 a and b: Intrinsic Dissolution profiles of IBU-PVPVA disks using modified USP apparatus 1, c and d: Dissolution profiles of IBU-PVPVA granules compared to related mixtures using USP apparatus 1 (basket). 100 rpm; medium volume 900 ml at pH 1.0 and pH 5.5; mean \pm SD; n = 3

The difference in IDR was, however, not significant between the co-milled and standard compacts of IBU-PVPVA at pH 1.0. This difference was significant and very much noticeable at pH 5.5, where IBU is partially ionized (Table 42).

At non-Sink conditions, the high-pressure compaction produced accelerated release kinetics for IBU out of the compacts granules as compared to the related mixtures in both media, with a less significant influence noticed at pH 5.5. The effect was obvious, especially for the standard formulation without a previous co-milling. The co-milled granules of PVPVA showed faster release than the corresponding mixtures at pH 1.0, whereas a similar dissolution was observed at pH 5.5 during the first 20 minutes. After that, the co-milled mixtures started to partially precipitate reaching a concentration plateau. On the other hand, the co-milled granules appeared to have precipitation-redissolution processes in succession, and revealed constant fluctuations in the IBU release.

Table 42 Intrinsic dissolution rates of IBU-PVPVA formulations and pure IBU

formulation	IDR pH 1.0	IDR pH 5.5	IDR factor pH 1.0	IDR factor pH 5.5
IBU-PVPVA ST-Tab	1.598 ± 0.063	4.657 ± 0.487	65.0	104.0
IBU-PVPVA COM-Tab	1.686 ± 0.024	5.752 ± 0.342	68.6	128.4
IBU cry	0.025 ± 0.003	0.045 ± 0.001		

7.2.2 Solubility determination of IBU-PVPVA formulations

7.2.2.1 Shake flask method

The measurements revealed a significant improvement of equilibrium solubility for the investigated granules at pH 1.0 as well as pH 5.5, as compared to the pure IBU and corresponding mixtures (Table 43).

Table 43 Saturation values and solubility factors of IBU-PVPVA formulations (physical mixtures, granules)

Formulation	Saturation Solubility P.M (pH 1.0)	Saturation Solubility Gr (pH 1.0)	Solubility factor P.M (pH 1.0)	Solubility factor Gr (pH 1.0)	Saturation Solubility P.M (pH 5.5)	Saturation Solubility Gr (pH 5.5)	Solubility factor P.M (pH 5.5)	Solubility factor Gr (pH 5.5)
	IBU-PVPVA ST-Tab	0.0437 ± 0.0013	0.0489 ± 0.0003	1.45	1.62	0.872 ± 0.0658	1.167 ± 0.0361	2.07
IBU-PVPVA COM-Tab	0.0462 ± 0.0014	0.0505 ± 0.0020	1.53	1.67	0.914 ± 0.0266	1.226 ± 0.0915	2.17	2.91
IBU-Cry	0.0302 ± 0.0025				0.4212 ± 0.0712			

As IDR data showed, the COM-compacts with PVPVA showed a higher impact on IBU solubility, manifested by higher values of solubility factors as compared to ST-compacts in both media. The difference was smaller at the acidic medium.

Each formulation revealed a higher solubility factor at pH 5.5 in comparison with pH 1.0.

7.2.2.2 CheqSol method

Significant differences for IBU intrinsic and kinetic solubilities were observed in the presence of PVPVA (Figure 44). The supersaturation ratios and increase in solubilities are summarized in Table 44.

The S_0 and S_k were increased by 5.4 and 2.1 folds respectively with PVPVA as compared to pure IBU. The supersaturation ratio showed a positive value (1.5). IBU precipitated out of IBU-PVPVA binary formulation at a concentration that was 8 times of the intrinsic solubility of pure IBU.

Table 44 Experimental solubility (S_0) data for IBU-PVPVA and IBU measured by CheqSol at 25 °C

	IBU-PVPVA (n=2)	IBU (n=4)
estimated S_0 pH 1.0 (mg/ml)	0.1963 ± 0.0012	0.0363 ± 0.0003
estimated S_0 pH 5.5 (mg/ml)	2.7820 ± 0.017	0.5141 ± 0.0043
S_0 increase	5.4	-
S_k increase	2.1	-
Supersaturation ratio S_k / S_0	1.5	-
Supersaturation ratio S_k / S_0 (to IBU)	8.1	3.4

The estimated solubility of 0.1963 mg/ml at pH 1.0 was much higher than the measured one 0.0437 mg/ml using the shake flask method. The increase in S_0 was also higher than the solubility factor calculated based on the shake flask findings (≈ 1.2) regarding the IBU-PVPVA ST-granules.

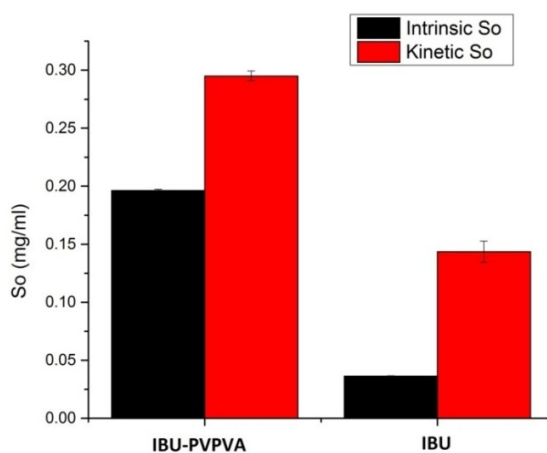


Figure 44 The intrinsic and kinetic solubility of IBU-PVPVA as compared to IBU

7.2.3 Solid-state analysis of IBU-PVPVA compacts

7.2.3.1 XRPD of IBU-PVPVA compacts

The tablets and mixtures were analyzed by XRPD at the same day of preparation.

XRPD of the fresh prepared standard mixtures contained all diagnostic representative peaks of the crystalline IBU; their patterns appeared as combined diffraction patterns of pure IBU and pure PVPVA, with no observation of a change in the total crystallinity (Figure 45).

IBU-PVPVA ST-tablets displayed increased hollow regions; less intensities were generally measured as compared to the related physical mixtures, indicating a partial loss in crystallinity upon compaction. In addition, the peaks of IBU at 14, 15 2θ disappeared; the ones between 18.7 and 20.16 theta slightly shifted. An almost hollow pattern of diffraction was monitored in the range between 25 and 45 2θ .

Table 45 The crystallinity determination of IBU-PVPVA formulations

Formulation	Sum of net intensity (cts)	Crystalline IBU%
IBU-PVPVA ST-Mix (fresh)	1190662	100
IBU-PVPVA ST-Tab (fresh)	355964	31
IBU-PVPVA COM-Mix (fresh)	0	0
IBU-PVPVA COM-Tab (fresh)	0	0
IBU-PVPVA ST-Mix (1 month)	413988	36
IBU-PVPVA ST-Tab (18 months, desiccator)	366741	32
IBU-PVPVA COM-Tab (18 months, desiccator)	0	0

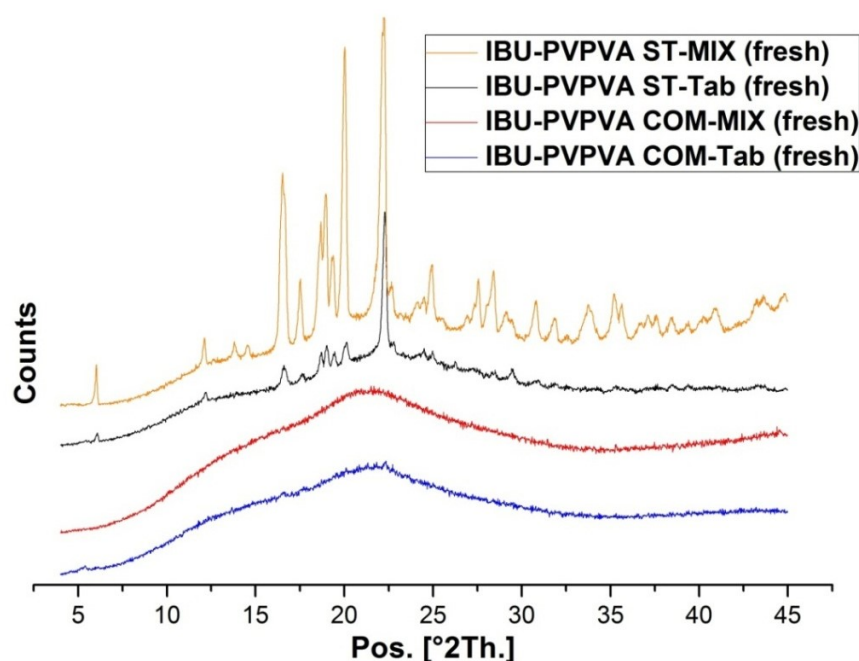


Figure 45 X-Ray diffraction patterns for IBU-PVPVA physical mixtures tested after preparation

The IBU-PVPVA co-milled mixtures as well as compacts showed completely hollow patterns without any diffraction peaks. The broad XRPD pattern is characteristic for no long-range three-dimensional molecular orders, relating to the amorphous materials.

The calculation of residual crystallinity revealed no influence on crystallinity degree in case of standard mixtures, whereas a conversion of around 69% into an amorphous form was estimated for the standard compacts. A full amorphous phase was recorded for the co-milled formulations.

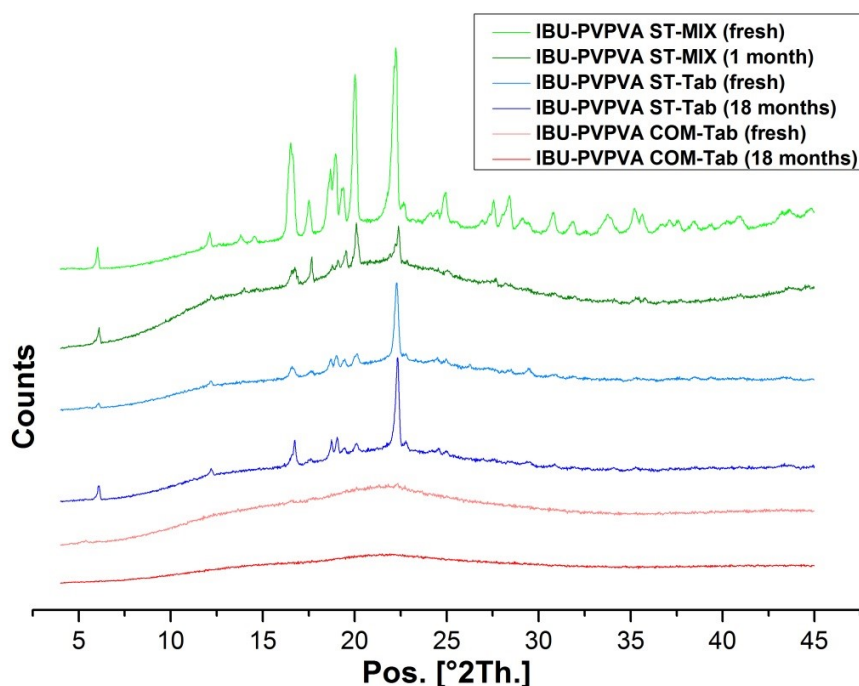


Figure 46 XRPD for freshly prepared and 1 month stored IBU-PVPVA physical mixture; and for ST and COM tablets after storage for 18 months in dissector

The intensity of X-ray diffraction peaks of IBU decreased within the physical mixture that was prepared one month before the measurement and stored at ambient conditions (Figure 46). Its pattern was very similar to the diffraction pattern of the standard compacts that have a partial loss of crystallinity. The mixture turned into a fully amorphous system after 3 months storing at room temperature, showing a conversion to glass-like sticky agglomerated masses.

No change could be seen in the XRPD patterns for the co-milled mixtures that were measured on the same day of the preparation or one month after the preparation. Only an optical change was observed, where the co-milled mixture turned transparent forming a glass-bulk.

Both types of tablets (ST and COM) were stored in desiccator with phosphorus pentoxide in a relative cold environment at 15-20 °C. These tablets revealed no change in the crystallinity, showing stable diffractions after around 18 months (Table 45, Figure 46). Moreover, the further observation of these tablets indicated a stable crystallinity for IBU-PVPVA ST-Tab and no recrystallization for the co-milled tablets for longer than 3 years.

7.2.3.2 DSC of IBU-PVPVA compacts

The melting point of IBU (onset) for ST-tablets was measured with a noticeable reduction at 56.22 °C (Table 46). Beside the depression in melting point, ST-tablets revealed that the integrated melting endotherm (endothermic area) was significantly smaller, indicating to a lower crystallinity 36.5%, based on the measured heat of enthalpy (see 4.2.4.2).

No existing of endothermic events related to a melting process could be recorded, for the IBU-PVPVA co-milled formulations in the first heating run, indicating the amorphous nature of IBU in the co-milled compacts and mixtures. The only endotherm observed was due to the absorbed residual water. Moreover, one Tg was obtained at 31.4 °C (onset) for the COM-Tab.

Table 46 DSC findings for IBU-PVPVA ST-Tab as compared to pure IBU

Sample	Enthalpy J/g	Crystalline IBU load%	Melting onset (°C)	Melting peak (°C)	Tm onset reduction	Tm peak reduction
IBU-PVPVA ST-Tab	7.61	7.29	56.22	66.67	-19.42	-11.41
IBU			75.64	78.08		

7.2.3.3 Optical observation and SEM of IBU-PVPVA compacts

The freshly prepared ST- and COM-compacts appeared as white condensed powder-bulks, showing one integrated matrix phase. The IBU-PVPVA ST-Tabs were bright snow-white tablets, whereas the co-milled compacts had rather off-white luminous surfaces. This appearance remained stable and unchanged for the samples stored in the desiccator for longer than three years (Figure 47).

The visual observation revealed an appearance of a glass-like form with stacked agglomerates for both the physical mixtures and compacts upon storage at room temperature for 3 weeks or at acceleration stability conditions for 2 days (Figure 48).

7. Incompatibilities of ibuprofen and copovidone under high-pressure compaction

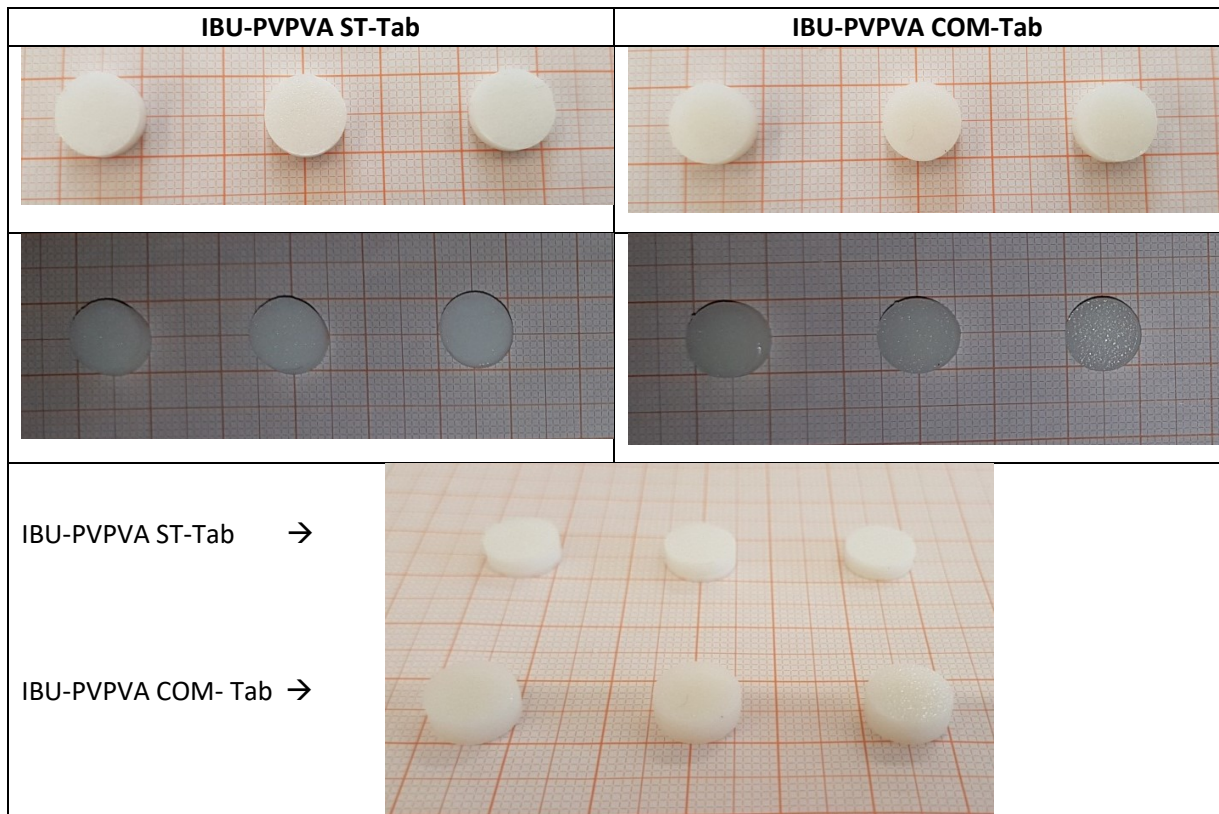


Figure 47 The appearance of IBU-PVPVA compacts stored in desiccator



Figure 48 The appearance of IBU-PVPVA compacts after 2 days at acceleration stability 40°C, 75% r.h.

The pure IBU appeared as needle-like rods and PVPVA looked as irregularly rounded disrupted spheroids. The morphologies of the individual components were deformed to big extent within IBU-PVPVA ST-Mix,

that were stored at room temperature for one month; new formed agglomerates could be seen (Figure 49).

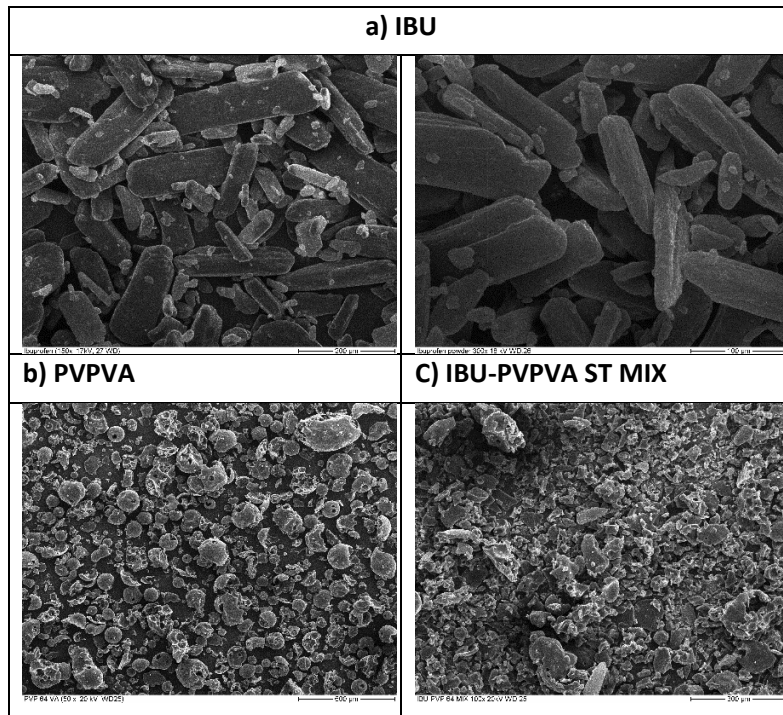


Figure 49 SEM images of a) IBU, b) PVPVA, and c) IBU-PVPVA ST-Mix one month after preparation

As shown in Figure 50, a high degree of agglomeration was observed for the compacts system and even more pronounced for the COM-compacts. The compacts exhibited one homogenous phase on the surface, showing melted-like appearance by SEM-COMP images obtained by BSE-detector. The particles appeared to sinter forming a smooth surface, especially for the COM-compacts, with no clear pores. SEM images of cross-sections demonstrated no distinguishable crystals of IBU within the compacts.

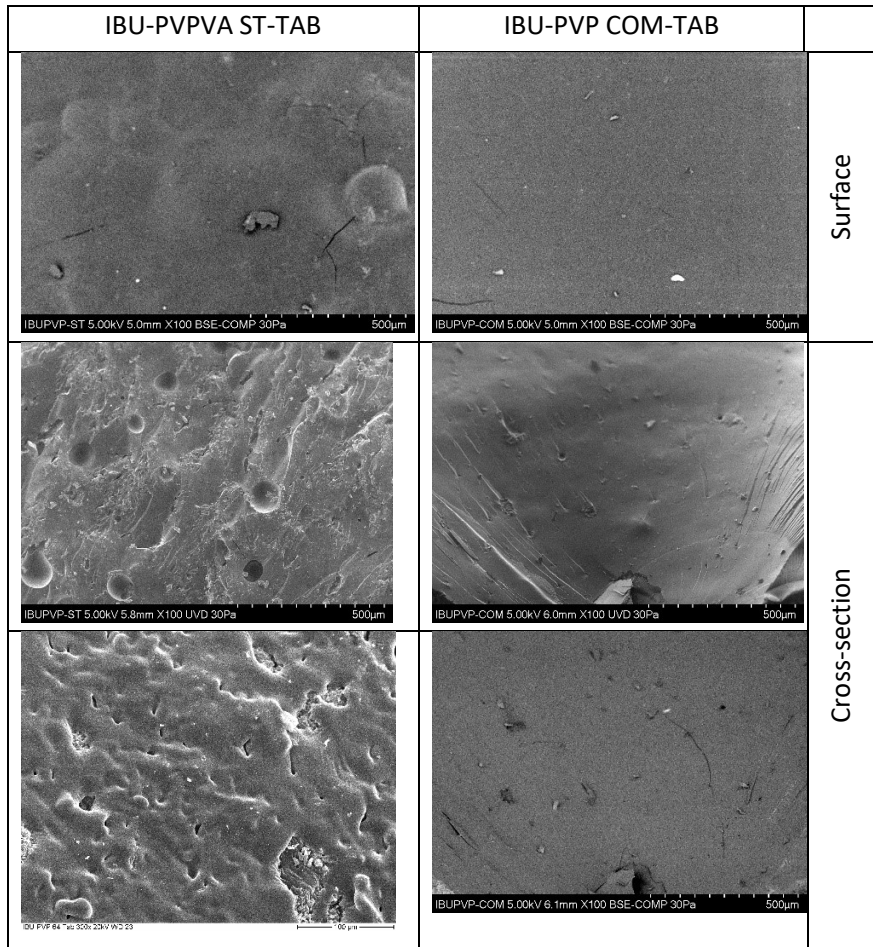


Figure 50 SEM of the surface and cross-sections of IBU-PVPVA tablets

7.2.4 Wetting studies of IBU-PVPVA compacts

7.2.4.1 Shape drop analysis of IBU-PVPVA compacts

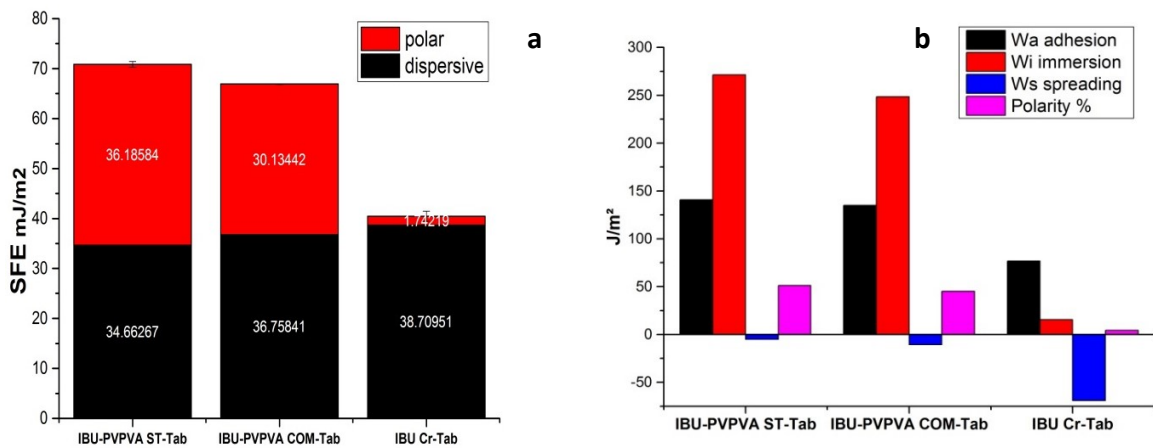


Figure 51 a) SFE and b) wetting kinetics of IBU-PVPVA compacts as compared to IBU

Both prepared compacts were characterized for their surface free energy using OWRK method and compared with the pure IBU-compacts.

As compared to pure IBU, both compacts revealed significantly lower contact angles with water and consequently, higher SFEs, that were accompanied with significantly bigger polar components (Figure 51). IBU-PVPVA ST-compacts showed smaller contact angles ($21.30^\circ \pm 2.54^\circ$) than the COM-compacts ($31.47^\circ \pm 1.25^\circ$) with a higher polarity (51 to 45%). The calculated values of polar/dispersive ratio (≈ 1) referred to similar contributions of the polar and dispersive components. The co-milled compacts showed a slight increase in the dispersive energy as compared to the corresponding standard compacts, hence, a higher tendency toward dispersive forces.

As the data of wetting kinetics revealed, both IBU-PVPVA compacts showed very high works of adhesion and an improvement of the immersion and spreading processes (Figure 51). The higher values were assigned to ST-compacts, leading to higher wettability as compared to the COM-Tabs.,

7.2.4.2 Tensiometer of IBU-PVPVA compacts

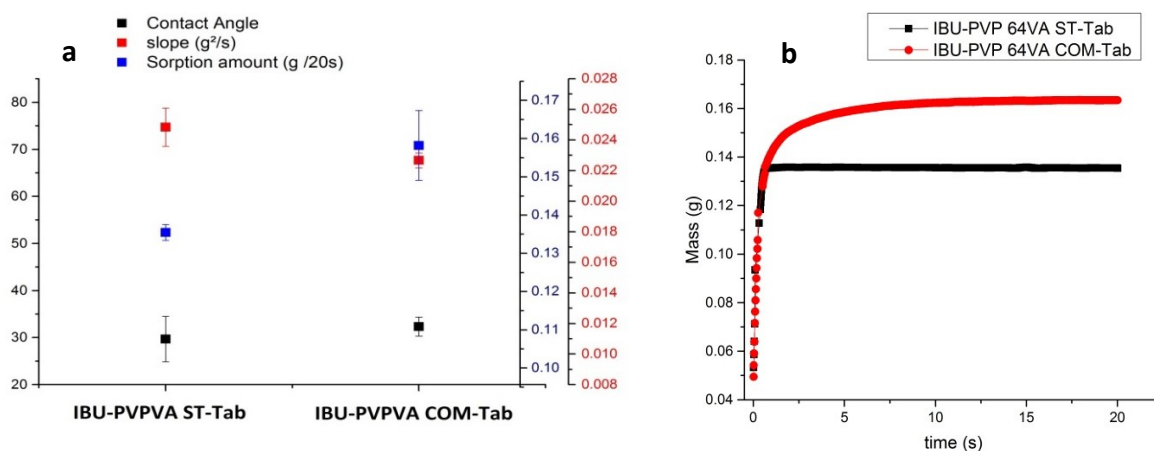


Figure 52 (a) values of contact angle, slope and sorption amount of both IBU-PVPVA compacts, (b) the mass uptake of water into tested compacts

Both compacts having identical weights were tested based on sorption behavior. The both tablets were measured first with n-hexane and then their contact angle measurement with water was performed.

As mentioned before, no measurement could be performed for the pure IBU-compacts. IBU-PVPVA ST-Tab exhibited smaller contact angles and superior slope (rate of adsorption) compared to the COM-compacts (Figure 52). However, IBU-PVPVA COM-compacts showed a higher value of the absorbed mass. Both compacts showed a similar behavior against n-Hexan.

The increased θ , for PVPVA COM-compacts in the presence of water as to ST compacts, indicated to a declined drug surface wetting upon co-milling. The difference in contact angle was, however, not significant.

7.2.5 Density and porosity of IBU-PVPVA compacts

A lower porosity was measured for COM-tablets as compared to their ST-compacts (Table 47). The true density of PVPVA-mixtures with and without co-milling was much similar, whereas the ST-mixture had significantly a lower apparent density. The tablets densities were high and much close to the true densities of the related mixture.

Table 47 Porosity, density of IBU-PVPVA compacts and apparent density of related mixture

formulation	Porosity%	Tablet Density	True density	Apparent density (MIX)
IBU-PVPVA ST-Tab	5.50 ± 0.20	1.13 ± 0.002	1.19 ± 0.002	0.213
IBU-PVPVA COM-Tab	2.43 ± 0.13	1.15 ± 0.002	1.18 ± 0.0002	0.395
IBU CR-Tab	4.28 ± 0.32	1.06 ± 0.004	1.11 ± 0.001	

7.2.6 Hg-porosimetry of IBU-PVPVA granules

The analysis of mercury porosimetry was performed for the prepared granules. Only the data of the instrument 440 were evaluated, to avoid the interference of any inter-granules voids on the obtained values.

The porosity values were lower than the measured ones for the corresponding tablets, showing however, the same trend. The ST-granules were characterized by a higher porosity than the COM-granules, but they presented bizarrely lower values for the total pore surface area. The median pore diameter was much similar (Table 48).

Table 48 Total surface area, porosity and pore diameter of IBU-PVPVA granules from mercury porosimeter

440	Porosity (%)	Total specific (pore) surface area (m ² /g)	r50 (nm)	d _{average} (nm)
IBU-PVPVA ST-Gr	4.3258	18.3440	4.104	8.30
IBU-PVPVA COM-Gr	1.3462	30.5870	5.271	9.24

The cumulative intrusion volume of mercury implied that the most pore volume related to the mercury intruded volume in the nanometer range (Figure 53); particularly for the co-milled granules.

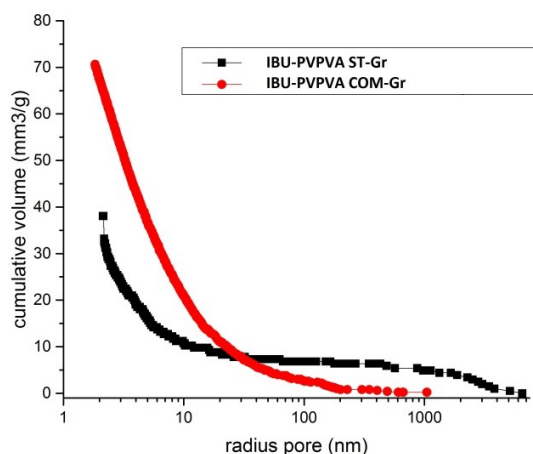


Figure 53 Mercury intrusion curves for IBU-PVPVA granules

7.2.7 PSD of IBU-PVPVA mixtures

Table 49 Particle size distribution of IBU-PVPVA mixtures, before and after milling

	ST-MIX				COM-MIX			
	X10	X50	X90	Span	X10	X50	X90	Span
IBU-PVPVA	30.98 ± 0.20	84.59 ± 1.37	141.50 ± 0.54	1.31 ± 0.02	3.25 ± 0.07	22.62 ± 0.34	61.25 ± 0.45	2.56 ± 0.06
IBU-Cr	10.06 ± 1.83	50.98 ± 1.01	119.29 ± 3.86	2.14 ± 0.00				

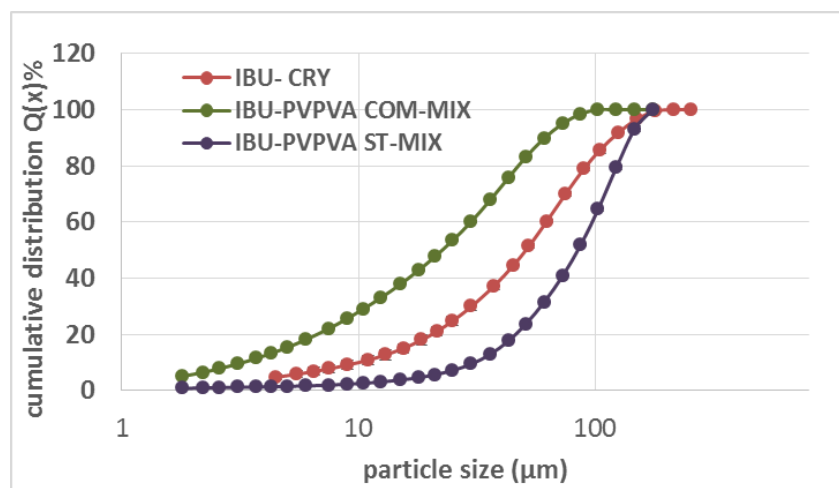


Figure 54 Particle size distributions of IBU-PVPVA mixtures before and after milling

The use of oscillating mill produced obviously an influence on the particle size. Regarding d_{90} , a particle size reduction to around 61 μm was obtained after co-milling. Besides, the volume median diameter of particles decreased from 85 μm up to 23 μm (Table 49). After co-milling, the mixtures were found to be

very fine with an average diameter d_{50} that was 3.7 folds smaller than that before co-milling (Figure 54). Span values of 1.3 and 2.6 were calculated, for ST- and COM-mixture respectively.

7.2.8 Effect of IBU: PVPVA ratio

Tablets of pure ingredients as well as of different IBU/excipient ratio (40: 60) were pressed applying the same conditions (500MPa) and examined regarding their SFE.

The compacts of IBU-PVPVA (20:80) displayed an improved spontaneity of water adhesion over the individual components, and showed a higher polar surface energy than the related compacts of the pure components. The σ^p increased as the PVPVA ratio increased (Figure 55).

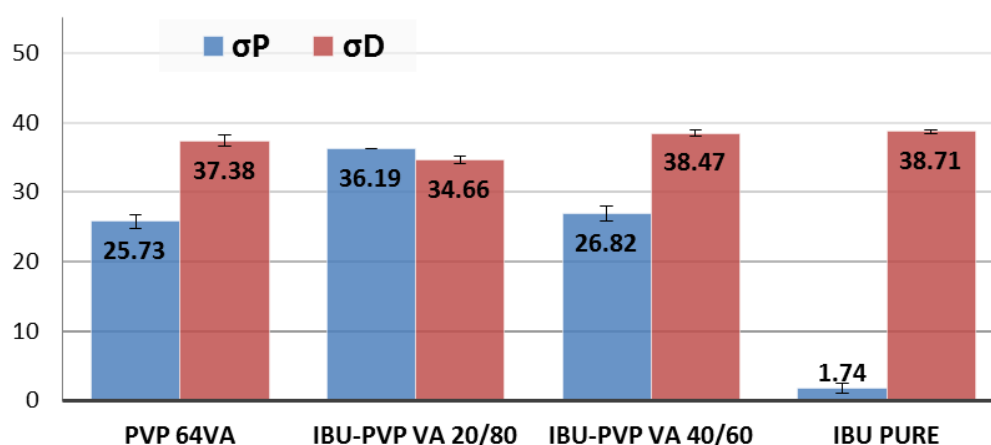


Figure 55 contact angle values for compacts of pure ingredients and of different IBU: PVPVA ratios

7.2.9 IBU-PVPVA compacts under 200MPa

A binary mixture of IBU-PVPVA was compacted under less pressure 200MPa and tested in comparison with of the compacts of 500MPa regarding IDR testing, the dissolution rate of granules at non-Sink condition and SFE.

The compacts under less pressure showed slower dissolution profiles with significantly lower values of the release's slope (IDR 0.957 ± 0.079) compared to those of high-pressure (Figure 56). The granules of 500MPa revealed a faster drug release over the whole testing time of 240 min. Although IBU-PVPVA 200MPa-Tab had a higher porosity ($10.92\% \pm 0.09$) resulting from their lower density ($1.06 \text{ g/cm}^3 \pm 0.001$), their tablets demonstrated a lower overall SFE with significantly lower polarity (38%) as compared to 51% polarity for 500MPa-compacts (Figure 57).

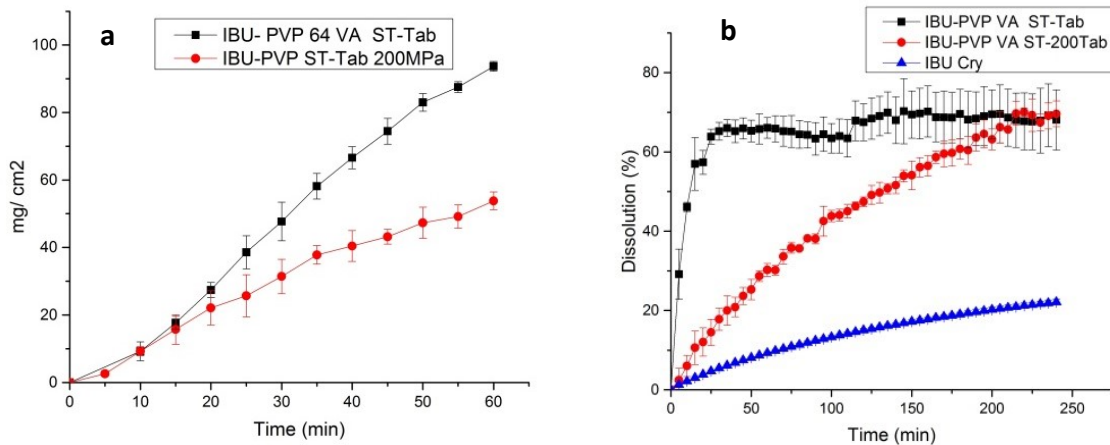


Figure 56 IBU-PVPVA compacts prepared at 200MPa as compared to 500MPa compacts at pH 1.0 (a) IDR (b) dissolution test of granules at non-sink condition

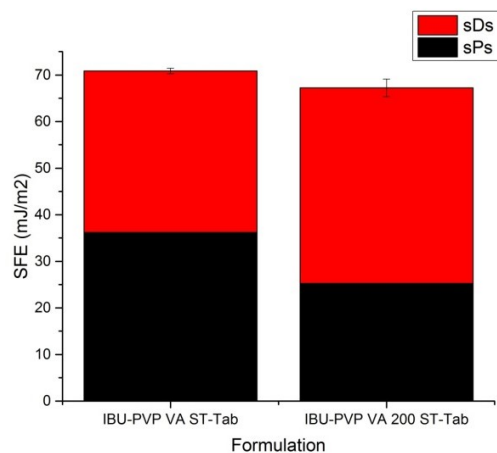


Figure 57 SFE data with polar and dispersive components of IBU-PVPVA compacts under 500 and 200MPa

7.2.10 IBU and PVPVA interactions: FTIR

The assignment of infrared characteristic peaks of the functional groups for neat IBU and PVPVA were described previously in 5.2.2 and 6.2.6 respectively, as. In addition to the narrow peak of C=O stretching of IBU at 1708.7 cm⁻¹, the frequency region of carbonyl was in the scope of investigation for the compacts, due to the stretching peak of C=O cyclic amide (pyrrole) at 1659 cm⁻¹ of PVP and the C=O stretching vibration of acetate ester in VA at 1730 cm⁻¹.

The following changes were observed among the compacts (Figure 58):

1- The stretching vibration bands, assigned to IBU cyclic dimerized OH groups at ~ 2630 and 2730 cm⁻¹ almost disappeared for the ST-compacts and totally disappeared for the COM-compacts. The bending OH

vibrations at 1229 cm^{-1} broadened and the stretching CO vibrations of IBU at 1183 cm^{-1} was almost missing for ST-compacts and entirely disappeared for COM-compacts.

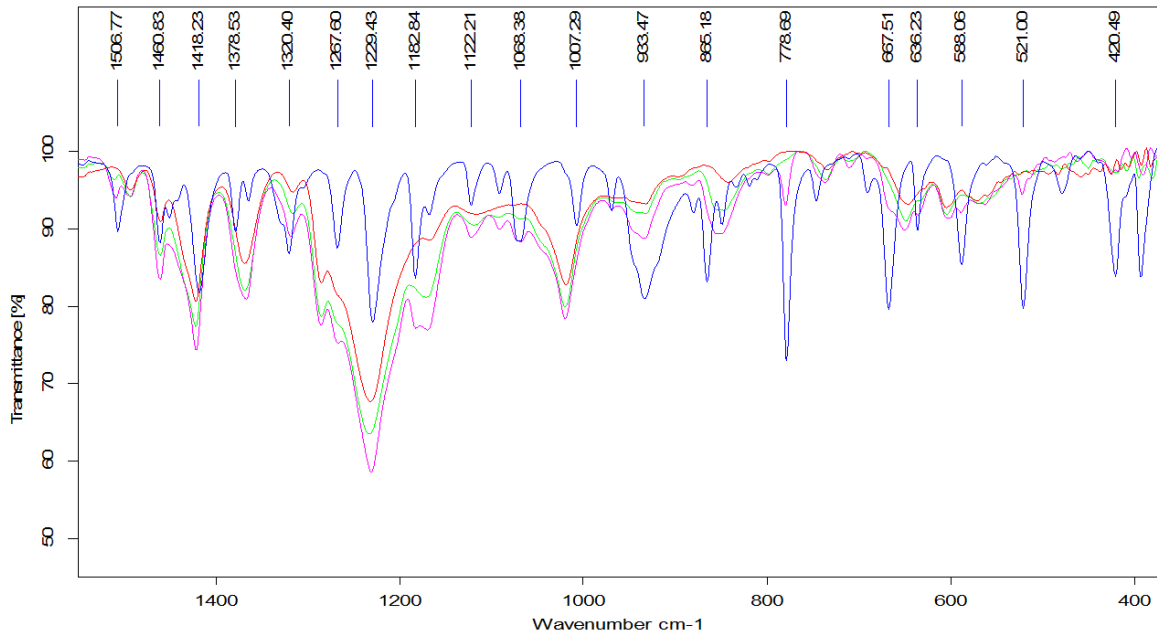
2- The reference band of the carboxylic carbonyl (C=O stretching of IBU) shifted from 1709 cm^{-1} . This was accompanied with a broadening and hypochromic shift to 1725 and 1730 cm^{-1} for the ST- and COM-tablets respectively that integrated within the carbonyl absorption of VA.

3- In parallel, the characteristic peak of carbonyl moiety stretching of the PVP cyclic amide (pyrrole group) was broadened at 1676 and 1673 cm^{-1} for ST- and COM-tablets respectively. Besides, an additional absorption shoulder with a bathochromic shift to a lower wavenumber at 1625 cm^{-1} was monitored, which might refer to a complex formation, most likely by H-bonds [167].

4- Apart from that, the OH stretching peaks of carboxylic acid observed in IBU at the range of $2850\text{-}3150\text{ cm}^{-1}$ were further broadened, revealing triplicate peaks due to the OH and CH stretching, showing a less defined peak that shifted down, especially for the COM-Tab. This manifested as a broad baseline over the range of $2500\text{-}3000\text{ cm}^{-1}$ for COM-compacts and $2500\text{-}3200\text{ cm}^{-1}$ for ST-compacts, which is indicative of H-bonding [167].

5- Specific changes could be seen in the "fingerprint" region, like the less sharpness defined and the disappearance of some peaks. The marked changes were related to the out-of-plane bending vibrations of the aryl substituents, such as the disappearance of the very strong peak at 779 cm^{-1} that linked to the out-of-plane deformation of CH group of the aromatic ring for the co-milled tablets. Similar observations were reported before [166].

7. Incompatibilities of ibuprofen and copovidone under high-pressure compaction



— IBU
— PVPVA
— IBU-PVPVA ST-Tab
— IBU-PVPVA COM-Tab

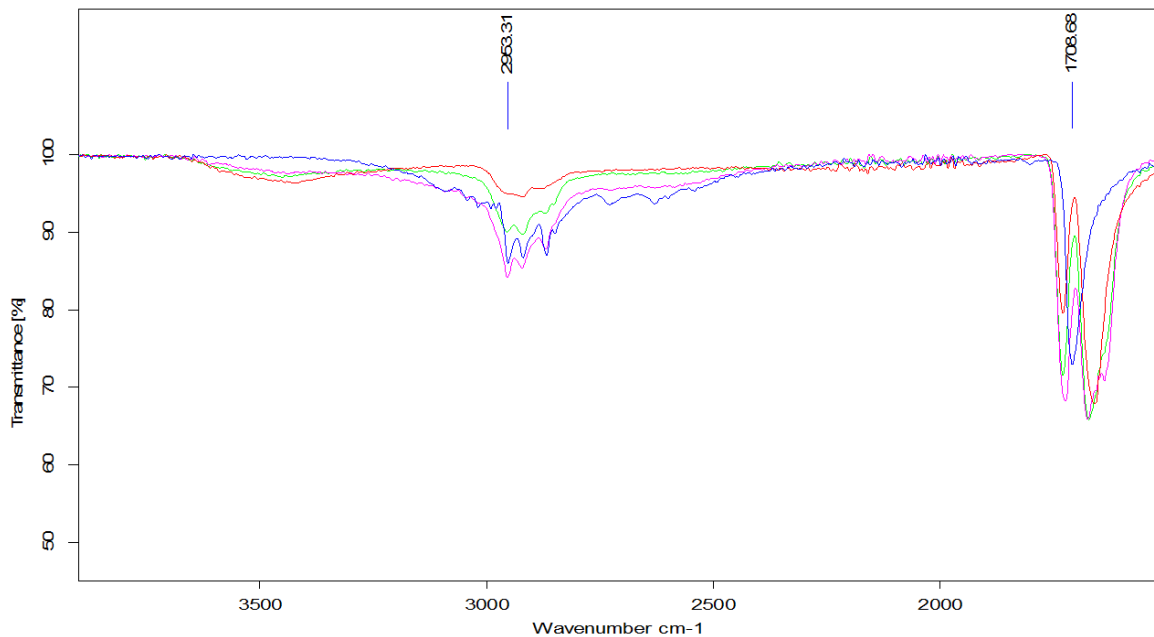


Figure 58 FTIR spectra of pure crystalline IBU, pure PVPVA and IBU-PVPVA ST, IBU-PVPVA COM compacts, the presented ranges refer to bands where prominent changes occurred

7.2.11 Dissolution profiles of stored IBU-PVPVA compacts

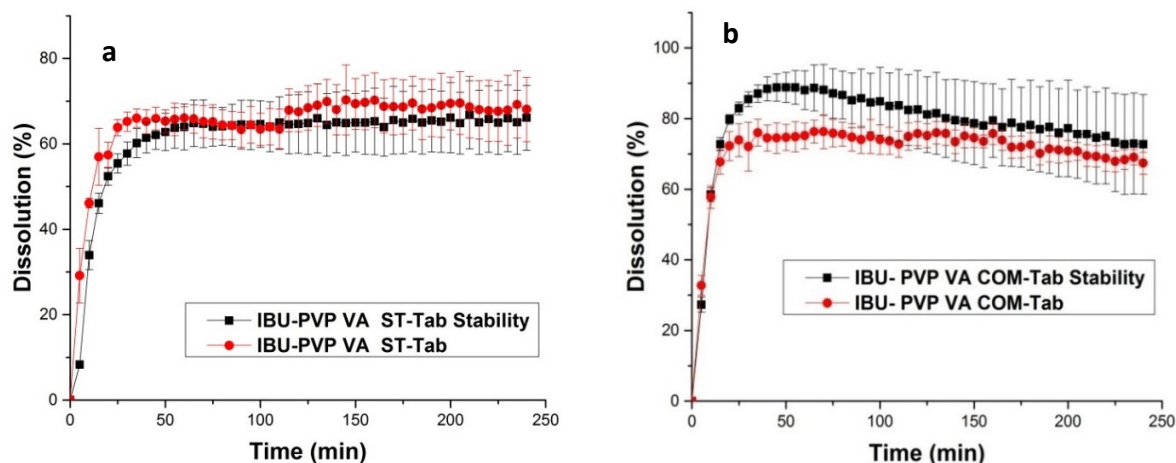


Figure 59 Dissolution profiles of compacts granules a) IBU-PVPVA ST, b) IBU-PVPVA COM; initial and 2 years storage using USP apparatus 1 (basket). 100 rpm; medium volume 900 ml at pH 1.0; mean \pm SD; n = 3

The presence of any reduction in the dissolution rate was investigated by repeating the dissolution test under non-Sink conditions at pH 1.0 for the compacts granules (both ST and COM), that were stored in the desiccator for 2 years and compared to that obtained as initial values for the fresh prepared compacts. No significant differences were observed between the compared dissolution profiles, indicating to a good shelf-life stability of the stored samples in terms of a stable release behavior. However, a slight increase of IBU release was seen for the stored co-milled granules showing a small increase in the precipitation degree (Figure 59).

7.3 Discussion

The impact of high-pressure compaction was clearly noticed that increased the dissolution rate and equilibrium solubility of IBU in the presence of PVPVA. The magnitude of increase was generally higher at pH 5.5. Hence, the ionization process seemed to have a synergy effect on the applied approach producing a stronger efficacy, as less energy is required to transfer IBU molecules into solubilized form in that medium. The additional observed benefits of the co-milling process can be related to the complete amorphousization induced (confirmed by XRPD, SEM and DSC measurements) as well as the reduction in the particle size regarding the dissolution test at non-sink conditions. However, this additive effect of co-milling was not significant in the medium where IBU is neutral. When IBU is able to ionize, the smaller particle size and higher amorphousity can then accelerate the transformation of IBU into the solution, as

higher energy and bigger contact area are provided. By IDR test, this impact was blinded to some extent as the difference between ST- and COM-disks was smaller. The presence of only a limited defined surface (during IDR test) exposed to the medium, besides, the formation of gel-layer by PVPVA, through which IBU molecules should permeate, could be responsible for that observation.

As discussed in section 4.2.6, the conversion of 68% into amorphous substance contributed to an increase of IDR for IBU to 1.3 and 2.2 folds at pH 1.0 and pH 5.5 correspondingly. Hence, the higher amorphousity of 30% for IBU within co-milled tablets could explain the increase in IDR as compared to ST-tablets.

Both XRPD and DSC data confirmed definitively the amorphous state of IBU for the co-milled formulations and the decrease of IBU crystallinity of ST-tablets samples. As the co-milled compacts exhibited higher release rate and solubility compared to the related co-milled mixtures, an extra impact of high-pressure compaction after co-milling could be recorded to accelerate the IBU dissolution process and maintain the supersaturation levels for longer time. This can be explained by increasing the IBU/PVPVA interactions and improving the wetting kinetics as revealed by FTIR and SFE studies respectively.

The solubilizing effect of PVPVA was evidenced by CheqSol analysis, increasing both the kinetic and intrinsic solubilities of IBU. The obtained supersaturation ratio (≈ 1.5) referred to close values of S_0 and S_k . Thus, a less degree of precipitation and a higher ability to preserve supersaturation can be concluded, which indicates to a high strength of interactions between IBU and PVPVA molecules within the aqueous medium.

Different behaviors of IBU solid-state as well as appearance were recorded for PVPVA formulations (compacts and mixtures), depending on the manufacturing procedure, holding time after preparation and storage conditions. The availability of humidity seemed to trigger certain changes in IBU solid-state, converting IBU gradually in a short time into amorphous form, to reach a complete amorphous system at the end, with a glass-like appearance. Apparently and based on the analysis of XRPD data, the application of high-pressure compaction or co-milling process could facilitate and accelerate this conversion process, due to the higher drug/polymer interactions induced.

For the physical mixtures, XRPD revealed that IBU undergoes a complete conversion into amorphous form upon storage at room temperature, which was consistent with a previous work [170]. In our case, the speed of occurrence of these changes was higher under accelerated storage conditions (higher

humidity%) and for the compacts as to the mixtures. Sekizaki *et al.* found a higher decrease in the intensity of IBU peaks for IBU/ PVP physical mixture after merely mixing as the standing time increased with an almost disappearance of the peaks after 14 days, creating a solid dispersion of IBU/ PVP [167]. The absorbed moisture may decrease the T_g of PVPVA and involve in H-bonding with PVPVA chains, leading to an increase in the polymer molecular mobility. This in addition to increasing the temperature may facilitate and speed up IBU/PVPVA interactions.

The change in the appearance, exhibited as glassy-form for the stored physical mixtures and compacts, was an indication of phase transformation into amorphous system. Since the compacts stored in the desiccator showed neither a significant altering in XRPD pattern nor a change in the appearance, prohibiting of IBU-PVPVA formulations from absorbing the ambient humidity could then stabilize the current solid-state of IBU.

The interactions between IBU and PVPVA in the solid-state were analyzed and confirmed by FTIR and DSC. The remarkable reduction in IBU T_m obtained for IBU-PVPVA ST-Tab indicated the induced crystal modification as well as high IBU/ PVPVA interactions [169].

However, the strength of IBU/PVP interactions was reported to be possibly depending on the particle size of IBU or affected by the ratio of both components [167,169]. The micronized IBU (by co-milling) offered a bigger contact area between the two ingredients; hence, the interaction process would speed up. Due to the reduction in the particle size after milling, the co-milled particles demonstrated as expected a higher ability to be condensed, generating a compacted bulk with less pores. However, both compacts had limited pores in the nanometer range.

The increased density by high-pressure compaction (manifested by SEM images) facilitated and ensured a high level of IBU-PVPVA interactions. The condensed alignment of the contiguous components, especially within the co-milled compacts would assure a higher stabilization effect of PVPVA.

The presence of one T_g for COM-Tab indicated the formation of a solid glassy solution. This recorded T_g was, however, lower than the theoretically calculated one of an IBU-PVPVA glass-solution (67 °C) according to Gordone Taylor equation as well as lower than the measured one at 47.1 °C for IBU-PVPVA amorphous free-water system revealed upon second heating. This can be assigned to the interference of residual water within the initial compacts that led to the decrease in the glass transition measured. Thus, a higher mobility of PVPVA molecules is expected with a higher ability to dissolve IBU molecules within the polymer chains by H-bonding.

The increased polarity for the compacts could be attributed to several factors. That includes the formation of H-bonding between IBU and PVPVA; the higher hydrophilicity of the surface due to the adsorbed PVPVA; new crystal habits and the induced amorphous materials.

The adhesion process was spontaneous for the prepared compacts manifested in the high calculated W_a values, that indicate stronger interactions with water.

The initial fast dissolution rate of the compacts can correlate with the high values of work of immersion. W_s values indicated a better spreadability of water on IDM-PVPVA ST-Tab than on co-milled tablets. In this context, the effect of the polymer on wetting studies was discussed in the previous chapters.

Although the ST-compacts showed lower contact angles, the co-milled compacts exhibited a higher ability to absorb water, which might be correlated with the higher drug/polymer interactions and/or the more amount of amorphous material.

A certain level of PVPVA to IBU as well as of the applied pressure has to be delivered in order to obtain a high strength of IBU/PVPVA interactions; as the 80% of PVPVA was superior to 60% for increasing the polarity of the compacts. Bogdanova *et al.* indicated that a low PVP content might cause an incomplete IBU/PVP interaction [166].

The IR data revealed remarkable differences for the compacts regarding the spectral behavior of IBU and PVPVA, manifested as changes in the regions of the carbonyl-, and dimerized hydroxyl groups as well as in the “fingerprints” region. The carbonyl region of PVP was most valuable to observe and understand the changes in IBU-PVPVA system.

Pure amorphous IBU is characterized with a vibration of non H-bonded C=O at a higher wavenumber ($\sim 1730\text{ cm}^{-1}$). The broadening and blueshifting of the IBU carboxylic carbonyl within the compacts is attributed to the alteration of IBU solid-state from crystalline to amorphous form and to destroying of the dimers structure of pure IBU. The vibrational modes were, generally, more broadly spread and have less sharpness, which is normally connected with amorphous materials. The observed changes in vibrational modes among compacts indicted some modifications of IBU structural order.

The apparent shift for OH vibration of IBU, the significant obvious broadening and the reduced frequency for the C=O stretching mode of PVP in the compact system imply the formation of H-bonding of OH groups of IBU to C=O of PVP [58,127], signifying the higher strength of IBU-PVP interactions within compacts. The non-shifting of C=O for vinyl-acetate moiety of PVPVA at 1730 cm^{-1} in case of co-milled compacts, and the minor shifting in case of ST-compacts inferred limited interactions involving this group moiety. Thus, the

main interactions between IBU and PVPVA occur preferentially by protonation of the C=O group of the pyrrole group rather than the C=O in vinyl-acetate group.

Each PVP monomer was proposed to react with one IBU dimer structure through H-bonding and aromatic interactions [166]. The high availability of PVPVA would ensure H-bonding for all IBU molecules. Hence, the excess of non H-bonded PVP can explain the absorption part of C=O PVP at 1676 and 1673 cm^{-1} for ST- and COM-tablets respectively. At low PVPVA concentrations, it is expected that IBU dimers could still present, since not enough PVP carbonyl groups are available to hydrogen bond with all IBU molecules.

FTIR data referred to strong H-bonds between IBU and PVPVA that were formed at the expense of internal H-bonds between IBU molecules, which became very weak or were eventually destroyed. The H-bonding within the dimers structure formed by the same IBU type enantiomers is weaker than that established between HBD of IBU (COOH) and external available HBA groups such as the amide oxygens of PVP [166].

The observation of no change in the dissolution profile for the stored samples in the desiccator was an indication of a stable solid-state of IBU within the stored compacts.

The crystallization is normally accompanied with higher internal H-bonds between the drug molecules. Thus, high-pressure compaction with PVPVA may hinder the recrystallization process of IBU by inhibiting the intermolecular H-bonding between IBU molecules in the single crystals for the favor of IBU-exipient interactions.

The XRPS data and the visual observation implied that no changes have occurred in the original solid-state of IBU for the compacts after being stored in desiccator under ambient conditions for long time. The high molecular weight of PVPVA could also kinetically stabilize the IBU amorphous portion through interactions with IBU in the absence of an extremely absorption of water.

7.4 Conclusion

The application of high-pressure compaction on the IBU/PVPVA binary mixture confirmed the effectiveness of the applied approach to increase the release rate and solubility of IBU, which was indicated previously with IBU/HPC, IBU/ISO, IDM/PVPVA and IDM/ISO systems. The IBU/PVPVA compacts were characterized with higher wettability, density and a new amorphous form of IBU, which was induced by merely compacting. The magnitude of the improvement (in dissolution and solubility) was even higher

by co-milling of the mixture prior to pressing that produced a full amorphousization of IBU, higher IBU/PVPVA interactions and smaller particle sizes.

The phenomenon of the transformation of IBU/PVPVA into supersaturated one amorphous phase and its impact was observed and evaluated for the prepared compacts. Herewith, the high-pressure compaction appears to accelerate this conversion as a high degree of IBU/excipient interactions was induced. However, the speed of this transformation was found to be directly proportional to IBU/PVPVA initial degree of interactions within the system (mainly related to the manufacturing procedure i.e. compaction with or without milling), storage conditions (humidity level) and the holding time after preparation. In spite of the high IBU/PVPVA interactions within the compacts, they revealed a high stability for at least 18 months by storing under dry conditions, showing neither a change in the initial solid-state nor a drop in the dissolution rate.

The involvement of the IBU hydroxyl groups and the PVPVA carbonyl groups (most likely of PVP) in H-bonds was confirmed by FTIR, which appeared to be facilitated, apart from the impact of absorbed water, by the delivered energy of high-pressure compaction and co-milling process. However, the nature and strength of IBU/PVPVA interactions seemed to be well controlled by protecting their formulations from the surrounding moisture.

8 Materials and methods

8.1 Materials

8.1.1 Ingredients for solid formulations

The following chemicals were obtained from commercial suppliers and used as received: Ibuprofen; indomethacin; Kollidon 64VA; low-viscosity hydroxypropylcellulose HPC-SSL; isomalt (GalenIQ 721 DC, agglomerated spherical isomalt with direct compression grade); mannitol (Pearlitol SD100, prepared by spray-drying of hydrogenated mannose solution); sorbitol (Neosorb P20/60, extra coarse sorbitol powder) and magnesium stearate.

Table 50 Overview of the used materials

Material name	Batch. number	Manufacturer / Supplier
Ibuprofen	HE-RO 0302	BASF AG (Ludwigshafen, Germany)
Indomethacin	IND/115003	Swati Spentose Pvt. Ltd. (Mumbai, India)
Kollidon 64VA	07449116KO	BASF AG (Ludwigshafen, Germany)
HPC-SSL	NCH-4021	NIPPON SODA (Tokyo, Japan)
Isomalt	L121494001	Beneo-Palatinit (Mannheim, Germany)
Mannitol	EO14D	Roquette (Lestrem, France)
Sorbitol	E374K	Roquette (Lestrem, France)
Magnesium stearate	LOT 2079	Bärlocher GmbH (Unterschleißheim, Germany)
Hydrochloric acid solution (37%)	17C284010	VWR International GmbH (Fontenay-sous-Bois, France)
Citric Acid Anhydrous	13J31-B03-292832	FAGRON GmbH (Barsbüttel, Germany)
Disodium hydrogen phosphate	10196355	ThermoFisher (Kandel, Germany)
Diiodomethane	STBH7092	Sigma-Aldrich (Steinheim, Germany)
n-Hexan	14A170510	VWR International GmbH (Darmstadt, Germany)
Phosphoric acid 85%	12B280522	VWR International GmbH (Fontenay-sous-Bois, France)
Potassium phosphate monobasic	Lot 82840	Carl Roth GmbH (Karlsruhe, Germany)
Acetonitrile	1716029	Fisher Scientific (Loughborough, U.K)

8.1.2 Chemicals for analytical assays

The hydrochloric acid solution HCl (aq)37% ($\approx 12M$) was used for preparation of the acidic medium HCL 0.1N (pH 1.0). Citric acid anhydrous and disodium hydrogen phosphate Na_2HPO_4 were utilized to prepare the McIlvaine buffer (pH 5.5; 0.05M). Diiodomethane and n-Hexan were applied for the wetting studies.

The following chemicals were used for the HPCL analysis: Phosphoric acid 85%; potassium phosphate monobasic KH₂PO₄; acetonitrile and MilliQ water. The acetonitrile and water were of HPLC grade and all other chemicals were of laboratory reagent grade.

The used ingredients and chemicals are summarized in Table 50.

8.2 Methods

8.2.1 Preparations of the tablets using high-pressure 500MPa

8.2.1.1 *ST-formulations*

Development batches of binary mixtures (drug/excipient) were prepared using a batch size of 40 g with a drug load of 20% (Figure 2). The mixtures were blended for 15 minutes in the Turbula T2A Mixer (W.A. Bachofen, Basel, Switzerland) at 70 rpm and further with magnesium stearate (0.5%) for additional one minute. The blends obtained were directly compressed on a single punch tablet press (FlexiTab, Röltgen GmbH & Co. KG, Solingen, Germany), using 10-mm round flat punches. The Dwell time was set at 500 ms and the compaction force was fixed to reach a pressure of 500MPa. The filling depth was adjusted to obtain 300 mg tablets for each formulation.

8.2.1.2 *COM-formulations (the oscillating mill function)*

Corresponding tablets were also prepared as described previously with the same compositions of ST-formulations, but using co-milled mixtures. The co-milling process was performed using the mechanical oscillating ball mill MM 400 (Retsch, Haan, Germany), as a medial step prior to the compression process, that intensively grind and mix the binary mixtures.

For the milling purpose, a cylindrical jar (internal volume of 50 ml) and a grinding ball (diameter= 25 mm); both made of stainless-steel, were used at frequency 12Hz for 20 min.

As mentioned previously, these tablets produced (Table 1, Table 2 and Table 3) are to be regarded as granules produced via briquetting. Hence, the obtained tablets were granulated by an Erweka Dry Granulator AR402 (Heusenstamm, Germany) as a final step to get dense granules, which would form multiparticulate tablets. The resultant granules were passed through sieves, but only the granules between 1.5 and 2 mm underwent further testing.

The tablets (Tab) for intrinsic dissolution/ wetting testing and the related granules (Gr) for aqueous solubility testing that have been prepared without milling, are referred to as standard compacts (ST), whereas the ones obtained from the milled blends are co-milled compacts (**COM**).

8.2.2 Preparations of IDR disks

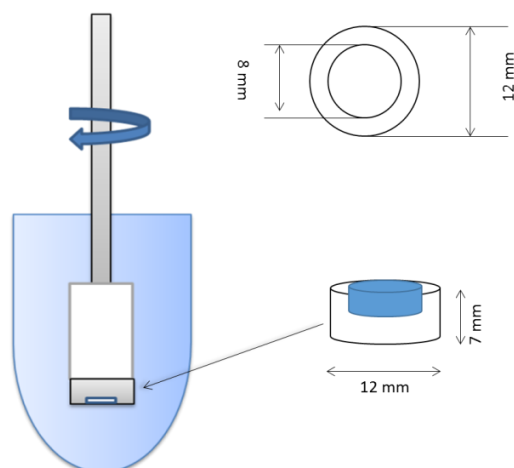


Figure 60 Technical diagram of the new fabricated dies and die assembly for the IDR testing

In order to make non-disintegrating IDR-disks of pure ingredients and all formulations (Table 1, Table 2 and Table 3) feasible at high-pressure, the operation of Flexi-Tab for the compaction was adjusted and modified. The binary mixtures (100 ± 0.5 mg) could then be subjected to 500MPa and compressed directly inside the new fabricated special dies (Figure 60) with known geometry and size ($\phi=8$ mm). This procedure produced disks with a flat surface and diameter of 8 mm at only one side of the die. The dies with the integrated disks were later coupled to the modified assembly of the dissolution tester SOTAX AT7 (Basel, Switzerland) as described further (8.2.3.2 and 8.2.3.3) to ensure one flat surface exposed to the release medium.

8.2.3 Dissolution studies

IBU is a pH-dependent drug. Based on the calculations of Dose number (**Do**) [79] and in order to reflect the pH-dependent solubility of weak acids, two aqueous media with different pH values were of interest to be more relevant to the in-vivo conditions, simulating the GI passage. The media included the simulated gastric fluid hydrochloric acid (HCL) 0.1N (pH 1.0) where ibuprofen is totally unionized, in addition to McIlvaine buffer 0.05 M (pH 5.5). The aqueous medium at pH 6.8 was neglected, considering this pH value corresponds to the region of the ileum, where IBU arrives already dissolved in an ionized form.

In this context, the calculation of D_0 of IBU and IDM at pH 1.0, pH 5.5 and pH 6.8 was performed, which is the dose concentration divided by the saturation solubility C_s (Eq. 5). It represents one of the important aspects that describe the absorption behavior of a drug through the gastrointestinal tract.

$$D_0 = \frac{M/V_0}{C_s} \quad \text{Eq. 5}$$

Where M is the drug dose, V_0 is the water volume ingested during drug administration (approx. 250 mL). To consider a drug as completely absorbed, it must present a value of $D_0 < 1$. The Dose number of IBU obtained at pH 6.8 was ≈ 1 , referring to an acceptable solubility of IBU in this medium. The results of the dose number obtained of IBU and IDM at pH 1.0 and pH 5.5 were obviously > 1 , thus, dissolution and solubility studies were operated at these two different pH levels separately.

8.2.3.1 Dissolution profiles (non-sink conditions)

In vitro drug release studies were carried out for the formulations granules using European Pharmacopoeia dissolution apparatus 1 (SOTAX AT7; Sotax AG, Basel, Switzerland) under non-sink condition in 900 ml of each medium over 4 h at 37 ± 0.5 °C and a stirring speed of 100 rpm. The samples were withdrawn automatically at predetermined time points and analyzed online by UV Spectrophotometer (Agilent 8453; Agilent Technologies GmbH, Waldbronn, Germany). For pH 1.0, IBU was detected at 264 nm for PVPVA formulations and at 220 nm for all other formulations, and) whereas IBU was analyzed at 264 nm for pH 5.5 (Table 51).

On the other hand, IDM was detected at 264 and 319 nm for pH 1.0 and pH 5.5 respectively (Table 52). All experiments were conducted in triplicate.

8.2.3.2 Intrinsic Dissolution procedure & Analysis (Modified apparatus)

To enable the performance of IDR test for the above-mentioned disks (8.2.2), a dissolution tester SOTAX AT7 (basket) was modified. The compact die assembly was built to suit the dissolution apparatus (Figure 60), considering the formal dimensions based on the description of rotating-disk system "Wood's apparatus" for IDR test [172]. This system is used very often compared with fixed-disk system. The IDR-disk dies were positioned centrally in the manufactured die holders, which were then coupled to the spindle of the dissolution equipment, providing a disk distance of 1 inch = 2.54 cm to the bottom of the vessel. This allows the compacted disks to be exposed downwards at one side, at a lower hydrodynamic variability, ensuring a constant disks surface ($\approx 0.5 \text{ cm}^2$) available for the dissolution medium.

IDR analysis was carried out in triplicate at 100 rpm and 37 ± 0.5 °C in 900 ml of each medium.

For IBU formulations at pH 1.0, the samples were withdrawn automatically at predetermined time intervals and analyzed online using Agilent 8453 UV-Vis Spectrophotometer (Agilent Technologies GmbH, Shanghai, China) at 220 nm (264 nm for PVPVA formulations). For pH 5.5, the samples were collected by an autosampler 850-DS Dissolution sampling station (Agilent Technologies, Waldbronn, Germany) at predetermined time intervals and analyzed by a Waters 2695 Separations Module HPLC system, equipped with a photodiode array detector (Waters 996). The separation was performed on a reverse-phase C18 column 5 μ m C18 100A, 150 x 4.6 mm (Inertsil 5 μ OS-3 100A). The mobile phase consisted of 20 mM phosphate potassium pH 2.5: Acetonitrile (50:50 v/v). The eluent was monitored at 230 nm with a flow rate of 1 ml/min (Table 51).

Regarding IDM formulations, the samples were withdrawn automatically at predetermined time intervals at pH 1.0 and pH 5.5 and analyzed online using Agilent 8453 UV-Vis Spectrophotometer at 264 nm (Table 52).

Determination of IDR value

Based on Noyes, Whitney and Nernst equation (Eq. 6), the dissolution rate dc/dt can be estimated.

$$\frac{dc}{dt} = \frac{DS}{Vh} (C_s - C_t) \quad \text{Eq. 6}$$

Where C_s is the saturation solubility at a given temperature; D is the diffusivity; S is the surface area; h is the diffusion layer thickness, and V is the medium volume.

The integration of mass dissolved $W = C \cdot V$ in the previous equation leads to the following Eq. 7:

$$W/S = K(C_s - C_t) \times t \quad \text{Eq. 7}$$

Where $K = D/h$. By holding S constant and plotting of the accumulated amount of drug dissolved per unit area W/S as a function of time t will generate a linear regression and the slope ($K C_s$) refers to mass dissolved per unit area per unit time, which is IDR [111].

8.2.3.3 Intrinsic dissolution test of pure excipients Novel instruments

An instrument was developed and adjusted to determine the IDR of pure excipients, which would help to distinguish its input on IDR of the formulations. The apparatus consists of three parts: A die holder assembly that is mounted to a rotating spindle; a capacitive sensor (BCS0011, BALLUFF, Germany) that is integrated within the spindle, and a time counter (Figure 61). Thereby, the die holder assembly was just fabricated as described previously in the preparation of IDR disks (8.2.2) for dies with $\phi=8$ mm.

The developed procedure enables the determination of the end-point time of IDR test by means of a capacitive sensor, which is sensitive to liquids. As soon as the whole tablet dissolves and the sensor comes into contact with water, the current circle will be broken and the time reader consequently stops counting. The end-point time of IDR-disk dissolution is now known. Depending on the concept of IDR, a linear regression can be extrapolated, whose slope refers to the IDR value. Disks (100 mg) via compaction of pure excipients on their own or after a previous milling were prepared at 500MPa and tested in 900 ml of pH 1.0 and pH 5.5 media at 100 rpm.

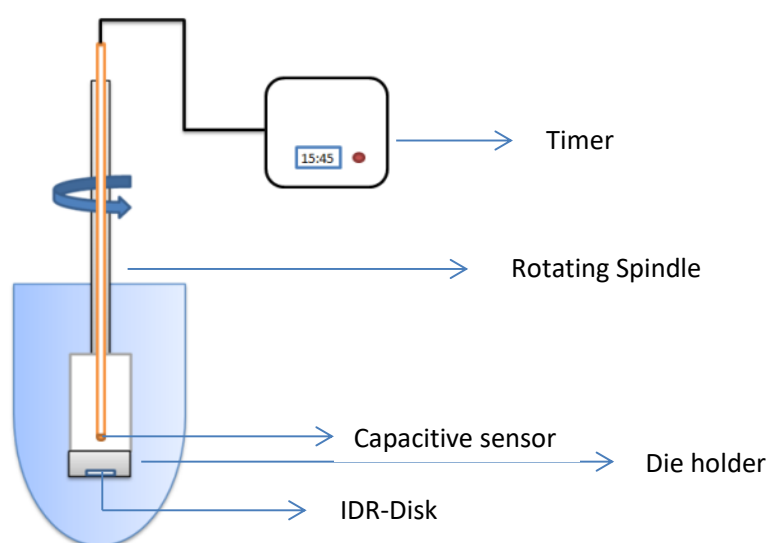


Figure 61 Configuration of IDR developed equipment for pure

8.2.4 Equilibrium solubility at different pH values by Shake flask Method

The determination of the equilibrium solubility of granules, the related mixtures and plain APIs was executed by the classical shake flask method in the same aqueous media used for dissolution studies (pH 1.0 and 5.5). The pH-value of the prepared media was determined prior and at the end of the solubility/dissolution tests using a glass-electrode pH meter, no pH-change (>0.05) of the media was observed. Saturated solutions were prepared by adding 50 ml of selected aqueous media into each flask which contained an excess quantity of the drug. The flasks were shaken for seven days under constant shaking rate of 50 agitations per minute and temperature (25 ± 1 °C) by using a shaking Bath (GFL 1083 Burgwedel, Germany), to ensure the solutions are equilibrated. The solutions were then filtered using cellulose filters with $0.45 \mu\text{m}$ pore size of. The first few drops of filtrate were discarded to avoid the filter absorption. The amount of dissolved IBU was determined in triplicate by an Agilent 8453 UV-Vis Spectrophotometer at

220 and 264 nm for pH 1.0 and pH 5.5 respectively (at 264 nm for PVPVA formulations). The amount of dissolved IDM was determined in triplicate at 264 and 319 nm for pH 1.0 and pH 5.5 respectively (Table 51 and Table 52).

Table 51 Results of UV-VIS calibration and HPLC calibration of ibuprofen for IBU formulations

Parameter	IBU (UV) pH 1.0 (220 nm)	IBU (UV) pH 1.0 (264 nm)	IBU (UV) pH 5.5 (264 nm)	IBU (HPLC) pH 5.5	Unit
slope	36.5239	1.4321	1.6862	5.885E+07	Abs*ml/mg (UV) AU/ mg (HPLC)
intercept	1.015E-02	5.334E-04	8.120E-03	-5.305E+03	Abs (UV) AU (HPLC)
Std.error intercept	7.821E-03	4.621E-04	3.899E-03	6.585E+03	
Correlation coefficient R ²	0.9996	0.9998	0.9998	0.9998	
Linearity range	0.004025 - 0.04025	0.008228 - 0.08228	0.06 - 0.6	0.00215 - 0.0344	mg/ ml
LOD	0.00071	0.00106	0.00763	0.00037	mg/ ml
LOQ	0.00214	0.00323	0.02321	0.00112	mg/ ml

Table 52 Results of UV-VIS calibration of indomethacin for IDM formulations and of fluorescein for the verification of IDR test of pure excipients

Parameter	IDM pH 1.0 (264 nm)	IDM * pH 5.5 (264 nm)	IDM pH 5.5 (319 nm)	Fluorescein (237.5 nm)	Unit
slope	42.9196	47.7237	19.1844	82.7326	Abs*ml/mg
intercept	-3.2479E-05	-2.224E-02	2.92E-04	-2.146E-02	Abs
Std.error intercept	1.057E-03	1.091E-02	6.28E-03	1.468E-02	
Correlation coefficient R ²	0.9995	0.9987	0.9989	0.9975	
Linearity range	0.00046 - 0.0046	0.002075 - 0.02905	0.002075 - 0.0664	0.0014 - 0.014	mg/ ml
LOD	0.00008	0.00075	0.00108	0.00059	mg/ ml
LOQ	0.00025	0.00229	0.00327	0.00177	mg/ ml

*used for IDR test

Theoretical estimation of IBU aqueous solubility increase for melt-quenched IBU and IBU-compacts

For melt-quenched IBU: Based on the variance in their free energy (ΔG), the aqueous solubility increase of the amorphous IBU to its crystalline form could be anticipated by applying Parks model (Eq. 8) [173].

$$\Delta G_c \approx RT \ln (S_{\text{amorphous}} / S_{\text{crystalline}}) \quad \text{Eq. 8}$$

Where R is the gas constant; T is the temperature, and S amorphous/S crystalline is the solubility ratio of the two forms. In order to estimate the free energy difference between the amorphous and crystalline

forms, Hoffman equation (Eq. 9) was applied, at which the melting temperature T_m and the heat of fusion H_f of the crystalline IBU are required.

$$\Delta G_c = \Delta H_f (T_m - T) T / T_m^2 \quad \text{Eq. 9}$$

In spite of the approximate values resulted, the Parks-Hoffman approach still provides a useful prediction of the solubility improvement degree that might be attained by amorphous systems.

For IBU-compacts: The theoretical maximum increase of the solubility for the metastable forms S_0^m to the crystalline IBU S_0^c was estimated applying the approach proposed by Hancock and Parks [42,173].

In an analogous manner to Eq. 9, the free energy difference $\Delta G (G_T^m - G_T^c)$ between metastable/crystalline forms defines the solubility ratio of the two forms S_0^m / S_0^c at the considered temperature T (Eq. 10).

$$\Delta G \approx RT \ln (S_0^m / S_0^c) \quad \text{Eq. 10}$$

To estimate $\Delta G (G_T^m - G_T^c)$, the differences of entropy $\Delta S_f^{m,c}$ and enthalpy $\Delta H_f^{m,c}$ between the two forms should be calculated based on T_m , the enthalpy ΔH_f and entropy of fusion ΔS_f of each form and the difference of the isobaric heat capacities ΔC_p (Eq. 11). The last value is normally considered as constant and approximated to be $\Delta C_p \approx 0$ or $\Delta C_p \approx \Delta S_f$, in case of no available experimental data at the interested temperature; $\Delta T = T_m - T$ and $\Delta S_f^c = \Delta H_f^c / T_m^c$.

$$G_T = (\Delta H_f - (\Delta C_p \times \Delta T)) - (T \times (\Delta H_f / T_m)) - (\Delta C_p \times \ln (T_m / T)) \quad \text{Eq. 11}$$

8.2.5 CheqSol

CheqSol is a novel potentiometric procedure and refers to Chasing Equilibrium Solubility of ionizable compounds. It enables rapid measurements of the kinetic K_s and intrinsic solubility S_0 . The kinetic solubility stands for the concentration of neutral species at the time when the dissolved drug first starts to precipitate. On the other hand, the intrinsic solubility indicates to the equilibrium solubility of the neutral form of an ionizable drug at the pH value where it is totally unionized [112,174]. The determination of the intrinsic and kinetic solubilities of pure ibuprofen as well as the binary mixtures was carried out by CheqSol method using InForm apparatus (Sirius Analytical Instruments Ltd., East Sussex, UK). The apparatus is equipped with an Ag/AgCl double junction reference pH-electrode; a fibre optic dip-probe with a path length of 10 mm that connected to a Sirius diode array spectrophotometer, which is used to record the UV spectra of the solution for the whole time. The system was supplied with Sirius software to refine the experimental data and calculate results. Solubility and pKa [144] experiments were conducted at room temperature 25 °C, in an ionic strength adjusted (ISA) deionized water solution containing 0.15M

NaCl under argon atmosphere. Precise aliquots of standardized 0.5M HCL and 0.5M NaOH were used as acid and base titrants respectively.

8.2.6 Solid-state analysis

8.2.6.1 X-Ray powder diffraction XRPD

For comparative purposes, pure ingredients, the tablets and correlating mixtures containing the corresponding drug/excipient ratio were evaluated using a Philips Expert pro MPD X-ray diffractometer (PANalytical, Almelo, Netherlands), operated at an accelerating voltage of 45 kV, a current of 40 mA and Ni-filtered radiation wavelength of Cu K α = 0.154 nm. The analysis was performed in the angle range of 4 to 45 °2 θ , with a step size of 0.0167 °2 θ at 50.165 times per step and scan speed of 0.042 °2 θ /s.

The X-Pert PRO MPD system was equipped with a 2 θ compensating slit and automatic divergence slit. Stainless steel plates were used for reflection measurements as sample holders with an internal diameter of the ring of 16 mm and the thickness of 2.4 mm. The following settings were applied: continuous rotation as scan mode, sample length of 10 mm, irradiated length of 8 mm and the movement spinning enabled. The diffractograms were analyzed with X'Pert HighScore Plus software (version 2.2c, PANalytical, Almelo, Netherland).

Determination of crystallinity degree by XRPD

The crystallinity of IBU within IBU: HPC, IBU: PVPVA mixtures and tablets as well as of IDM within IDM: PVPVA mixtures and tablets was quantified based on a linear relationship established between the sum of all diffracted peaks intensities (neat areas) in the range 5 to 45 Theta° and the crystalline amount% of the drug.

For the calibration, different amounts of the crystalline drug were mixed with corresponding amount of the polymer in 50 ml high-density polyethylene bottles by a Turbula T2A Mixer at 70 rpm for 15 minutes and analyzed. The analysis was performed in triplicate in case of IBU: HPC and IDM: PVPVA formulations. Plotting the sum of all drug peaks intensities versus the percentage of the crystalline drug generated a linear correlation regression R²=0.99 for both IBU and IDM with an acceptable variation within the measurements (Table 53).

A change in either the crystal habit or in crystalline form can be accompanied by a change in intensities of some peaks or by differential diffraction patterns respectively. The calculation of the crystallinity of IBU based on one specific peak area would deliver a false expression. It is advised to perform the evaluation by XRPD carefully, in particular when any crystal modifications could occur upon pharmaceutical

processing. Hence, it was decided to use the sum of all net intensities by integrating the area under all diffracted peaks in the range of 5 to 45 Theta° for the calculation of crystallinity.

For the determination of the sum of all net areas, the instrumental background contribution to the whole XRPD pattern was offset. Subsequently, the areas of the peaks of crystalline IBU or IDM were differentiated and integrated.

Table 53 Results of XRPD calibration of IBU and IDM for the formulations of IBU-HPC, IBU-PVPV and IDM-PVPVA

Parameter	IBU-PVPVA	IBU-HPC	IDM-PVPVA	Unit
slope	6.061E+04	1.332E+04	1.287E+04	Cts/ Cry%
intercept	-1.399E+05	-1.026E+04	2.416E+04	Cts
Std.error intercept	1.201E+05	4.025E+04	2.525E+04	
Correlation coefficient R ²	0.9919	0.9883	0.9947	
Linearity range	5 - 100	15 - 100	15 - 100	Cry%
LOD	6.54	9.97	6.48	Cry%
LOQ	19.82	30.21	19.63	Cry%

8.2.6.2 Differential Scanning Calorimetry DSC Analysis

DSC studies were performed in order to identify any possible solid-state interactions between API and the excipients. The DSC analysis for individual ingredients, all mixtures and paired granules was done using a DSC2 METTLER TOLEDO (Mettler-Toledo GmbH, Gießen, Germany), equipped with a nitrogen cooling system. Samples (4-16 mg) were weighed into 40µl crucible aluminum-pans (Type: ME- 26763, Mettler Toledo GmbH, Gießen, Germany) with pierced lid and crimped; subsequently, subjected to a successive heating-cooling-heating loop with heating/cooling rates of 10 K/min, and nitrogen as purge gas at a flow of 30 ml/min. The end temperature for the heating cycles was set above the melting temperatures of IBU and IDM. The melting point and enthalpy of fusion of each single compound were measured during the first heating run (conventional DSC mode). The glass transition temperature for neat HPC was measured using TOPEM- mode DSC-measurements with multi-frequency temperature modulation). The data obtained were analyzed with a STARe software DB V13.00 (Mettler-Toledo).

Indium was used as standard for the calibration of the DSC module in the range of 120 to 180 °C with a heating rate of 10 °C/ min, applying the following specifications: 27.45 to 29.45 J/g for the fusion enthalpy and 156.3 to 156.9 °C for the melting point.

Determination of crystallinity degree by DSC

Due to the relatively low drug load (20%) and the crystalline nature of the used excipients other than HPC and PVPVA, the peaks from IBU and IDM overlapped with the excipient peaks in the XRPD diffractograms,

therefore, it was difficult to employ XRPD to quantify the crystallinity degree upon processing for the sugar-alcohols compacts [122]. DSC was also applied for the crystallinity determination as following.

For IBU-formulations:

The samples crystallinity was estimated by quantifying the heat associated with the enthalpy of fusion for IBU. The normalization of the measured heat of fusion within the sample (ΔH_m) to that for a reference of 100% crystalline IBU (ΔH_m°) resulted in the percentage of crystallinity.

$$\text{Crystallinity \%} = [\Delta H_m - \Delta H_c] / \Delta H_m^\circ \times 100\% \quad \text{Eq. 12}$$

In Eq. 12, ΔH_m , ΔH_m° and cold recrystallization ΔH_c were determined by integrating the areas (J/g) under the melting peaks.

For IDM-formulations:

Although the melting point of IDM interfered with the melting endotherm of ISO, the determination of heat of fusion for IDM and consequently the calculation of IDM crystallinity was estimated by applying the following modified Eq. 13. The percent crystallinity was calculated based on the measured $\Delta H_{m1}^\circ = 100.9$ J/g for 100% crystalline IDM and $\Delta H_{m2}^\circ = 87.56$ J/g for 100% crystalline ISO as reference values. Hereby, the weight ratio of IDM: ISO (0.2: 0.8) was taken into consideration as described in the equation, where the sample's heat of melting ΔH_m is determined by integrating the areas (J/g) under the melting peaks. In case of IDM/PVPVA mixtures, ΔH_{m2}° was set to be 0.

$$\text{Crystallinity \%} = \frac{\Delta H_m}{(\Delta H_{m1}^\circ * 0.2) + (\Delta H_{m2}^\circ * 0.8)} \times 100\% \quad \text{Eq. 13}$$

8.2.7 Scanning electron microscopy (SEM)

An estimate of the morphological changes can be obtained by means of the SEM photographs observation. A microscopic assessment was applied by taking images of the tablets surfaces as well as cross-sections of the tablets using a SEM (Hitachi SU 3500, Tokyo, Japan) and comparing them with images of pure ingredients and related mixtures. The SEM analysis was performed via different detectors.

The samples were spread on SEM aluminum stubs by a double side adhesive tape and sputtered with gold. The scanning electron microscope operated at high Vacuum mode with an excitation voltage of 10 Kv using Secondary Electron (SE) detector and Backscattered Electron (BSE) detector.

SEM was also used to examine the surface topography and composition of the tablets surface at VP mode (variable pressure operation) using Ultra Variable-Pressure Detector (UVD) or Backscattered Electron

(BSE) detector. For VP mode, imaging was performed directly on the samples without coating with gold, to obtain the image surface information at low vacuum and low accelerating voltages, facilitating the analysis of surface phase's combination. The samples were fixed in this case on a double-sided adhesive carbon tape, mounted on aluminum specimen holders.

BSE imaging, at low vacuum and low accelerating voltages, provides an image contrast as a function of the elemental composition.

8.2.8 Wetting studies

For wettability studies, the tested tablets were compressed without Mg-stearate, to avoid any interference with the measured angles; the abundance of methyl CH₃ and methylene CH₂ groups on the surface would be reflected in poor wetting properties.

8.2.8.1 Drop Shape Analysis (SFE & wetting kinetics)

Contact angle measurements of the tablets were carried out goniometry by applying Drop Shape Analysis **DSA** using an Easy Drop FM40 (Krüss GmbH, Hamburg, Germany); with a sessile drop type method. Drops of tested solutions were deposited on the compacts flat surface, where the compacts were laid on a metal adjustable table. Images were captured by the FTA image analyzer, supported with a DSA 20E software. The image of the sessile drop was analyzed at the points of intersections (three-phase contact points) between the drop contour, air and the tablet's surface (baseline in the image). Depending on the drop formed shape, different fitting mathematical expressions were employed for calculation of the contact angle through determining the slope of the tangent to the drop at the interface line of liquid-solid-vapor phases. Water and Diiodomethane were used as testing liquids. The drop dosing volume was set to 6 μ l and 3 μ l for water and Diiodomethane respectively, using a dosing needle \varnothing = 0.8 mm. All angles were recorded one minute after the deposition of the testing drop on the tablets surface by a high speed camera at room temperature. The reported values are an average of three measurements.

The drop size, dynamic effects and the measurement technique will affect the obtained values. Other measurement procedures saturate the bed with the liquid and then place a small drop on surface, but this can lead to a swelling and deformation of the surface. Therefore, the measurement time was fixed at one minute after placing of the drop to avoid any problem regarding structural integrity [135], which was not changed during the measurements.

The applied technique was simple and relatively reproducible with an error of around ± 3 . The data revealed even low values of error (less than ± 1) and higher reproducibility for very smooth model surfaces. The smooth surfaces of prepared compacts decreased the hysteresis of the measured contact angles. The abrasions sizes for some tablets were too small to change or affect the measured angles.

The measurements on various points over the compacts surface revealed rather a homogeneous nature. This is important, because vapours can sometimes adsorb onto different sites producing faces with different compositions (dirty surface), which can affect the measurements.

The measured contact angles with water and Diiodomethane on the surfaces were utilized to estimate the average dispersive and polar components of surface free energy SFE. The SFE value represents the solid-vapour interfacial energy, and describes the nature of solid surface. Hence, its measurement was preferred as appropriate technique to provide some understanding of the compacts surface characterizations. As all compacts showed relatively flat nonporous surfaces, especially with HPC and PVPVA, the effect of hysteresis on the results was not considerable.

As stated by Young (Eq. 14), there is a relationship between the solid SFE (σ_s), the contact angle θ , the liquid surface tension (σ_l) and the interfacial tension between the liquid and the solid (σ_{sl}) [135,175].

$$\sigma_s = \sigma_{sl} + \sigma_l \cdot \cos \theta \quad \text{Eq. 14}$$

The hydrophilic nature of the compacts can be determined via SFE, which is for solids equal to the surface tension of liquids and has to be considered when water has to spread over solid [82]. SFE of a solid refers to the work, which has to be expended in order to increase the size of the solid surface [176]. It is estimated as energy per unit area (mJ/m^2 or mN/m).

Since initial calculations, applying the basis equation of SFE theories, revealed values over $20 \text{ mJ}/\text{m}^2$; therefore, the OWRK (Owens-Wendt-Rabel-Kaelble) method was chosen preferably as an appropriate method for the calculation (Eq. 15). The effect of polar and disperse intermolecular interactions of the compacts are then investigated regarding the wettability and adhesion processes [175].

According to OWRK, SFE is divided into individual components associated with distinct interactions, assuming that σ_{sl} is an outcome of various interfacial interactions that relate to the properties of both the measured solid and the measurement liquids.

$$\sqrt{\sigma_{sv}^d \sigma_{lv}^d} + \sqrt{\sigma_{sv}^p \sigma_{lv}^p} = 0.5 \sigma_{lv} (1 + \cos \theta_Y) \quad \text{Eq. 15}$$

Where θ_Y is Young's contact angle, σ_{sv}^p and σ_{sv}^d refer to the polar and dispersive parts of SFE respectively, that are unknown. Thus, two liquids with known polar σ_{lv}^p and dispersive σ_{lv}^d fractions of the surface tension σ_{lv} are required to solve this equation, wherein at least one of two liquids must have a polar part > 0 . Water was preferred as a testing liquid with a dominant polar component and Diiodomethane was chosen as a dispersive liquid; both liquids are most often utilized [177,178]. The properties of both liquids are summarized in Appendix Table 56. The final calculation of SFE was done according to DIN 55660-2:2011-12.

Furthermore, there is a need to develop and establish a relationship between the wetting kinetics of tablets and the obtained dissolution rates. Hence, the wetting kinetics were reviewed and investigated as an alternative approach for understanding the measured IDR.

The wetting kinetics were inspected based on the contact angle values with water and the interfacial tension. The impact of high-pressure compaction on processes of adhesion, immersion, and spreading was demonstrated, calculated as described in Eq. 16, Eq. 17 and Eq. 18 respectively that derived from the Young's equation.

The work of adhesion W_a per unit area, that induces solid-liquid interface at the expense of the other phases' interfaces (solid-vapour SV and liquid-vapour LV), can be presented as

$$W_a = \sigma_{SL} - (\sigma_{SV} + \sigma_{LV}) = \sigma_{LV} (\cos \theta + 1) \quad \text{Eq. 16}$$

The higher the W_a is, the higher are the adhesive forces between water and solid.

The immersion process W_i [134] describes the change of 4 interfaces of solid-vapour to solid-liquid SL interfaces, whereas liquid-vapour interfaces don't change.

$$W_i = 4\sigma_{SL} - 4\sigma_{LV} = 4\sigma_{LV} (\cos \theta) \quad \text{Eq. 17}$$

The work of spreading W_s refers to the amount of energy expended to spread (complete wetting) a liquid on a solid surface per unit area. The energy required is equal to the difference between the work of cohesion of the spreading liquid and the work of adhesion (between two phases). It describes the replacement of solid-liquid interface by the other phases interfaces [135] as

$$W_s = \sigma_{LV} (\cos \theta - 1) \quad \text{Eq. 18}$$

8.2.8.2 *Tensiometer: Sorption behaviour*

Based on the capillary rise principle, the dynamic fluid sorption technique was used to determine the wettability of the tablets using an automated Tensiometer K100 (Krüss, GmbH, Hamburg, Germany) with a surface sensitivity detection of 0.005 g. The modified tablets holder, which was mounted to a force sensor and Washburn approach [139] enabled measuring the contact angle. Besides, the sorption behaviour was analyzed by measuring the increasing tablet mass due to the amount of absorbed liquid via a force sensor with respect to time.

Compacts with an identical weight (300 ± 5 mg) were tested, this is crucial to get comparable results.

$$\frac{m^2}{t} = \frac{C \cdot P^2 \cdot \sigma \cdot \cos \theta}{\eta} \quad \text{Eq. 19}$$

As soon as the tablet and liquid are brought into contact, the increase in mass of the tablet due to the capillary force is measured against time.

As seen in Eq. 19, plotting the square of the mass m^2 against time t shows a linear correlation regression, the slope of which, for known liquid parameters (σ surface tension, ρ density and η viscosity), contains only two unknowns: the capillary constant C and the contact angle θ . By determining C values, contact angle calculations with a liquid like water could be then performed.

The C value is characteristic value of each material that depends on the porosity of the compacts bed (Eq. 20), thus, C determination for each tested sample would normalize its porosity.

$$C = r_{eff} A^2 \epsilon^2 / 2 \quad \text{Eq. 20}$$

Where r_{eff} refers to the effective radius of each individual capillary tube within the capillary bundles; A is the area of the cross-section of packed tube and ϵ is the porosity of packing material. In order to estimate the material capillary constant of each formulation, all compacts were measured first with n-hexane as a completely wetting liquid, which has a very low surface tension and θ can, thus, be assumed to be zero ($\cos \theta = 1$). The estimated C value for each sample was employed later to measure the contact angle of each sample with water, utilizing the slope of the uptake curves, viscosities, densities, and surface tensions of the test-liquids. All experiments were run in triplicate.

The Washburn method is normally performed with loosely packed bed of the solid [82] and it has some analytical issues to consider, such as the assumption of a cylindrical pore shape for all materials and a similar radius r of all parallel capillaries for the same material. Other issues include the flow type of the liquid movement and the possible liquid separation from the unwetted, which can affect the results. Nevertheless, it provided a good indication of each compact's wettability and ability to uptake water.

8.2.9 Fourier transform infrared spectroscopy FTIR-ATR

The inspection of any modification in the environment of ibuprofen and indomethacin functional groups was performed by FTIR-spectroscopy studies. The presence of certain interactions between chemical moieties can be detected as well as the type of these interactions (intermolecular or intramolecular). Besides, having shifts in the vibrations' positions in the IR spectrum or changes in their peaks shapes can also refer to changes in the drug solid-state.

ATR-FTIR technique was employed; it allows a direct observation of the sample, without any special preparations that could alter their characteristics. The FTIR spectra of the compacts and pure ingredients were recorded by a Bruker ALPHA (Ettlingen, Germany) in combination with a diamond Attenuated Total Reflection (ATR) unit over a wavenumber range of 400 to 4000 cm^{-1} . The samples were measured at a resolution of 2 cm^{-1} and an accumulation of 20 scans, where the average of these successive scans was collected at a scanning speed 2 U/s.

The samples were dried before analysis under vacuum in a vacuum oven (WTC binder 9030-0010, Tuttlingen, Germany) at 25°C over night, so that the changes in the extent of the drug-polymer interactions would not be masked by any absorbed moisture and water interference. The samples were not subjected to any special further preparation except being positioned between the diamond crystal of ATR unit and the anvil. The evaluation of data was supported by Bruker's spectroscopy software OPUS® 6.5.

8.2.10 Tablets Porosity

The total porosity of the tablets was estimated based on solid fraction calculations [179] as shown in Eq. 21, by measuring the tablets dimensions (diameter and thickness) using an electronic digital caliper (Fisher Scientific, UK).

The true density of corresponding mixtures was determined using a Pycnometer AccuPyc 1330 (Micromeritics GmbH, Aachen, Germany), where the sample volume was determined using helium gas. The operation included 20 runs of purges and maximum 25 runs of procedures. The measurement stopped as soon as the standard deviation for five measurements in succession was less than 0.005%.

$$\text{Tablet porosity} = \left[1 - \frac{\left(\frac{\text{tablet weight}}{\text{tablet volume}} \right)}{\text{true density of mixtures}} \right] \times 100 \quad \text{Eq. 21}$$

8.2.11 Mercury porosimeter

The obtained tablets were subjected to the mercury intrusion porosimetry. The experiments were carried out with PASCAL 140 and PASCAL 440 (Porotec GmbH, Hofheim/Ts, Germany). The method is based on the intrusion process of mercury into pores and capillaries. The intrusion is controlled by an applied pressure from just above vacuum to 400 MPa, which is reduced again during the extrusion process.

The intruded volume of mercury is measured with each pressure change, by which the volume of pores in the corresponding size will be determined. A mercury penetrometer (electrical capacitance dilatometer) measured the volume of mercury that intruded into the pores. Laplace-Washburn equation (Eq. 22) was applied to convert the pressure values into pore diameters as following [180]:

$$d = - \frac{4 \gamma \cos \theta}{P} \quad \text{Eq. 22}$$

Where d is the pore diameter; γ is the interfacial tension between mercury, solid, and vacuum that assumed to be 0.48 Nm^{-1} ; θ is the contact angle and P is the applied pressure.

For a porous material, a relationship between the pore diameter and pore volume can be established by measuring the apparent volume and the volume of mercury intruded. PASCAL 140 is able to measure the diameter of pore sizes in the range $3.8 - 116 \mu\text{m}$, whereas 440 can measure from $15 \mu\text{m}$ down to 3.6 nm . Beside porosity, this test also provides information about bulk; apparent densities, and porosity parameters, such as the average pore diameter, total pore specific area and pore size distributions.

The test was performed first for the tablets (one tablet each formulation). The tablets were evacuated to remove any residual moisture and analyzed at room temperature. Since the dimensions of the tablets are well measured before performing the test, their bulk density **BD** could be accurately determined and employed with the total volume of mercury intrusion that is obtained from the test V_{max} to determine the tablets total porosity **POR%** (Eq. 23). **POR%** was finally calculated as the ratio between the sample void volumes (inter and intra porosity) and its external volume (inverse of bulk density).

$$\text{POR}\% = [V_{\text{max}} / (1 / \text{BD})] \times 100 \quad \text{Eq. 23}$$

The bulk density is the density of the tablet that referred to its external volume (g/cc).

The average of pore diameter d_{average} was calculated from the following equation (Eq. 24):

$$d_{\text{average}} = 4 V_{\text{max}} / S \quad \text{Eq. 24}$$

S is the total pore surface area.

The r_{50} was determined as the pore radius at 50% of the maximum cumulative intrusion volume of mercury.

Additionally, the analysis of mercury porosimetry was also performed for the prepared granules for comparison purpose.

Artificial pores (inter-granules voids) could be created due to the packing of the granules under increasing pressure inside the penetrometer cell, which may lead to fault values. This kind of error, however, can be significant regarding almost non-porous samples [143]. Therefore, to avoid this interference with the obtained data for the granules' porosity, subtracting the spaces and voids between the sample pieces has to be executed. The presence of these voids is not expected in case of the analysis of complete tablets. Thus, the previous analysis, which was executed for each formulation with one tablet, was employed to determine the maximum value of pores sizes that could be presenting within the compacts. This threshold value was used to offset the data of granules obtained from both 140 and 440 instruments, and only the points corresponding to the internal pores were included for the evaluation. Accordingly, the intruded volume of mercury and total pore surface area were corrected; the apparent density, average of pores diameter and total porosity were calculated.

The apparent density AD is calculated as described in **Eq. 25**.

$$AD = 1 / [(1 / BD) - V_{max}] \quad \text{Eq. 25}$$

AD describes the true density of the sample. The bulk density BD is the density of granules referred to its external volume that can be estimated as described in Eq. 26 and V_{max} is the total volume of mercury penetrated.

$$BD = SM / [(WD + Hg - WD) / HgDB - (WD + Hg + Sco - WD - SM) / HgDA] \quad \text{Eq. 26}$$

Where SM is the sample mass (g); HgDB is the density of mercury calculated at blank temperature (g/cc); HgDA is the density of mercury calculated at the analysis temperature (g/cc); WD is the weight of empty dilatometer (g); WD + Hg is the weight of dilatometer plus mercury in the blank (g) and WD + Hg + Sco is the weight if dilatometer plus mercury plus sample, this weight is corrected (g).

The average of pore diameter $d_{average}$, r_{50} and porosity% were finally calculated as described above for the tablets.

8.2.12 Particle size distribution (PSD) of ST and COM mixtures

The Helos KA/LA 644 laser diffraction testing instrument (Sympatec GmbH, Clausthal-Zellerfeld, Germany) was used to evaluate PSD of the physical mixtures (ST) and their co-milled counterparts, supported with

Windox 3.4 software for the calculations. A Rodos module SR 544 from Sympatec was used as a dry dispersing system. Lenses with different focal lengths were used; the air pressure was adjusted to assure a good dispersion of the bulk samples. The calculations were conducted based on the Fraunhofer diffraction theory. The distribution width was expressed by calculating the span as defined in Eq. 27.

$$\text{Span} = d_{90} - d_{10} / d_{50} \quad \text{Eq. 27}$$

d_{90} , d_{50} and d_{10} are the average diameters (μm) at the respective percentile of accumulation. d_{50} refers to the diameter size where half of distribution lies above and half below this diameter. 90 percent of the distribution lies below the d_{90} value, and 10 percent of the distribution lies below the d_{10} .

8.2.13 Specific area

The determination of specific surface areas for the granules was carried out according to adsorption isotherm derived by the Brunauer, Emmet and Teller method (BET), using a high speed gas sorption analyzer Nova 3200 Series Model 6.11 (Quantachrome GmbH & Co. KG, Odelzhausen, Germany).

A sample weight of a range between 3 - 4.5 g was first degassed under vacuum and dried for 24 h at pre-specified temperature that was below the melting point of the tested drug and excipients. Nitrogen was used as an adsorbent gas. One measurement for each formulation was considered sufficient [69]. The granules underwent physical adsorption of nitrogen at ≈ -195.79 °C by immersing the sample holder in a liquid nitrogen bath during the test. As the adsorption started, the volume of nitrogen adsorbed as a function of its relative pressure was recorded. A single point BET at a relative pressure of ≈ 0.3 as well as five points (BET multipoint) at a range of relative pressures (0.09 – 0.3) were obtained. The results listed are from the 5 points BET. The correlation coefficients as well as the BET constant for all measurements were acceptable.

The following settings were hold during the measurements. Adsorption setup: tolerance 0.10 mm Hg; equilibrium time 180 s and dwell time 360 s. Desorption setup: tolerance 0.10 mm Hg; equilibrium time 60 s and dwell time 180 s.

8.2.14 Preparation of melt quenched IBU (IBU-MQ)

Due to the expected increased solubility of amorphous forms as to the crystalline counterparts, a metastable IBU that possesses a high amorphous fraction was prepared by the direct melt quenching method. This might help to estimate the specific contribution of the amorphous part on the increased solubility and IDR for IBU-HPC COM-formulation, which has a partial amorphousity. The procedure included melting of IBU in an electrical furnace and keeping it in a ceramic crucible for 15 min at 100 °C,

which is around 20 °C above IBU melting point. This was followed by immediately quick cooling of the IBU-melt through direct pouring of liquid nitrogen LiN₂. The bottom of ceramic crucible was then carefully dipped into a shallow pool of LiN₂ for another 15 min to prevent the melt from coming into a warm environment again. The quenched IBU was then equilibrated and dried under vacuum in a vacuum oven (WTC binder9030-0010, Tuttlingen, Germany) at 25 °C, to protect it from humidity, and stored immediately in a desiccator containing silica gel (phosphorous pentoxide) at -7 °C to be tested.

The melt quenched IBU was analyzed by XRPD, IDR and shake flask method and the results compared to that of the crystalline IBU.

8.2.15 Data analysis

The data were analyzed by one-way analysis of variance ANOVA, using OriginPro statistical package, to observe and evaluate differences within the formulations regarding the measured variables and tested parameters. The differences were considered significant when p-value was lower than $p < 0.05$ (significance level). The IDR values were obtained as the slope of the fitted line through the time intervals points for all compacts and compared by linear regression. Principal Components Analysis (PCA) was carried out to condense the data obtained from the original examined factors (that could affect the drug release such as solubility, polarity etc.) into a smaller set of new composite dimensions, and to reveal relationships between those factors themselves and between the factors and formulations' performance regarding the obtained IDR values, thereby allowing better interpretations of the results.

9 Summary and outlook

Many of the new API candidates are impaired by low aqueous solubility and slow dissolution rates, which may hinder their pharmacological response. Therefore, there is an increasing need to investigate and implement new approaches that are easily applicable in the formulation development to enhance solubility and/or dissolution kinetics of sparingly soluble APIs.

The purpose of this research was to develop new carrier systems for an optimized administration of borderline poorly soluble drugs, giving more attention to the formulation assessment, since an appropriate formulation is of key importance to achieve successful drug delivery.

The design of enabling formulations was proposed that enables a reliable drug therapy based on the manipulation of the drug solid-state as well as the bulk surface properties, particularly for poorly soluble drugs that exhibit limited absorption as a consequence of low GIT available concentration. The strategy of the enabling formulation involves the preparation of solid compacts composing of binary mixtures of a crystalline API and a hydrophilic excipient that has polar functional groups, compressed under very high-pressure.

Ibuprofen and indomethacin, as model compounds, as well as five excipients were used. The low-viscosity hydroxypropylcellulose and copovidone were selected as polymeric model excipients. The three sugar-alcohols based model excipients were isomalt, mannitol and sorbitol. Two potential impacts can be induced by this process on the physicochemical properties of API within the formulated product, through which the API solubility and dissolution rate can be improved. The first impact relates to the ability to induce a crystal modification on the neat API solid-state attributes (including crystallinity, crystal defects/polymorphism and crystal habits). The second potential impact relates to the manipulation of the overall tablet solid surface and its wettability.

The high-pressure compaction of IBU and IDM with polyols, namely isomalt, improved the solubility and intrinsic dissolution rate significantly, without changing the crystalline state of drugs. In combination with the polymers HPC and PVPVA, the effect on solubility and dissolution was even more pronounced, but with a high degree of drug transformed into amorphous state for the co-milled formulation. In general, the magnitude of the increase in solubility and IDR was carrier-dependent and did not necessarily require a co-milling step of the binary mixture prior to compaction.

The developed systems exhibited an adequate and sufficient preservation of the supersaturation state of model-drugs and a fast release with an acceptable stability of the dissolved drug in the dissolution medium, which might assure no drug precipitation during the GI-passage. Moreover, acceptable shelf-life stabilization was monitored for IBU and IDM in an amorphous state regarding HPC and PVPVA co-milled compacts, respectively.

Based on the data collected, the process appeared to trigger and induce a kind of modification in either the crystal properties of API or in the solid surface properties which produced a hydrophilization effect on the resulted compacts surfaces. A higher strength of interactions was obtained between the two adjacent components in the final formed matrix, which consequently possessed a high surface energy. This was reflected particularly in the higher polarity and stronger attractive forces toward aqueous media. Thus, improved wettability was observed.

The analysis of XRPD, DSC and FTIR might not suggest the existence of enantiotropic or monotropic polymorphs. However, the data indicated a lattice modification of ibuprofen and indomethacin, even to a partial extent, which most likely occurred on the surface.

Three main effects could be generated due to the high level of mechanical energy applied. These effects comprised a change in crystal habits, partial polymorphism and/ or amorphousization. These solid-state transformations and changes caused a kind of “mechanochemically-transformed” or “activated” drug, i.e., a higher internal released energy, thus, better solubility was obtained. Higher magnitude of changes was connected with higher IDR and solubility values.

The wetting analysis data of compacts indicated a new favourable exposure of hydrophilic crystal facets emerging on the surface, as a result of internalization, positioning and merging of the excipient’s polar functional groups of the on the bulk surface (with possible H-bond interactions with API). The compacts possessed a higher degree of hydrophilic interactions with the aqueous media, which resulted in better wettability and faster drug release.

The data suggests a high strength of API/excipient interactions produced upon the applied compaction. In this context, the existence of specific parts of the API molecule that can be either protonated (weak base) or deprotonated (weak acid) is apparently crucial to obtain high potential interactions, damaging the self-association of the drug molecules. The drug/excipient new interactions could assure the stabilization of the API kinetically within the crystalline dispersion matrix, which reduce the tendency of

any polymorphic transition. Taking the increased interactions accompanied to some co-milled formulations into account, a certain range of the particle size of both ingredients might be required to facilitate and ensure a suitable environment for API/excipient. For systems that own the property to build strong interactions in the solution like IDM-PVPVA, a further investigation should be performed to determine the required pressure to trigger such interactions and to proof the feasibility of the application of the method.

Generally, all compacts revealed low porosity. This is an important aspect for IDR testing and the shape drops analysis, where a low porosity is required to perform the tests.

The presence of a high ratio of the hydrophilic excipient seems to be essential to restrict the water self-association and its ability to drive out non-polar drug molecules. For the prepared compacts, the dissolution process can be considered as carrier dependent process. Herewith, the type and properties of the used excipient proved to be crucial for forming a high level of interactions with IBU or IDM. The neat excipients were determinant of the overall generated effects regarding the API kinetic solubility, intrinsic solubility, compacts wettability and dissolution performances. The high intensity of the proposed process to increase the wettability and IDR appeared to be as a function of several factors. These factors included a higher excipient load, higher solubilizing efficacy of the excipient to produce supersaturation state of API and last, but not least the higher IDR of pure excipient for the sugar-alcohols. In this context, the new IDR developed procedure for estimation of the carrier IDR was successfully implemented to quantify the mass dissolved of pure polyols-disks.

Furthermore, the dissolution process of the compacts can be considered as drug dependent as well, where the API will be released in a new activated form and the drug's induced physicochemical properties are dominant for the overall performance.

The modified intrinsic dissolution apparatus was confirmed as a feasible and reliable procedure to measure IDR of the compacts prepared under high-pressure. The IDR test has been verified as a forecast tool for the drug release at non-sink condition that easily discriminates between formulations, at least for the first phase of release. Moreover, the IDR test has been certified as an evaluation tool to assess the impact of different materials and solid-bulk properties on the product performance, as certain relationships were obtained between several parameters (API solid-state, solubility and SFE) and IDR values. Based on PCA, higher values of IDR out of the prepared compacts were correlated with higher amorphousity%, higher solubility factor, higher polar component of SFE and the reduction in T_m of API.

The correlation between the wettability findings and IDR may establish a tool to predict whether the proposed approach will be effective or not, directly from the analysis of drug and excipient structure, and their ability to interact by calculating the polar component of SFE.

IDR values could be overestimated for the compacts prepared with a relatively low pressure due to the interfering porosity and some erosion of surface during the test. Herewith, for certain substances it is recommended that more investigations are done to identify the most appropriate pressure, by which the intrinsic properties of ingredients are expressed and no change in the physical properties is produced. More informative IDR values will then be obtained, which would optimize the interpretation of IDR values and the correlation to the formulations' properties.

Furthermore, an investigation of any polymorphic transformation of the API during the non-sink dissolution test or for the residual solid, recovered at the end of the test, may be of interest in the future studies.

Regarding the porosity, the total pore surface area and median pore diameter may affect the drug dissolution rate, but they undergo some changes during the dissolution test. Thus, further in-situ examination of these parameters during the dissolution test might be important to correlate the changes with dissolution behaviours.

Finally, the results of this research suggest screening high-pressure compaction as a means to potentially improve solubility and IDR in a roller compaction process as dry granulation technique. This can be promising for the pharmaceutical industry to produce tablets in a secondary manufacturing of borderline poorly soluble drugs, especially which are sensitive to heat and/or moisture. However, the combination with co-milling of the substrates prior to compaction should be evaluated carefully, as milling did not always improve solubility and IDR performance of IBU or IDM and posed a higher likelihood to facilitate the formation of an amorphous drug. Withal, it is recommended that further experiments be performed to evaluate the application of this approach in the pharmaceutical development fields. Additional work investigating the potential benefits of the process described in this research, would be invaluable in evaluating and correlating the influencing factors with the dissolution rates obtained. Different formulations should be prepared from several APIs, which have different physicochemical properties, in the presence of a wide range of excipients. Consequently, the interplay between process-dependent, API-dependent and excipient-dependent influences could be better understood.

10 PUBLICATIONS

“Influence of high-pressure compaction on solubility and dissolution of ibuprofen binary mixtures employing nonfunctional excipients”, Ibraheem, et.al., IJPX,2021.

11 Appendix

Table 54 Saturation solubility values of IBU formulations (mixtures, granules) at pH 1.0 and pH 5.5

Formulation	Saturation Solubility Mix (pH 1.0)	Saturation Solubility Gr (pH 1.0)	Saturation Solubility Mix (pH 5.5)	Saturation Solubility Gr (pH 5.5)
IBU-HPC ST-TAB	0.0334 ± 0.0016	0.0411 ± 0.0021	0.5317 ± 0.0424	0.6226 ± 0.0080
IBU-HPC COM-TAB	0.0385 ± 0.0012	0.0439 ± 0.0014	0.5820 ± 0.0413	0.6496 ± 0.0414
IBU-ISO ST-TAB	0.0328 ± 0.0005	0.0370 ± 0.0006	0.4341 ± 0.0262	0.5853 ± 0.0591
IBU-ISO COM-TAB	0.0352 ± 0.0008	0.0365 ± 0.0005	0.4443 ± 0.0317	0.5448 ± 0.0069
IBU-MANN ST-TAB	0.0333 ± 0.0001	0.0355 ± 0.0006	0.4296 ± 0.0357	0.5094 ± 0.0248
IBU-MANN COM-TAB	0.0347 ± 0.0003	0.0359 ± 0.0004	0.4417 ± 0.0412	0.5297 ± 0.0123
IBU-SORB ST-TAB	0.0340 ± 0.0001	0.0339 ± 0.0001	0.4319 ± 0.0145	0.4324 ± 0.0280
IBU-SORB COM-TAB	0.0346 ± 0.0002	0.0353 ± 0.0005	0.4505 ± 0.0225	0.5309 ± 0.0310
IBU-Cry	0.0302 ± 0.0025		0.4212 ± 0.0712	

Table 55 Contact angle values of IBU compacts and related pure excipient compacts with water and Diiodomethane

Sample	contact angle		contact angle of related pure excipient	
	water	Diiodomethane	water	Diiodomethane
IBU-HPC ST-Tab	28.23 ± 1.99	55.00 ± 1.28	47.00 ± 2.52	74.07 ± 3.01
IBU-HPC COM-Tab	24.10 ± 1.73	60.43 ± 3.86	40.30 ± 2.60	69.45 ± 2.33
IBU-ISO ST-Tab	14.97 ± 3.78	65.03 ± 1.77	24.20 ± 1.95	43.07 ± 0.95
IBU-ISO COM-Tab	29.77 ± 5.00	61.10 ± 1.56	17.80 ± 1.92	39.20 ± 0.44
IBU-MANN ST-Tab	55.33 ± 2.02	45.50 ± 1.35	48.63 ± 2.06	34.00 ± 0.70
IBU-MANN COM-Tab	47.60 ± 2.86	40.00 ± 3.49	34.07 ± 1.98	41.87 ± 2.83
IBU-SORB ST-Tab	60.77 ± 1.58	51.47 ± 1.40	47.80 ± 1.48	32.23 ± 0.45
IBU-SORB COM-Tab	58.93 ± 1.05	48.03 ± 2.95	39.13 ± 0.42	43.53 ± 0.15
IBU-HPC ST-Tab200	36.33 ± 0.92	71.77 ± 2.25	47.00 ± 2.52	74.07 ± 3.01
IBU-ISO ST-Tab200	36.47 ± 1.35	48.33 ± 3.68	24.20 ± 1.95	43.07 ± 0.95
IBU-PVPVA ST-Tab	21.30 ± 2.54	49.90 ± 5.24	38.80 ± 1.00	44.30 ± 1.65
IBU-PVPVA COM-Tab	31.47 ± 1.25	44.90 ± 1.57	36.40 ± 3.24	29.23 ± 1.15
IBU-PVPVA ST-Tab200	35.13 ± 2.58	35.07 ± 2.45	38.80 ± 1.00	44.30 ± 1.65
IBU-CRY	86.93 ± 3.16	41.77 ± 0.57		
IBU-MQ	61.57 ± 2.21	47.33 ± 0.40		

Table 56 The surface tension and its fractions of the testing liquids [178]

Test liquid	Surface tension/ σ mN/m	Dispersive fraction D/σ mN/m	Polar fraction P/σ mN/m
Water	72.8	21.8	51.0
Diiodomethane	50.8	50.8	0.0
n-Hexan	18.4	18.4	0.0

Table 57 IDR measurements of disks prepared from pure excipients at pH 1.0

Excipient	IDR mg/min/cm ²
ISO	30.238 ± 6.582
MANN	15.957 ± 1.899
SORB	12.689 ± 2.217

Table 58 Saturation solubility values of IDM formulations (mixtures, granules) at pH 1.0 and pH 5.5

Formulation	Saturation Solubility Mix (pH 1.0)	Saturation Solubility Gr (pH 1.0)	Saturation Solubility Mix (pH 5.5)	Saturation Solubility Gr (pH 5.5)
IDM-PVPVA ST-TAB	0.0029 ± 0.0002	0.0045 ± 0.0005	0.023 ± 0.001	0.031 ± 0.001
IDM-PVPVA COM-TAB	0.0032 ± 0.0002	0.0046 ± 0.0002	0.034 ± 0.001	0.036 ± 0.001
IDM-ISO ST-TAB	0.0016 ± 0.0001	0.0033 ± 0.0001	0.021 ± 0.002	0.024 ± 0.001
IDM-ISO COM-TAB	0.0017 ± 0.0002	0.0028 ± 0.0002	0.028 ± 0.002	0.025 ± 0.001
IDM	0.0015 ± 0.0001		0.012 ± 0.001	

All values of solubility are in mg/ ml

Table 59 Contact angle values of IDM compacts and related pure excipient compacts with water and Diiodomethane

Sample	contact angle	
	water	Diiodomethane
IDM-PVPVA ST-Tab	28.40 ± 2.00	22.60 ± 1.31
IDM-PVPVA COM-Tab	33.77 ± 2.87	17.57 ± 1.80
IDM-ISO ST-Tab	45.50 ± 0.75	39.00 ± 1.18
IDM-ISO COM-Tab	51.77 ± 1.72	23.80 ± 2.55
IDM-CRY	93.67 ± 3.18	8.37 ± 0.96

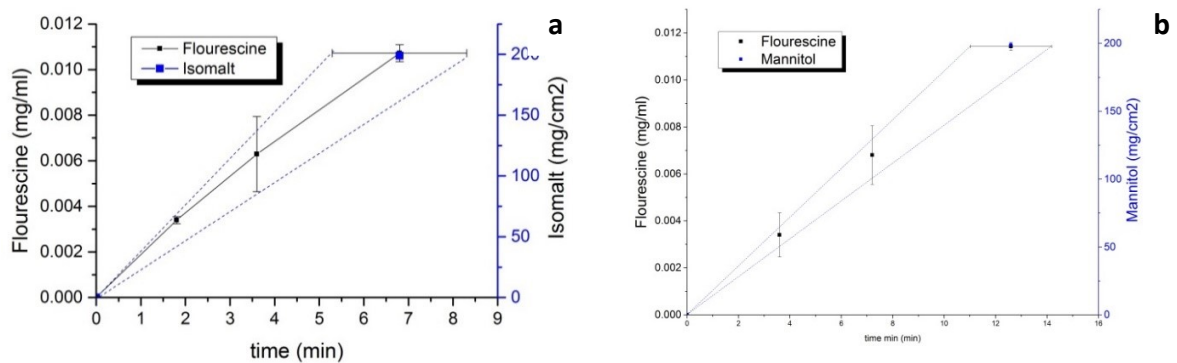


Figure 62 IDR measurements of a) pure isomalt and b) pure mannitol by the developed equipment with the verification of the method by determination of the dissolved fluorescein

11. Appendix

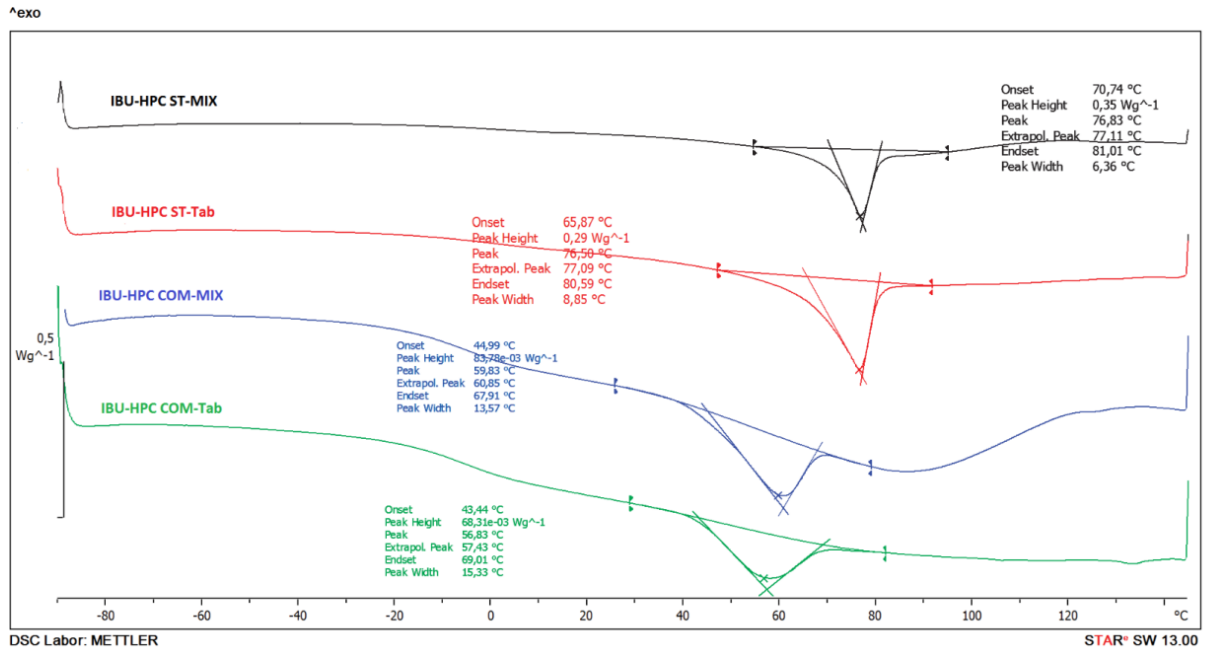


Figure 63 DSC thermograms of IBU-HPC binary mixtures and corresponding compacts

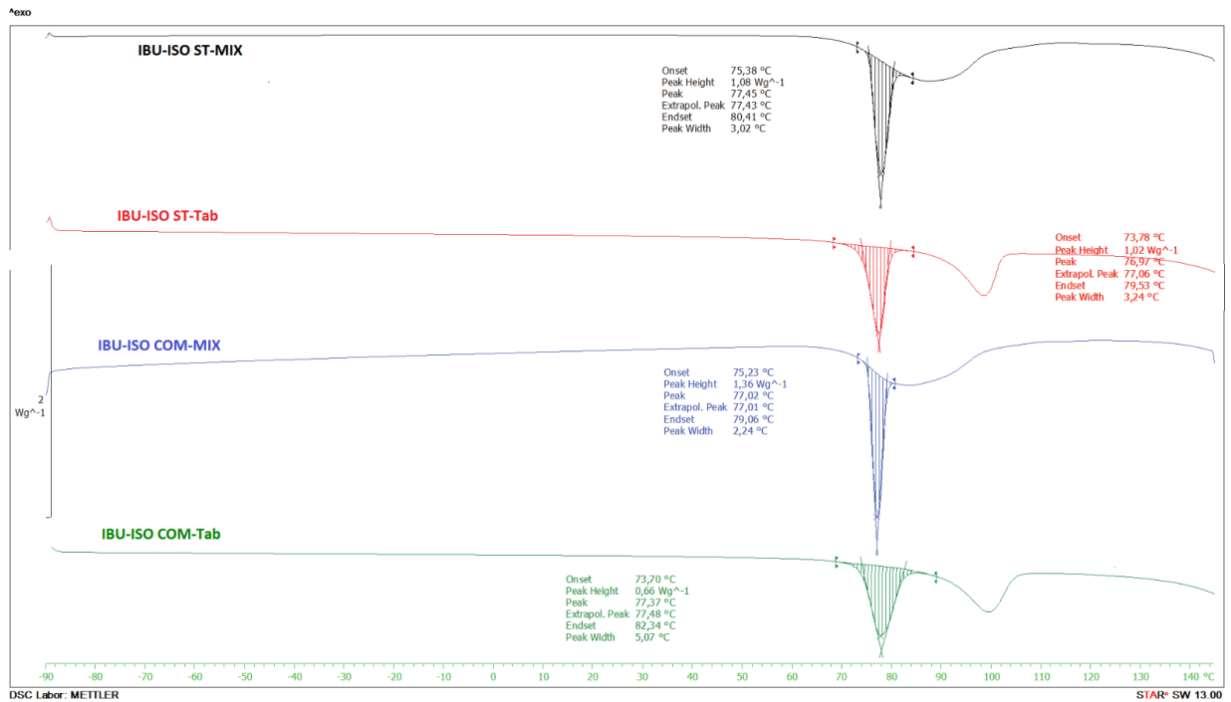


Figure 64 DSC thermograms of IBU-ISO binary mixtures and corresponding compacts

11. Appendix

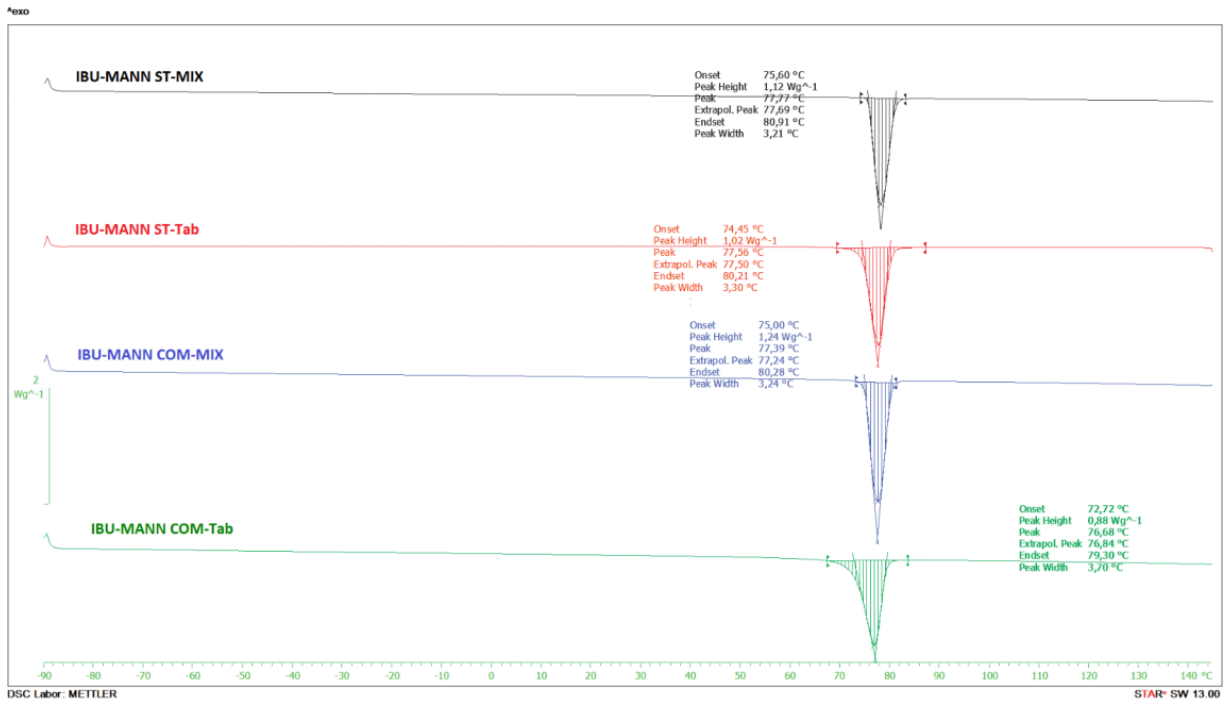


Figure 65 DSC thermograms of IBU-MANN binary mixtures and corresponding compacts

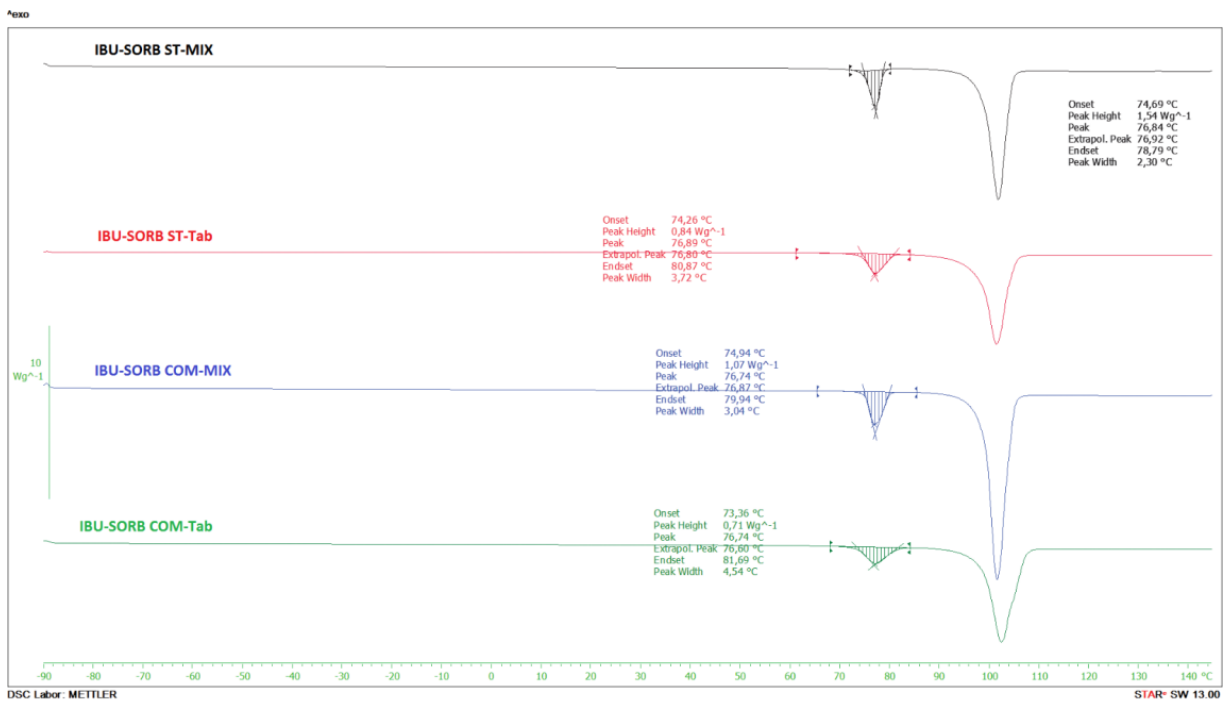


Figure 66 DSC thermograms of IBU-SORB binary mixtures and corresponding compacts

12 References

- [1] N. Rasenack, B.W. Müller, Poorly water-soluble drugs for oral delivery - A challenge for pharmaceutical development. Part I: Physicochemical and biopharmaceutical background/strategies in pharmaceutical development, *Pharm. Ind.* 67 (2005) 323–326.
- [2] S.T. Buckley, K.J. Frank, G. Fricker, M. Brandl, Biopharmaceutical classification of poorly soluble drugs with respect to “enabling formulations,” *European Journal of Pharmaceutical Sciences.* 50 (2013) 8–16. <https://doi.org/10.1016/j.ejps.2013.04.002>.
- [3] A. Fahr, X. Liu, Drug delivery strategies for poorly water-soluble drugs, *Expert Opinion on Drug Delivery.* 4 (2007) 403–416. <https://doi.org/10.1517/17425247.4.4.403>.
- [4] N. Rasenack, B.W. Müller, Poorly water-soluble drugs for oral delivery - A challenge for pharmaceutical development. Part II: Micronization technologies and complex formation, *Pharm. Ind.* 67 (2005) 447–451.
- [5] N. Rasenack, B.W. Müller, Poorly water-soluble drugs for oral delivery - A challenge for pharmaceutical development. Part III: Drug delivery systems containing the drug molecularly dispersed / Aspects on in vitro and in vivo characterization, *Pharm. Ind.* 67 (2005) 583–591.
- [6] P. Khadka, J. Ro, H. Kim, I. Kim, J.T. Kim, H. Kim, J.M. Cho, G. Yun, J. Lee, Pharmaceutical particle technologies: An approach to improve drug solubility, dissolution and bioavailability, *Asian Journal of Pharmaceutical Sciences.* 9 (2014) 304–316. <https://doi.org/10.1016/j.ajps.2014.05.005>.
- [7] A. Singh, Z.A. Worku, G. Van den Mooter, Oral formulation strategies to improve solubility of poorly water-soluble drugs, *Expert Opinion on Drug Delivery.* 8 (2011) 1361–1378. <https://doi.org/10.1517/17425247.2011.606808>.
- [8] V.R. Vemula, V. Lagishetty, S. Lingala, Solubility enhancement techniques, *International Journal of Pharmaceutical Sciences Review and Research.* 5 (2010) 41–51.
- [9] Bindu MB, K. B, D. Banji, NOVEL STRATEGIES FOR POORLY WATER SOLUBLE DRUGS, *International Journal of Pharmaceutical Sciences Review and Research.* 4 (2010) 76–84.
- [10] R. Laitinen, K. Löbmann, H. Grohgan, P. Priemel, C.J. Strachan, T. Rades, Supersaturating drug delivery systems: The potential of co-amorphous drug formulations, *International Journal of Pharmaceutics.* 532 (2017) 1–12. <https://doi.org/10.1016/j.ijpharm.2017.08.123>.
- [11] S. Janssens, G. Van den Mooter, Review: physical chemistry of solid dispersions, *Journal of Pharmacy and Pharmacology.* 61 (2009) 1571–1586. <https://doi.org/10.1211/jpp/61.12.0001>.
- [12] S.J. Dengale, H. Grohgan, T. Rades, K. Löbmann, Recent advances in co-amorphous drug formulations, *Advanced Drug Delivery Reviews.* 100 (2016) 116–125. <https://doi.org/10.1016/j.addr.2015.12.009>.
- [13] C. Leuner, J. Dressman, Improving drug solubility for oral delivery using solid dispersions, *Eur J Pharm Biopharm.* 50 (2000) 47–60.
- [14] A. Das, A.K. Nayak, B. Mohanty, S. Panda, Solubility and Dissolution Enhancement of Etoricoxib by Solid Dispersion Technique Using Sugar Carriers, *ISRN Pharmaceutics.* 2011 (2011) 1–8. <https://doi.org/10.5402/2011/819765>.
- [15] N. Zajc, A. Obreza, M. Bele, S. Srčić, Physical properties and dissolution behaviour of nifedipine/mannitol solid dispersions prepared by hot melt method, *International Journal of Pharmaceutics.* 291 (2005) 51–58. <https://doi.org/10.1016/j.ijpharm.2004.07.042>.
- [16] R.P. Patel, D.J. Patel, D.B. Bhimani, J.K. Patel, Physicochemical Characterization and Dissolution Study of Solid Dispersions of Furosemide with Polyethylene Glycol 6000 and Polyvinylpyrrolidone K30, *Dissolution Technologies.* 15 (2008) 17–25. <https://doi.org/10.14227/DT150308P17>.
- [17] R.J. Chokshi, H. Zia, H.K. Sandhu, N.H. Shah, W.A. Malick, Improving the Dissolution Rate of Poorly Water Soluble Drug by Solid Dispersion and Solid Solution—Pros and Cons, *Drug Delivery.* 14 (2007) 33–45. <https://doi.org/10.1080/10717540600640278>.

- [18] D.N. Bikiaris, Solid dispersions, Part I: recent evolutions and future opportunities in manufacturing methods for dissolution rate enhancement of poorly water-soluble drugs, *Expert Opinion on Drug Delivery*. 8 (2011) 1501–1519. <https://doi.org/10.1517/17425247.2011.618181>.
- [19] D.N. Bikiaris, Solid dispersions, Part II: new strategies in manufacturing methods for dissolution rate enhancement of poorly water-soluble drugs, *Expert Opinion on Drug Delivery*. 8 (2011) 1663–1680. <https://doi.org/10.1517/17425247.2011.618182>.
- [20] D.E. Zecevic, R. Meier, R. Daniels, K.-G. Wagner, Site specific solubility improvement using solid dispersions of HPMC-AS/HPC SSL – Mixtures, *European Journal of Pharmaceutics and Biopharmaceutics*. 87 (2014) 264–270. <https://doi.org/10.1016/j.ejpb.2014.03.018>.
- [21] P. Pandi, R. Bulusu, N. Kommineni, W. Khan, M. Singh, Amorphous solid dispersions: An update for preparation, characterization, mechanism on bioavailability, stability, regulatory considerations and marketed products, *International Journal of Pharmaceutics*. 586 (2020) 119560. <https://doi.org/10.1016/j.ijpharm.2020.119560>.
- [22] M. Helliwell, D. Taylor, Solid oral dosage forms, *Prof Nurse*. 8 (1993) 313–317.
- [23] Z.H. Loh, A.K. Samanta, P.W. Sia Heng, Overview of milling techniques for improving the solubility of poorly water-soluble drugs, *Asian Journal of Pharmaceutical Sciences*. 10 (2015) 255–274. <https://doi.org/10.1016/j.ajps.2014.12.006>.
- [24] Y. Kawabata, K. Wada, M. Nakatani, S. Yamada, S. Onoue, Formulation design for poorly water-soluble drugs based on biopharmaceutics classification system: Basic approaches and practical applications, *International Journal of Pharmaceutics*. 420 (2011) 1–10. <https://doi.org/10.1016/j.ijpharm.2011.08.032>.
- [25] D. Yang, R. Kulkarni, R.J. Behme, P.N. Kotiyan, Effect of the melt granulation technique on the dissolution characteristics of griseofulvin, *Int J Pharm*. 329 (2007) 72–80. <https://doi.org/10.1016/j.ijpharm.2006.08.029>.
- [26] M.E. Aulton, *Pharmaceutics: The Science of Dosage Form Design*, in: *Pharmaceutics: The Science of Dosage Form Design*, 2nd ed., Churchill Livingstone, 2001: pp. 16–32.
- [27] S.W. Ahjel, D. Lupuleasa, Enhancement of solubility and dissolution rate of different forms of atorvastatin calcium in direct compression tablet formulas, *Farmacia*. 57 (2009) 290–300.
- [28] R.G. Strickley, Solubilizing Excipients in Oral and Injectable Formulations, *Pharmaceutical Research*. 21 (2004) 201–230. <https://doi.org/10.1023/B:PHAM.0000016235.32639.23>.
- [29] J.W. Millard, F.A. Al, Solubilization by cosolvents Establishing useful constants for the log \bar{A} /linear model, *International Journal of Pharmaceutics*. (2002) 14.
- [30] K.P.R. Chowdary, T. Manjula, Effect Of Surfactants On The Solubility And Dissolution Rate Of Nimesulide From Tablets, *Indian J. Pharm. Sci*. 62 (2000) 97–101.
- [31] S.-H. Park, H.-K. Choi, The effects of surfactants on the dissolution profiles of poorly water-soluble acidic drugs, *International Journal of Pharmaceutics*. 321 (2006) 35–41. <https://doi.org/10.1016/j.ijpharm.2006.05.004>.
- [32] C.O. Rangel-Yagui, A. Pessoa, L.C. Tavares, Micellar solubilization of drugs, *J Pharm Pharm Sci*. 8 (2005) 147–165.
- [33] S. Thakkar, K. Sharma, S. Khurana, A.K. Bansal, Excipients and their Functionality for Enabling Technologies in Oral Dosage Forms, in: O.M.Y. Koo (Ed.), *Pharmaceutical Excipients*, John Wiley & Sons, Inc., Hoboken, NJ, USA, 2016: pp. 97–143. <https://doi.org/10.1002/9781118992432.ch3>.
- [34] K. Pitt, C. Sinka, Chapter 16 Tableting, in: *Handbook of Powder Technology*, Elsevier, 2007: pp. 735–778. [https://doi.org/10.1016/S0167-3785\(07\)80051-0](https://doi.org/10.1016/S0167-3785(07)80051-0).
- [35] I.C. Sinka, F. Motazedian, A.C.F. Cocks, K.G. Pitt, The effect of processing parameters on pharmaceutical tablet properties, *Powder Technology*. 189 (2009) 276–284. <https://doi.org/10.1016/j.powtec.2008.04.020>.

- [36] Q. Fu, H.-D. Lu, Y.-F. Xie, J.-Y. Liu, Y. Han, N.-B. Gong, F. Guo, Salt formation of two BCS II drugs (indomethacin and naproxen) with (1R, 2R)-1,2-diphenylethylenediamine: Crystal structures, solubility and thermodynamics analysis, *Journal of Molecular Structure*. 1185 (2019) 281–289. <https://doi.org/10.1016/j.molstruc.2019.02.104>.
- [37] H.S. Smith, Nonsteroidal Anti-Inflammatory Drugs; Acetaminophen, in: *Encyclopedia of the Neurological Sciences*, Elsevier, 2014: pp. 610–613. <https://doi.org/10.1016/B978-0-12-385157-4.00214-1>.
- [38] C. Álvarez, I. Núñez, J.J. Torrado, J. Gordon, H. Potthast, A. García-Arieta, Investigation on the Possibility of Biowaivers for Ibuprofen, *Journal of Pharmaceutical Sciences*. 100 (2011) 2343–2349. <https://doi.org/10.1002/jps.22472>.
- [39] A.J. Romero, L. Savastano, C.T. Rhodes, Monitoring crystal modifications in systems containing ibuprofen, *International Journal of Pharmaceutics*. 99 (1993) 125–134. [https://doi.org/10.1016/0378-5173\(93\)90354-1](https://doi.org/10.1016/0378-5173(93)90354-1).
- [40] E. Dudognon, F. Danède, M. Descamps, N.T. Correia, Evidence for a New Crystalline Phase of Racemic Ibuprofen, *Pharm Res*. 25 (2008) 2853–2858. <https://doi.org/10.1007/s11095-008-9655-7>.
- [41] M.G. Papich, Indomethacin, in: *Saunders Handbook of Veterinary Drugs*, Elsevier, 2016: pp. 396–397. <https://doi.org/10.1016/B978-0-323-24485-5.00307-7>.
- [42] B.C. Hancock, M. Parks, What is the true solubility advantage for amorphous pharmaceuticals?, *Pharm. Res*. 17 (2000) 397–404.
- [43] J. Comer, S. Judge, D. Matthews, L. Towers, B. Falcone, J. Goodman, J. Dearden, The intrinsic aqueous solubility of indomethacin, ADMET & DMPK. 2 (2014). <https://doi.org/10.5599/admet.2.1.33>.
- [44] X. Wang, H. Dearmas, N. Blaton, A. Michoel, G. Vandemooter, Phase characterization of indomethacin in binary solid dispersions with PVP VA64 or Myrj 52, *International Journal of Pharmaceutics*. 345 (2007) 95–100. <https://doi.org/10.1016/j.ijpharm.2007.05.046>.
- [45] E. Sangeetha, V.U. Rao, M. Sudhakar, S. Manisha, Enhancement of Solubility and Bioavailability of Hydrochlorothiazide Using Solid Dispersion Technique, (n.d.) 9.
- [46] B. Wang, D. Wang, S. Zhao, X. Huang, J. Zhang, Y. Lv, X. Liu, G. Lv, X. Ma, Evaluate the ability of PVP to inhibit crystallization of amorphous solid dispersions by density functional theory and experimental verify, *European Journal of Pharmaceutical Sciences*. 96 (2017) 45–52. <https://doi.org/10.1016/j.ejps.2016.08.046>.
- [47] E. Khodaverdi, N. Khalili, F. Zangiabadi, A. Homayouni, Preparation, Characterization and Stability Studies of Glassy Solid Dispersions of Indomethacin using PVP and Isomalt as carriers, *Iran J Basic Med Sci*. 15 (2012) 820–832.
- [48] F. Frizon, J. de O. Eloy, C.M. Donaduzzi, M.L. Mitsui, J.M. Marchetti, Dissolution rate enhancement of loratadine in polyvinylpyrrolidone K-30 solid dispersions by solvent methods, *Powder Technology*. 235 (2013) 532–539. <https://doi.org/10.1016/j.powtec.2012.10.019>.
- [49] T. YAMADA, N. SAITO, T. IMAI, M. OTAGIRI, Effect of Grinding with Hydroxypropyl Cellulose on the Dissolution and Particle Size of a Poorly Water-Soluble Drug, *CHEMICAL & PHARMACEUTICAL BULLETIN*. 47 (1999) 1311–1313. <https://doi.org/10.1248/cpb.47.1311>.
- [50] R. Talukder, C. Reed, T. Dürig, M. Hussain, Dissolution and Solid-State Characterization of Poorly Water-Soluble Drugs in the Presence of a Hydrophilic Carrier, *AAPS PharmSciTech*. 12 (2011) 1227–1233. <https://doi.org/10.1208/s12249-011-9697-8>.
- [51] A. Ito, T. Shimotori, N. Honma, S. Tsue, Evaluation of Hydroxypropyl Cellulose for Solubility Enhancement of Poorly Water-Soluble Drug Using Spray Dry Method, (n.d.) 1.

- [52] A.L. Sarode, R. Cheng, C. Cote, D.R. Worthen, Dissolution Rate Enhancement of Poorly Water Soluble Drugs by Spray Drying and Hot Melt Mixing Techniques Using a Super Special Low Viscosity Grade of Hydroxypropyl Cellulose (HPC-SSL) Polymer, (n.d.) 1.
- [53] A. Sarode, P. Wang, C. Cote, D.R. Worthen, Low-Viscosity Hydroxypropylcellulose (HPC) Grades SL and SSL: Versatile Pharmaceutical Polymers for Dissolution Enhancement, Controlled Release, and Pharmaceutical Processing, *AAPS PharmSciTech.* 14 (2013) 151–159. <https://doi.org/10.1208/s12249-012-9897-x>.
- [54] HYDROXYPROPYL CELLULOSE API | Drug Information, Uses, Side Effects, Chemistry, *PharmaCompass.Com.* (n.d.). <https://www.pharmacompass.com/chemistry-chemical-name/hydroxypropyl-cellulose> (accessed March 16, 2019).
- [55] J.S. LaFountaine, J.W. McGinity, R.O. Williams, Challenges and Strategies in Thermal Processing of Amorphous Solid Dispersions: A Review, *AAPS PharmSciTech.* 17 (2016) 43–55. <https://doi.org/10.1208/s12249-015-0393-y>.
- [56] A.C.F. Rumondor, P.J. Marsac, L.A. Stanford, L.S. Taylor, Phase Behavior of Poly(vinylpyrrolidone) Containing Amorphous Solid Dispersions in the Presence of Moisture, *Molecular Pharmaceutics.* 6 (2009) 1492–1505. <https://doi.org/10.1021/mp900050c>.
- [57] A. Fini, C. Cavallari, F. Ospitali, Raman and thermal analysis of indomethacin/PVP solid dispersion enteric microparticles, *European Journal of Pharmaceutics and Biopharmaceutics.* 70 (2008) 409–420. <https://doi.org/10.1016/j.ejpb.2008.03.016>.
- [58] L.S. Taylor, G. Zografi, Spectroscopic characterization of interactions between PVP and indomethacin in amorphous molecular dispersions, *Pharm. Res.* 14 (1997) 1691–1698.
- [59] A. Madgulkar, M. Bandivadekar, T. Shid, S. Rao, Sugars as solid dispersion carrier to improve solubility and dissolution of the BCS class II drug: clotrimazole, *Drug Development and Industrial Pharmacy.* 42 (2016) 28–38. <https://doi.org/10.3109/03639045.2015.1024683>.
- [60] M. Langer, Investigations on the predictability of the formation of glassy solid solutions of drugs in sugar alcohols, *International Journal of Pharmaceutics.* 252 (2003) 167–179. [https://doi.org/10.1016/S0378-5173\(02\)00647-6](https://doi.org/10.1016/S0378-5173(02)00647-6).
- [61] K. Sakeer, H. Al-Zein, I. Hassan, S. Desai, A. Nokhodchi, Enhancement of dissolution of nystatin from buccoadhesive tablets containing various surfactants and a solid dispersion formulation, *Archives of Pharmacal Research.* 33 (2010) 1771–1779. <https://doi.org/10.1007/s12272-010-1109-1>.
- [62] B.K. Nanjwade, S. Ali M, V.K. Nanjwade, F. Manvi, Effect of Compression Pressure on Dissolution and Solid State Characterization of Cefuroxime Axetil, *Journal of Analytical & Bioanalytical Techniques.* 1 (2010). <https://doi.org/10.4172/2155-9872.1000112>.
- [63] Y.-C. Tseng, M. Patel, Y. Zhao, Determination of Intrinsic Dissolution Rate Using Miniaturized Rotating and Stationary Disk Systems, *Dissolution Technologies.* 21 (2014) 24–29. <https://doi.org/10.14227/DT210214P24>.
- [64] L.X. Yu, A.S. Carlin, G.L. Amidon, A.S. Hussain, Feasibility studies of utilizing disk intrinsic dissolution rate to classify drugs, *International Journal of Pharmaceutics.* 270 (2004) 221–227. <https://doi.org/10.1016/j.ijpharm.2003.10.016>.
- [65] T.A. Iranloye, E.L. Parrott, Effects of Compression Force, Particle Size, and Lubricants on Dissolution Rate, *Journal of Pharmaceutical Sciences.* 67 (1978) 535–539. <https://doi.org/10.1002/jps.2600670424>.
- [66] K. Wlodarski, W. Sawicki, K.J. Paluch, L. Tajber, M. Grembecka, L. Hawelek, Z. Wojnarowska, K. Grzybowska, E. Talik, M. Paluch, The influence of amorphization methods on the apparent solubility and dissolution rate of tadalafil, *European Journal of Pharmaceutical Sciences.* 62 (2014) 132–140. <https://doi.org/10.1016/j.ejps.2014.05.026>.

- [67] K. Löbmann, K. Flouda, D. Qiu, T. Tsolakou, W. Wang, T. Rades, The Influence of Pressure on the Intrinsic Dissolution Rate of Amorphous Indomethacin, *Pharmaceutics*. 6 (2014) 481–493. <https://doi.org/10.3390/pharmaceutics6030481>.
- [68] L. Giorgetti, M.G. Issa, H.G. Ferraz, The effect of dissolution medium, rotation speed and compaction pressure on the intrinsic dissolution rate of amlodipine besylate, using the rotating disk method, *Brazilian Journal of Pharmaceutical Sciences*. 50 (2014) 513–520. <https://doi.org/10.1590/S1984-82502014000300009>.
- [69] F.O. Costa, A.A.C.C. Pais, J.J.S. Sousa, Analysis of formulation effects in the dissolution of ibuprofen pellets, *International Journal of Pharmaceutics*. 270 (2004) 9–19. <https://doi.org/10.1016/j.ijpharm.2003.10.002>.
- [70] L.R. Shaw, W.J. Irwin, T.J. Grattan, B.R. Conway, The Effect of Selected Water-Soluble Excipients on the Dissolution of Paracetamol and Ibuprofen, *Drug Development and Industrial Pharmacy*. 31 (2005) 515–525. <https://doi.org/10.1080/03639040500215784>.
- [71] S.-Y. Chan, Y.-Y. Chung, X.-Z. Cheah, E.Y.-L. Tan, J. Quah, The characterization and dissolution performances of spray dried solid dispersion of ketoprofen in hydrophilic carriers, *Asian Journal of Pharmaceutical Sciences*. 10 (2015) 372–385. <https://doi.org/10.1016/j.ajps.2015.04.003>.
- [72] J.E. Hilton, M.P. Summers, The effect of wetting agents on the dissolution of indomethacin solid dispersion systems, *International Journal of Pharmaceutics*. 31 (1986) 157–164. [https://doi.org/10.1016/0378-5173\(86\)90226-7](https://doi.org/10.1016/0378-5173(86)90226-7).
- [73] S.R. Modi, A.K.R. Dantuluri, S.R. Perumalla, C.C. Sun, A.K. Bansal, Effect of Crystal Habit on Intrinsic Dissolution Behavior of Celecoxib Due to Differential Wettability, *Crystal Growth & Design*. 14 (2014) 5283–5292. <https://doi.org/10.1021/cg501084a>.
- [74] S.R. Modi, A.K.R. Dantuluri, V. Puri, Y.B. Pawar, P. Nandekar, A.T. Sangamwar, S.R. Perumalla, C.C. Sun, A.K. Bansal, Impact of Crystal Habit on Biopharmaceutical Performance of Celecoxib, *Crystal Growth & Design*. 13 (2013) 2824–2832. <https://doi.org/10.1021/cg400140a>.
- [75] M. Tenho, P. Heinänen, V.P. Tanninen, V.-P. Lehto, Does the preferred orientation of crystallites in tablets affect the intrinsic dissolution?, *Journal of Pharmaceutical and Biomedical Analysis*. 43 (2007) 1315–1323. <https://doi.org/10.1016/j.jpba.2006.10.038>.
- [76] P. Zakeri-Milani, M. Barzegar-Jalali, M. Azimi, H. Valizadeh, Biopharmaceutical classification of drugs using intrinsic dissolution rate (IDR) and rat intestinal permeability, *European Journal of Pharmaceutics and Biopharmaceutics*. 73 (2009) 102–106. <https://doi.org/10.1016/j.ejpb.2009.04.015>.
- [77] H.-K. Chan, D.J.W. Grant, Influence of compaction on the intrinsic dissolution rate of modified acetaminophen and adipic acid crystals, *International Journal of Pharmaceutics*. 57 (1989) 117–124. [https://doi.org/10.1016/0378-5173\(89\)90299-8](https://doi.org/10.1016/0378-5173(89)90299-8).
- [78] J. Jinno, D. Oh, J.R. Crison, G.L. Amidon, Dissolution of Ionizable Water-Insoluble Drugs: The Combined Effect of pH and Surfactant, *JPharmSci*. 89 (2000) 268–274. [https://doi.org/10.1002/\(SICI\)1520-6017\(200002\)89:2<268::AID-JPS14>3.0.CO;2-F](https://doi.org/10.1002/(SICI)1520-6017(200002)89:2<268::AID-JPS14>3.0.CO;2-F).
- [79] M.G. Issa, H.G. Ferraz, Intrinsic Dissolution as a Tool for Evaluating Drug Solubility in Accordance with the Biopharmaceutics Classification System, *Dissolution Technologies*. 18 (2011) 6–13. <https://doi.org/10.14227/DT180311P6>.
- [80] A.B. Dezani, T.M. Pereira, A.M. Caffaro, J.M. Reis, C.H. dos R. Serra, Equilibrium solubility versus intrinsic dissolution: characterization of lamivudine, stavudine and zidovudine for BCS classification, *Brazilian Journal of Pharmaceutical Sciences*. 49 (2013) 853–863.
- [81] G. Buckton, Assessment of the wettability of pharmaceutical powders, *Journal of Adhesion Science and Technology*. 7 (1993) 205–219. <https://doi.org/10.1163/156856193X00664>.
- [82] G. Buckton, Contact angle, adsorption and wettability — a review with respect to powders, *Powder Technology*. 61 (1990) 237–249. [https://doi.org/10.1016/0032-5910\(90\)80090-L](https://doi.org/10.1016/0032-5910(90)80090-L).

- [83] M. Doreth, K. Löbmann, H. Grohganz, R. Holm, H. Lopez de Diego, T. Rades, P.A. Priemel, Glass solution formation in water - In situ amorphization of naproxen and ibuprofen with Eudragit® E PO, *Journal of Drug Delivery Science and Technology*. 34 (2016) 32–40. <https://doi.org/10.1016/j.jddst.2016.02.003>.
- [84] N. Blagden, M. de Matas, P.T. Gavan, P. York, Crystal engineering of active pharmaceutical ingredients to improve solubility and dissolution rates, *Advanced Drug Delivery Reviews*. 59 (2007) 617–630. <https://doi.org/10.1016/j.addr.2007.05.011>.
- [85] V.J. Stella, K.W. Nti-Addae, Prodrug strategies to overcome poor water solubility, *Advanced Drug Delivery Reviews*. 59 (2007) 677–694. <https://doi.org/10.1016/j.addr.2007.05.013>.
- [86] M. Maghsoodi, Role of Solvents in Improvement of Dissolution Rate of Drugs: Crystal Habit and Crystal Agglomeration, Tabriz University of Medical Sciences, 2015. <https://doi.org/10.5681/apb.2015.002>.
- [87] A. Nokhodchi, A. Homayouni, R. Araya, W. Kaialy, W. Obeidat, K. Asare-Addo, Crystal engineering of ibuprofen using starch derivatives in crystallization medium to produce promising ibuprofen with improved pharmaceutical performance, *RSC Advances*. 5 (2015) 46119–46131. <https://doi.org/10.1039/C5RA06183K>.
- [88] M. Tenho, J. Aaltonen, P. Heinänen, L. Peltonen, V.-P. Lehto, Effect of texture on the intrinsic dissolution behaviour of acetylsalicylic acid and tolbutamide compacts, *Journal of Applied Crystallography*. 40 (2007) 857–864. <https://doi.org/10.1107/S0021889807034553>.
- [89] P. Bukovec, P. Benkic, M. Smrkolj, F. Vrečer, Effect of crystal habit on the dissolution behaviour of simvastatin crystals and its relationship to crystallization solvent properties, (2016) 263–268. <https://doi.org/10.1691/ph.2016.5163>.
- [90] P. Bukovec, A. Meden, M. Smrkolj, F. Vrečer, Influence of Crystal Habit on the Dissolution of Simvastatin Single Crystals, *Acta Chimica Slovenica*. (2015) 958–966. <https://doi.org/10.17344/acsi.2015.1849>.
- [91] J.-P. Brog, C.-L. Chanez, A. Crochet, K.M. Fromm, Polymorphism, what it is and how to identify it: a systematic review, *RSC Advances*. 3 (2013) 16905. <https://doi.org/10.1039/c3ra41559g>.
- [92] R. Censi, P. Di Martino, Polymorph Impact on the Bioavailability and Stability of Poorly Soluble Drugs, *Molecules*. 20 (2015) 18759–18776. <https://doi.org/10.3390/molecules201018759>.
- [93] Y. Namatame, H. Sato, Evaluation of polymorphic forms by powder X-ray diffraction and thermal analysis methods, (2013) 8.
- [94] A.J. Aguiar, J. Krc, A.W. Kinkel, J.C. Samyn, Effect of polymorphism on the absorption of chloramphenicol from chloramphenicol palmitate, *Journal of Pharmaceutical Sciences*. 56 (1967) 847–853. <https://doi.org/10.1002/jps.2600560712>.
- [95] A.J. Aguiar, J.E. Zelmer, Dissolution Behavior of Polymorphs of Chloramphenicol Palmitate and Mefenamic Acid, *Journal of Pharmaceutical Sciences*. 58 (1969) 983–987. <https://doi.org/10.1002/jps.2600580817>.
- [96] A. Chaudhary, U. Nagaich, N. Gulati, V.K. Sharma, R.L. Khosa, Enhancement of solubilization and bioavailability of poorly soluble drugs by physical and chemical modifications: A recent review, (2012) 36.
- [97] Y. Kobayashi, S. Ito, S. Itai, K. Yamamoto, Physicochemical properties and bioavailability of carbamazepine polymorphs and dihydrate, *Int J Pharm*. 193 (2000) 137–146.
- [98] D. Sharma, M. Soni, S. Kumar, G. Gupta, Solubility Enhancement – Eminent Role in Poorly Soluble Drugs, (2009) 5.
- [99] S.B. Murdande, M.J. Pikal, R.M. Shanker, R.H. Bogner, Solubility advantage of amorphous pharmaceuticals: I. A thermodynamic analysis, *J Pharm Sci*. 99 (2010) 1254–1264. <https://doi.org/10.1002/jps.21903>.

- [100] M. Fujii, H. Okada, Y. Shibata, H. Teramachi, M. Kondoh, Y. Watanabe, Preparation, characterization, and tableting of a solid dispersion of indomethacin with crospovidone, *International Journal of Pharmaceutics*. 293 (2005) 145–153. <https://doi.org/10.1016/j.ijpharm.2004.12.018>.
- [101] J. Comer, *How CheqSol works*, (2011).
- [102] J. Comer, *Physicochemical Properties and their relation to ADMET*, (2013).
- [103] D.N. Kapote, K.G. Wagner, Influence of shellac on the improvement of solubility and supersaturation of loratadine amorphous solid dispersion using a new grade of HPMC, *Journal of Drug Delivery Science and Technology*. 61 (2021) 102116. <https://doi.org/10.1016/j.jddst.2020.102116>.
- [104] S.B. Murdande, M.J. Pikal, R.M. Shanker, R.H. Bogner, Solubility Advantage of Amorphous Pharmaceuticals: II. Application of Quantitative Thermodynamic Relationships for Prediction of Solubility Enhancement in Structurally Diverse Insoluble Pharmaceuticals, *Pharmaceutical Research*. 27 (2010) 2704–2714. <https://doi.org/10.1007/s11095-010-0269-5>.
- [105] K. Nidhi, S. Indrajeet, M. Khushboo, K. Gauri, D.J. Sen, HYDROTROPY: A PROMISING TOOL FOR SOLUBILITY ENHANCEMENT: A REVIEW, (2011) 8.
- [106] S.A. Vshivkov, E.V. Rusinova, Phase diagrams of a hydroxypropyl cellulose-water system under static conditions and in the shear field, *Polymer Science Series B*. 49 (2007) 209–212. <https://doi.org/10.1134/S1560090407070093>.
- [107] K.Y. Rhee, H.K. Cho, J.S. Hong, An Investigation on the Application of Cryogenic Ball Milling to Ibuprofen Particle and Its Characteristics, *MSF*. 505–507 (2006) 355–360. <https://doi.org/10.4028/www.scientific.net/MSF.505-507.355>.
- [108] T. Niwa, One-step preparation of pharmaceutical nanocrystals using ultra cryo-milling technique in liquid nitrogen, *European Journal of Pharmaceutical Sciences*. (2010) 8.
- [109] S. Mallick, S. Pattnaik, K. Swain, P.K. De, A. Saha, G. Ghoshal, A. Mondal, Formation of physically stable amorphous phase of ibuprofen by solid state milling with kaolin, *European Journal of Pharmaceutics and Biopharmaceutics*. 68 (2008) 346–351. <https://doi.org/10.1016/j.ejpb.2007.06.003>.
- [110] M. Descamps, J.F. Willart, E. Dudognon, V. Caron, Transformation of Pharmaceutical Compounds upon Milling and Comilling: The Role of Tg, *Journal of Pharmaceutical Sciences*. 96 (2007) 1398–1407. <https://doi.org/10.1002/jps.20939>.
- [111] M. Skinner, THE ROLE OF INTRINSIC DISSOLUTION RATE IN THE ASSESSMENT OF SOLID ORAL DOSAGE FORMS, (2009).
- [112] M. Stuart, K. Box, Chasing Equilibrium: Measuring the Intrinsic Solubility of Weak Acids and Bases, *Analytical Chemistry*. 77 (2005) 983–990. <https://doi.org/10.1021/ac048767n>.
- [113] K. Etherson, G. Halbert, M. Elliott, Determination of excipient based solubility increases using the CheqSol method, *International Journal of Pharmaceutics*. 465 (2014) 202–209. <https://doi.org/10.1016/j.ijpharm.2014.02.007>.
- [114] S.A. Speakman, Basics of X-Ray Powder Diffraction, (2011). <http://prism.mit.edu/xray/Basics%20of%20X-Ray%20Powder%20Diffraction.pdf>.
- [115] M. Otsuka, F. Kato, Y. Matsuda, Comparative evaluation of the degree of indomethacin crystallinity by chemoinformetrical fourie-transformed near-infrared spectroscopy and conventional powder X-ray diffractometry, *AAPS PharmSci*. 2 (2000) 80–87. <https://doi.org/10.1208/ps020109>.
- [116] X. Huang, Y. Liu, J. Deng, B. Yi, X. Yu, P. Shen, S. Tan, A novel polymer gel electrolyte based on cyanoethylated cellulose for dye-sensitized solar cells, *Electrochimica Acta*. 80 (2012) 219–226. <https://doi.org/10.1016/j.electacta.2012.07.014>.
- [117] M. Sugisaki, H. Suga, S. Seki, Calorimetric Study of the Glassy State. IV. Heat Capacities of Glassy Water and Cubic Ice, *BCSJ*. 41 (1968) 2591–2599. <https://doi.org/10.1246/bcsj.41.2591>.

- [118] M. Skinner, I. Kanfer, Intrinsic dissolution rate and solubility studies on josamycin, a macrolide antibiotic, *International Journal of Pharmaceutics*. 88 (1992) 151–158. [https://doi.org/10.1016/0378-5173\(92\)90311-O](https://doi.org/10.1016/0378-5173(92)90311-O).
- [119] D. Douroumis, A. Fahr, eds., *Drug Delivery Strategies for Poorly Water-Soluble Drugs: Douroumis/Drug*, John Wiley & Sons Ltd, Oxford, UK, 2013. <https://doi.org/10.1002/9781118444726>.
- [120] E. Baka, J.E.A. Comer, K. Takács-Novák, Study of equilibrium solubility measurement by saturation shake-flask method using hydrochlorothiazide as model compound, *Journal of Pharmaceutical and Biomedical Analysis*. 46 (2008) 335–341. <https://doi.org/10.1016/j.jpba.2007.10.030>.
- [121] F. Flicker, V.A. Eberle, G. Betz, Recrystallization of Commercial Carbamazepine Samples—A Strategy to Control Dissolution Variability, *Pharmaceutics*. 4 (2012) 58–70. <https://doi.org/10.3390/pharmaceutics4010058>.
- [122] D.H. Barich, J.M. Davis, L.J. Schieber, M.T. Zell, E.J. Munson, Investigation of Solid-State NMR Line Widths of Ibuprofen in Drug Formulations, *Journal of Pharmaceutical Sciences*. 95 (2006) 1586–1594. <https://doi.org/10.1002/jps.20564>.
- [123] M. Doreth, M.A. Hussein, P.A. Priemel, H. Grohgan, R. Holm, H. Lopez de Diego, T. Rades, K. Löbmann, Amorphization within the tablet: Using microwave irradiation to form a glass solution in situ, *International Journal of Pharmaceutics*. 519 (2017) 343–351. <https://doi.org/10.1016/j.ijpharm.2017.01.035>.
- [124] V.-P. Lehto, M. Tenho, K. Vähä-Heikkilä, P. Harjunen, M. Päällysaho, J. Väliisaari, P. Niemelä, K. Järvinen, The comparison of seven different methods to quantify the amorphous content of spray dried lactose, *Powder Technology*. 167 (2006) 85–93. <https://doi.org/10.1016/j.powtec.2006.05.019>.
- [125] A. Fini, C. Cavallari, F. Ospitali, Effect of Ultrasound on the Compaction of Ibuprofen/Isomalt Systems, *Pharmaceutics*. 1 (2009) 3–19. <https://doi.org/10.3390/pharmaceutics1010003>.
- [126] P. Tran, Y.-C. Pyo, D.-H. Kim, S.-E. Lee, J.-K. Kim, J.-S. Park, Overview of the Manufacturing Methods of Solid Dispersion Technology for Improving the Solubility of Poorly Water-Soluble Drugs and Application to Anticancer Drugs, *Pharmaceutics*. 11 (2019) 132. <https://doi.org/10.3390/pharmaceutics11030132>.
- [127] S.O. Kyeremateng, M. Pudlas, G.H. Woehrle, A Fast and Reliable Empirical Approach for Estimating Solubility of Crystalline Drugs in Polymers for Hot Melt Extrusion Formulations, *Journal of Pharmaceutical Sciences*. 103 (2014) 2847–2858. <https://doi.org/10.1002/jps.23941>.
- [128] N. Eguchi, K. Kawabata, H. Goto, Electrochemical Polymerization of 4,4-Dimethyl-2,2'-Bithiophene in Concentrated Polymer Liquid Crystal Solution, *Journal of Materials Science and Chemical Engineering*. 05 (2017) 64–70. <https://doi.org/10.4236/msce.2017.52007>.
- [129] M. Chawla, G. Srinivasan, Evaluation of galen IQ polymer in Tramadol Hydrochloride orally disintegrating tablet., (2011) 17.
- [130] V.K. Sharma, D.S. Kalonia, Effect of vacuum drying on protein-mannitol interactions: the physical state of mannitol and protein structure in the dried state, *AAPS PharmSciTech*. 5 (2004) E10. <https://doi.org/10.1208/pt050110>.
- [131] H.K. Stulzer, M.P. Tagliari, A.P. Cruz, M.A.S. Silva, M.C.M. Laranjeira, Compatibility studies between piroxicam and pharmaceutical excipients used in solid dosage forms, *Pharmaceutical Chemistry Journal*. 42 (2008) 215–219. <https://doi.org/10.1007/s11094-008-0091-0>.
- [132] S.F. Shaikh, R.S. Mane, B.K. Min, Y.J. Hwang, O. Joo, D-sorbitol-induced phase control of TiO₂ nanoparticles and its application for dye-sensitized solar cells, *Scientific Reports*. 6 (2016). <https://doi.org/10.1038/srep20103>.

- [133] P. Di Martino, M. Beccerica, E. Joiris, G.F. Palmieri, A. Gayot, S. Martelli, Influence of crystal habit on the compression and densification mechanism of ibuprofen, *Journal of Crystal Growth*. 243 (2002) 345–355. [https://doi.org/10.1016/S0022-0248\(02\)01523-3](https://doi.org/10.1016/S0022-0248(02)01523-3).
- [134] S. Verma, V.S. Rudraraju, Wetting Kinetics: an Alternative Approach Towards Understanding the Enhanced Dissolution Rate for Amorphous Solid Dispersion of a Poorly Soluble Drug, *AAPS PharmSciTech*. 16 (2015) 1079–1090. <https://doi.org/10.1208/s12249-014-0281-x>.
- [135] G. Buckton, The assessment, and pharmaceutical importance, of the solid/liquid and the solid/vapour interface: a review with respect to powders, *International Journal of Pharmaceutics*. 44 (1988) 1–8. [https://doi.org/10.1016/0378-5173\(88\)90093-2](https://doi.org/10.1016/0378-5173(88)90093-2).
- [136] B.C. Lippold, A. Ohm, Correlation between wettability and dissolution rate of pharmaceutical powders, *International Journal of Pharmaceutics*. 28 (1986) 67–74. [https://doi.org/10.1016/0378-5173\(86\)90148-1](https://doi.org/10.1016/0378-5173(86)90148-1).
- [137] G. Buckton, The estimation and application of surface energy data for powdered systems, *Drug Development and Industrial Pharmacy*. 18 (1992) 1149–1167. <https://doi.org/10.3109/03639049209046326>.
- [138] S. Young, G. Buckton, Particle growth in aqueous suspensions: the influence of surface energy and polarity, *International Journal of Pharmaceutics*. 60 (1990) 235–241. [https://doi.org/10.1016/0378-5173\(90\)90077-H](https://doi.org/10.1016/0378-5173(90)90077-H).
- [139] A. Alghunaim, S. Kirdponpattara, B.Z. Newby, Techniques for determining contact angle and wettability of powders, *Powder Technology*. 287 (2016) 201–215. <https://doi.org/10.1016/j.powtec.2015.10.002>.
- [140] M. Newa, K.H. Bhandari, D.H. Oh, Y.R. Kim, J.H. Sung, J.O. Kim, J.S. Woo, H.G. Choi, C.S. Yong, Enhanced dissolution of ibuprofen using solid dispersion with poloxamer 407, *Archives of Pharmacal Research*. 31 (2008) 1497–1507. <https://doi.org/10.1007/s12272-001-2136-8>.
- [141] Y. Guan, Y. Zhang, T. Zhou, S. Zhou, Stability of hydrogen-bonded hydroxypropylcellulose/poly(acrylic acid) microcapsules in aqueous solutions, *Soft Matter*. 5 (2009) 842. <https://doi.org/10.1039/b815913k>.
- [142] J.J. Sousa, A. Sousa, M.J. Moura, F. Podczeczek, J.M. Newton, The influence of core materials and film coating on the drug release from coated pellets, *International Journal of Pharmaceutics*. 233 (2002) 111–122. [https://doi.org/10.1016/S0378-5173\(01\)00921-8](https://doi.org/10.1016/S0378-5173(01)00921-8).
- [143] H. Giesche, Mercury Porosimetry: A General (Practical) Overview, *Particle & Particle Systems Characterization*. 23 (2006) 9–19. <https://doi.org/10.1002/ppsc.200601009>.
- [144] D. Schönherr, U. Wollatz, D. Haznar-Garbacz, U. Hanke, K.J. Box, R. Taylor, R. Ruiz, S. Beato, D. Becker, W. Weitschies, Characterisation of selected active agents regarding pKa values, solubility concentrations and pH profiles by SiriusT3, *European Journal of Pharmaceutics and Biopharmaceutics*. 92 (2015) 155–170. <https://doi.org/10.1016/j.ejpb.2015.02.028>.
- [145] M. Otsuka, F. Kato, Y. Matsuda, Y. Ozaki, Comparative determination of polymorphs of indomethacin in powders and tablets by chemometrical near-infrared spectroscopy and X-ray powder diffractometry, *AAPS PharmSciTech*. 4 (2003) 58–69. <https://doi.org/10.1208/pt040219>.
- [146] S.A. Surwase, J.P. Boetker, D. Saville, B.J. Boyd, K.C. Gordon, L. Peltonen, C.J. Strachan, Indomethacin: New Polymorphs of an Old Drug, *Molecular Pharmaceutics*. 10 (2013) 4472–4480. <https://doi.org/10.1021/mp400299a>.
- [147] N. Kaneniwa, M. Otsuka, T. Hayashi, Physicochemical characterization of indomethacin polymorphs and the transformation kinetics in ethanol., *CHEMICAL & PHARMACEUTICAL BULLETIN*. 33 (1985) 3447–3455. <https://doi.org/10.1248/cpb.33.3447>.
- [148] T. Van Duong, D. Lüdeker, P.-J. Van Bockstal, T. De Beer, J. Van Humbeeck, G. Van den Mooter, Polymorphism of Indomethacin in Semicrystalline Dispersions: Formation, Transformation, and

- Segregation, *Molecular Pharmaceutics*. 15 (2018) 1037–1051. <https://doi.org/10.1021/acs.molpharmaceut.7b00930>.
- [149] B. Legendre, Y. Feutelais, Polymorphic and Thermodynamic Study of Indomethacin, *Journal of Thermal Analysis and Calorimetry*. 76 (2004) 255–264. <https://doi.org/10.1023/B:JTAN.0000027824.55280.37>.
- [150] E. Atef, H. Chauhan, D. Prasad, D. Kumari, C. Pidgeon, Quantifying Solid-State Mixtures of Crystalline Indomethacin by Raman Spectroscopy Comparison with Thermal Analysis, *ISRN Chromatography*. 2012 (2012) 1–6. <https://doi.org/10.5402/2012/892806>.
- [151] T. Matsumoto, G. Zografi, Physical properties of solid molecular dispersions of Indomethacin with PVP and PVPVA in relation to Indomethacin recrystallization, 1999. <https://doi.org/10.1023/A:1018906132279>.
- [152] R.P. D'Amelia, S. Gentile, W.F. Nirode, L. Huang, Quantitative Analysis of Copolymers and Blends of Polyvinyl Acetate (PVAc) Using Fourier Transform Infrared Spectroscopy (FTIR) and Elemental Analysis (EA), *World Journal of Chemical Education*, *World Journal of Chemical Education*. 4 (2016) 25–31. <https://doi.org/10.12691/wjce-4-2-1>.
- [153] M.A.-F. Basha, Magnetic and optical studies on polyvinylpyrrolidone thin films doped with rare earth metal salts, *Polym J*. 42 (2010) 728–734. <https://doi.org/10.1038/pj.2010.60>.
- [154] I.A. Safo, M. Werheid, C. Dosche, M. Oezaslan, The role of polyvinylpyrrolidone (PVP) as a capping and structure-directing agent in the formation of Pt nanocubes, *Nanoscale Adv*. 1 (2019) 3095–3106. <https://doi.org/10.1039/C9NA00186G>.
- [155] E. Bubev, A. Georgiev, M. Machkova, ATR-FTIR spectroscopy study of the photodegradation protective properties of BP-4 and 4HBP in polyvinyl acetate thin films, *Journal of Molecular Structure*. 1118 (2016) 184–193. <https://doi.org/10.1016/j.molstruc.2016.04.013>.
- [156] N. Zhang, S. Wang, M.E. Gibril, F. Kong, The copolymer of polyvinyl acetate containing lignin-vinyl acetate monomer: Synthesis and characterization, *European Polymer Journal*. 123 (2020) 109411. <https://doi.org/10.1016/j.eurpolymj.2019.109411>.
- [157] D. Bahl, R.H. Bogner, Amorphization Alone Does Not Account for the Enhancement of Solubility of Drug Co-ground with Silicate: The Case of Indomethacin, *AAPS PharmSciTech*. 9 (2008) 146–153. <https://doi.org/10.1208/s12249-007-9013-9>.
- [158] T. Watanabe, S. Hasegawa, N. Wakiyama, A. Kusai, M. Senna, Comparison between polyvinylpyrrolidone and silica nanoparticles as carriers for indomethacin in a solid state dispersion, *International Journal of Pharmaceutics*. 250 (2003) 283–286. [https://doi.org/10.1016/S0378-5173\(02\)00549-5](https://doi.org/10.1016/S0378-5173(02)00549-5).
- [159] T. Watanabe, S. Hasegawa, N. Wakiyama, A. Kusai, M. Senna, Prediction of apparent equilibrium solubility of indomethacin compounded with silica by ¹³C solid state NMR, *International Journal of Pharmaceutics*. 248 (2002) 123–129. [https://doi.org/10.1016/S0378-5173\(02\)00428-3](https://doi.org/10.1016/S0378-5173(02)00428-3).
- [160] X. Pan, T. Julian, L. Augsburg, Quantitative measurement of indomethacin crystallinity in indomethacin-silica gel binary system using differential scanning calorimetry and X-ray powder diffractometry, *AAPS PharmSciTech*. 7 (2006) E72–E78. <https://doi.org/10.1208/pt070111>.
- [161] M. O'Brien, J. McCauley, E. Cohen, Indomethacin, in: K. Florey (Ed.), Academic Press, 1984: pp. 211–238. [https://doi.org/10.1016/S0099-5428\(08\)60192-6](https://doi.org/10.1016/S0099-5428(08)60192-6).
- [162] D.E. Zecevic, K.G. Wagner, Rational Development of Solid Dispersions via Hot-Melt Extrusion Using Screening, Material Characterization, and Numeric Simulation Tools, *Journal of Pharmaceutical Sciences*. 102 (2013) 2297–2310. <https://doi.org/10.1002/jps.23592>.
- [163] E. Kaminska, K. Adrjanowicz, M. Tarnacka, K. Kolodziejczyk, M. Dulski, E.U. Mapesa, D. Zakowiecki, L. Hawelek, I. Kaczmarczyk-Sedlak, K. Kaminski, Impact of Inter- and Intramolecular Interactions on the Physical Stability of Indomethacin Dispersed in Acetylated Saccharides, *Molecular Pharmaceutics*. 11 (2014) 2935–2947. <https://doi.org/10.1021/mp500286b>.

- [164] J. Larsson, *Methods for measurement of solubility and dissolution rate of sparingly soluble drugs*, Lunds Universitet, 2009.
- [165] T. Matsumoto, G. Zografi, Physical properties of solid molecular dispersions of indomethacin with poly(vinylpyrrolidone) and poly(vinylpyrrolidone-co-vinyl-acetate) in relation to indomethacin crystallization, *Pharm. Res.* 16 (1999) 1722–1728.
- [166] S. Bogdanova, I. Pajeva, P. Nikolova, I. Tsakovska, B. Müller, Interactions of Poly(vinylpyrrolidone) with Ibuprofen and Naproxen: Experimental and Modeling Studies, *Pharmaceutical Research.* 22 (2005) 806–815. <https://doi.org/10.1007/s11095-005-2598-3>.
- [167] H. Sekizaki, K. Danjo, H. Eguchi, Y. Yonezawa, H. Sunada, A. Otsuka, Solid-State Interaction of Ibuprofen with Polyvinylpyrrolidone., *CHEMICAL & PHARMACEUTICAL BULLETIN.* 43 (1995) 988–993. <https://doi.org/10.1248/cpb.43.988>.
- [168] H.M. Maswadeh, Incompatibility study of ibuprofen in ternary interactive mixture by using differential scanning calorimetry, *Journal of Thermal Analysis and Calorimetry.* 123 (2016) 1963–1971. <https://doi.org/10.1007/s10973-015-4773-z>.
- [169] A. Allahham, H.M. Maswadeh, Study of Dissolution Kinetics for Poorly Water-Soluble Drugs from Ternary Interactive Mixtures in Comparison with Commercially Available Capsules, *Journal of Pharmaceutical Innovation.* 9 (2014) 106–114. <https://doi.org/10.1007/s12247-014-9177-2>.
- [170] BASF, Technical information (Ibuprofen), 2010. <https://products.basf.com/documents/pim;view/en/8805242579413.Ibuprofen%20-%20Technical%20Information.pdf>.
- [171] P.J. Marsac, D.P. Romary, S.L. Shamblin, J.A. Baird, L.S. Taylor, Spontaneous crystallinity loss of drugs in the disordered regions of poly(ethylene oxide) in the presence of water, *J Pharm Sci.* 97 (2008) 3182–3194. <https://doi.org/10.1002/jps.21237>.
- [172] D.A.-V.D.R. Schmiedel, USP 40 - NF 35 The United States Pharmacopeia and National Formulary 2017 Main edition plus Supplements 1 and 2, 2016.
- [173] G.K. Webster, J.D. Jackson, R.G. Bell, *Poorly soluble drugs: dissolution and drug release*, 2017. <http://www.crcnetbase.com/isbn/9789814745468> (accessed June 14, 2018).
- [174] G. Cimpan, K. Box, J. Comer, S. Stones, *Measuring Drug Solubility at 37°C*, (n.d.) 1.
- [175] Owens, Wendt, Rabel and Kaelble (OWRK) method, (2018). <https://www.kruss-scientific.com/services/education-theory/glossary/owens-wendt-rabel-and-kaelble-owrk-method/> (accessed July 6, 2018).
- [176] Interfacial tension, (2018). <https://www.kruss-scientific.com/services/education-theory/glossary/interfacial-tension/> (accessed August 4, 2019).
- [177] Surface free energy - theory and calculations, (n.d.). <https://cdn2.hubspot.net/hubfs/516902/Pdf/Attension/Tech%20Notes/AT-TN-04-Surface-free-energy-theory.pdf?t=1530862737635>.
- [178] DIN 55660-2:2011-12, Beschichtungsstoffe_- Benetzbarkeit_- Teil_2: Bestimmung der freien Oberflächenenergie fester Oberflächen durch Messung des Kontaktwinkels, Beuth Verlag GmbH, n.d. <https://doi.org/10.31030/1823008>.
- [179] C.K. Tye, C. (Calvin) Sun, G.E. Amidon, Evaluation of the effects of tableting speed on the relationships between compaction pressure, tablet tensile strength, and tablet solid fraction, *Journal of Pharmaceutical Sciences.* 94 (2005) 465–472. <https://doi.org/10.1002/jps.20262>.
- [180] G.M. Laudone, C.M. Gribble, G.P. Matthews, Characterisation of the porous structure of Gilsocarbon graphite using pycnometry, cyclic porosimetry and void-network modeling, *Carbon.* 73 (2014) 61–70. <https://doi.org/10.1016/j.carbon.2014.02.037>.